

GEOLOGICA ULTRAIECTINA
Mededelingen van de Faculteit Geowetenschappen
Universiteit Utrecht
No. 312

**Quantifying nutrient cycling and retention in coastal
waters
at the global scale**

Goulven G. Laruelle

Promotor: Prof. Dr. P. Van Cappellen
Department of Earth Science - Geochemistry
Faculty of Geosciences, Utrecht University

Co-Promotor: Dr. C. P. Slomp
Department of Earth Science - Geochemistry
Faculty of Geosciences, Utrecht University

Members of the dissertation committee:

Prof. dr. D.J. Conley *Lund University, Lund, Sweden*

Prof. dr. J.J. Middelburg *Utrecht University, Utrecht, the Netherlands*

Prof. dr. G.J. de Lange *Utrecht University, Utrecht, the Netherlands*

Prof. dr J. Garnier *Université Pierre et Marie Curie, Paris, France*

**Quantifying nutrient cycling and retention in coastal
waters
at the global scale**

*Kwantificering van nutriënten kringlopen en retentie in kustwateren op
mondiale schaal*
(met een samenvatting in het Nederlands)

PROEFSCHRIFT

ter verkrijging van de graad van doctor aan de Universiteit Utrecht op
gezag van de rector magnificus, prof.dr. J.C. Stoof, ingevolge het besluit
van het college voor promoties in het openbaar te verdedigen op vrijdag 18
september 2009 des ochtends te 10.30 uur

door
Goulven Gildas Laruelle

geboren op 1 mei 1978
te Morlaix, Frankrijk

Promotor: Prof. dr. P. van Cappellen
Co-promotor: Dr. C.P. Slomp

The research presented in this thesis was conducted at the
Department of Geosciences, Utrecht University, the Netherlands.

ISBN: 978-90-5744-174-5

“Il n’y a rien de tel que les fainéants quand ils s’y mettent...”
Gérard Cadiou

INTRODUCTION

1. General background

It has long been thought that the presence of liquid water is a unique characteristic of Earth (McKay, 1997). While the evidence for recent surface runoff on Mars proves this to be incorrect (Malin and Edgett, 2000), no one will deny the importance of water for our planet. Water covers 70% of the Earth's surface. Water also played a critical role in the appearance and development of life (Kasting and Catling, 2003) and acts as a major transport agent, solvent and chemical reactant on land and in the oceans. As a consequence, an intimate link exists between the global water cycle (Figure 1) and the biogeochemical cycles of the main constituents of all living organisms: carbon (C), hydrogen (H), nitrogen (N), oxygen (O), phosphorus (P) and sulfur (S).

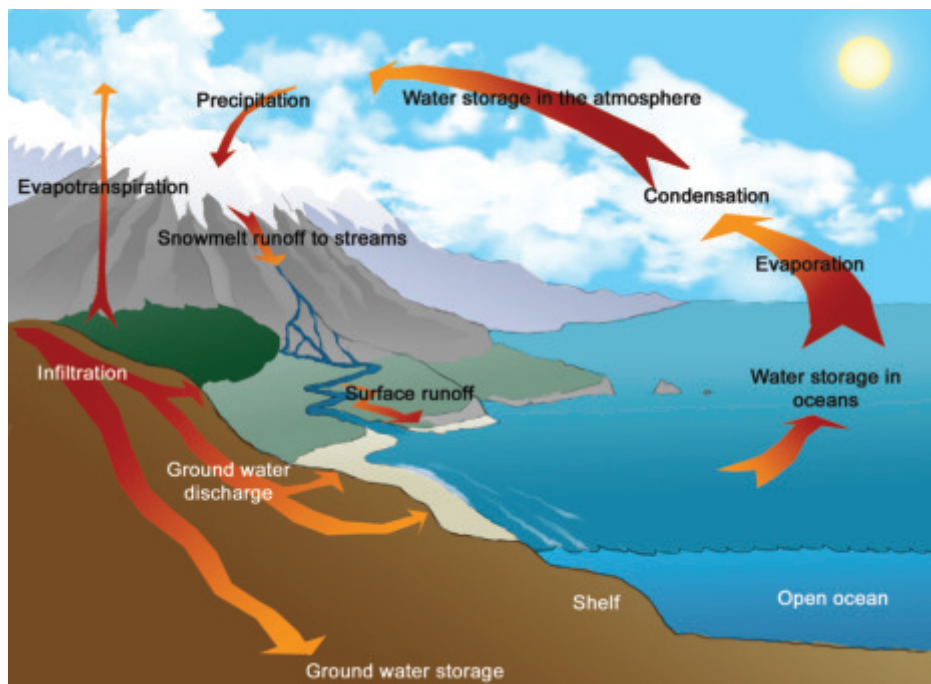


Figure 1: The global water cycle

The oceans alone, account for almost half of the global production of plant biomass on earth (Field et al, 1998, Falkowski et al., 2000) and the magnitude of nutrient recycling fluxes within the oceanic realm are similar to those on land. Coastal waters in particular are subject to intensive biogeochemical cycling (Mackenzie et al., 1998) characterized by complex spatial and temporal trends. The geomorphology and biogeochemical dynamics of this transition zone between the continents and the oceans are the topic of study for a wide range of scientific communities, including those of physical geographers, biogeochemical modellers and marine geochemists. Besides classical field work and sampling, typical approaches employed to study the coastal ocean include the use of types or clusters of the various coastal systems (Talaue-McManus et al. 2003; Crossland et al. 2005; Buddemeier et al. 2008), and the development and application of box models and numerical models that include physical and/or biogeochemical processes.

Over the past decades, an increasing number of coastal ecosystems have been perturbed by human activities. Examples of such perturbations include increased nutrient inputs from land associated with land use changes and urbanization (Mackenzie et al., 2005), changes in river inputs of nutrients due to river damming (Conley, 1993), increased input of domestic and industrial waste water and the proliferation of invasive species (Ragueneau et al., 2005). All of these perturbations have been shown to modify carbon and nutrient cycling in coastal waters and, in many cases, disrupt ecosystem dynamics. The manifestations of such changes often consist of alterations in nutrient ratios in coastal waters, eutrophication and modifications of phytoplankton communities and their seasonal dynamics. In an increasing number of cases, coastal hypoxia develops, with the Gulf of Mexico and Baltic Sea being two of the most pertinent examples (Díaz and Rosenberg, 2008). In addition, harmful algal blooms (HABs) may develop that endanger fisheries and ecosystem services (Crossland et al., 2005). Human activities are also severely modifying riverine carbon export to the coastal zone (Cole et al., 2007), thus potentially affecting the role of near-coastal waters as a source of atmospheric CO₂ (Borges et al., 2005; Crossland et al. 2005; Sarmiento and Gruber, 2006).

Various modeling approaches are currently being used to quantitatively

assess the response of nutrient and carbon dynamics in the global coastal ocean to environmental change. These include the use of global scale box models, where the continental margins are represented by one or two homogeneous reservoirs with a single river input (e.g. Ver, 1999; Rabouille et al., 2001; Slomp and Van Cappellen, 2004). With this method, the spatial heterogeneity in input fluxes (Smith et al., 2003; Seitzinger et al., 2005) and coastal ecosystem characteristics including the hydrodynamics are ignored. Alternatively, Ocean General Circulation Models (OGCMs) can be used to assess short-term effects of changes in river inputs on nutrient cycling on the open continental shelves in relatively coarse spatial resolution (Bernard et al., 2009). While a multitude of local 1- 2- and 3-dimensional biogeochemical models and flux estimates are available for many near-coastal systems, upscaling and extrapolation of the results to the global scale is hampered by computational costs and a lack of insight in the spatial boundaries and areas of the various types of coastal systems and the relevant temporal variability.

The aim of this thesis is to obtain more insight in the biogeochemical cycles of carbon and nutrients in the global coastal ocean and their response to perturbation, mostly on time scales of decades to a century. To reach this aim, various tools are developed, including models of the cycling of silica, phosphorus and nitrogen in coastal waters, a box model of the global silica cycle and a global coastal zone typology. A specific effort is made to go beyond traditional boundaries between scientific fields. As a consequence, this work combines typical resources and tools used by physical geographers (e.g., maps and geographical information systems) and those of biogeochemical modelers (e.g., elemental budgets, box models and general circulation models). In the following three sections, I will give a brief description of the biogeochemical cycling of nutrients along the land-ocean continuum, the modeling tools that are commonly used to study these cycles and the topics that are addressed in this thesis.

2. Biogeochemical cycling of nutrients along the land-ocean continuum

There are many similarities in the dynamics of the biogeochemical cycling of phosphorus (P), nitrogen (N) and silica (Si) both on land and in the ocean. For example, in all cases recycling is dominated by uptake by various types of plants

and remineralization or redissolution of the produced organic or mineral material. Another common characteristic is the significant retention of nutrients in soils or sediments. Although, on the global scale, the biomass of terrestrial systems is significantly larger than that of aquatic systems, recycling fluxes of Si, P and N on land and in the ocean are of the same order of magnitude.

The ultimate source of P and Si on land and in the oceans is the weathering of continental rocks. For Si, hydrothermal inputs are an additional minor source (Tréguer et al., 1995). The major source of N, in contrast, is fixation of N_2 from the atmosphere through the activity of terrestrial and aquatic micro-organisms. Over the past century, human-induced increases in inputs of P and N, mostly from fertilizer and sewage, have become important (Seitzinger et al., 2005). Once introduced into the aquatic realm, the fate of these nutrients is tightly linked to the water cycle. This connection allows the nutrients to travel along the land-ocean continuum from rivers and lakes to the open ocean. During this journey, a multitude of transformations occur between dissolved and particulate and inorganic and organic nutrient forms.

Phytoplankton are responsible for the major proportion of the transformation of dissolved inorganic nutrients to organic matter in aquatic systems. The relative contribution of pelagic versus benthic phytoplankton (e.g. microphytobenthos and macroalgae) in a given system depends on the water depth and penetration of light, with benthos being most important in the intertidal zone (Heip et al., 1995). While N and P are essential nutrients for all plant life, Si is only necessary for diatoms, radiolarians and sponges (and higher terrestrial plants; Conley, 2002). Diatoms are a major phytoplankton species in coastal environments and use the Si to form frustules (Figure 2) of biogenic Si.

Remineralisation is the process by which, after the death of the organisms, particulate organic matter is converted again to a dissolved inorganic form. Micro-organisms are usually responsible for this multi-step degradation of organic matter. In the particular case of Si, the term dissolution is more appropriate since biogenic Si is an amorphous mineral phase. Remineralisation and dissolution occur both within the water column and, after settling of the organic or inorganic material from the water column, in the surface layer of the sediment. The dissolved products may

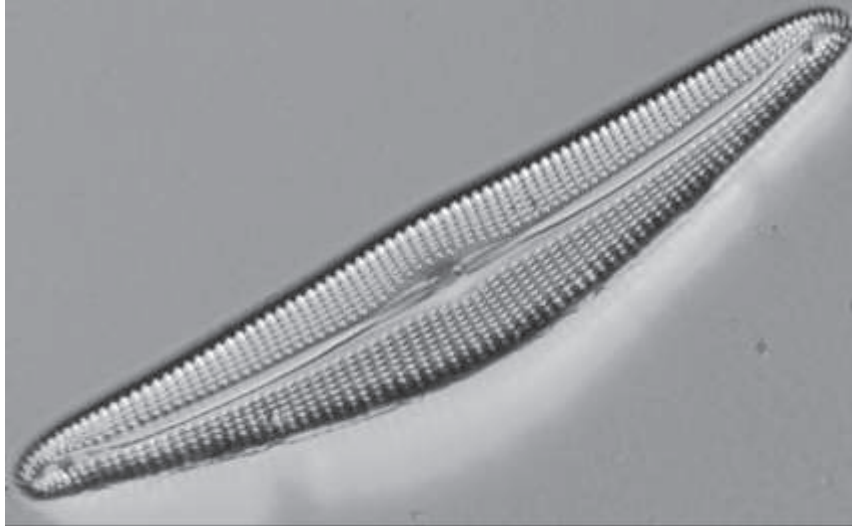


Figure 2: *Cymbella Helvetica*, fresh water diatom (size: 60µm, photos by Vincent Roubéix).

then be released through sediment-water exchange (“benthic-pelagic coupling”) or retained through additional diagenetic processes (e.g. reverse weathering for Si, authigenic Ca-P formation for P) and burial. Direct burial of particulate organic N and P and biogenic Si and transformation of inorganic N forms to N_2 are also major sinks for nutrients in aquatic systems.

A significant fraction of the N, Si and P is thus retained in riverine and estuarine systems. Nonetheless, the ultimate destination of the major proportion of the transported nutrients is the coastal and open ocean. While it is well-known that the rivers, estuaries, continental margins and regional seas behave as successive filters for nutrients along the land-ocean continuum, the recycling and burial of nutrients in these environments is still poorly quantified at the global scale.

3. Quantification of biogeochemical cycling:

Currently, three main approaches are used to quantitatively assess the biogeochemical dynamics of nutrients in aquatic systems. By increasing order of complexity, these consist of biogeochemical budgets, box models and reactive transport models (RTM). Biogeochemical budgets are simple mass balance calculations for specific variables for a well-defined system over a given time

period (Gordon et al., 1996). A box model is typically based on such a budget for a system which is then divided into various reservoirs. Simple rate laws are used to describe the fluxes between those reservoirs (Mackenzie et al., 1993). Reactive transport models allow a truly mechanistic description of coupled transport and reaction processes (e.g. Soetaert and Herman, 2008).

The widest range of modeling approaches is used at the local scale (typically < 100 km in length). The use of budgets to quantify nutrient cycling in these systems was made particularly popular by the LOICZ program (Gordon et al., 1996). While several box models have been derived from the LOICZ budgets, most local coastal studies involve RTMs of various degrees of complexity. In linear estuaries, 1-dimensional models are sometimes used, thus ignoring most of the geometry of the system (Regnier et al, 1997; Hoffmann et al., 2008). Horizontal 2 dimensional models allow the reproduction of currents and the inclusion of advection and diffusion terms (Arndt et al, 2009). When vertical stratification of the water column occurs or when depth dependant processes initiate a strong vertical heterogeneity, fully developed 3-dimensional models can be used to represent the physics of the systems. In such cases, the computation cost may become a concern for long term simulations.

Note that various types of budgets and models can be developed for sub-systems such as the sediment layer, the inter-tidal zone (Guarini, 2000) or a particular location within an ecosystem. As an example, diagenetic models can range from simple box models to vertical multi-variable RTMs (Soetaert et al., 2000).

Regional scale systems range in size from ca. 100 km in length to a whole oceanic basin. With the exception of a few well-known areas (North East US coast, North and Mediterranean seas), data availability often limits the calibration and validation of biogeochemically complex models. The inherent assumption of homogeneity also limits box modeling approaches to (semi-)enclosed systems such as, for example, the Mediterranean Sea (Sarmiento et al., 1988). Sometimes, several, smaller order box models are combined to represent each section of a system (Nielsen, 1995).

At the global scale, both reactive transport models for the ocean, which

are more commonly denoted as Ocean General Circulation Models (Heinze et al., 1991, 1999), and a variety of box models have been developed over the years (Broecker and Peng, 1982; Ver, 1998; Yool and Tyrell, 2003, 2005; Slomp and Van Cappellen, 2004; 2007). Box models have been used by oceanographers in various applications for many decades (Broecker and Peng, 1982). They require only limited data and calculation cost. Applications commonly focus either on the world's ocean as a whole (e.g. Ver, 1998), a specific region of interest such as the coastal zone (e.g. Rabouille et al., 2001) or the various oceanic basins (Broecker and Peng, 1982). While OGCMs allow more mechanistic descriptions of physical and biogeochemical processes in the ocean, they only poorly resolve coastal zone processes. In addition, they have a high computational demand. Box model approaches thus are particularly useful for studies of coastal waters at the global scale.

4 Thesis outline

This thesis concentrates on the relatively short-term processes affecting nutrient and carbon cycling and fluxes in coastal waters at the global scale. The research comprised of the development and application of various tools for the quantification of cycling and retention of nutrients. This included the development of a global scale coastal typology and associated model for N and P retention in the near-coastal zone. The work was carried out within the framework of a larger project on Global Nutrient Fluxes at the Land-Ocean Interface (G-NUX).

In **chapter 1**, a fully transient two dimensional hydrodynamic model is coupled to a biogeochemical model for N and Si cycling to assess the effect of two perturbations, namely increased nutrient loads and colonization by invasive species, on a small tidal Bay (Bay of Brest). The model results emphasize the role of seasonal retention and redissolution of silica in determining the resistance of the system to eutrophication.

Chapter 2 focuses on the global cycle of Si along the land-ocean continuum. Four major compartments are distinguished. These are the continents, proximal coastal zone, distal coastal zone and open ocean and an updated budget for reactive Si for these compartments is established. In a next step, a first order

kinetic box model is derived from the established reservoir sizes and fluxes. A sensitivity analysis of the global Si cycle to temperature rise and river damming demonstrates the role of the coastal zone as a buffer between the terrestrial and oceanic domains.

In **chapter 3**, a comparison is made between the performance of the box model for the global Si cycle of chapter 2 and two Ocean General Circulation Models (HAMOCC2, Heinze et al, 2003 and HAMOCC5, Bernard et al, 2009). Similar scenarios for short (150 yrs) and long (150 kyrs) time scales are used in this comparison. The results demonstrate that the average global ocean response to changes in river input is similar on time scales up to 150 kyrs.

In **chapter 4**, a spatially-explicit global typology for estuarine ecosystems is presented. This typology is based on morphological, lithological and hydrological criteria and provides new insights in the spatial distribution and inherent heterogeneity of the estuarine filter worldwide. As an application of this typology, a re-estimate of the global estuarine surface area is provided.

In **chapter 5**, the global estuarine typology is used as the basis for a spatially explicit model for N and P cycling and retention. The model consists of a ribbon of 6200 generic box models distributed along the world coastline, and is designed to be compatible with outputs of GIS-based riverine nutrient fluxes from global watershed models (GLOBAL NEWS, Seitzinger et al., 2005). The global estimates for N and P retention calculated for the estuarine filter are lower than values reported in previous studies.

Finally, in **chapter 6** a simplified continental shelf typology is presented and combined with the estuarine typology of chapter 5 to reevaluate the global CO₂ exchange at the air-water interface of the coastal ocean. When compared to the earlier work of Borges et al. (2005), the improved surface areas, and spatially-explicit typological approach allow for a more accurate upscaling of average CO₂ exchange fluxes from local studies to the global scale.

References:

- Arndt S., P. Regnier and J-P. Vanderborcht (2009) Seasonally-resolved nutrient filtering capacities and export fluxes in a macrotidal estuary. *Journal of Marine Systems*. In press.
- Bernard C. Y., H. H. Durr, C. Heinze, J. Segschneider and E. Maier-Reimer (2009) Contribution of riverine nutrients to the silicon biogeochemistry of the global ocean - a model study, *Biogeosciences Discuss.* 6:1091-1119.
- Borges A.V., B. Delille and M. Frankignoulle (2005) Budgeting sinks and sources of CO₂ in the coastal ocean: Diversity of ecosystems counts. *Geophysical Research Letters* 32, L14601, doi:10.1029/2005GL023053.
- Broecker W. S. and T.-H. Peng (1982) *Tracers in the Sea*. A publication of the L-D geological Observatory. Columbia University, Palisades, New York. Eldigio Press.
- Buddemeier R.W., S.V. Smith, D.P. Swaney, C.J. Crossland and B.A. Maxwell (2008) Coastal typology: An integrative “neutral” technique for coastal zone characterization and analysis. *Estuarine, Coastal and Shelf Science*. 77 (2):197-205. doi:10.1016/j.ecss.2007.09.021
- Conley, D.J., C.L. Schelske, and E. F. Stoermer (1993) Modification of the Biogeochemical Cycle of Silica with Eutrophication, *Marine Ecology Progress Series*, 101:179-192.
- Conley D.J. (2002) Terrestrial ecosystems and the global biogeochemical silica cycle. *Global Biogeochem. Cycle* 16, 1121, doi: 10.1029/2002GB001894.
- Cole, J. J., Y. T. Prairie, N. F. Caraco, W. H. McDowell, L. J. Tranvik, R. G. Striegl, C. M. Duarte, P. Kortelainen, J. A. Downing, J. J. Middleburg and J. Melakck (2007) Plumbing the global carbon cycle: integrating inland waters into the terrestrial carbon budget. *Ecosystems* 10: 171–184.
- Crossland C. J., H. H. Kremer, H. J. Lindeboom, J. I. Marshall Crossland and M.D.A. LeTissier (2005). *Coastal Fluxes in the Anthropocene*. *Global Change - The IGBP Series*: Berlin, Heidelberg, Springer, 232pp.
- Díaz R. J. and R. Rosenberg (2008) Spreading dead zone and consequences for marine ecosystems. *Science* 321: 926–929.
- Falkowski P., R. J. Scholes, E. Boyle, J. Canadell, D. E. Canfield, J. Elser, N.

- Gruber, K. Hibbard, P. Hogberg, S. Linder, F. T. Mackenzie, B. Moore, T. Pdersen, Y. Rosenthal, S. Seitzinger, V. Smetacek and W. Steffen (2000) The global carbon cycle: A test of our knowledge of earth as a system. *Science* 290: 291–296.
- Field C. B., M. J. Behrenfeld, J. T. Randerson and P. Falkowski (1998) Primary Production of the Biosphere: Integrating Terrestrial and Oceanic Components. *Science, New Series*. 281: 237-240
- Guarini J. M., G. F. Blanchard, Ph. Gros, D. Gouleau and C. Bacher (2000) Dynamic model of the short-term variability of microphytobenthic biomass on temperate intertidal mudflat, *Mar. Ecol. Prog. Ser.* 195: 291–303.
- Gordon J. D. C., P. R. Boudreau, K. H. Mann, J. E. Ong, W. L. Silvert, S. V. Smith, G. Wattayakorn, F. Wulff and T. Yanagi (1996) LOICZ Biogeochemical Modelling Guidelines. LOICZ Reports & Studies, (ed.), 5, Texel, The Netherlands: LOICZ, pp. 1 - 96.
- Heinze C. and E. Maier-Reimer (1999) The Hamburg Oceanic Carbon Cycle Circulation Model Version “HAMOCC2s” for long time integrations. Deutsches Klimarechenzentrum. Technical Report No. 20, 71pp.
- Heinze C., E. Maier-Reimer and K. Winn (1991) Glacial pCO₂ reduction by the world ocean: experiments with the Hamburg carbon cycle model. *Paleoceanography* 6: 395–430.
- Heinze C., A. Hupe, E. Maier-Reimer, N. Dittert and O. Ragueneau (2003) Sensitivity of the marine biospheric Si cycle for biogeochemical parameter variations, *Global Biogeochemical Cycles* 17(3), 1086, doi:10.1029/2002GB001943
- Heip C. H. R., N. K. Goosen, P. M. J. Herman, J. Kromkamp, J. J. Middelburg and K. Soetaert (1995) Production and consumption of biological particles in temperate tidal estuaries. *Oceanogr Mar Biol Annu Rev* 33:1–150.
- Hoffmann A. F., K. Soetaert and J. J. Middelburg (2008) Present nitrogen and carbon dynamics in the Scheldt estuary using a novel 1D-model. *Biogeosciences* 5: 981-1006.
- Kasting J.F. and D. Catling (2003) Evolution of a habitable planet. *Annual Review*

- of Astronomy and astrophysics. 41: 429-463.
- Malin M. C. and K. S. Edgett (2000) Evidence for Recent Groundwater Seepage and Surface Runoff on Mars. *Science, New Series*. 288: 2330-2335.
- McKay C. P. (1997) The search for life on Mars. *Origins of Life and Evolution of the Biosphere* 27: 263–289.
- Mackenzie F. T., A. Lerman and L. M. Ver (1998) Role of the continental margin in the global carbon balance during the past three centuries. *Geology* 26: 423–426.
- Mackenzie F. T., L. M. Ver, C. Sabine, M. Lane and A. Lerman (1993) C, N, P, S global biogeochemical cycles and modeling of global change. in *Interactions of C, N, P and S Biogeochemical Cycles and Global Change*, edited by Wollast, R., F. T. Mackenzie and L. Chou., Springer-Verlag, pp. 1–62.
- Mackenzie F. T., A. J. Andersson, A. Lerman and L. M. Ver (2005) Boundary exchanges in the global coastal margin: Implications for the organic and inorganic carbon cycles. In: Robinson, A. R., Brink, K. H. (Eds.), *The Global Coastal Ocean- Multi-scale Interdisciplinary Processes*, Harvard University Press, Cambridge, pp. 193–225.
- Nielsen S. P. (1995) A box model for North-East Atlantic coastal waters compared with radioactive tracers, *J. Mar. Syst.* 6: 545–560.
- Rabouille C., F. T. Mackenzie and L. M. Ver (2001) Influence of the human perturbation on carbon, nitrogen, and oxygen biogeochemical cycles in the global coastal ocean. *Geochim. Cosmochim. Acta*, 65(21): 3615-3641.
- Ragueneau O., L. Chauvaud, B. Moriceau, A. Leynaert, G. Thouzeau, A. Donval, F. Le Loc'h and F. Jean (2005) Biodeposition by an invasive suspension feeder impacts the biogeochemical cycle of Si in a coastal ecosystem (Bay of Brest, France). *Biogeochemistry*, doi:10.1007/s10533-004-5677-3.
- Regnier P., R. Wollast and C. I. Steefel (1997) Long-term fluxes of reactive species in macrotidal estuaries: Estimates from a fully transient, multicomponent reaction-transport model. *Marine Chemistry* 58: 127–145.
- Sarmiento J. L. and N. Gruber (2006) *Ocean Biogeochemical Dynamics*. Princeton University Press, Princeton.

- Sarmiento J. L., T. Herbert and J. R. Toggweiler (1988) Mediterranean nutrient balance and episodes of anoxia. *Global Biogeochemical Cycles* 2: 427-444.
- Seitzinger S. P., J. A. Harrison, E. Dumont, A. H. W. Beusen and A. F. Bouwman (2005) Sources and delivery of carbon, nitrogen, and phosphorus to the coastal zone: An overview of Global Nutrient Export from Watersheds (NEWS) models and their application. *Global Biogeochemical Cycles*, 19, GB4S01, doi: 10.2029/2005GB002606: 1-11.
- Slomp C. P. and P. Van Cappellen (2004) Nutrient inputs to the coastal ocean through submarine groundwater discharge: controls and potential impact. *Journal of Hydrology*, 295 (1-4): 64 - 86.
- Slomp C. P. and P. Van Cappellen (2007) The global marine phosphorus cycle: sensitivity to oceanic circulation. *Biogeosciences* 4: 155-171.
- Smith S. V., D. P. Swaney, L. Talaue-McManus, J. D. Bartley, P. T. Sandhei, C. McLaughlin, V. C. Dupra, C. J. Crossland, R. W. Buddemeier, B. A. Maxwell and F. Wulff (2003) Humans, hydrology, and the distribution of inorganic nutrient loading to the ocean, *Bioscience* 53: 235–245.
- Soetaert K and P. M. Herman (2008). *ecolMod*: “A practical guide to ecological modelling – using R as a simulation platform”. R package version 1.1.
- Soetaert K., J. J. Middelburg, P. M. J. Herman and K. Buis (2000) On the coupling of benthic and pelagic biogeochemical models. *Earth-Science Reviews* 51: 173–201.
- Talaue-McManus L., S. V. Smith and R. W. Buddemeier (2003). Biophysical and socio-economic assessments of the coastal zone: the LOICZ approach. *Ocean & Coastal Management* 46(3–4): 323–333.
- Tréguer P., D. M. Nelson, A. J. Van Bennekom, D. J. DeMaster, A. Leynaert and B. Queguiner (1995) The silica balance in the world ocean: A reestimate, *Science New Series* 268(5209): 375-379.
- Ver L. M. (1998) Global kinetic models of the coupled C, N, P, and S biogeochemical cycles: Implications for global environmental change. Ph.D. dissertation, University of Hawaii.
- Yool A. and T. Tyrrell (2003) The role of diatoms in regulating the ocean’s silicon

cycle. Glob. Biogeochem. Cycles 17, 1103, doi:10.1029/2002GB002018.
Yool A. and T. Tyrrell (2005) Implications for the history of Cenozoic opal
deposition from a quantitative model. Palaeogeography, Palaeoclimatology,
Palaeoecology 218: 239–255.

CHAPTER 1

Benthic-pelagic coupling and the seasonal silica cycle in the Bay of Brest (France): New insights from a coupled physical-biological model

Laruelle, G. G., Regnier P., Ragueneau, O., Kempa, M., Moriceau, B., Ni Longphuir, S., Leynaert, A., Thouzeau, G. and Chauvaud, L.

Published in Marine Ecology Progress Series

Vol. 385: 15–32, June 2009, doi: 10.3354/meps07884

Abstract

A fully-transient, two-dimensional physical and biological model has been developed to quantify the seasonal cycle of silica in the estuaries - coastal zone continuum of the Bay of Brest (France). The numerical model includes an explicit representation of the benthic-pelagic coupling, which is stimulated by the increasing density of an invasive megabenthic filter feeder (*Crepidula fornicata*), a slipper limpet. The selected spatial resolution allows resolving the heterogeneous density distribution of these organisms in the bay. Results show that the benthic dynamics is highly variable and strongly depends on the local conditions. This heterogeneity is not reflected in the pelagic dynamics because transport and mixing homogenize the distributions of nutrients and biomasses. A seasonally-resolved silica budget over the entire bay and estuaries emphasizes the important contribution of the benthic recycling fluxes to the supply of dissolved silica (dSi) during the productive period (~ 50 % over the period 1 April to 1 September). In a prognostic scenario which forecasts the impact of removing the invasive benthic filter feeders, the dSi efflux is reduced by 63 % and a pronounced harmful algal bloom of dinoflagellates develops in late summer.

1. Introduction

Like many other coastal areas over the world (Cloern 2001), the Bay of Brest (NW France) is a macrotidal embayment which is subject to major anthropogenic pressure. In this ecosystem, nitrogen inputs from agricultural practices in the watersheds have doubled since the 70's (Le Pape et al. 1996). At the same time, the gastropod *Crepidula fornicata* invaded the bay and became the main benthic suspension feeder within the megafauna during the early 90's. (Chauvaud et al. 2000). In 2000, it covered about half of the entire benthic surface area of the bay (Chauvaud, 1998).

Despite the marked increase in dissolved inorganic nitrogen (DIN) inputs, the Bay of Brest has not experienced any major eutrophication events so far. Such dynamics has been attributed to the fact that most of the nutrient delivery occurs before the start of the productive season. In addition, it has been argued that the estuarine processes occurring upstream and the macrotidal dynamics in the bay itself were not providing favorable conditions for the onset of eutrophication (Le Pape et al. 1996). More surprisingly, however, no significant perturbation of the pelagic food-web structure related to the long-term decline in the dSi:DIN ratio which accompanied the increase in nitrate inputs has yet been observed (Ragueneau 1994). In many ecosystems, such a decline has induced changes in phytoplankton dynamics, the increase in non-siliceous phytoplankton species at the expense of the diatoms having important implications for the pelagic and benthic food webs (Smayda 1990, Conley et al. 1993, Turner et al. 1998). However, as recently reviewed by Ragueneau et al. (2006a), such a shift in phytoplankton abundances due to modifications in nutrient ratio does not always occur. In particular, it has been advocated that the intensity of dSi recycling within a specific ecosystem plays an essential role in controlling the characteristics and succession of phytoplankton species. The recycling intensity modifies the properties of the various diatom species (Roberts et al. 2003), especially their degree of silicification (Rousseau et al. 2002), and ultimately, favor the switch from diatom to non-diatom species when the dSi stress becomes too strong (Officer & Ryther 1980).

Until very recently, diatoms have dominated the phytoplankton biomasses during the whole productive period in the Bay of Brest (Del Amo et al. 1997a,

Beucher et al. 2004), despite indirect (Ragueneau et al. 1994) and direct (Del Amo 1997b, Ragueneau et al. 2002) evidence of a dSi limitation during spring. On the one hand, physical factors have been proposed (Ragueneau et al. 1996) to explain the limited occurrence of dinoflagellates, which generally prefer stratified water bodies (Margalef 1978). On the other hand, dSi recycling is significant in this ecosystem, both in the water column (Beucher et al. 2004) and in the sediments (Ragueneau et al. 1994, Martin et al. 2007), and, therefore, could explain the high resistance of the diatoms towards the decrease in the dSi:DIN ratio. Del Amo et al. (1997b) have suggested the existence of a coastal silicate pump similar to that of the oceanic silicate pump proposed by Dugdale et al. (1995), which extracts dSi from the surface waters, but instead of transferring it to the deep layers of the open ocean, would here be directly transported and temporarily stored in the sediments. The subsequent benthic recycling flux of dSi during late spring and summer could then explain the maintenance of diatoms throughout the entire productive period. Since it has been suggested that the invasion of *C. fornicata* increase significantly the efficiency of the silicate pump in the Bay of Brest (Chauvaud et al., 2000), the two major anthropogenic perturbations (nutrient loads increase and invasive species) strongly interact in this ecosystem. The efficiency of the silicate pump is improved by the filtering and biodeposition activities of the benthic filter feeder, leading to a significant storage of biogenic silica (bSiO_2) in the sediments, followed by dissolution later in the season when temperature increases. If true, such hypothesis implies that the proliferation of the benthic filter feeder may have helped preventing, at least for some time, the expected switch in phytoplankton dominance. From an Integrated Coastal Zone Management (ICZM) perspective, the possible positive effect of the invasive species, that is, its ability to prevent the development of non-diatom, possibly harmful, algal blooms should thus be balanced with its negative impact on other native benthic species in the bay (e.g. the Great scallop, *Pecten maximus*).

Previous experimental studies have already investigated the direct impact of the presence of *C. fornicata* on the magnitude of benthic recycling fluxes of dSi (Ragueneau et al. 2002, 2006b). In addition, seasonal and annual budgets of Si have been proposed (Ragueneau et al. 2005) and the importance of the benthic

filter feeders in the Si seasonal cycle has clearly been established. Yet, the feedback of this biologically-driven silicate pump on the phytoplankton dynamics in the bay and, more specifically, its ability to maintain the diatom dominance despite the observed widespread dSi limitation are important research questions that remain essentially unanswered. These research questions are however essential if one aims to forecast the potential effect of benthic filter feeder eradication on both the eutrophication and food-web structure in the bay. Such an engineered intervention is now planned since the early 2000's and, therefore, prognostic simulations are particularly timely to help design the best sustainable management strategy for the Bay of Brest.

In this paper, a 2 dimensional, depth-averaged, hydrodynamic and reactive-transport model has been developed for the estuaries and the Bay of Brest. The ecological and biogeochemical reaction network includes the dominant processes of the Si, C and N cycles in the water column and surficial layers of the sediments. In particular, the model explicitly accounts for the feeding and biodeposition activities of *C. fornicata* at the sediment-water interface. Model results are not only compared with measurements of standing stocks of nutrients and chl *a*, but also with in-situ flux and rate measurements (e.g. silica production, benthic fluxes...). Mesocosm experiments (Fouillaron et al., 2007) have shown that observations on process rates and material fluxes are essential to understand the biogeochemical dynamics in the bay. The model allows advancing our understanding of the Si dynamics in the bay, to establish temporally and spatially resolved budgets of silica, and to conduct prognostic simulation addressing the ecological consequences of eradicating partly the benthic filter feeder from the sea bed.

2. Model Set-Up

2.1. Hydrodynamics and transport

Support

A two-dimensional, vertically integrated numerical model (MIKE 21, www.dhisoftware.com/mike21) is used to compute the flow field in the Aulne and Elorn estuaries, the Bay of Brest and the inner part of the Iroise Sea (Fig. 1). The

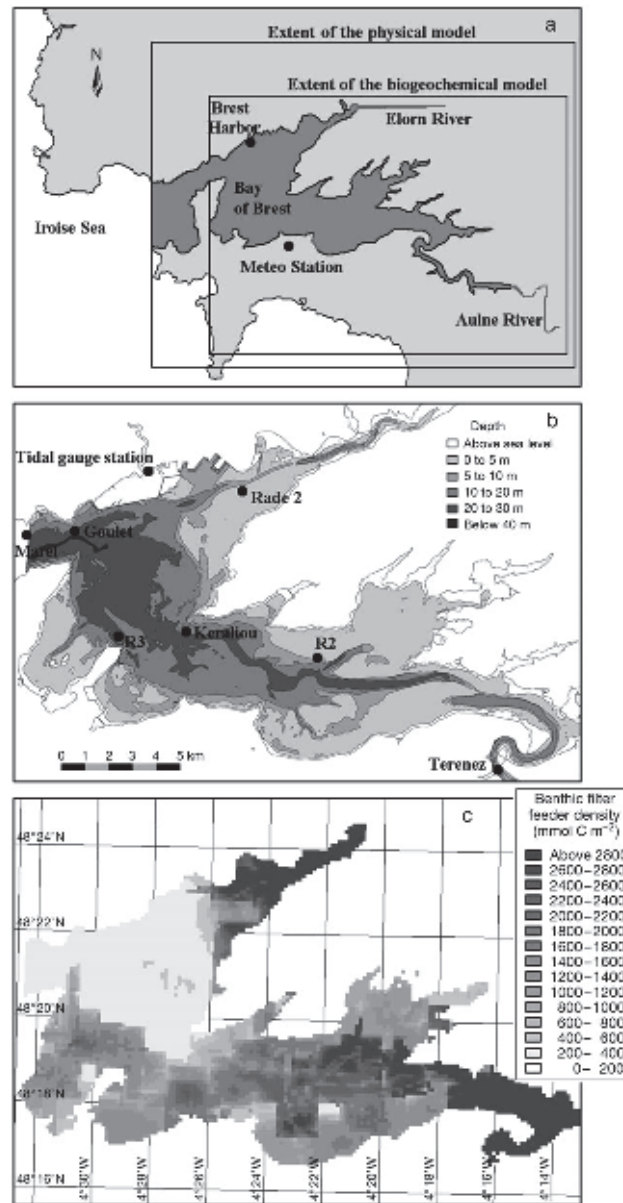


Figure 1: (a) Geographical extent of the model, (b) bathymetric map of the Bay of Brest, France, and (c) spatial distribution of benthic filter feeder density. All locations and stations referred to in the text are shown in (a) and (b).

model extends upstream in the Aulne and Elorn up to the limit of tidal influence where unidirectional flow is maintained at all times. The marine boundary in the Iroise Sea is set to longitude 4°36'W. The land boundaries and the bathymetry are obtained from the SHOM (Service hydrologique et océanographique de la marine) digital charts. Spatial resolution of the bathymetric surveys in the Iroise, the bay and the estuaries are in the order of 500, 100 and 200 m, respectively. The hydrodynamic model is run over the entire domain with a spatial resolution of 150m x 150m. Time series of water elevation are then extracted along a transect through the narrow strait between the bay and the Iroise sea ('Goulet', Fig. 1) and used to force a smaller-scale, coupled physical-biological model which is run over the entire year of 2001.

Hydrodynamics

The hydrodynamic model is based on the vertically integrated volume (eq. 1) and momentum conservation equations (eq. 2 and 3) for barotropic flow:

$$\frac{\partial \zeta}{\partial t} + \frac{\partial p}{\partial x} + \frac{\partial q}{\partial y} = 0 \quad (1)$$

$$\begin{aligned} \frac{\partial p}{\partial t} + \frac{\partial}{\partial x} \left(\frac{p^2}{h} \right) + \frac{\partial}{\partial y} \left(\frac{pq}{h} \right) + gh \frac{\partial \zeta}{\partial x} + \frac{gp\sqrt{p^2+q^2}}{M^2 h^{1/3} h^2} \\ - \left[E_x \frac{\partial^2 p}{\partial x^2} + E_y \frac{\partial^2 p}{\partial y^2} \right] - \Omega q - f(V)V_x = 0 \end{aligned} \quad (2)$$

$$\begin{aligned} \frac{\partial q}{\partial t} + \frac{\partial}{\partial y} \left(\frac{q^2}{h} \right) + \frac{\partial}{\partial x} \left(\frac{pq}{h} \right) + gh \frac{\partial \zeta}{\partial y} + \frac{gq\sqrt{p^2+q^2}}{M^2 h^{1/3} h^2} \\ - \left[E_x \frac{\partial^2 q}{\partial y^2} + E_y \frac{\partial^2 q}{\partial x^2} \right] + \Omega p - f(V)V_y = 0 \end{aligned} \quad (3)$$

This set of coupled non-linear partial differential equations (PDE's) resolves the spatial (x,y) and temporal (t) dynamics of surface water elevation, ζ [m], and scalar components of the momentum fluxes, p and q , [$m^2 s^{-1}$]. The flux densities p and q are defined per unit length along the y and x coordinates, respectively. In eqs. (2) and (3), h [m] is the water depth, g [$m \cdot s^{-2}$] is the Earth's gravitation constant, Ω [s^{-1}] is the Coriolis parameter and M [$m^{1/3} s^{-1}$] is the Manning-Strickler coefficient

which is used to constrain the bed friction. The effect of wind stress (last term on the left side of eqs. 2 and 3) is also taken into account in the momentum balance, using daily data of wind speed (V) and direction obtained 10 m above the surface at the Lanvéoc Poulmic meteorological station (48°16'57.11" N 004°26'37.29" W, Fig. 1). The wind friction factor $f(V)$ is calculated according to Smith and Bank (1992). The system of PDE's is solved by finite differences with appropriate initial and boundary conditions, using a non-iterative alternating direction implicit algorithm (Abbott 1979).

The Manning-Strickler number M and eddy viscosity coefficients $E_{x,y}$ [$\text{m}^2 \text{s}^{-1}$] are model calibration parameters that must be specified. Eddy viscosity coefficients are proportional to the local current velocities and calculated with the Smagorinsky formula (Smagorinsky 1963) using a proportionality constant of 0.5. For bed friction, a Manning-Strickler of 60 has been used over the entire domain.

Transport

The mass conservation equation for scalar components (salt and biogeochemical variables) is based on the vertically integrated advection-dispersion equation:

$$\begin{aligned} \frac{\partial}{\partial t}(hc) + \frac{\partial}{\partial x}(uhc) + \frac{\partial}{\partial y}(vhc) - \frac{\partial}{\partial x}\left(h \cdot D_x \frac{\partial c}{\partial x}\right) \\ - \frac{\partial}{\partial y}\left(h \cdot D_y \frac{\partial c}{\partial y}\right) + \Sigma R + S = 0 \end{aligned} \quad (4)$$

where c is the species concentration [mol m^{-3}], $u=p/h$ and $v=q/h$ are the horizontal components of the velocity vector [m s^{-1}], D_x and D_y are the eddy dispersion coefficients [$\text{m}^2 \text{s}^{-1}$]. The hydrodynamic model provides the horizontal velocity components u and v as well as the water depth, h [m]. In equation (4), ΣR is the rate of production or consumption of the species by the sum of biogeochemical processes, defined per unit surface area [$\text{mol m}^{-2} \text{s}^{-1}$] and S [$\text{mol m}^{-2} \text{s}^{-1}$] is a source/sink term defining the local exchange of the species between the water column and the sediment.

The equation is solved for the spatial and temporal evolution of the concentration field using appropriate initial and boundary conditions (see below).

Numerical integration of equation (4) is performed using the third-order, explicit finite difference scheme QUICKEST (Ekebjærg & Justesen 1991). The dispersion coefficients D_x and D_y in equation (4) are model parameters that are set proportional to the local current velocities. The proportionality constant has been adjusted until agreement with observed salinity profiles was achieved. Both the hydrodynamic and salt transport models are run with a time step of 20 seconds that guarantees stability of the numerical schemes. The biogeochemical model used to calculate the ΣR and S terms is numerically decoupled from the transport algorithm using an operator-splitting approach. To decrease computational times, it is run with a larger time step of numerical integration of 360 seconds.

2.2. Biogeochemistry

Reaction network and state variables

The biogeochemical model is based on a reaction network (RN) that describes the pelagic and benthic processes involved in the Si and associated C, and N cycles (Fig. 2). The biogeochemical model was implemented within the ECOLab© environmental modeling tool of DHI (e.g. Vanderborght et al., 2007; Arndt et al., 2007). All pelagic state variables are subject to fluid flow motion while the benthic variables are fixed on the bed and, thus, not explicitly transported. The benthic compartment consists of the top layer of the sediment where biological activity is most intense. The pelagic RN is a slightly modified version of the reaction set proposed by Le Pape et al. (1996). The formulation of benthic processes also follows these authors, except for the dynamics of benthic diatoms (microphytobenthos) and filter feeders, as well as for an improved formulation of opal dissolution. Table 1 lists all state variables and their respective units.

Briefly, two phytoplankton groups (diatoms [Dia] and dinoflagelates [Dino]) are distinguished in the model (Fig. 2). Pelagic diatom growth consumes both dissolved silica [dSi] and dissolved inorganic nitrogen [DIN], dinoflagelates only requiring DIN. Both phytoplankton species are grazed by zooplankton [Zoo]. The death of diatoms supports a pool of freshly dead diatoms [FDDia] which in turn, are decomposed in detritic nitrogen [NDet] and detritic silica [SiDet] (Jean 1994). A simpler formulation is used for the Dino and Zoo, which assumes a direct

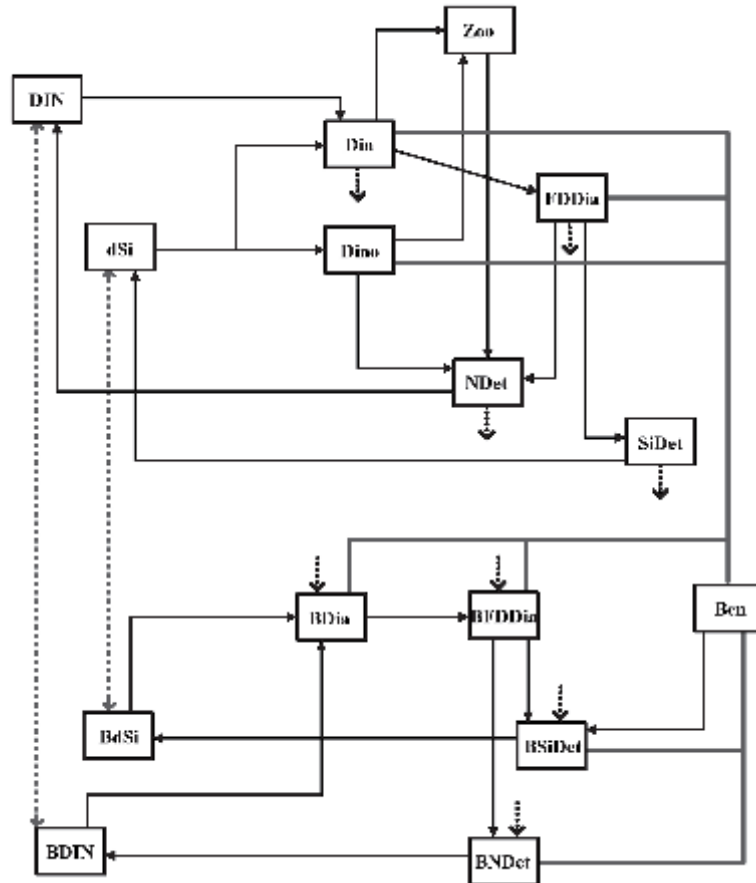


Figure 2: Schematic representation of the biogeochemical model. The boxes and arrows represent the state variables and processes, respectively. The thin lines characterize the pelagic and benthic processes. The benthic-pelagic coupling occurs through grazing by benthic filter feeders (thick lines), sedimentation (black dotted lines), and diffusion (grey dashed lines).

transformation into $NDet$ upon death of organisms. Zooplankton also excretes DIN . The detritic material ($[SiDet]$ and $[NDet]$) is partially mineralized in the water column and leads to the production of dissolved nutrients ($[dSi]$ and $[DIN]$).

Overall, the state variables involved in the benthic RN are similar to the ones implemented in the pelagic compartment. The model accounts for living and freshly dead benthic diatoms ($[BDia]$ and $[BFDDia]$), detritic pools of Si and N ($[BSiDet]$ and $[BNDet]$), and pore water dissolved inorganic nutrients ($[BdSi]$ and

Table 1: State variables of the models with their units and abbreviations

Symbol	Definition	Unit
Dia	Diatoms	$\mu\text{mol C l}^{-1}$
Dino	Dinoflagelates	$\mu\text{mol C l}^{-1}$
Zoo	Zooplankton	$\mu\text{mol C l}^{-1}$
DIN	Pelagic Dissolved Inorganic Nitrogen	$\mu\text{mol N l}^{-1}$
NDet	Pelagic Detritic Nitrogen	$\mu\text{mol N l}^{-1}$
dSi	Pelagic Dissolved Silica	$\mu\text{mol Si l}^{-1}$
SiDet	Pelagic Detritic Silica	$\mu\text{mol Si l}^{-1}$
FDDia	Freshly Dead Diatoms	$\mu\text{mol C l}^{-1}$
BDIN	Dissolved Inorganic Nitrogen in pore waters	mmol N m^{-2}
BNDet	Benthic Detritic Nitrogen	mmol N m^{-2}
BdSi	Dissolved Inorganic Silica in pore waters	mmol Si m^{-2}
BSiDet	Benthic Detritic Silicon	mmol Si m^{-2}
BDia	Benthic Diatoms	mmol C m^{-2}
BFDDia	Benthic Freshly Dead Diatoms	mmol C m^{-2}
Ben	Benthic filter feeders	mmol C m^{-2}

[BDIN]). Benthic filter feeders [Ben], which graze on pelagic ([Dia], [FDDia] and [Dino]) and benthic ([BDia] and [BFDDia]) microalgae groups are also explicitly represented. The grazing on benthic diatoms implicitly assumes that re-suspension may occur (Richard, 2005; Guarini et al., 2008). BDia consume both the silica and nitrogen present in the pore water. Their death and subsequent decomposition follows the same dynamics as the one of the corresponding pelagic variable. Ben mortality increases the BNDet pool, excretion releases BDIN and egestion produces both BSiDet and BNDet. Finally, the mineralization of BSiDet and BNDet releases inorganic nutrients ([BdSi] and [BDIN]).

Besides benthic grazing, the coupling between the pelagic and benthic compartments is realized through the sedimentation of Dia, FDDia, NDet and SiDet (S term negative in eq. 4) which feeds the pools of BDia, BFDDia, BNDet and BSiDet, respectively. The diffusive fluxes of dissolved inorganic nutrients through the sediment water interface J_B [$\text{mol m}^{-2} \text{s}^{-1}$] provide a source of DIN and dSi to the water column (S term positive in eq. 4). This flux is positive out of the sediment and the mass balance for the benthic variables reads therefore:

$$\frac{\partial(H_{\text{sed}} c_B)}{\partial t} = v_{\text{sed}} \cdot c - J_B + \sum R_B \quad (5)$$

where H_{sed} [m] is the thickness of the benthic layer, v_{sed} [m s^{-1}] is the

sedimentation rate, c_b [$\text{mol}\cdot\text{m}^{-3}$] is the concentration of the benthic state variable and R_b [$\text{mol}\cdot\text{m}^{-2}\cdot\text{s}^{-1}$] is the net benthic flux, accounting for both production (positive) and consumption (negative) processes affecting the chemical species considered.

All physiological and mineralization processes are temperature dependent. In addition, the growth of pelagic and benthic microalgae depends both on light and nutrient availability, whose respective limitations are combined using Liebig's law (Von Liebig 1840). A detailed description of the equations implemented in our RN, including all parameter values, is given in the appendix.

Boundary conditions

The SOMLIT database (http://www.domino.u-bordeaux.fr/somlit_national/pSiteBrest.php) and the buoy-mounted MAREL (http://www.ifremer.fr/sismer/UK/catal/base/edmed_an.html?CBASE=MAREL2) automated acquisition system (Fig. 1) provide high frequency nutrient and total Chl a data (sampling interval between 20 and 60min) at the Goulet site for the year 2001. At this location, the annual evolution of the relative proportions of diatoms and dinoflagelates is taken from Beucher et al. (2004). Following Le Pape (1996), the zooplankton is set to 10% of the total phytoplankton concentration.

Nutrient concentrations at the upstream limits of the model domain are specified using weekly measurements performed in the framework of the ECOFlux program (<http://www.univ-brest.fr/IUEM/observation/ecoflux/ecoflux.htm>). In the present version of the model, it is assumed that no phytoplankton or zooplankton is introduced in the system through the upper boundaries. There are only very few phytoplankton measurements at the upstream boundaries of the model and the few available data provide only information on total biomasses without any further details on species distribution. Nutrient data are linearly interpolated between each sampling time interval to provide upstream concentrations at the frequency of the biogeochemical model resolution. The temporal evolution of water discharge, dSi and DIN in the Aulne and the Elorn estuaries during the year 2001 are illustrated in Fig. 3. The changes in forcing conditions (temperature and incident solar radiation) in the bay are also shown.

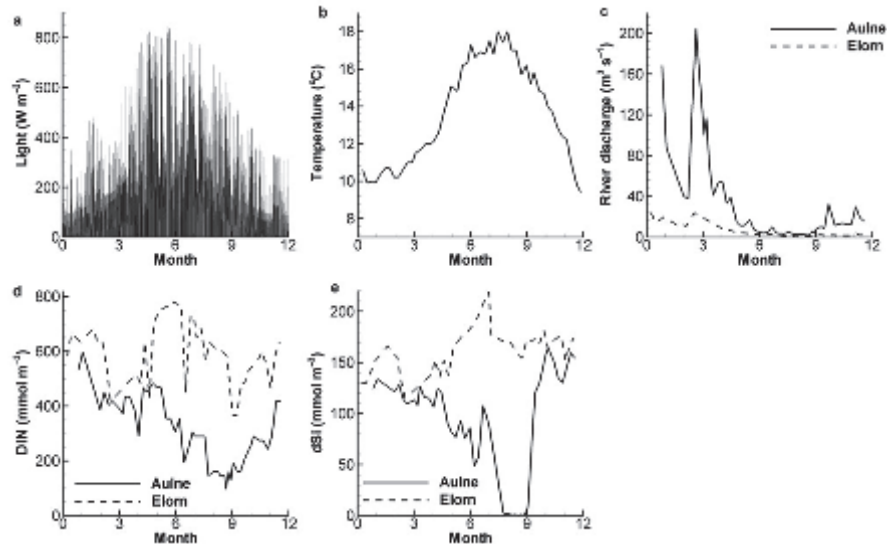


Figure 3: Model forcing (a-b) and upstream boundary conditions (c-e) for the year 2001. Incident solar radiation (a) and (b) average temperature for the whole bay, river discharge (c), DIN (d) and dSi (e) concentrations.

Initial conditions

The spin-up time for pelagic state variables in the model is on the order of one month. To provide realistic initial conditions for the simulation, the model is launched on December 1st 2000, starting with spatially homogeneous concentrations. The benthic state variables exhibit however much longer spin-up times and, therefore, the model is run twice over the year 2001. Simulations reveal that in this case, the intra-annual seasonal variation is much larger than the inter-annual variability recorded from the difference between the end of the first and second years, respectively. Note that for computational efficiency, the initial conditions are distributed homogeneously for all variables but the benthic filter feeders. The latter are estimated from recent maps of spatial distribution of *Crepidula Fornicata* in the Bay of Brest (Guérin 2004), combined with an older estimate of the biomass of other benthic filter feeders (Chauvaud 1998, Jean & Thouzeau 1995). The spatial distribution of *Crepidula Fornicata* was determined at 127 locations in the bay during the fall of 2000. The density at each model grid point in the bay was then determined by linear interpolation. Rivers were excluded from the survey and assumed here to be free of any benthic filter feeders.

An average value of 0.056 g C per individual [ind] (Jean 1994) was used to convert the population density [ind m²] into carbon biomass. The contribution of all other benthic filter feeders (Jean & Thouzeau 1995) was then added to *Crepidula Fornicata* to obtain the initial spatial distribution of total benthic filter feeder biomass. In what follows, all model results correspond to the second year of simulation.

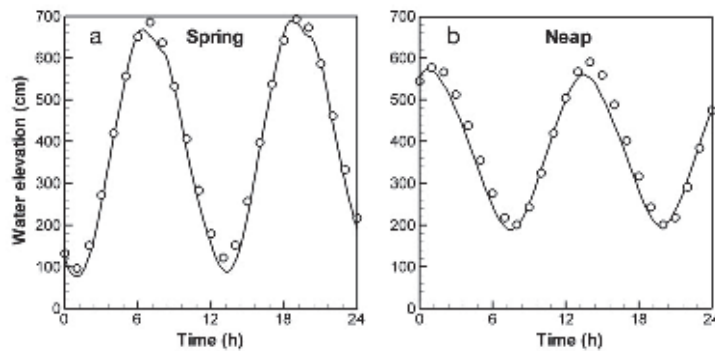


Figure 4: Time series of simulated (line) and measured (points) surface water elevation at Brest harbor for spring (top) and neap (bottom) tidal conditions.

3. Results and Discussion

3.1. Hydrodynamics and transport

Hydrodynamics

Model validation was performed on both water elevation and instantaneous tidal current velocities. Fig. 4 compares simulated and measured elevations recorded at the single tidal gauge station located in the bay (Fig. 1), for both spring and neap tide conditions. Overall agreement between modelled and measured tides is achieved with an error in tidal amplitude on the order of 5 % and a deviation in phase never exceeding 15 minutes. Fig. 5 shows the simulated and measured components of the velocity vector at four locations in the bay (Fig. 1). One station (Terenez, lower panel) is located near the mouth of the Aulne estuary while the other stations are representative of the conditions encountered in the centre of the bay. Results reveal that both the magnitude and direction of the flow field are well captured by the model. The time lags among the various stations are also properly reproduced. In particular, the good fit at station Terenez, which is located

the further upstream, indicates that the tidal wave propagates accurately within the system.

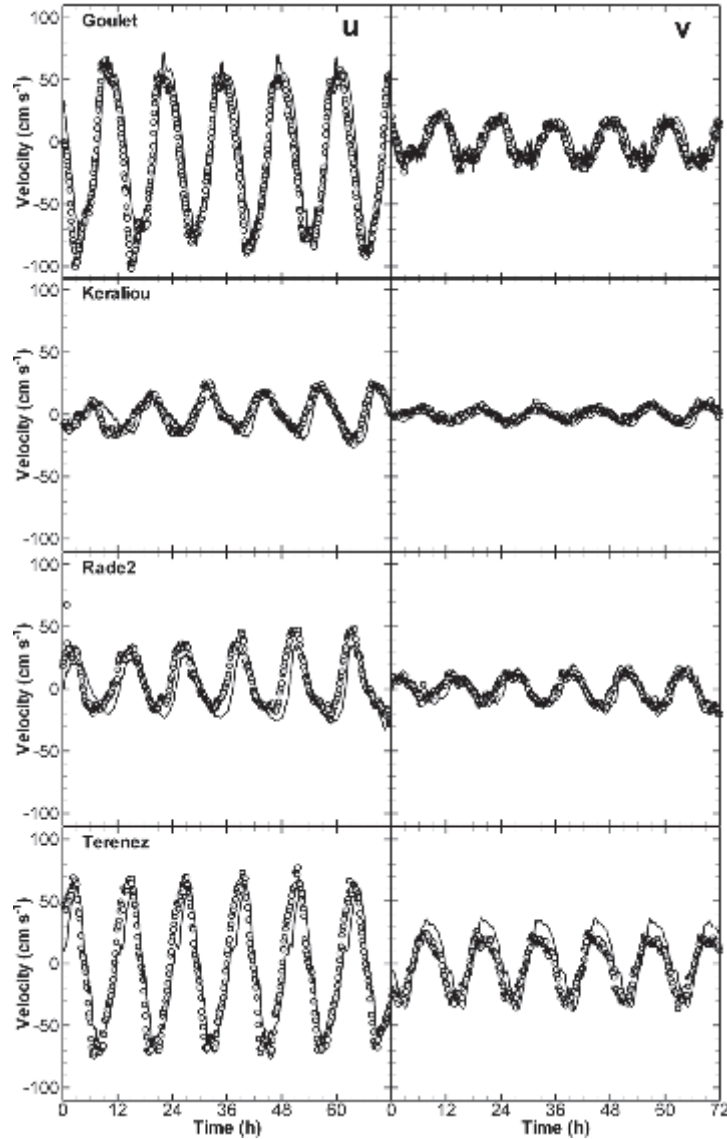


Figure 5: Time series of simulated (lines) and measured (points) components of the velocity vector u (left panels) and v (right panels) at four locations in the Bay. u and v represent the velocity of the current along the East-West and South-North direction, respectively. Measured current velocities from the Service Hydrologique et Oceanographique de la Marine Francaise (SHOM).

The predicted tidal and residual circulations are in good agreement with previous hydrodynamic modelling studies (e.g. Le Pape 1996, Salomon & Breton 1991). Model results show that the hydrodynamics is strongly dominated by the tidally induced circulation of semi-diurnal period. At each tide, the seawater volume that is exchanged with the Iroise Sea amounts roughly to 50 % of the total volume of water in the bay (Chauvaud 1998). Fig. 6 shows the development of large gyres in the center of the bay and very strong currents in the narrow strait connecting the bay to the ocean (“Goulet”). During the flood, the formation of the well-documented large central cyclonic gyre (Salomon & Breton 1991) can be identified in the model results. Several smaller anti-cyclonic gyres characterized by significantly lower velocities also develop in the Northern and Southern basins. During ebb, all large circulation features disappear and a uniform, retreating seaward flux of the water masses can be observed in the entire bay (Fig. 6b). The calculated residual circulation, which filters out the short-term (< 1 day) tidal components, reveals the existence of a well established central cyclonic gyre, and a complex circulation pattern in the Goulet, with water entering and leaving the bay by the Southern and Northern sides of this narrow strait, respectively. The residual circulation leads to freshwater residence times in the bay typically comprised between 10 and 20 days (Le Pape 1996).

Transport

Calibration of the dispersion coefficients ($D_{x,y}$) was performed using a set of salinity data from 1993 (not shown). Three salinity profiles collected in 2001 along a longitudinal transect within the Aulne estuary and the inner bay were then used for validation of the transport model (Fig. 7). In August and November 2001, river discharges from the Aulne river were low ($\sim 10 \text{ m}^3 \cdot \text{s}^{-1}$ and $\sim 5 \text{ m}^3 \cdot \text{s}^{-1}$, respectively). In contrast, May 2001 was characterized by much higher values ($\sim 50 \text{ m}^3 \cdot \text{s}^{-1}$). Comparison between simulated and measured profiles reveals that under low flow conditions, characteristic of the summer period, the fully-transient model captures properly the estuarine salt intrusion. A slightly larger deviation is observed in May 2001, which can be explained by the onset of a vertical stratification of the water masses in the vicinity of the estuarine mouth when river

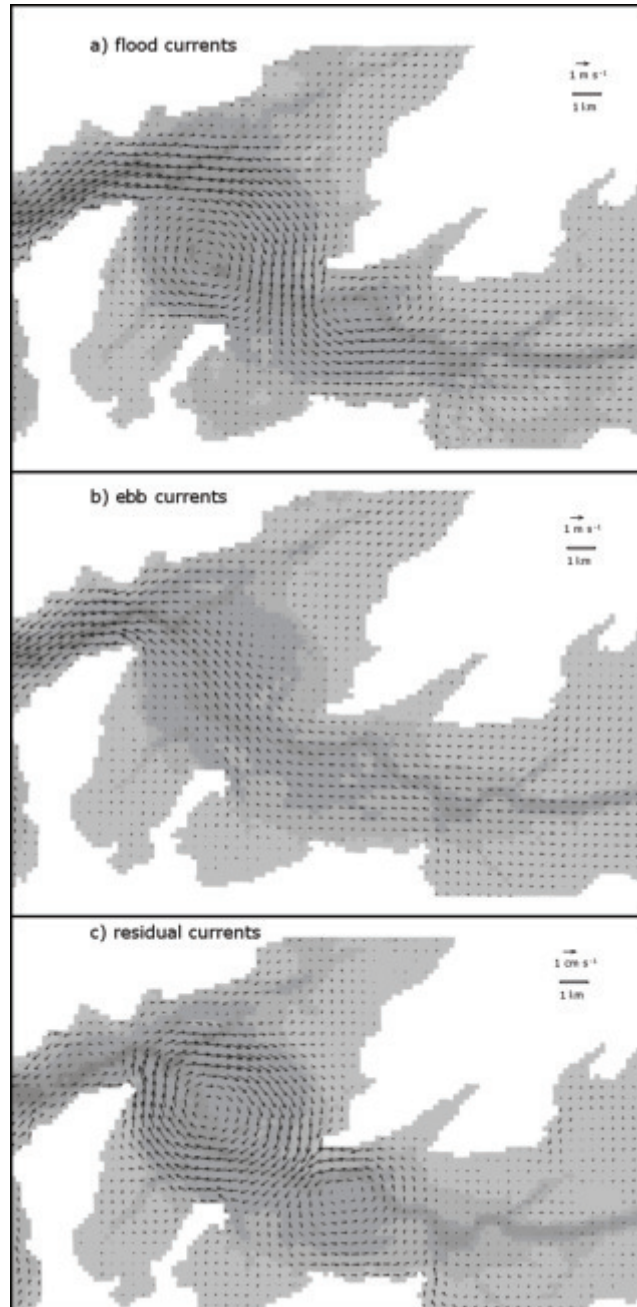


Figure 6: Snapshot of the velocity vector field at flood tide (a) and ebb tide (b). Panel (c) shows the computed Eulerian residual circulation in the Bay of Brest.

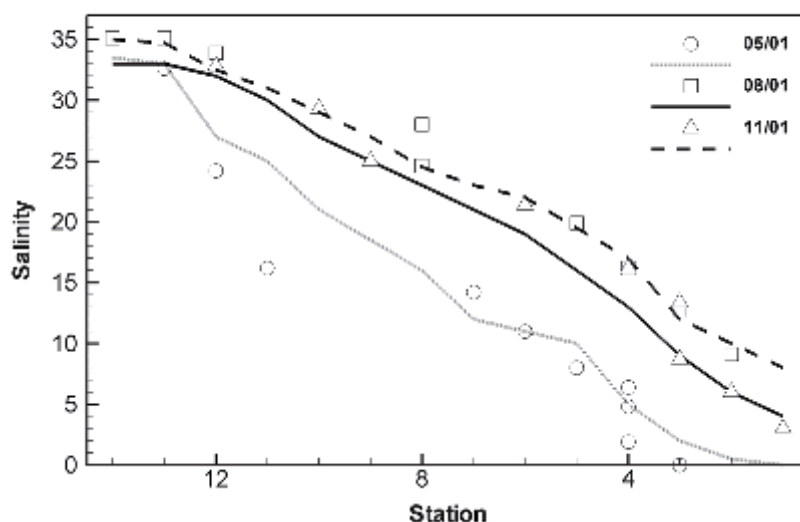


Figure 7: Simulated (lines) and measured (points) transient longitudinal salinity profiles at various stations in the Aulne estuary for 3 river discharges (Q) in 2001. May: $Q=15 \text{ m}^3 \cdot \text{s}^{-1}$, August: $Q=2 \text{ m}^3 \cdot \text{s}^{-1}$, November: $Q=30 \text{ m}^3 \cdot \text{s}^{-1}$.

flow increases. The simulated depth-averaged salinities are therefore higher than the observed values collected 1 m below the water surface. Note however that the stratification is significant only in a small portion of the longitudinal transect within the estuary ($\sim 10 \text{ km}$ into the bay from the Aulne's riverine boundary) and is generally negligible within the bay during the biologically productive period (Salomon & Breton 1991, Le Pape 1996).

3.2. Biogeochemistry

Seasonal dynamics

The Bay of Brest and estuaries are characterized by different hydrodynamic and transport regimes, and, therefore, by distinct biogeochemical behavior. In what follows, the estuarine processes are only analyzed in the extensively surveyed Aulne estuary, which accounts for 80% of the annual water and nutrient discharges to the bay. The transition between the Aulne and the bay can conveniently be located in the area where a sudden increase in cross section occurs (Pont de Terenez, Fig. 1). In the estuary, the dynamics are essentially one-dimensional and important

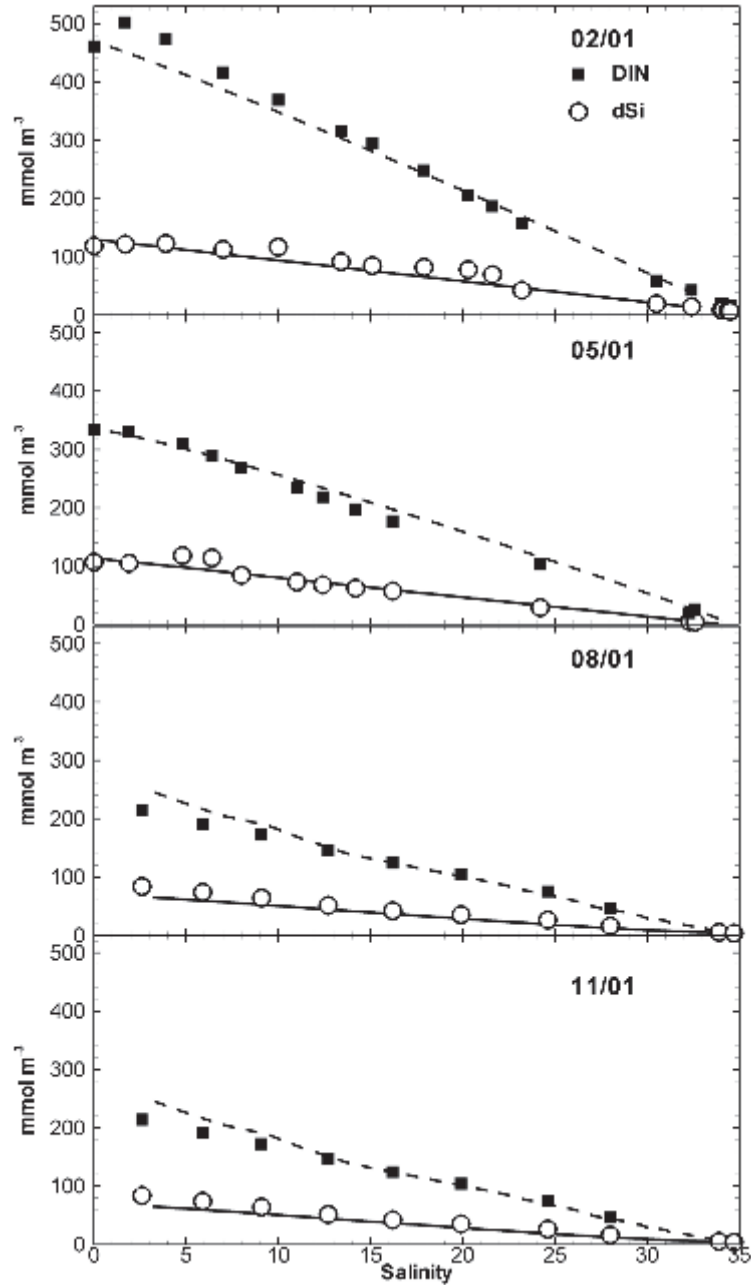


Figure 8: Simulated (lines) and measured (points) transient longitudinal profiles of dSi and DIN as a function of salinity in the Aulne estuary in February, May, August and November 2001.

concentration gradients are established along the longitudinal curvilinear axis of the system. In the bay, the spatial variability in the concentration fields is limited due to low river discharge and intense tidal mixing (Fig. 8). Field observations at various locations in the bay show, however, that seasonal changes in biogeochemical variables are significant.

Fig. 8 compares fully-transient longitudinal profiles of dSi and DIN with measurements performed along the salinity gradient of the Aulne estuary in February, May, August and November 2001. Results show that the model captures the main features of the spatial and temporal distributions of nutrients in the estuary. The property-salinity plots reveal an almost conservative behavior, even during the biologically productive period. Transport and mixing are therefore always dominant over internal transformation processes. The dilution between the freshwater end-member and the water masses discharging in the bay provokes a one order of magnitude decrease in nutrient concentration.

Fig. 9a-b shows the simulated seasonal variations of dSi and DIN over the year 2001 at two locations (R2 and R3, Fig. 1) in the bay. Stations R2 and R3 are representative of the dynamics in the Southern basin and in the center of the bay, respectively (Jean 1994, Ragueneau et al. 1994, Le Pape et al. 1996, Le Pape et al., 1999). The two stations have been extensively surveyed since the 1990's (Le Pape 1996, Del Amo 1996, Chauvaud 1998, Lorrain 2002) and are currently sampled on a yearly basis. Nutrient distributions are characterized by high values during winter followed by a rapid decrease in late April at both stations (Fig. 9a-b), when estuarine discharge is reduced and biological uptake is promoted by an increase in temperature and incident solar radiation (Fig. 3). dSi is consumed slightly earlier in the season than DIN, the former remaining limiting for phytoplankton growth for at least two months. Simulated nutrient concentrations increase again in the summer for dSi and only in the fall for DIN, in agreement with field observations.

The nutrient consumption in late April 2001 corresponds to the development of a diatom dominated early spring bloom (Fig. 9c). The model predicts a switch from diatom to dinoflagellate dominance in August, in agreement with field observations (Chauvaud et al. 1998, Beucher et al. 2004). The occurrence of such late summer dinoflagellate blooms has recently been reported for the years 1995,

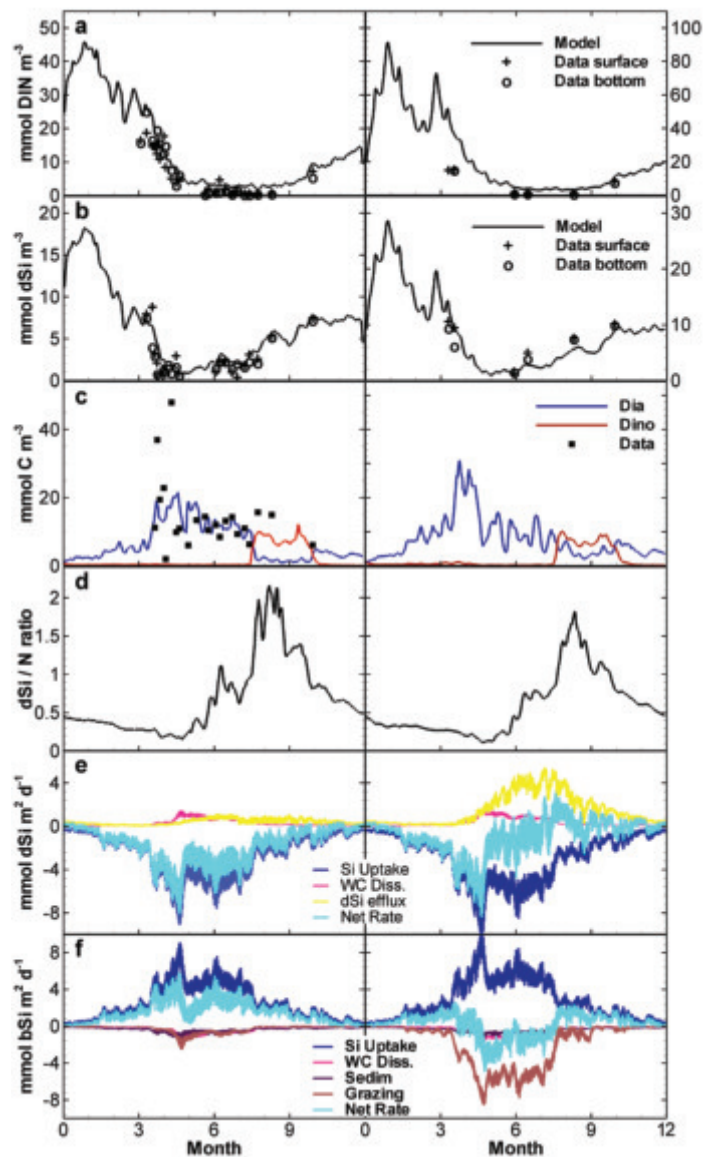


Figure 9: Seasonal evolution of DIN (a), dSi (b), phytoplankton biomass (c) and dSi:DIN ratio (d) in the water column at stations R3 (left panels) and R2 (right panels). Measured nutrient concentrations at the surface and the bottom of the Bay are also shown in panels a and b and Chl a measurements converted into carbon unit in panel c. The seasonal evolution of process rates affecting the pelagic dSi and bSiO₂ concentrations is illustrated in panels e and f, respectively. WC diss.: water column dissolution; Sedim.: sedimentation rate, the Net Rate is the sum of all positive and negative processes.

1998, 1999 and 2001 (Chauvaud et al. 1998, Lorrain 2002). The phytoplankton succession explains partly why, after the depletion period, dSi concentrations increase earlier in the season than DIN. This succession explains also high Chl *a* concentrations from spring to fall and leads to a fairly long productive period. Such dynamics differs from the conditions that prevailed in the years 1970-1980 when the first diatom spring bloom was usually of larger magnitude (up to 10 μg Chl *a* l^{-1} which represents 60-70 $\mu\text{mol C l}^{-1}$ in the model) and the productive period of shorter duration (Chauvaud et al. 2000). The simulated dSi uptake by diatoms is in good agreement with in-situ rate measurements based on ^{32}Si incorporation (Fig. 10a, Ragueneau et al., 2005), except for the two very high uptake rates recorded at the early stages of the productive period. This discrepancy might be attributed to the succession of distinct diatom species characterized by different Si:C ratios, a feature not accounted for in the model. The observed phytoplankton which remained in the fall of 2001 (up to 1.5 μg Chl *a* l^{-1} , Lorrain (2002)) when dSi uptake is low must be attributed to non siliceous algal development, a result consistent with the simulated phytoplankton succession (Fig. 9c). As already reported in previous modeling studies (Monbet 1992, Pondaven et al. 1998), the zooplankton dynamics follows that of phytoplankton with a time lag of about 10 days, consistent with a typical predator-prey relationship for this kind of ecosystem (not shown).

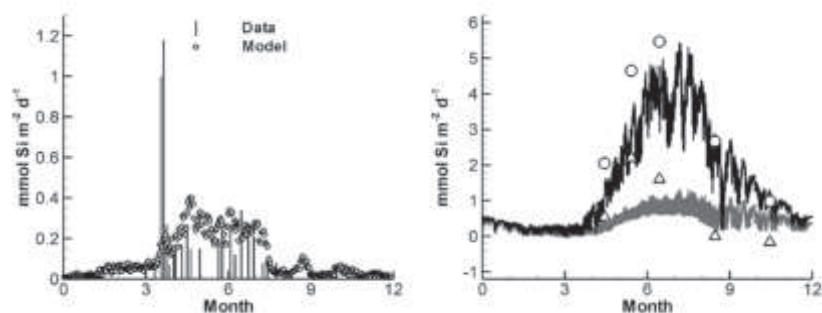


Figure 10: Simulated (points) and measured (vertical bars) pelagic dSi uptake rates (left panel). Comparison of silica benthic fluxes through the sediment-water interface simulated (lines) and measured (points) at a station with (circles, black line) and without (triangles, grey line) *Crepidula Fornicata* (right panel). Data from Ragueneau et al., 2005.

The evolution of water column variables at stations R2 and R3 exhibits similar patterns and, thus, limited spatial variability in the pelagic dynamics. At this site, the high density of filtering organisms leads to a benthic exchange flux through the sediment-water interface of similar magnitude than the pelagic uptake of dSi. In contrast, the biomass of benthic filter feeders shows a high degree of heterogeneity over short distances (Fig. 1). The intra-annual variability in biomass of benthic filter feeders is of the order of 40-50 %, in agreement with previous modeling studies in the bay (Jean, 1994; Grall et al. 2006). Typically, the seasonal evolution of the biomass is characterized by a decrease during winter followed by a growth period between April and September and, during fall, a decrease back to the original winter conditions (Grall et al. 2006).

Fig. 9e-f compares the process rate distributions affecting dSi (d) and BSi (e) at stations R2 and R3. Model results reveal that the pelagic uptake of dSi and the dissolution of dead diatoms in the water column are of similar magnitude at both stations. Benthic processes show however a much larger variability, the grazing of diatoms by benthic filter feeders and the dSi efflux out of the sediments being roughly one order of magnitude higher at R2. At this site, benthic exchanges through the sediment-water interface are of similar magnitude than the pelagic uptake of dSi due to the high density of filtering organisms. In contrast, the local dynamics at R3 is by far dominated by the pelagic activity of the phytoplankton. As a result, the dynamic balance between processes remains always negative for dSi at this site, indicating continuous, net silica uptake over a seasonal cycle. The pattern in net rate is more complex at R2 as a result of the dynamic interplay between pelagic production, grazing and benthic BSi dissolution. The benthic flux of silica reach values as high as $6 \text{ mmol Si m}^{-2} \text{ d}^{-1}$ and exceeds the dSi uptake during a large part of the productive period.

The magnitude and timing of this high recycling flux of bSiO_2 is in good agreement with direct flux measurements based on sediment cores incubations (Fig. 10b, Ragueneau et al. 2005). The drop in dSi efflux in the absence of filtering organisms is also captured by our model, even though the seasonal variation in the simulated flux is of smaller magnitude than actually observed. The comparison between the pelagic dynamics at R2 and R3 shows that the intense turbulent mixing

leads to an homogeneization of water column properties that does not reflect the spatial heterogeneity in benthic process intensities. Field observations focusing only on the time evolution of the pelagic variables (DIN, dSi, phytoplankton) are therefore of limited value to capture the biogeochemical dynamics in the Bay of Brest.

Temporally-resolved budget of Silica

Fig. 11 presents a temporally-resolved budget of silica in the estuaries and the Bay of Brest for the year 2001. Each simulated process rate is integrated over the whole model domain, and then time-integrated over monthly periods. The extent of the benthic-pelagic coupling is summarized in Fig. 11a. The total deposition flux of BSi due to sedimentation and grazing remains roughly constant during the months May-July and reaches values of up to $20 \cdot 10^6$ moles Si month⁻¹ (about 4 mmoles Si m⁻².d⁻¹). The benthic recycling flux of dSi to the water column follows the deposition pulse with a time lag of 1-2 months and reaches maximum values in August ($\sim 15 \cdot 10^6$ moles Si month⁻¹ or 3 mmoles Si m⁻².d⁻¹). Such a time lag falls within the range of benthic flux responses determined from a sensitivity analysis performed with a transient, vertically-resolved, early diagenetic model of silica (Arndt & Regnier 2007). Yearly-integrated deposition and recycling fluxes of silica amount to 0.56 and 0.48 moles Si m⁻², respectively. The preservation of biogenic silica in the sediments after one year of simulation represents $\sim 14\%$ of the supply flux by riverine inputs.

The importance of benthic-pelagic coupling for the silica cycle in the water column of the bay is shown in Fig. 11b. Results reveal that the total dSi flux in the bay exceeds the uptake by diatoms during a significant fraction of the year. A reverse trend is however observed between April and August and leads to a significant depletion of the total mass of dSi in the system during the productive period (Fig. 9c). The river input is larger than the recycling fluxes of dSi in the water column and in the sediments until May. From then onwards, the benthic-pelagic coupling becomes the main source of dSi to the water column until fall. At its maximum value in August, the benthic flux is roughly one order of magnitude larger than both river input and water column dissolution and sustains almost entirely the late

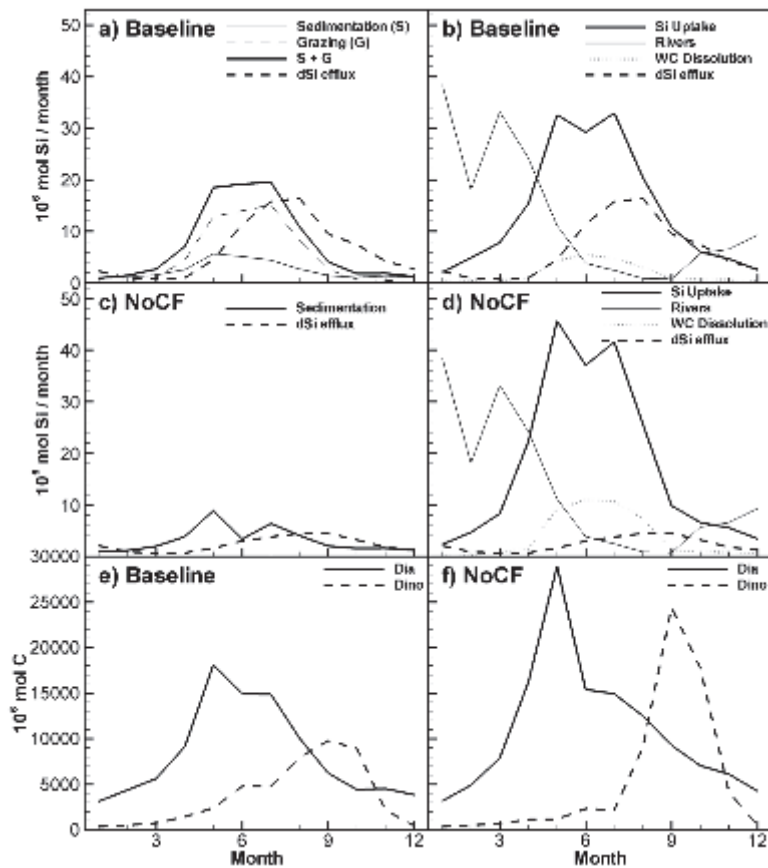


Figure 11: Monthly resolved budget of silica for the Bay of Brest and estuaries. Fluxes from the baseline simulation are shown in the top Panels for the benthic-pelagic exchange (a) and dSi processes in the water column (b). The results of the scenario without *Crepidula Fornicata* (NoCF) are presented in the middle Panels (c, d). The monthly resolved masses of diatom and dinoflagellate biomasses in the system are shown in the lower panels for the baseline (e) and NoCF (f) simulations.

summer diatom bloom in the bay. If one excludes the winter months during which most of the dSi is transported as a passive tracer through the system (freshwater residence times ~ 10 days for a typical winter river discharge), the relative contributions of the benthic flux, the river input and the water-column dissolution to the dSi supply during the period April-September amounts to 48, 36, and 16 %, respectively. Therefore, benthic-pelagic coupling sustains an important part of the annual diatoms productivity in the bay.

The monthly-resolved budgets can be integrated and compared with previously established seasonal budgets during the winter/fall and spring/summer periods of 2001 (Ragueneau et al. 2005). The seasonal budgets were constructed from local measurements of silica production and dissolution in the water column, as well as from experimentally-derived dSi benthic fluxes through the sediment-water interface. The extrapolation for the production flux was based on weekly surveys performed at a single site (station R3). The agreement with the model predictions is nevertheless satisfactory, a result which can be explained by the fairly homogeneous dSi uptake rates over the entire area of the bay. Overall agreement in dSi benthic flux estimates is also achieved and reflects the dominant control of *C. fornicata* on the magnitude of these fluxes, a factor which was already accounted for in the experimentally-derived budgets (Ragueneau et al. 2005). A larger discrepancy is obtained for the deposition flux, the yearly integrated estimates agreeing within 30%. The winter/fall prediction from the model is only about half that of Ragueneau et al. (2005). Yet, because most of the internal Si cycling in the bay occurs during the spring/summer period, this variability has a limited effect at the yearly time scale.

The most important deviation between estimates is obtained for the water column dissolution. The model-based calculations suggest that this process accounts for only 13% of the annual silica production, whereas the estimate from direct measurements by Beucher et al. (2004) leads to a significantly higher relative contribution (45%). Interestingly, a similar discrepancy between the estimates of Beucher et al. (2004) and those established by mass balance calculations (18%) was already reported by Ragueneau et al. (2005) and attributed to the fact that the direct measurements represent a (maximum) potential dissolution flux from the diatom community if they were to remain permanently in suspension in the water column. However, the Bay of Brest is very shallow and diatoms are settling rapidly; therefore, they are being heavily grazed by suspension feeders and the magnitude of the model-derived pelagic dissolution should logically be smaller than the experimentally-derived estimate. Obviously, a significant fraction of the preserved diatoms will actually dissolve in the sediments. However, as already discussed above, it is important to obtain accurate estimates of the relative contribution of

water column and benthic dissolution fluxes as this factor is instrumental for the determination of the time delays in Si dynamics and, thus, for the phytoplankton dynamics in the bay.

Reduction in biomass of benthic filter feeders

The model is used here for prognostic purposes and is a first attempt at quantifying the effect of eradicating an invasive benthic filter on the Si dynamics and phytoplankton succession in the bay. Fig. 11c shows the magnitude of the benthic-pelagic coupling in a scenario without *C. Fornicata* (referred to as ‘NoCF’ in what follows) and should be compared with the results of the baseline simulation discussed above (Fig. 11a-b). Simulations reveal that in the NoCF scenario, the supply flux of BSi to the sediments and the dSi flux back to the water column are both significantly smaller than in the baseline run. On a yearly integrated basis, the amount of BSi reaching the benthic compartment decrease from $89 \cdot 10^6$ moles/yr to $37 \cdot 10^6$ moles/yr when the benthic filter feeders are removed. Although removing the grazing term leads to a slightly higher sedimentation flux (+29 %) in the NoCF scenario, this increase does not compensate the uptake by the grazers and, therefore, the dSi efflux is roughly 3 times smaller in this case.

The effect of the benthic-pelagic coupling on the amount of dSi available to sustain the pelagic primary production is summarized in Fig. 11d. In the baseline simulation, the benthic dSi flux to the bay is largely dominant from early June until November, the riverine inputs contributing most during the winter period. In the NoCF case, the benthic return flux remains small throughout the year. Yet, because of the increased residence time of the phytoplankton within the water column (both living and dead), the pelagic dissolution of dead diatoms is twice larger during most of the summer period, and partly compensates the drop in benthic flux. A major difference between both scenarios, however, is the overall reduction of the dSi flux during late summer and fall, which was mainly sustained by the time-delayed efflux from the sediments in the baseline simulation.

The temporal distribution of dSi uptake (Fig. 11d) and phytoplankton succession (Fig. 11e-f) partly reflects the variation in dSi supply when benthic filter feeders are removed from the seabed. In the NoCF scenario, results reveal

that during the spring/early summer when the total dSi inputs from the various sources are already reduced but not limiting, both the silica uptake and the total diatom biomass are increased compared to the baseline simulation. Such behavior might appear counterintuitive but can be explained by the significantly larger residence times of living diatoms in the bay when the sink term due to grazing is suppressed. As a result, the total diatom biomass which develops during the April-July period increases by 32 % in the NoCF scenario. Results reveal also a more distinct phytoplankton succession when the influence of the benthic-pelagic coupling is reduced. In the NoCF case, the total biomass of dinoflagelates is up to twice that of the baseline scenario. The hypothesis that an engineered intervention aiming at removing *C. Fornicata* from the bay might sustain enhanced harmful dinoflagelate blooms is thus supported by the results of the present study.

4. Conclusion

A reactive-transport modeling approach has been used to identify and quantify the dominant pelagic and benthic processes of the Si cycle in the estuaries and the Bay of Brest (France). The simulations resolved the seasonal variations in process intensities and helped unravel the role of the benthic filter feeders on the magnitude and timing of the benthic-pelagic coupling in this shallow coastal ecosystem. Results from the hydrodynamics and transport showed that the dominant physical controls on biological processes were properly represented in our numerical model. The biogeochemical dynamics in the estuaries revealed limited biogeochemical transformation but significant dilution upon estuarine mixing. In the bay, the model results were in good agreement with the measured seasonal evolution in nutrient concentration, dSi uptake and benthic fluxes. Simulations revealed that the intense mixing in the bay limits the spatial variability in the pelagic phytoplankton dynamics. In contrast, the benthic processes showed a high degree of heterogeneity which is correlated with the spatial distribution of benthic filter feeders. The magnitude of the benthic efflux of dSi to the water column can vary by up to one order of magnitude and, in areas densely populated by *Crepidula fornicata*, it may reach values comparable to the local uptake by diatoms in the overlying water column. The dSi efflux followed also the deposition

pulse with a typical time lag of 1 to 2 months and, on a yearly basis, preservation of BSi remained limited. Our model approach was particularly suitable to provide temporally resolved Si budgets for the entire bay and estuarine areas. Results revealed that the benthic recycling fluxes of dSi during the productive period was the main source (40%) of this nutrient to the bay and sustained almost entirely the late summer diatom bloom. A prognostic scenario of reduction in biomass of benthic filter feeders revealed that the magnitude and timing of the pelagic diatom bloom is only moderately affected by the decrease in intensity of the benthic-pelagic coupling. On the other hand, the hypothesis that the removal of the filtering organisms on the seabed might enhance the development of harmful dinoflagellate blooms in the bay is supported by our model results.

Acknowledgments

This work has been financially supported by the EU-RTN Si-WEBS (contract number HPRN-CT-2002-000218), by the Netherlands Organization for Scientific Research (NWO) (VIDI award 864.05.007 to PR) and by the government of the Brussels-Capital region (Brains Back to Brussels award to PR).

References

- Abbott MB (1979). Computational hydraulics: Elements of the theory of free surface flows. Pitman, London.
- Andersen V, Nival P (1988) A pelagic ecosystem model simulating production and sedimentation of biogenic particules – Role of salps and copepods. Ecol. Prog. Ser. 44: 37–50
- Andersen, V., 1985. Modélisation d' écosystèmes pélagiques. Étude de processus. PhD thesis, Université Pierre et Marie Curie, Paris
- Antia NJ, McAllister CD, Parsons TR, Stephens K, Strickland JDH (1963). Further measurements of primary production using a large-volume plastic sphere. Limnol. Oceanogr. 8: 166-183.
- Arndt S, Regnier P (2007) A model for the benthic-pelagic coupling of silica in estuarine ecosystems: sensitivity analysis and system scale simulation. Biogeosciences 4: 331-352.
- Arndt, S., Vanderborght, J.-P., Regnier, P., 2007. Diatom growth response to physical forcing in a macrotidal estuary: coupling hydrodynamics, sediment transport and biogeochemistry. Journal of Geophysical Research 112. doi:10.1029/2006JC003581
- Baretta-Becker JG, Riemann B, Baretta JW, Rasmussen EK (1994) Testing the microbial loop concept by comparing mesocosm data with results from a dynamical simulation model. Mar. Ecol. Prog. Ser., 106: 187–198
- Beucher C, Tréguer P, Corvaisier R, Hapette AM, Elskens M (2004) Production and dissolution of biosilica, and changing microphytoplankton dominance in a coastal ecosystem of western Europe. Mar. Ecol. Prog. Ser. 267: 57–69.
- Chapelle A (1991) Modélisation d'un écosystème marin crier soumis à l'eutrophisation: la baie de Vilaine (sud Bretagne). Etude du phytoplancton et du bilan en oxygène. Ph-D thesis. Université Pierre et Marie Curie, Paris VI, Paris.

- Chauvaud L (1998) La coquille Saint-Jacques en Rade de Brest: un modèle biologique d'étude des réponses de la faune benthique aux fluctuations de l'environnement. Ph-D thesis. Université de Bretagne Occidentale, Brest, 265 pp.
- Chauvaud L, Thouzeau G, Paulet YM (1998) Effects of environmental factors on the daily growth rate of *Pecten maximus* juveniles in the Bay of Brest (France). *J. Exp. Mar. Biol. Ecol.* 227: 83–111.
- Chauvaud L, Jean F, Ragueneau O, Thouzeau G (2000) Long-term variation of the Bay of Brest ecosystem: benthic–pelagic coupling revisited. *Mar. Ecol. Prog. Ser.* 200: 35–48.
- Cloern JE (2001) Our evolving conceptual model of the coastal eutrophication problem. *Mar. Ecol. Prog. Ser.* 210: 223-253.
- Conley DJ, Schelske CL, Stoermer EF (1993) Modification of the biogeochemical cycle of silica with eutrophication. *Mar. Ecol. Prog. Ser.* 101: 179-192.
- Del Amo Y (1996) Dynamique et structure des communautés phytoplanctoniques en écosystème côtier perturbé; cinétiques de l'incorporation du silicium par les diatomées. Thèse de Doctorat, Université de Bretagne Occidentale, Brest, France.
- Del Amo Y, Quéguiner B, Tréguer P, Breton H, Lampert L (1997a). Impacts of high-nitrate freshwater inputs on macrotidal ecosystems. II. Specific role of the silicate pump in the yearround dominance of diatoms in the Bay of Brest (France). *Mar. Ecol. Prog. Ser.* 161: 225-237.
- Del Amo Y, Le Pape O, Tréguer P, Quéguiner B, Menesguen A, Aminot A (1997b) Impacts of high-nitrate freshwater inputs on macrotidal ecosystems. I. Seasonal evolution of nutrient limitation for the diatom-dominated phytoplankton of the Bay of Brest (France). *Mar. Ecol. Prog. Ser.* 161: 213-224.
- Dugdale RC, Wilkerson FP, Minas HJ (1995) The role of a silicate pump in driving new production. *Deep-Sea Res.* 42: 697-719.

- Ekebjaerg L, Justesen P (1991) An explicit scheme for advection-diffusion modelling in two dimensions, *Computer methods in Applied Mechanics and Engineering* 88: 3–8.
- Eppley, R. W. (1972) Temperature and phytoplankton growth in the sea. *Fishery* 21 Bull. 70: 1063-1085.
- Foullaron P, Leynaert A, Claquin P, L'Helguen S, Huonnic P, Martin-Jézéquel V, Masson A, Ni Longphuir S, Pondaven P, Thouzeau G (2007) Response of a phytoplankton community to increased nutrient inputs: a mesocosm experiment in the Bay of Brest (France). *Journal of Experimental Marine Biology and Ecology* 351 (1-2): 188-198. doi:10.1016/j.jembe.2007.06.009
- Grall J, Le Loc'h F, Guyonnet B, Riera P (2006) Community structure and food web analysis based on stable isotopes. *Journal of Experimental Marine Biology and Ecology* 338 (1): 1-15.
- Guarini JM, Sari N, Moritz C (2008) Modelling the dynamics of the microalgal biomass in semi-enclosed shallow-water ecosystems. *Ecological Modeling* 211 (3-4): 267-278.
- Guérin L (2004) La crépidule en rade de Brest: un modèle biologique d'espèce introduite proliférante en réponse aux fluctuations de l'environnement. Ph-D thesis. Université de Bretagne Occidentale, spécialité Océanologie Biologique, Brest, 361 pp
- Jean F, Thouzeau G (1995) Estimation des variables d'état d'un modèle de réseau trophique benthique en rade de Brest. *C R Acad Sci Paris Sci Vie* 318:145-154
- Jean F (1994) Modélisation à l'état stable des transferts de carbone dans le réseau trophique benthique de la Rade de Brest (France). Ph-D thesis. Université de Bretagne Occidentale, Brest, 170 pp.
- Le Pape O (1996) Modélisation des cycles biogéochimiques des éléments limitant la production phytoplanctonique en rade de Brest. Ph-D thesis. Ecole Nationale supérieure d'Agronomie de Rennes, Rennes, 195 pp.

- Le Pape O, Del Amo Y, Ménesguen A, Aminot A, Quéguiner B, Tréguer P (1996) Resistance of a coastal ecosystem to increasing eutrophic conditions: the Bay of Brest (France), a semi-enclosed zone of Western Europe, *Cont. Shelf Res.* 16: 1885–1907.
- Lorrain A (2002) Les structures calcifiées des invertébrés marins témoins des fluctuations de l'environnement côtier. Ph-D thesis. Université de Bretagne Occidentale, Brest.
- Margalef R (1978) Life-forms of phytoplankton as survival alternatives in an unstable environment. *Oceanol Acta*, 1: 493-509.
- Martin S, Clavier J, Chauvaud L, Thouzeau G (2007). Community metabolism in temperate maerl beds. II. Nutrient fluxes. *Mar. Ecol. Prog. Ser.* 335: 31-41.
- Monbet Y (1992) Control of phytoplankton biomass in estuaries: A comparative analysis of microtidal and macrotidal estuaries. *Estuaries* 15(4), 563-571.
- Moriceau B (2002) La dissolution de la silice biogénique dans la Rade de Brest: influence des Crépîdules. Master thesis. Université de Bretagne Occidentale, Brest, 27 pp.
- Officer CB, Ryther JH (1980) The possible importance of silicon in marine eutrophication. *Mar. Ecol. Prog. Ser.* 3: 83-91.
- Paasche E (1973) Silicon and the ecology of marine plankton diatoms: II. Silicate-uptake kinetics in five diatom species. *Mar. Biol.* 19: 262–269.
- Radach G, Moll A (1993) Estimation of the variability of production by simulating annual Cycles of phytoplankton in the central North Sea. *Prog. Oceanogr.*, 31: 339-419.
- Ragueneau O (1994) La dynamique du phytoplancton en écosystèmes macrotidaux: couplage avec l'hydrodynamique et le cycle biogéochimique du silicium. Ph-D thesis. Université de Bretagne Occidentale, Brest, 334 pp.
- Ragueneau O, De Blas Varela E, Tréguer P, Quéguiner B, Del Amo Y (1994) Phytoplankton dynamics in relation to the biogeochemical cycle of silicon

in a coastal ecosystem of western Europe. *Mar. Ecol. Prog. Ser.* 106: 157-172.

Ragueneau O, Quéguiner B, Tréguer P (1996). Contrast in biological responses to tidally induced vertical mixing for two macrotidal ecosystems of Western Europe. *Est Coast Shelf Sci*, 42: 645-665.

Ragueneau O, Chauvaud L, Leynaert A, Thouzeau G, Paulet YM, Bonnet S, Lorrain A, Grall J, Corvaisier R, Le Hir M, Jean F, Clavier J (2002) Direct evidence of a biologically active coastal silicate pump: Ecological implications. *Limnol. Oceanog.* 47 (6): 1849-1854.

Ragueneau O, Chauvaud L, Moriceau B, Leynaert A, Thouzeau G, Donval A, Le Loc'h F, Jean F (2005) Biodeposition by an invasive suspension feeder impacts the biogeochemical cycle of Si in a coastal ecosystem (Bay of Brest, France). *Biogeochemistry*, DOI 10.1007/s10533-004-5677-3.

Ragueneau O, Conley DJ, Ni Longphuir S, Slomp C, Leynaert A (2006a) A review of the Si biogeochemical cycle in coastal waters, I: diatoms in coastal food webs and the coastal Si cycle. Dans: *Land-Ocean nutrient fluxes: silica cycle*. Ittekkot, V., Humborg, C., Garnier, J. (Eds.), SCOPE Book, Island Press, pp. 163-195.

Ragueneau O, Conley DJ, Ni Longphuir S, Slomp C, Leynaert A (2006b) A review of the Si biogeochemical cycle in coastal waters, II: anthropogenic perturbation of the Si cycle and responses of coastal ecosystems. Dans: *Land-Ocean nutrient fluxes: silica cycle*. Ittekkot, V.,

Humborg, C., Garnier, J. (Eds.), SCOPE Book, Island Press, pp. 197-213. Redfield AC (1934) On the proportions of organic derivations in sea water and their relation to the composition of plankton. In *James Johnson Memorial Volume*. (ed. R.J. Daniel). University Press of Liverpool, pp. 177-192.

Richard J (2005) *Crepidula fornicata* : un modèle biologique pour l'étude du rôle de la variabilité des caractères phénotypiques (reproduction, croissance et nutrition) sur les processus de colonisation en milieu marin. Ph-D thesis,

Université de Genève, Switzerland, 128pp.

- Roberts EC, Davidson K, Gilpin LC (2003) Response of temperate microplankton communities to N:Si ratio perturbation. *J. Plankton Res.* 25: 1485–1495.
- Rousseau V, Leynaert A, Daoud N, Lancelot C (2002) Diatom succession, silicification and silicic acid availability in Belgian coastal waters (Southern North Sea). *Mar. Ecol. Prog. Ser.* 236: 61-73.
- Salomon JC, Breton M (1991) Numerical study of the dispersive capacity of the Bay of Brest, France, towards dissolved substances, in Lee Cheung (ed.), *Environmental Hydraulics*, Balkema, Rotterdam, pp. 459–464.
- Smagorinsky J (1963) General Circulation experiments with the primitive equations. *Mon. Wea. Rev.* 91: 99-164.
- Smayda TJ (1990) Novel and nuisance phytoplankton blooms in the sea: evidence for a global epidemic. In: Graneli E., Sundström B., Edler L. and Anderson D.M. (Eds.) *Toxic Marine Phytoplankton* (pp. 29-40). Elsevier, Inc., Amsterdam.
- Smith SJ, Bank LC (1992). Modifications to beam theory for bending and twisting of open section composite beams-Experimental verification. *Composite Structures* 22: 169-177.
- Turner RE, Qureshi N, Rabalais NN, Dortch Q, Justic D, Shaw RF, Cope J (1998) Fluctuating silicate:nitrate ratios and coastal plankton food webs. *Proc. Natl. Acad. Sci. USA*, 95: 13048-13051.
- Van Cappellen, P, S Dixit and J. Van Beusekom, 2002. Biogenic silica dissolution in the oceans: reconciling experimental and field-based dissolution rates. *Global Biogeochem. Cycles*, 16(4), 1075, doi: 10.1029/2001GB001431
- Vanderborght, J.P., Folmer, I., Aguilera, D.R., Uhrenholdt, T., Regnier, P., 2007. Reactive-transport modelling of a river-estuarine-coastal zone system: application to the Scheldt estuary. *Marine Chemistry* 106, 92–110.
- Von Liebig J (1840) *Die Organische Chemie in Ihrer Anwendung auf Agrikultur*

und Physiologie. Friedrich Vieweg.

Appendix:

Symbol	Description	value	unit	References
k_{NDet}	NDet mineralisation rate at 0°C in the water column	0.03	d ⁻¹	Baretta-Becker et al., 1994
k_{SiDet}	SiDet mineralisation rate at 0°C in the water column	0.06	d ⁻¹	Le Pape, 1996
$vsed$	Sedimentation rate for Dia and detritic matter	1.5	mol C/ l	Andersen and Nival, 1988
kd_{FDDia}	FDDia degradation rate to detritic mater	0.1	d ⁻¹	Le Pape, 1996
kd_{BFDDia}	BFDDia degradation rate to detritic mater	0.1	d ⁻¹	Le Pape, 1996
μ_{max_Dia}	Maximum growth rate at 0°C for pelagic diatoms	0.5	d ⁻¹	Chapelle, 1991
$Iopt_{Dia}$	Optimal light intensity for Dia	100	W m ⁻²	Andersen, 1985
$Iopt_{Dino}$	Optimal light intensity for Dino	140	W m ⁻²	Andersen, 1985
kN_{Dia}	Half saturation constant for Nitrogen for Dia	2	µmol N.l ⁻¹	Eppley et al., 1972
kN_{Dino}	Half saturation constant for N for Dino	2	µmol N.l ⁻¹	Le Pape, 1996
kSi_{Dia}	Half saturation constant for Silica for Dia	1	µmol N.l ⁻¹	Paasche, 1973
η_{Dia}	Mortality rate at 0°C for pelagic Diatoms	0.02	d ⁻¹	Andersen, 1985
η_{Dino}	mortality rate at 0°C for Dinoflagelates	0.02	d ⁻¹	Radach & Moll, 1993
μ_{max_Dino}	Maximum growth rate at 0°C for Dinoflagelates	0.4	d ⁻¹	Calibration
C/N	C over N ratio for Phytoplankton	6.62	mol C/mol N	Redfield, 1934
Si/N	Silica over Nitrogen ratio	1	-	Redfield, 1934
$N/Chla$	N over Cl. A ratio for Phytoplankton	1	-	Antia et al., 1963
K_{nc}	Non chlorophilian light extinction coefficient	0.1	-	calibration
l	Maximum depth over which the sedimentation rate is maximum	30	m	Le Pape, 1996
k_{DNDet}	BNDet mineralisation rate at 0°C in the sediment	0.003	d ⁻¹	Le Pape, 1996
k_{BSiDet}	Silica mineralisation rate at 0°C in the sediment	0.006	d ⁻¹	Moriceau, 2002
$Hsed$	Active sediment depth	0.01	m	Calibration
k_{diffSi}	Diffusion coefficient for Silica	0.0001	-	Calibration
k_{diffN}	Diffusion coefficient for Nitrogen	0.0001	-	Calibration

ε_{Dia}	Egestion rate of benthic filter feeders for Dia	0.4	-	Le Pape <i>et al.</i> , 1999
ε_{NDet}	Egestion rate of benthic filter feeders for Detritic mater	0.8	-	Le Pape <i>et al.</i> , 1999
ε_{BDia}	Egestion rate of benthic filter feeders for BDia	0.4	-	Le Pape <i>et al.</i> , 1999
ε_{Dino}	Egestion rate of benthic filter feeders for Dino	0.4	-	Le Pape <i>et al.</i> , 1999
Aff_{Dia}	Affinity of bethic feeders for Dia	0.35	-	Calibration
Aff_{Dino}	Affinity of bethic feeders for Dino	0.35	-	Calibration
Aff_{BDia}	Affinity of bethic feeders for BDia	0.3	-	Calibration
Aff_{NDet}	Affinity of bethic feeders for detritic mater	0	-	Calibration
$SMin_{Dia}$	Minimum slop of predation rate for Ben on Dia	3	mmol C m ⁻³	calibration
$SMax_{Dia}$	Maximum slop of predation rate for Ben on Dia	11	mmol C m ⁻³	calibration
$SMin_{Dino}$	Minimum slop of predation rate for Ben on Dino	3	mmol C m ⁻³	calibration
$SMax_{Dino}$	Maximum slop of predation rate for Ben on Dino	11	mmol C m ⁻³	calibration
$SMin_{BDia}$	Minimum slop of predation rate for Ben on BDia	200	mmol C m ⁻²	calibration
$SMax_{BDia}$	Maximum slop of predation rate for Ben on BDia	500	mmol C m ⁻²	calibration
$SMin_{Ben}$	Ben biomass below which grazing stops	3000	mmol C m ⁻²	calibration
$SMax_{Ben}$	Saturation threshold for Ben	18000	mmol C m ⁻²	calibration
η_{Ben}	Mortality rate at 0°C for benthic filter feeders	0.0005	d ⁻¹	Calibration
ρ_{Ben}	Excretion rate at 0°C for Benthic filter feeders	0.0005	d ⁻¹	Calibration
τ_{Ben}	Maximum ingestion rate at 0°C for Ben	0.017	d ⁻¹	Le Pape <i>et al.</i> , 1996
p_{Dia}	Affinity for Dia by Zoo	0.5	-	Pondaven <i>et al.</i> , 1998
p_{Dino}	Affinity for Dino by Zoo	0.5	-	Pondaven <i>et al.</i> , 1998
K_{Zoo}	Half saturation constant for chlorophyll for zooplankton	4.6		Pondaven <i>et al.</i> , 1998
η_{Zoo}	maximum death rate a 0 C for Zoo	0.06	d ⁻¹	Pondaven <i>et al.</i> , 1998
ρ_{Zoo}	excretion rate at 0 C for Zoo	0.01	d ⁻¹	Pondaven <i>et al.</i> , 1998
ε_{Zoo}	Egestion rate for zooplankton	0.4	-	Pondaven <i>et al.</i> , 1998
$m0$	Minimum mortality rate for Zoo	0	d ⁻¹	Pondaven <i>et al.</i> , 1998
mdd	Density-dependent mortality rate for Zoo	0.0002	d ⁻¹	Pondaven <i>et al.</i> , 1998

bur_{BSiDet}	Accumulation rate within the sediment for BSiDet	0.003		Calibration
bur_{BNDet}	Accumulation rate within the sediment for BNDet	0.003		Calibration
kSi_{BDia}	Half saturation constant for Si for benthic diatoms	1		Calibration
kN_{BDia}	Half saturation constant for N benthic diatoms	2		Calibration
$Iopt_{BDia}$	Optimal light intensity for benthic diatoms	100	W m ⁻²	Calibration
μ_{max_BDia}	maximum growth rate at 0°C for BDia	0.25	d ⁻¹	Calibration
η_{BDia}	mortality rate at 0°C Diaben	0.02	d ⁻¹	Calibration

State variable	Equation
Dia	$\frac{\partial Dia}{\partial t} = Dia \times [\mu_{\max, Dia} \times f(T) \times \min(f(I)_{Dia}, f(N)_{Dia}, f(S)_{Dia}) - \eta_{Dia} \times f(T)] - sed_{Dia} - C_{Zoo}^{Dia} - C_{Ben}^{Dia}$ <p>with $f(N) = \exp^{(0.07 \times T)}$ for the temperature function</p> $f(N)_{Dia} = \frac{DIN}{DIN + kN_{Dia}}$ <p>for diatom growth limitation by DIN availability</p> $sed_{Dia} = Dia \times \frac{1}{H} \times v_{sed} \times \min\left(1, \frac{H}{l}\right)$ <p>for the sedimentation of diatoms where H is water depth</p> <p>and $f(I)_{Dia} = \frac{1}{H} \times \int_0^H \frac{I_z \cdot P_{ant}}{I_{opt, Dia}} \times \exp\left(1 - \frac{I_z \cdot P_{ant}}{I_{opt, Dia}}\right) dz$ for the light limitation function for diatoms</p> <p>using $I_z = I_{surf} \times \exp^{(-k \times z)}$ and $K = K_{nc} + 0.04 \times (Dia + Dino)^{0.6}$</p>
Dino	$\frac{\partial Dino}{\partial t} = Dino \times [\mu_{\max, Dino} \times f(T) \times \min(f(I)_{Dino}, f(N)_{Dino}) - \eta_{Dino} \times f(T)] - C_{Zoo}^{Dino} - C_{Ben}^{Dino}$
Zoo	$\frac{\partial Zoo}{\partial t} = Zoo \times [\mu_{Zoo} \cdot f(T) - \eta_{Zoo} \cdot f(T) - \rho_{Zoo} \cdot f(T)]$ <p>with $\mu_{Zoo} = (1 - \epsilon_{Zoo}) \cdot (C_{Zoo}^{Dia} + C_{Zoo}^{Dino})$ where $C_{Zoo}^{Dia} = \mu_{max}^{Dia} \frac{I_{Dia}}{K_{Zoo} + F}$ and $C_{Zoo}^{Dino} = \mu_{max}^{Dino} \frac{I_{Dino}}{K_{Zoo} + F}$</p> $F = Dia \cdot \rho_{Dia} + Dino \cdot \rho_{Dino}$ $I_{Dia} = \frac{Dia \cdot P_{Dia}}{Dia \cdot P_{Dia} + Dino \cdot P_{Dino}} \quad \text{and} \quad I_{Dino} = \frac{Dino \cdot P_{Dino}}{Dia \cdot P_{Dia} + Dino \cdot P_{Dino}}$ <p>and $\eta_{Zoo} = \max(m_0, m_{gd}) \cdot Zoo$</p> <p>Thus $C_{Zoo}^{Dia} = Zoo \times f(T) \times C_{Zoo}^{Dia}$ and $C_{Zoo}^{Dino} = Zoo \times f(T) \times C_{Zoo}^{Dino}$</p>

DIN	$\frac{\partial \text{DIN}}{\partial t} = k_{\text{NDet}} \times f(T) \times \text{NDet} - \text{N:C} \times \sum_{\text{prey}} \mu_{\text{prey}} + Z_{\text{oo}} \times \rho_{Z_{\text{oo}}} \times f(T) \times \text{N:C} + \text{diffN}$ <p>with $\text{diffN} = -k_{\text{diffN}} \times \frac{\text{BDIN} - \text{DIN}}{I}$</p>
NDet	$\frac{\partial \text{NDet}}{\partial t} = (\text{Dino} \cdot \rho_{\text{Dino}} + \text{FDDia} \cdot k_{\text{FDDia}} + Z_{\text{oo}} \cdot \rho_{Z_{\text{oo}}}) \times f(T) \cdot \text{N:C} - k_{\text{NDet}} \times f(T) \times \text{NDet} - \text{BNDet} + \varepsilon_{Z_{\text{oo}}} \times (C_{Z_{\text{oo}}}^{\text{Dia}} + C_{Z_{\text{oo}}}^{\text{Dino}})$
dSi	$\frac{\partial \text{dSi}}{\partial t} = k_{\text{SDet}} \times f(A) \times \text{SIDet} - \text{Si:C} (\text{Dia} \times \mu_{\text{Dia}}) + \text{diffSi}$ <p>with $f(A) = A \cdot \exp\left(-\frac{E_{\text{app}}}{R \cdot T}\right)$ for the Si dissolution</p>
	$\text{and } \text{diffSi} = -k_{\text{diffSi}} \times \frac{\text{BdSi} - \text{dSi}}{I}$
SIDet	$\frac{\partial \text{SIDet}}{\partial t} = \text{Si:C} [\text{FDDia} \times k_{\text{FDDia}} \times f(T)] - \text{SIDet} \times k_{\text{SDet}} \times f(A) - \text{sed}_{\text{SIDet}} + \text{Si:C} [C_{Z_{\text{oo}}}^{\text{Dia}} + C_{Z_{\text{oo}}}^{\text{FDDia}}]$
FDDia	$\frac{\partial \text{FDDia}}{\partial t} = \eta_{\text{Dio}} \times f(T) \times \text{Dia} - \text{FDDia} \times f(T) \times k_{\text{FDDia}} - \text{sed}_{\text{FDDia}} - C_{\text{Ben}}^{\text{FDDia}}$
BDIN	$\frac{\partial \text{BDIN}}{\partial t} = \text{BNDet} \times k_{\text{BNDet}} \times f(T) - \text{diffN} + \rho \times f(T) \times \text{Ben} \times \text{N:C}$
BNDet	$\frac{\partial \text{BNDet}}{\partial t} = -k_{\text{BNDet}} \times f(T) \times \text{BNDet} + \text{N:C} \times H \times \text{sed}_{\text{NDet}} + \eta \times f(T) \times \text{Ben} + \text{N:C} \times \sum_i (1 - \varepsilon_{\text{prey}}) \cdot C_{\text{prey}} - \text{BNDet} \times k_{\text{BNDet}} \times f(T) - \text{BNDet} \times \text{bu}_{\text{BNDet}}$

$$\begin{aligned}
\text{BdSi} \quad \frac{\partial \text{BdSi}}{\partial t} &= \text{BSiDet} \times k_{\text{resid}} \times f(A) - \text{diffSi} \\
\text{BSiDet} \quad \frac{\partial \text{BSiDet}}{\partial t} &= kd_{\text{prey}} \times f(T) \times \text{BFDDia} \times \text{Si} \cdot C + H \times \text{sed}_{\text{prey}} + \text{Si} \cdot C \times [C_{\text{ben}}^{\text{Dia}} + C_{\text{ben}}^{\text{BDDia}} + C_{\text{ben}}^{\text{BDDia}} + C_{\text{ben}}^{\text{BDDia}}] \\
&\quad - \text{BSiDet} \times k_{\text{resid}} \times f(A) - \text{BSiDet} \times \text{bur}_{\text{resid}} \\
\text{BDia} \quad \frac{\partial \text{BDia}}{\partial t} &= \text{BDia} \times \mu_{\text{max}} \times f(T) \times \min(f(\eta_{\text{Dia}}), f(N)_{\text{Dia}}) - \text{BDia} \times \eta_{\text{Dia}} \times f(T) - C_{\text{dia}}^{\text{BDia}} + H \cdot \text{sed}_{\text{Dia}} \\
\text{BFDDia} \quad \frac{\partial \text{BFDDia}}{\partial t} &= \eta_{\text{BDia}} \times f(T) \times \text{BDia} - \text{BFDDia} \times f(T) \times kd_{\text{BFDDia}} - C_{\text{ben}}^{\text{BFDDia}} + H \cdot \text{BFDDia} \\
\text{Ben} \quad \frac{\partial \text{Ben}}{\partial t} &= \left[\sum \tau_{\text{lum}} \times \text{Aff}_{\text{prey}} \times \rho_{\text{prey}} \times \text{ddl}_{\text{ben}} \times (1 - \epsilon_{\text{prey}}) \times \text{ddl}_{\text{lum}} - [\eta \text{Ben} + \rho \text{Ben}] \times f(T) \times \text{Ben} \right. \\
&\quad \left. \text{with } \rho_{\text{prey}} = \max \left(0, \min \left(1, \frac{\rho_{\text{prey}} - S_{\text{min,prey}}}{S_{\text{max,prey}} - S_{\text{min,prey}}} \right) \right) \right] \\
&\quad \text{and } \text{ddl}_{\text{ben}} = \max \left[\frac{\eta_{\text{Ben}} + \rho_{\text{Ben}}}{\tau_{\text{Ben}} \times (1 - \epsilon_{\text{Ben}})}, 1 - \left[\left(1 - \frac{\eta_{\text{Ben}} + \rho_{\text{Ben}}}{\tau_{\text{Ben}} \times (1 - \epsilon_{\text{Ben}})} \right) \times \left(\min \left[1, \frac{\text{Ben} - S_{\text{min,Ben}}}{S_{\text{max,Ben}} - S_{\text{min,Ben}}} \right] \right) \right] \right] \\
\text{Thus: } C_{\text{ben}}^{\text{prey}} &= \text{Berr} \times f(T) \times \tau_{\text{Ben}} \times \text{Aff}_{\text{prey}} \times \rho_{\text{prey}} \times \text{ddl}_{\text{ben}}
\end{aligned}$$

CHAPTER 2

Anthropogenic perturbations of the silicon cycle at the global scale: the key role of the land-ocean transition

G. G. Laruelle, V. Roubeix, A. Sferratore, B. Brodherr, D. Ciuffa, D. J. Conley, H. H. Dürr, J. Garnier, C. Lancelot, Q. Le Thi Phuong, J.-D. Meunier, M. Meybeck, P. Michalopoulos, B. Moriceau, S. Ni Longphuir, S. Loucaides, L. Papush, M. Presti, O. Ragueneau, P. A. G. Regnier, L. Saccone, C. P. Slomp, C. Spiteri, P. Van Cappellen

Accepted by *Global Biogeochemical Cycles*

July 2009

Abstract

Silicon (Si), in the form of dissolved silicate (DSi), is a key nutrient in marine and continental ecosystems. DSi is taken up by organisms to produce structural elements (e.g., shells and phytoliths) composed of amorphous biogenic silica (bSiO₂). A global mass balance model of the biologically active part of the modern Si cycle is derived based on a systematic review of existing data regarding terrestrial and oceanic production fluxes, reservoir sizes, and residence times for DSi and bSiO₂. The model demonstrates the high sensitivity of biogeochemical Si cycling in the coastal zone to anthropogenic pressures, such as river damming and global temperature rise. As a result, further significant changes in the production and recycling of bSiO₂ in the coastal zone are to be expected over the course of this century.

1. Introduction

Silicon (Si) is the second most abundant element in the Earth's crust after oxygen. Most Si, however, is bound in the form of quartz and silicate minerals, and is therefore unavailable for uptake by organisms. Thus, despite its abundance, Si is a major limiting element in many aquatic systems (Conley and Malone, 1992; Egge and Aksnes, 1992; Paasche, 1980; Leynaert et al., 2001), and is also an essential nutrient for the growth of many terrestrial plants (Epstein, 1999; Datnoff et al., 2001). Key aspects of the global biogeochemical silicon cycle remain poorly understood, such as the biological cycling of Si on the continents (Conley, 2002a), the role of the coastal zones in regulating the transfer of reactive Si from land to the open ocean (Conley, 1997; DeMaster, 2002), the fate of biogenic silica produced in oceanic surface waters and its decoupling from carbon during sinking (Nelson et al., 1995; Ragueneau et al., 2002, 2006a), and ongoing changes to the Si cycle by human activities (Chauvaud et al., 2000; Conley et al., 1993; Friedl and Wuest, 2002; Friedl et al., 2004; Humborg et al., 2000, 2006; Ragueneau et al., 2005, 2006b, 2006c, Conley et al., 2008).

Global scale studies of the biogeochemical Si cycle have focused mainly on the marine aspect. An important landmark in the assessment of Si fluxes in the world ocean is the work of Tréguer et al. (1995). These authors, however, provide no estimates of the amounts of biogenic silica stored in the oceans and underlying sediments. Furthermore, only a crude representation of the land-ocean interface is included in their global Si budget. In this respect, the current state of knowledge and modeling of global carbon, nitrogen, phosphorus and sulfur cycles (Mackenzie et al., 1993, 1998; Ver, 1998; Rabouille et al., 2001) are significantly more advanced than for silicon.

In this study, we provide global scale estimates of reservoir sizes and fluxes of reactive Si on the continents in the ocean and at the continent-to-ocean transition. Emphasis is placed on the biogeochemical dynamics of Si at the Earth's surface, from the recent past to the end of the 21st century. We therefore do not explicitly represent the long-term endogenic Si cycling, but rather include the Earth's lithosphere as the ultimate source and sink of reactive Si. The two forms of reactive Si considered are dissolved silicate (DSi) and biogenic silica (bSiO₂). The

main transformation processes in the global biogeochemical Si cycle are uptake of DSi followed by biomineralization as bSiO₂ in terrestrial plants and aquatic organisms, and the dissolution of bSiO₂ into DSi.

The resulting mass balance model is used to explore the sensitivity of the global Si cycle and gain insight into its function. Special attention is paid to the role of the coastal zone and continental shelves on the coupling of terrestrial and oceanic Si dynamics. In addition, the response of the global biogeochemical Si cycle to two anthropogenically-driven forcings is analyzed: global temperature rise and river damming. These forcings are selected because both siliceous production and bSiO₂ dissolution are sensitive to temperature (Wollast 1974; Cossins and Bowler, 1987; Rickert, 2000; Van Cappellen et al., 2002), while increased river damming, especially since the 1950's, has considerably modified the reactive Si delivery to the oceans (Conley, 2002b, Humborg et al., 2006).

2. Global biogeochemical Si model

2.1. Water cycle

The Earth's surface environment is divided into four compartments (Figure 1): continents (box 1), proximal (box 2) and distal (box 3) coastal zones, and the open ocean (box 4). The proximal and distal coastal zones are those proposed by Rabouille et al. (2001). As shown by these authors, this division of the global coastal zone provides a more realistic representation of the role of continent to ocean transition in the biogeochemical cycling of carbon and nutrients. The proximal zone consists of large bays, the open water parts of estuaries, inner deltas, inland seas and coastal marshes (Woodwell et al., 1973). The distal zone comprises the rest of the continental margins up to the shelf break.

These compartments are linked to one another via the water cycle (Figure 1). Water on the continents is subdivided into an aquatic reservoir, which comprises exorheic rivers and lakes including their floodplains (Box 1a), and a groundwater reservoir (Box 1b). The open ocean is by far the largest compartment, with a mean water depth of 3600 m and covering 92% of the world ocean (Tréguer et al., 1995). Three vertical subcompartments of the water column are considered: a 100 m thick surface layer where photosynthesis takes place (Box 4a), mesopelagic oceanic

waters (100-1000 m depth) (Box 4b) and deep waters (Box 4c).

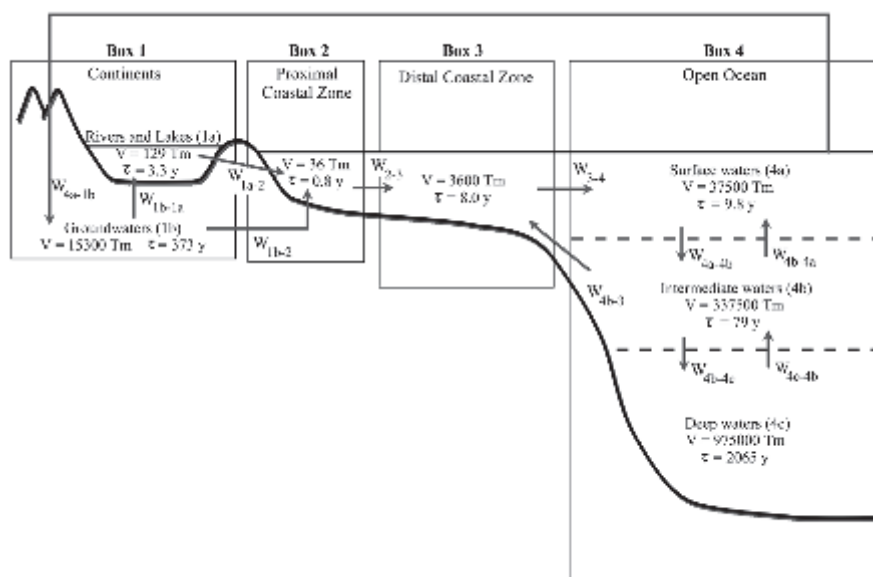


Figure 1: Global Water Cycle with water masses in Tm^3 and water fluxes (W) in $Tm^3 y^{-1}$. V = volume and τ = residence time.

Water fluxes (W) considered in the baseline scenario are based on the simplified steady-state water cycle summarized in Table 1. It should be noted that a contribution from subsurface groundwater discharge to the proximal coastal zone is explicitly considered (W_{1b-2} , Slomp and Van Cappellen, 2004). The combination of water reservoir sizes with water fluxes yields water residence times that agree well with previous studies (Garrels and Mackenzie, 1971; Broecker and Peng, 1982; Macdonald, 1998).

2.2. Reactive Si reservoirs

The DSi and bSiO₂ reservoir masses are time-dependent variables of the Si cycle model (Figure 2). DSi mainly consists of undissociated monomeric silicic acid, Si(OH)₄, and represents the main form under which silicon can be assimilated by organisms (Del Amo and Brzezinski, 1999). Organisms use DSi to build structural elements made of amorphous, hydrated silica, part of which is preserved after the death of the organisms (Simpson and Volcani, 1981; Conley

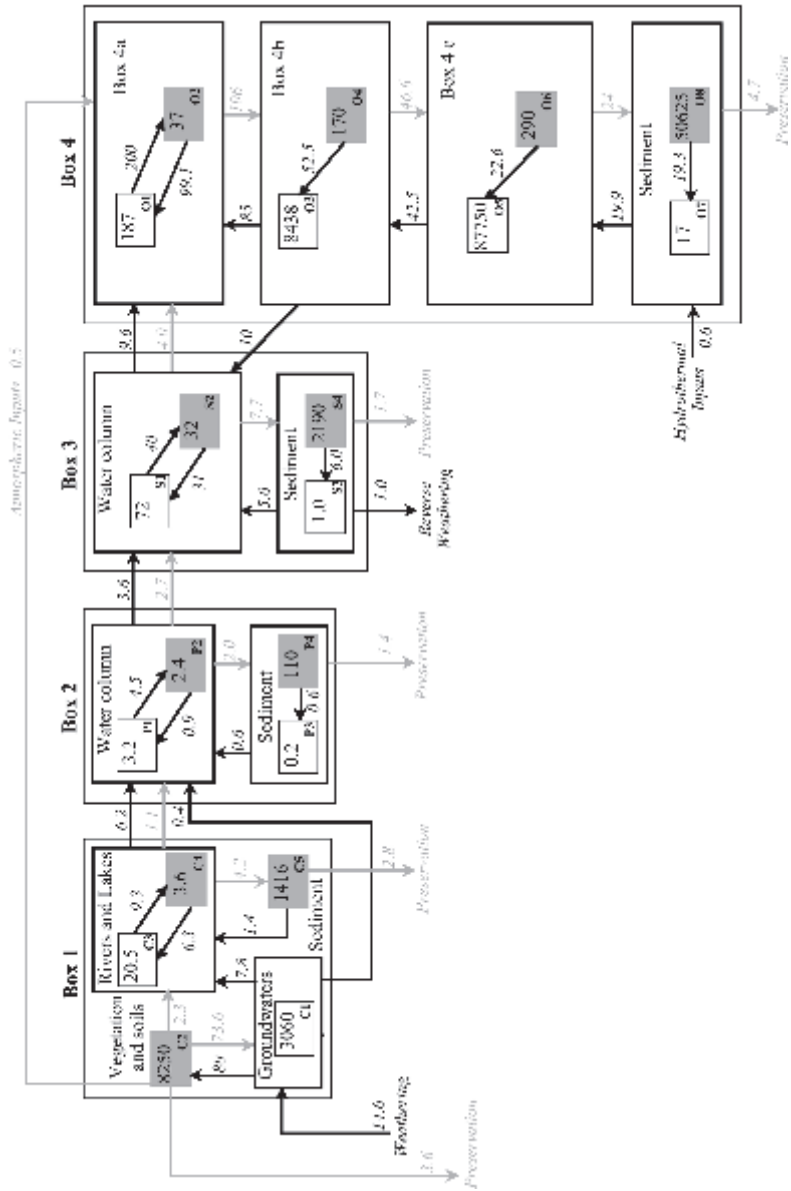


Figure 2: Steady state biogeochemical cycle of silicon, with reservoirs in Tmol Si y⁻¹. Shaded squares represent bSiO₂ reservoirs, open squares represent DSi reservoirs. The steady state cycle of Si is used as initial condition (nominally 1950) in the perturbation simulations.

and Schelske, 2001). Here, bSiO_2 includes the amorphous silica in both living biomass and biogenic detritus in open waters, soils and sediments. It should be noted that bSiO_2 may undergo significant chemical and mineralogical changes (Van Cappellen et al., 2002), even including a complete diagenetic transformation of the opaline silica into aluminosilicate minerals (Michalopoulos et al., 2000).

Table 1: Calculations and references used to constrain the water fluxes in the model.

Flux	Value ($\text{Tm}^3 \text{y}^{-1}$)	Calculation	Reference
W_{1b-1a}	39	-	(1)
W_{1a-2}	39	$W_{4a-1} - W_{1b-2}$	-
W_{1b-2}	2	-	(2)
W_{2-3}	41	$W_{1a-2} + W_{1b-2}$	-
W_{3-4}	441	$W_{2-3} - W_{4-3}$	-
W_{4-3}	400	-	(3,4,5)
W_{4a-4b}	3800	$W_{4b-4a} + W_{3-4} - W_{4a-1}$	-
W_{4b-4a}	3400	-	(6)
W_{4b-4c}	472	-	(6)
W_{4c-4b}	472	W_{4b-4c}	-
W_{4a-1b}	41	-	(7)

(1) Fekete et al., 2002; (2) Slomp and Van Cappellen, 2004; (3) Brink et al., 1995; (4) Ver, 1998 ; (5) Rabouille et al., 2001 ; (6) Deduced from residence time in Broecker and Peng, 1982; (7) Anikouchine and Sternberg (1981);

In marine environments, the major producers of bSiO_2 are diatoms, although other organisms, such as radiolarians, sponges, and chrysophytes, may locally be important sources of bSiO_2 (Simpson and Volcani, 1981). On land, large quantities of DSi are fixed by higher plants and deposited as amorphous silica in so-called phytoliths (Piperno, 1988). The significant contribution of phytolith production and dissolution in the global Si cycle has only recently been highlighted (Bartoli, 1983; Meunier et al., 1999; Conley, 2002a).

Estimations of DSi and bSiO_2 reservoir sizes in the four earth surface compartments are summarized in Table 2. Reservoir masses are mostly derived from estimates of the average DSi or bSiO_2 concentrations and the volumes of the corresponding reservoirs. In some cases, however, the reservoir mass is calculated from flux estimates, assuming steady-state conditions. For example, the mass of DSi in the water column of the distal coastal ocean (72 Tmol Si) is obtained from

Table 2: Reservoir sizes of dissolved silicate (DSi) and biogenic silica (bSiO₂) in the model. V(x) and VS(x) refer to the volumes of water and sediment reservoirs of box x as described in Figure 1. The porosity ($\phi = 0.7$) and the density ($\rho = 2.5 \text{ g cm}^{-3}$) of the sediments are taken from Maher et al. (2004). M(Si) and M(SiO₂) stand for the atomic mass of Si and molar weight of SiO₂ respectively.

Reservoir	Size (Tmol Si)	Calculation	Reference
Continents			
C1	3060	200 $\mu\text{mol Si L}^{-1(a)} \times V(1b)^{(b)}$ a- average DSi concentration in ground waters b- volume of ground waters	- (1) (2)
C2	8250	$0.42 \text{ g Si}^{-1(e)} \times 0.005 \text{ g g}^{-1(b)} \times (75 \cdot 10^{18} \text{ m}^2)^{(c)} \times 1 \text{ m}^{(d)} \times 2.65 \text{ g cm}^{-3(e)} \times 0.55^{(f)} / \text{M(Si)}$ a- mass of Si per gram of phytoliths b- average mass of phytoliths per gram of soil c- global surface area covered by soils d- assumed global average soil depth e- average dry density of soils f- solid fraction of soils	- (2) (3) (4) (5) (5) (6)
C3	3.6	-	(6)
C4	20.5	$(9.3 \text{ mg Si L}^{-1(a)} \times V(1b)^{(b)}) / \text{M(Si)}$ a- average DSi concentration in rivers b- global volume of lakes and floodplains	- (7)
C5	1416	$50 \text{ mg SiO}_2 \text{ g sediment}^{-1(e)} / \text{M(SiO}_2) \times \text{VS}(1)^{(b)} \times (1 - \phi) \times \rho$ a- average bSiO ₂ content of river sediments b- volume of lake plus river sediments	(8)

Proximal Coastal Zone			
P1	DSi in the water column	3.2	$F_{\text{P1Si}} \times V(2)/W_{2-3}$
P2	bSiO ₂ in the water column	2.4	$F_{\text{P2SiO}_2} \times V(2)/W_{2-3}$
P3	pore water DSi in sediments	0.2	$300 \mu\text{mol Si L}^{-1} \times VS(2) \times \phi$
P4	bSiO ₂ in sediments	110	$0.02 \text{ g Si g}^{-1} \text{ (a)} \times VS(2) \times (1-\phi) \times \rho / M(\text{Si})$ a- mass of Si as bSiO ₂ in proximal coastal sediments (2 wt%)
Distal Coastal Zone			
S1	DSi in the water column	72	$F_{\text{S101}} \times V(3) / W_{3-4a}$
S2	bSiO ₂ in the water column	32	$F_{\text{S202}} \times V(3) / W_{3-4a}$
S3	pore water DSi in sediments	1	$300 \mu\text{mol Si L}^{-1} \times VS(3) \times \phi$
S4	bSiO ₂ in sediments	2190	$0.03 \text{ g Si g}^{-1} \text{ (a)} \times VS(3) \times (1-\phi) \times \rho / M(\text{Si})$ a- mass of Si as bSiO ₂ in distal coastal sediments (3 wt%)
Open Ocean			
O1	DSi in the surface ocean	187	$5 \mu\text{mol L}^{-1} \times V(4a)$
O2	bSiO ₂ in the surface ocean	37	$1 \mu\text{mol L}^{-1} \times V(4a)$
O3	DSi in intermediate waters	8438	$25 \mu\text{mol L}^{-1} \times V(4b)$
O4	bSiO ₂ in intermediate waters	170	$0.5 \mu\text{mol L}^{-1} \times V(4b)$
O5	DSi in deep sea	87750	$100 \mu\text{mol L}^{-1} \times V(4c)$
O6	bSiO ₂ in deep sea	290	$0.1 \mu\text{mol L}^{-1} \times V(4c)$
O7	pore water DSi in sediments	17	$300 \mu\text{mol Si L}^{-1} \times VS(4) \times \phi$
O8	bSiO ₂ in sediments	50625	$0.05 \text{ g Si g}^{-1} \text{ (a)} \times VS(4) \times (1-\phi) \times \rho / M(\text{Si})$ a- mass of Si as bSiO ₂ in deep sea sediments (5 wt%)

Sources : (1) J.-D. Meunier, comm. pers. ; (2) Berner and Berner, 1996 ; (3) Conley, 2002b ; (4) FAO/UNESCO soil map of the world, 1986 ; (5) Schroeder, 1978 ; (6) Conley, 1997 ; (7) Dürr et al., submitted ; (8) Conley, 1988 ; (9) Jahnke et al., 1982 ; (10) Ledford-Hoffman et al., 1986 ; (11) Nelson et al., 1995 ; (12) Yool and Tyrrell, 2003 ; (13) Conkright et al., 1994 ; (14) Dittmar and Birkicht, 2001 ; (15) Hill and Wheeler, 2002 ; (16) Bonn, 1995

the export flux of DSi and the water flux to the open ocean (Table 2). This estimate, combined with the reservoir volume (3600 Tm^3 , Figure 1), then yields an average DSi concentration of the distal ocean of $20 \mu\text{M}$, which can be compared to the wide range of observed, depth-integrated DSi concentrations in shelf waters from $<5 \mu\text{M}$ (Alvarez-Salgado et al., 1997; Gibson et al., 1997, Lacroix et al., 2007) to $\sim 15 \mu\text{M}$ (Heiskanen and Keck, 1996) to $>30 \mu\text{M}$, (Serebrennikova and Fanning, 2004; Zhang, 2002).

The ultimate source of DSi for the global Si cycle is chemical weathering of silicate rocks of the continental and oceanic crust (Gerard and Ranger, 2002). The total mass of silicate rock exposed at the Earth's surface largely exceeds that of the reactive DSi plus bSiO_2 reservoirs. Thus, on the time scales investigated (years to centuries), the reservoir size of silicate rocks remains essentially unchanged. A large fraction of DSi released by weathering is converted by plants into phytoliths and temporarily stored in soils (Saccone et al., 2008; Figure 2). A rough estimate of the reservoir mass of bSiO_2 in soils is obtained based on average phytolith concentrations for different types of soils (Conley et al., 2002b), the average soil bSiO_2 concentration, and the global volume of soils. The latter is derived from the FAO world soil map (FAO/UNESCO, 1986), assuming a mean soil depth of 1 meter (Pouba, 1968; Batjes, 1997).

The sediment reservoirs correspond to the topmost layers where decomposition of biogenic constituents drives the return of dissolved nutrient species to the water column (including DSi). The corresponding volumes (V_S , Table 2) are estimated by assigning a mean thickness of 10 cm to the active layer of aquatic sediments on the continents and in the proximal coastal zone (Heinze et al., 1999), and 20 cm for distal coastal zone and deep sea sediments (De Master, 2002). An average porosity of 0.7 and an average dry density of 2.5 g cm^{-3} are assumed for all sediments (Maher et al., 2004). The calculated sediment volumes of boxes 1, 2, 3 and 4 are 1.73, 0.18, 5.5 and 75 Tm^3 , respectively.

2.3. Reactive Si fluxes

The fluxes of reactive Si are obtained from the literature, or constrained by assuming that the Si cycle is initially at steady-state (Table 3). The assumption

Table 3: Silicon fluxes in the model. V and VS refer to the volumes of water and sediment reservoirs, respectively, Si/C is the molar Si to carbon ratio of primary production, M(Si) and M(C) stand for the atomic mass of Si and C respectively.

	Flux (Tmol.y ⁻¹)	Calculation or explanation	Reference
Continents			
F _w	14.6	F _{C1C2} - F _{C2C1} + F _{C1C3} + F _{C1P1}	(1)
F _{C2-burial}	3.6	25% of F _w	(2)
F _{C1C2}	80	reported range: 60 to 200 Tmol Si.y ⁻¹	
F _{C1C3}	7.8		(3)
F _{C1P1}	0.4	W _{lb-2} x 200 μmol Si L ⁻¹ in ground waters	(1)
F _{C2C1}	73.6	92% of F _{C1C2}	(4)
F _{C2O2}	0.5		
F _{C2C4}	2.3		
F _{C3C4}	9.3	61% ^(a) of carbon primary production × 17.10 ²² m ² · m ³ · yr ⁻¹ × (Si/C) ^(b) / M(C) × 13.5g C m ⁻² yr ⁻¹ × (Si/C) ^(b) / M(C)	(5)
		a- fraction of primary production due to diatoms in fresh waters	(6)
		b- surface of rivers and lakes	(7)
		c- Average riverine primary production in carbon	(8)
		d- molar Si to C ratio of 0.79±0.43	(9)
F _{C3P1}	6.2		(7)
F _{C4C3}	6.3		
F _{C4C5}	4.2	F _{C2C4} + F _{C3C4} - F _{C4P1} - F _{C4C3}	(2)
F _{C4P2}	1.1		
F _{C5C3}	1.4		
F _{C5-burial}	2.8		
Proximal Coastal Zone			
F _{P1P2}	4.5	75% ^(a) of carbon primary production (40 Tmol C.y ⁻¹ · (b)) × (Si/C) ^(c)	(10)
		a- fraction of primary production due to diatoms in the coastal zone	(11)
		b- primary production in the proximal coastal zone in carbon	
		c- molar Si to C ratio of 0.15	

F_{P1S1}	DSi export from box 2	3.6	$P1 \times W_{2,3}$	
F_{P2P1}	bSiO ₂ dissolution	0.9	$F_{P1P2} + F_{C4P2} - F_{P2S2} - F_{P2P4}$	
F_{P2P4}	Sedimentation	2	$F_{P4P3} + F_{P4-burial}$	
F_{P2S2}	bSiO ₂ export from box 2	2.7	$F_{P1P2} - F_{P2P4} - F_{P2P1}$	(12)
F_{P3P1}	DSi efflux	0.6	Within the range of 0.8 ± 0.4 Tmol Si y ⁻¹ given by 3.6 Tm ² $\times 22 \pm 11 \cdot 10^{-2}$ mol Si y ⁻¹ m ⁻²	
F_{P4P3}	Sediment bSiO ₂ dissolution	0.6	F_{P3P1}	(13)
$F_{P4-burial}$	bSiO ₂ Burial	1.4	$P4 \times 0.13$ cm y ⁻¹ (a)/ 10 cm ^(b) (and so that $F_{P4-burial} + F_{S4-burial} = 3.1$)	(11)
			a- sediment accumulation rate in the proximal coastal zone	(14)
			b- depth of the active sediment layer in the proximal coastal zone	
Distal Coastal Zone				
F_{S1S2}	DSi uptake	40	$[18\%^{(a)}$ of global siliceous primary production (240 Tmol Si y ⁻¹ (b))]- F_{P1P2}	(15)
			a- fraction of the global marine primary production occurring in the coastal zone	(4)
			b- estimate of the global marine siliceous production	
F_{S2S1}	bSiO ₂ dissolution	31	$F_{S2S1} + F_{S3S1} + F_{O3S1} + F_{P4S1} - F_{S1S2}$	
F_{S1O1}	bSiO ₂ export from box3	9.6	$F_{S1S2} + F_{P2S2} - F_{S2S4} - F_{S2O2}$	
F_{S2S1}	bSiO ₂ dissolution	31	$F_{S4-burial} + F_{S4S3}$	(15,16,17)
F_{S2S4}	Sedimentation	7.7	assuming the same export rate as organic carbon, 10% of F_{S1S2}	
F_{S2O2}	bSiO ₂ export from box3	4	within the range of 6 ± 3 Tmol Si y ⁻¹ given by 27 Tm ² (a)	
F_{S3S1}	DSi efflux	5	$\times 0.22 \pm 0.11$ mol Si y ⁻¹ m ⁻²	
			a- surface area of the distal coastal zone	(11)
			b- estimate of benthic efflux rate for the continental shelf	(12)
F_{S3-rw}	Reverse weathering	1	$F_{S3-rw} + F_{S3S1}$	(13)
F_{S4S3}	bSiO ₂ dissolution	6	$S4 \times 0.016$ cm y ⁻¹ (a)/ 20 cm ^(b) (so that $F_{P4-burial} + F_{S4-burial} = 3.1$)	(11)
$F_{S4-burial}$	bSiO ₂ Burial	1.7	a- sediment accumulation rate in the proximal coastal zone	(13)
			b- depth of the active sediment layer in the proximal coastal zone	

Open Ocean				
F_{0102}	DSi uptake	200	$240 \text{ Tmol Si y}^{-1} - F_{\text{SiS2}}$	(4)
F_{0201}	bSiO_2 dissolution	104.9	within the range of 100 – 120 Tmol Si y^{-1} (50 ^(a) to 60 ^(b) % of F_{0102})	(4)
			a- fraction of bSiO_2 production preserved in the water column (lower estimate)	(4)
			b- fraction of bSiO_2 production preserved in the water column (upper estimate)	(10)
F_{0204}	Sedimentation	99.1	$F_{0102} + F_{\text{atm}} - F_{0204}$	
F_{03S1}	Coastal upwelling	10	$[\text{O}_3 / \text{V}(4b)] \times W_{4-5}$	
F_{0301}	Oceanic upwelling	85	$F_{0403} + F_{0303} - F_{03S1}$	
F_{0403}	bSiO_2 dissolution	52.5	$(F_{0605} + F_{0403} = 38\% \text{ of } F_{0102})^{(1)}$	(4)
F_{0406}	Sedimentation	46.6	$F_{0204} - F_{0403}$	
F_{0503}	Deep upwelling	42.5	$F_{0605} + F_{0705}$	
F_{0605}	bSiO_2 dissolution	22.6	$(F_{0605} + F_{0403} = 38\% \text{ of } F_{0102})^{(1)}$	(4)
F_{0608}	Sedimentation	24	12% of F_{0102}	(4)
F_{0705}	DSi efflux	19.9	within the range of $23 \pm 15 \text{ Tmol Si y}^{-1}$	(4)
F_{0807}	Sediment bSiO_2 dissolution	19.3	$F_{0705} - F_{\text{hyd}}$	
$F_{08\text{-burial}}$	bSiO_2 burial	4.7	within the range of 4.1-4.3 Tmol Si y^{-1} (a) and 6 Tmol Si y^{-1} (b)	(13)
			a- estimate of bSiO_2 preservation in marine sediments	(4)
			b- assuming 3% preservation of opal in marine sediments	(4)
F_{hyd}	Hydrothermal input	0.6		

(1) Alexandre et al., 1997; (2) Conley, 2002b; (3) Appelo and Postma, 1996; (4) Tréguer et al., 1995; (5) Arhonditsis and Brett, 2005; (6) Berner and Berner, 1996; (7) Garnier et al., 2002; (8) Conley et al., 1989; (9) Dürr et al., submitted; (10) Nelson et al., 1995; (11) Rabouille et al., 2001; (12) Berelson et al., 1987; (13) De Master, 2002; (14) Heinz et al., 1999; (15) Biscaye et al., 1994; (16) Wollast, 1991; (17) Michalopoulos and Aller, 2004

of an initial steady-state is a common practice in the modeling and budgeting of global elemental cycles (e.g., Mackenzie et al., 1993; Tréguer et al., 1995; Yool and Tyrrell, 2003). It is most likely that, given the oceanic residence time of reactive Si is 15000-17000 years (Tréguer et al., 1995), the marine Si cycle was not at steady state prior to 1950, due to glacial-interglacial changes. Nonetheless, considering the time scales investigated in the simulations (≤ 150 years), these much longer term changes have little effect on the system's response to the imposed perturbations.

The fluxes include the sources and sinks of reactive Si for the Earth's surface environment (Figure 2). The sources are chemical weathering on land (F_w) and flux of DSi to the oceans resulting from basalt-seawater interactions (F_{hyd}). The sinks are burial of bSiO₂ in sediments ($F_{C5-burial}$, $F_{P4-burial}$, $F_{S4-burial}$, $F_{O8-burial}$), and removal of DSi due to reverse weathering reactions in shelf sediments (F_{S3rw} ; Mackenzie and Garrels, 1966; Michalopoulos and Aller, 1995, 2004). Note that, because we assume an initially steady-state Si cycle, the sinks and sources of reactive Si balance each other exactly.

All other fluxes either transform or transport reactive Si within the Earth's surface environment and are thus internal fluxes. Si fluxes are represented by the symbol "F" followed by a subscript that identifies the initial (source) and final (sink) reservoir. The reservoir symbols are listed in Tables 1 and 2, for water and reactive Si reservoirs, respectively. Fluxes describing the uptake of DSi by organisms to produce bSiO₂ (F_{C1C2} , F_{C3C4} , F_{P1P2} , F_{S1S2} , F_{O1O2}) scale to the primary production rates in the various compartments of the earth surface environment (Table 3). Most bSiO₂ is efficiently recycled via dissolution in the water column (F_{C4C3} , F_{P2P1} , F_{S2S1} , F_{O2O1} , F_{O4O3} , F_{O6O5}), soils (F_{C2C1}) and sediments (F_{C5C3} , F_{P4P3} , F_{S4S3} , F_{O8O7}). The accumulation of DSi in the pore waters of sediments and progressive loss in the reactivity of biogenic silica surfaces (ageing) ultimately allows a small fraction of bSiO₂ production to be buried and preserved in sediments (Van Cappellen et al., 2002).

The groundwater discharge flux of DSi to the coastal zone (F_{C1P1}) is derived from the corresponding water flux (W_{1a-2} in Figure 1) and the average DSi concentration in groundwater. The riverine supply of DSi to the proximal zone (F_{C3P1}) is derived by averaging the estimated river DSi delivery fluxes computed

for 150 coastal segments in the GEMS-GLORI (Meybeck and Ragu, 1995) and GEMS-PRISRI (Meybeck et al., 2003) databases, under pristine conditions, that is, prior to human perturbation (Dürr et al., submitted). The estimated river DSi flux (6.2 Tmol y^{-1}) thus implicitly corrects for the drop in DSi concentration in the downstream reaches of rivers that has accompanied the extensive building of dams since the 1950s (Humborg et al., 2006). Note that, while the main source of reactive Si for the oceans is in the form of DSi, the contribution of riverine bSiO_2 delivery (F_{C4P2}) is far from negligible (Conley et al., 2000). Reactive Si is also supplied to the oceans via the atmosphere with eolian dust (F_{C2O2}), although this flux is most likely very small (Tréguer et al. 1995) and its origin (biogenic vs. mineral) remains poorly known (Cole et al., 2009; Dürr et al., submitted).

Transport fluxes of DSi into the ocean ($F_{\text{P1S1}}, F_{\text{S1O1}}, F_{\text{O3S1}}, F_{\text{O3O1}}, F_{\text{O5O3}}$), as well as export fluxes of bSiO_2 from the proximal zone to the distal zone (F_{P2S2}) and from the distal zone to the open ocean (F_{S2O2}), are assumed to be directly coupled to the water cycle. That is, the flux of DSi or bSiO_2 exiting the reservoir is related to the mass of DSi or bSiO_2 in that reservoir according to:

$$\frac{F_{ij}}{S_i} = \frac{Q_{ij}}{V_i} \quad (1)$$

where F_{ij} and Q_{ij} are, respectively, the fluxes of reactive Si and water from reservoir i to reservoir j , S_i is the mass of DSi or bSiO_2 in reservoir i , and V_i is the volume of the reservoir.

The remaining transport fluxes correspond to sedimentation ($F_{\text{O2O4}}, F_{\text{O4O6}}$) and deposition of bSiO_2 ($F_{\text{C4C5}}, F_{\text{P2P4}}, F_{\text{S2S4}}, F_{\text{O6O8}}$), and the efflux of DSi from sediments ($F_{\text{C5C3}}, F_{\text{P3P1}}, F_{\text{S3S1}}, F_{\text{O7O6}}$). In the marine realm, these fluxes are relatively well constrained by observations. Sedimentation rates and DSi fluxes from sediments can be determined directly with sediment traps and benthic chambers, respectively (Koning et al., 1997; Rao and Jahnke, 2004). Furthermore, numerous estimates of benthic DSi efflux have been calculated from measured pore water profiles (Rabouille et al., 1993; Dixit and Van Cappellen, 2003).

A widely used approach in biogeochemical box modeling is to relate the

reservoir sizes and fluxes via linear expressions,

$$F_{ij} = k_{ij} S_i \quad (2)$$

where k_{ij} is a first order rate constant (Lasaga, 1981; Chameides and Perdue, 1997; Mackenzie et al., 1998). Values of k_{ij} range from values of 1 y^{-1} , for example for biological DSi uptake and bSiO_2 dissolution in aquatic environments, to values of 10^{-3} y^{-1} or less for groundwater transport of DSi or burial of bSiO_2 in the deep-sea sediments.

2.4. Model simulations

The mass balance equations for the various reactive Si reservoirs, based on the linear flux equations (2), are solved in MATLAB using Euler's method. The steady-state silica cycle represented in Figure 2 is taken as the initial condition. After verifying that the state variables exhibit no drift under time-invariant conditions, a time-dependent change in forcing is imposed, as detailed below. The system behavior is monitored for a period of 150 years, using an integration time step of 0.01 y. The starting time of the imposed perturbations is nominally set to 1950.

To simulate the response of the Si cycle to a global temperature increase, three different time-courses for mean surface air temperature are considered (low, medium and high; Figure 3), based on projections of the Intergovernmental Panel on Climate Change (IPCC, 1995). The three scenarios diverge after the year 2000. For simplicity, linear functions are used to describe the rising air-temperature. Temperatures of surface waters (Box 1a, Box 2, Box 3 and Box 4a) are assumed to follow air temperature, while the magnitude of the temperature rise of the intermediate oceanic waters is four times lower (Levitus, 2000). The initial temperature of the intermediate water is set to 5°C (Yool and Tyrell, 2003).

The processes that are directly affected by temperature in the simulations are biological DSi uptake, bSiO_2 dissolution and chemical weathering. The model assumes that, at the spatial and temporal scales resolved, an increase (decrease) in siliceous phytoplankton production results in an increase (decrease)

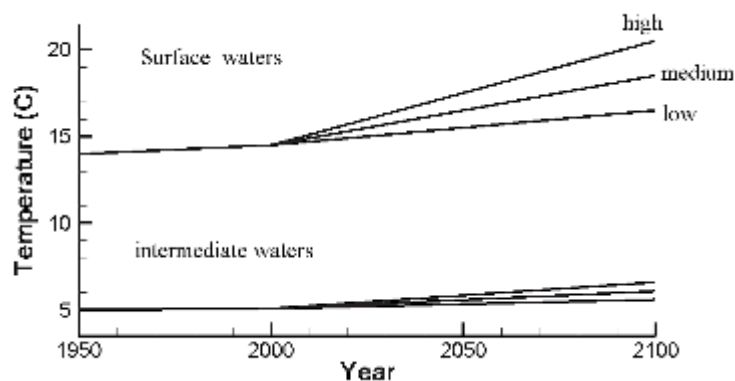


Figure 3: Temperature scenarios for surface and intermediate waters used as forcing functions in the simulations.

in DSi fixation. In particular, we assume that a temperature-dependent change in primary production by diatoms causes a proportional change in DSi uptake. The temperature dependence of DSi uptake in continental and marine environments is described by the Eppley function (uptake rate $\propto e^{(0.07 \cdot T)}$, where T is temperature in °C, Eppley, 1972). This exponential function is widely used to describe the response of planktonic communities to temperature variations, except under extreme temperature conditions (Pasquer et al., 2005). This formulation implies the assumption that changes in DSi uptake linearly follow diatom growth. In the absence of relationships specifically describing the temperature dependence of DSi uptake by higher plants on land, we opt for a simple Q_{10} function, whereby the uptake rate doubles with every 10°C temperature increase (Winkler et al., 1996). The Arrhenius equation is used to correct the rates of bSiO₂ dissolution and silicate weathering (Lasaga, 1998). Reported activation energies for the dissolution of framework silicates and bSiO₂ fall mostly in the range 25-90 kJ mol⁻¹ (Blum and Stillings, 1995; Van Cappellen et al., 2002). Here, a single Arrhenius activation energy of 60 kJ mol⁻¹ is imposed, to account for the effect of temperature changes on both silicate rock weathering and bSiO₂ dissolution.

Another major effect of human activity on the cycling of reactive Si at the Earth's surface is the construction of dams, known to trap large quantities of bSiO₂ (Conley et al., 2000; Humborg et al., 2006). To test the sensitivity to damming, a

correction coefficient is added to the flux equation describing bSiO_2 accumulation in sediments on the continents (F_{C4C5}). This coefficient is assigned a value of 1 at the start of the simulation and afterwards varies proportionally with changes in the number of dams. Gleick (2003) has projected future damming pressure over the next 25 years by relating global water use to the number of new dams (Rosenberg et al., 2000). Based on this work, and the assumption that global water use is proportional to the world's population, we estimate that the number of dams should increase by 20% with an increase of the world's population by 1.9 billion people. Three damming scenarios are then considered, based on three projections for the change in the world population until the year 2100 (UN, 2005). The low, medium, and high damming scenarios are shown in Figure 4.

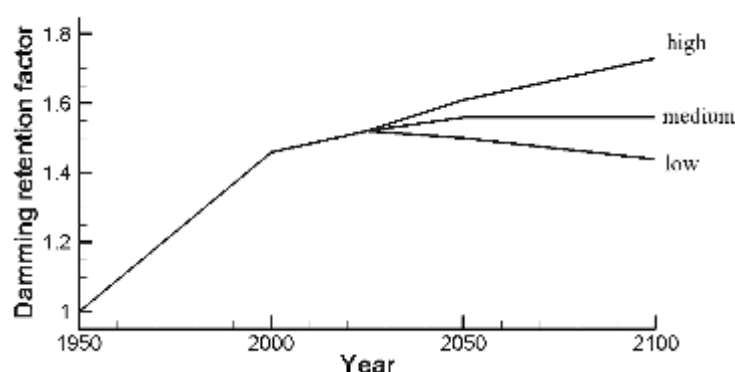


Figure 4: River damming scenarios used in the simulations. The three curves represent the relative change in damming pressure, relative to 1950, for low, medium and high damming scenarios.

Additional effects of anthropogenic modifications of the earth surface environment are likely to affect Si cycling along the land-to-ocean continuum. On the time scales considered here (≤ 150 years), shifts in precipitation patterns and vegetation, changes in land-use and erosion will affect the cycling of Si on land and the delivery of reactive Si to the oceans (Conley et al., 2008). On even longer time scales, changes in thermohaline circulation accompanying a warming of the surface ocean will modify the exchanges of DSi between the surface and deeper parts of the oceans, thereby affecting marine biosiliceous productivity

(see, e.g., Yool and Tyrell, 2005). A complete assessment of the response of the biogeochemical Si cycle to human-induced global change will thus require further work.

3. Results and Discussion

3.1. The global silica cycle

Most previous global scale mass balance studies of the Si cycle have focused on the oceans (Tréguer et al., 1995; De Master, 2002; Ragueneau et al., 2002; Yool and Tyrell, 2003, 2005; De La Rocha and Bickle, 2005). A novelty of the Si cycle presented here is that it includes an explicit representation of DSi and bSiO₂ cycling on the continents. Nevertheless, due to the relative scarcity of data, the estimates of the continental reservoir masses and fluxes have large uncertainties associated with them. For instance, the calculation of bSiO₂ stock in soils assumes an average concentration of 5 mg phytoliths per g of soil. While the latter value is consistent with the bSiO₂ determinations in soils that have been made so far (Alexandre et al., 1997; Conley, 2002b; Clarke, 2003; Sferratore et al., 2006), it remains to be seen how representative the relatively limited set of existing measurements is for the global soil reservoir.

According to our estimates, phytoliths in soils and living terrestrial biomass constitute the largest fraction (65%) of the continental reactive Si reservoir. The amount of Si fixed by terrestrial and aquatic organisms on the continents on a yearly basis is estimated to be 89 Tmol y⁻¹. This value lies within the range of 60-209 Tmol y⁻¹ given in the literature (Conley, 2002b) and is of the same order of magnitude as the rate of Si fixation in the oceans (244 Tmol y⁻¹). Thus, Si biomineralization on the continents is an important component of biological Si cycling on Earth (Conley, 2002a). As in the marine realm, siliceous productivity on the continents relies on the efficient regeneration of nutrient DSi through bSiO₂ dissolution. In our budget, 80% of the continental bSiO₂ produced is recycled, while the remainder accumulates in lacustrine sediments and in soils (Kendrick and Graham, 2004), or is exported to the oceans. Based on the estimates in Figure 2, the residence time of reactive Si on the continents is estimated to be 775 years.

Most reactive Si is delivered to the oceans by rivers under the form of

DSi (F_{CIP1} ; 6.2 Tmol y^{-1}). Nonetheless, the alternative supply routes of riverine bSiO₂ delivery (F_{C4P2} ; 1.1 ± 0.2 Tmol y^{-1}), submarine groundwater discharge (F_{CIP1} ; 0.4 ± 0.4 Tmol y^{-1}) and atmospheric transport (F_{C2O2} ; 0.5 ± 0.5 Tmol y^{-1}), together contribute about 25% of the transfer of reactive Si from the continents to the oceans. When hydrothermal inputs are also included (F_{hyd} ; 0.6 ± 0.4 Tmol y^{-1}), we estimate the total reactive Si delivery to the ocean to be 8.8 ± 1.5 Tmol y^{-1} . In comparison, Tréguer et al. (1995) estimated the total reactive Si supply to the oceans to be 6.7 ± 1.5 Tmol y^{-1} . These authors, however, did not account for the reactive Si input from groundwater discharge and riverine bSiO₂. It should further be recognized that all regional sources of Si may not have been identified yet. For example, the venting of crustal fluids in the North Pacific has only recently been suggested to contribute as much as 1.5 ± 0.5 Tmol y^{-1} to the global oceanic Si budget (Johnson et al., 2006).

Assuming an initial steady-state, the sum of the inputs to the ocean is balanced by that of the outputs, and thus burial and reverse weathering should together yield a total removal flux of 8.8 Tmol y^{-1} . This value falls within the range for total reactive Si removal from the ocean of 8.4 to 9.4 Tmol y^{-1} , obtained when combining the estimated sediment burial fluxes of biogenic Si of DeMaster (2002; 7.4 - 8.4 Tmol y^{-1}) with that for reverse weathering (1.0 Tmol y^{-1}).

The explicit consideration of the proximal coastal zone enables us to account for the important filter function of estuaries, lagoons and embayments in nutrient cycles (Rabouille et al. 2001; Wollast, 1993; Seitzinger, 1996; Mackenzie et al., 2000). Significant Si processing decreases the DSi/bSiO₂ ratio from around 3 in rivers to 1.2 in the proximal zone. A net transformation of DSi into bSiO₂ is commonly observed in nearshore environments and causes a large fraction (43%, according to our model) of reactive Si to be delivered from the proximal to the distal coastal zone in the form of bSiO₂.

The fluxes in Figure 2 emphasize the role of the continental margins in removing reactive Si by sediment burial. Although the proximal and distal zones are only responsible for about 18% of the total biological fixation of DSi in the oceans, they may account for 40% of the total marine bSiO₂ burial, in line with the assessment of DeMaster (2002). The sum of the bSiO₂ burial fluxes in the proximal

and distal coastal zones in our budget (3.1 Tmol y⁻¹) corresponds to the maximum of the range estimated by DeMaster (2002) for bSiO₂ burial along the continental margins (2.4 - 3.1 Tmol y⁻¹). It should be noted, however, that DeMaster's oceanic silica budget omits riverine supply of bSiO₂ and groundwater DSi discharge. Our relatively high estimate for bSiO₂ accumulation in coastal sediments is consistent with the inclusion of these additional reactive Si inputs to the coastal zone, as well as the upward revision of the riverine DSi supply (6.2 versus 5.6 Tmol y⁻¹). The preferential burial of bSiO₂ in nearshore and shelf sediments is not only due to the relatively high sedimentation rates, but also to enhanced preservation resulting from interactions between deposited bSiO₂ and constituents solubilized from lithogenic minerals and the formation of new aluminosilicate phases (Van Cappellen et al., 2002; Dixit and Van Cappellen, 2003; Michalopoulos and Aller, 1995, 2004). In the proximal zone and especially in deltaic settings, there is a tight coupling between biogenic Si burial and reverse weathering, and analytical procedures for the measurement of biogenic silica account for reverse weathering products (Michalopoulos et al, 2000, Michalopoulos and Aller 1995, 2004., Presti and Michalopoulos 2008). Thus, the Si burial flux used here for the proximal zone may include reverse weathering products.

The main inflow of DSi to the distal zone is caused by coastal upwelling, which is estimated to be on the order of 10 Tmol y⁻¹ (Figure 2). The intermediate water masses of the open ocean (100-1000 m water depth) are assumed to be the source region for coastal upwelling. This assumption is consistent with mesopelagic DSi concentrations (25-30 μmol kg⁻¹; Dittmar and Birkicht, 2001; Brezinski et al., 1997), and Si/N ratios close to one (Hill and Wheeler, 2002; Brzezinski et al., 1997) reported for coastal upwelling waters. Deeper source regions (i.e., >1000 m) would yield higher DSi concentrations and Si/N ratios between 2 and 3 (Sverdrup et al., 1942).

Tréguer et al. (1995) estimated the whole-ocean residence time of reactive Si to be on the order of 15000 years. The latter value likely represents a lower limit, however, as these authors excluded the active surface layer of marine sediments in their calculation. According to the reservoir masses considered here, reactive Si in the water column and surface sediments of the proximal coastal zone, distal coastal

zone, plus the open ocean amounts to 149927 Tmol. The removal rate of reactive Si through burial and reverse weathering of 8.8 Tmol y⁻¹ then implies a whole-ocean residence time of 17037 years. If the proximal coastal zone is excluded, the oceanic residence time of reactive Si is 20245 years. Estimated residence times for various marine reservoirs and their combinations are summarized in Table 4.

Table 4: Reactive silica contents and residence times in the various compartments of the earth surface environment.

	<i>DSi + bSiO₂</i> (Tmol Si)	<i>Export + Burial</i> (Tmol Si y ⁻¹)	<i>Residence</i> <i>time (y)</i>	<i>Uptake /</i> <i>(Export+ Burial)</i>
Continents (box1)				
Terrestrial	11310	14.6	775	0.9
Rivers and Lakes	24.1	10.1	2.1	5.5
River and Lakes + Sediment	1441.1	10.1	143	-
Proximal Coastal Zone (box 2)				
Water Column	5.6	7.7	0.7	0.6
Water Column + Sediment	115.6	7.7	15	-
Distal Coastal Zone (box 3)				
Water Column	104	16.3	4.9	2.5
Water Column + Sediment	2295	16.3	141	-
Open Ocean (box 4)				
Water Column	96875	14.6	6635	13.7
Water Column + Sediment	147517	14.6	10104	-
World Ocean (box 2+3+4)				
Water Column	96984.6	8.8	11021	27.8
Water Column + Sediment	149927.8	8.8	17037	-

Interestingly, the residence times of reactive Si in the open ocean (10104 years) and the distal coastal zone (141 years) alone are significantly lower than the whole-ocean residence time (17037 years). This reflects the large exchange fluxes of reactive Si between the continental margins and the open ocean. For the distal zone in particular, these exchanges dominate the inputs and outputs of reactive Si and, hence, explain the relatively short residence time of reactive Si on the continental shelves.

Water column residence times of reactive Si are somewhat shorter than the corresponding water residence times (Table 4), because sinking of bSiO₂ by sedimentation decouples the Si cycle from the water cycle. Nonetheless, they are significantly lower than the values obtained when including sediments. The relative

differences are particularly large for the proximal and distal coastal zone, because of the importance of benthic exchange fluxes of reactive Si. This is especially the case in the distal coastal zone, where benthic regeneration of silica accounts for nearly one-third of the reactive Si influx and is, therefore, a major source of reactive Si sustaining siliceous productivity in the overlying water column (Ragueneau et al., 2005).

3.2. Sensitivity analysis

To identify the most sensitive processes controlling Si cycling across the continent-ocean transition, we compute the relative changes in water column DSi and bSiO₂ concentrations of the coastal proximal and distal zones, induced by varying the rate constants k_{ij} in the flux equations (Equation 2). In each simulation the value of one rate constant is increased by 50%, while all other model parameters remain unchanged. The sensitivity of the model to continental rock weathering (F_w) is similarly tested by increasing the value of F_w by 50%. Sensitivities are expressed as relative changes in DSi and bSiO₂ concentrations after 150 years of simulation time, relative to the initial, steady-state values.

The rate constants included in the sensitivity analysis correspond to the reactive Si fluxes that are not directly coupled to the water cycle via Equation (1). These fluxes include uptake and biomineralization of DSi, dissolution, sedimentation, and burial of bSiO₂, plus DSi efflux across the sediment-water interface. In addition, on the time scale considered (150 years), Si cycling in the proximal zone is not affected by processes occurring in the downstream distal coastal zone and open ocean reservoirs. Hence, the sensitivity analysis for the proximal zone is further limited to rate constants k_{ij} corresponding to processes occurring in the upstream, continental reservoir or within the proximal zone itself. In contrast, Si cycling in the distal coastal zone may also be affected by processes in the downstream open ocean reservoir, because of the return of oceanic waters onto the shelves via coastal upwelling.

The results of the sensitivity analysis are summarized in Table 5. DSi and bSiO₂ concentrations of proximal coastal waters are most sensitive to chemical weathering of continental rocks (F_w), terrestrial (F_{C1C2}), riverine (F_{C3C4})

Table 5: Sensitivity analysis: % change in DSi and bSiO₂ concentrations in proximal (Box 2) and distal coastal zone (Box3) 150 years after increasing the corresponding flux or rate constant by 50%.

Modified parameter	Type of process	in box 2		in box 3	
		% DSi	% bSiO ₂	% DSi	% bSiO ₂
Fw	Weathering	7	6	2	2
k _{C1C2}	Uptake	-13	-11	-3	-4
k _{C2C1}	Dissolution	14	12	3	4
k _{C3C4}	Uptake	-15	-9	-3	-4
k _{C4C3}	Dissolution	13	8	3	3
k _{C4C5}	Sedimentation	-10	-13	-3	-4
k _{C5-burial}	Burial	-1	-1	0	0
k _{C5C3}	Dissolution	5	5	1	1
k _{P1P2}	Uptake	-21	15	-2	-1
k _{P2P1}	Dissolution	5	-4	0	0
k _{P2P4}	Sedimentation	0	-15	-2	-2
k _{P3P1}	Efflux	0	0	0	0
k _{P4-burial}	Burial	-2	-2	-1	-1
k _{P4P3}	Dissolution	3	3	1	1
k _{S1S2}	Uptake	-	-	-25	11
k _{S2S1}	Dissolution	-	-	21	-10
k _{S2S4}	Sedimentation	-	-	-9	-17
k _{S3-rw}	Reverse weathering	-	-	-2	-2
k _{S3S1}	Efflux	-	-	2	2
k _{S4-burial}	Burial	-	-	-1	-1
k _{S4S3}	Dissolution	-	-	10	9
k _{O1O2}	Uptake	-	-	0	0
k _{O2O1}	Dissolution	-	-	0	0
k _{O4O3}	Dissolution	-	-	1	1
k _{O6O5}	Dissolution	-	-	0	0
k _{O6O8}	Sedimentation	-	-	0	0
k _{O7O5}	Efflux	-	-	0	0
k _{O8-burial}	Burial	-	-	0	0
k _{O8O7}	Dissolution	-	-	0	0

and proximal coastal siliceous production (F_{P1P2}), and bSiO₂ dissolution on the continents (F_{C2C1} , F_{C4C3} , F_{C5C3}). Overall, enhanced production and sedimentation lead to lower DSi and bSiO₂ concentrations, while increased dissolution results in larger stocks of reactive Si in the water column. The main difference in the sensitivity of DSi and bSiO₂ concentrations in the proximal zone is related to the

deposition of bSiO₂ in nearshore sediments (F_{p2p4}). While increasing k_{p2p4} causes a significant drop (-15%) of the bSiO₂ concentration in proximal waters, the DSi concentration is hardly affected. The latter reflects the fact that internal recycling of DSi via dissolution of bSiO₂ within the proximal zone (F_{p2p1} , F_{p4p3}) is much less important than continental DSi input (Figure 2). Thus, with the exception of nearshore siliceous production, reactive Si dynamics in the proximal zone are primarily controlled by processes taking place on the continents.

The sensitivity analysis reveals a different picture for the distal coastal zone (Table 5). DSi and bSiO₂ concentrations in the distal coastal waters are most sensitive to internal processes. These include DSi uptake and bSiO₂ dissolution in the water column (F_{s1s2} , F_{s2s1}), as well as deposition (F_{s2s4}) and dissolution of bSiO₂ in the sediments (F_{s4s3}). Among the sensitive upstream processes, those on the continents, especially terrestrial bSiO₂ production and dissolution (F_{c1c2} , F_{c2c1}) and weathering (F_w), are more important than those in the adjacent proximal coastal zone, although absolute changes larger than 4% are not observed. Reactive Si cycling in the distal coastal zone is also sensitive to downstream processes, foremost open ocean water column dissolution and sinking of bSiO₂ (F_{o4o3} , F_{o4o6}), as these processes control the accumulation of DSi in the source waters of coastal upwelling.

On the time scale investigated, permanent removal of reactive Si through burial plays a minor role in Si cycling at the Earth's surface. This contrasts with the dominant role of sedimentary burial in the global biogeochemical Si cycle on geological time scales (De Master, 2002; Van Cappellen, 2003). Nonetheless, even on the time scale of decades and centuries, benthic-pelagic coupling is crucial to Si cycling in distal coastal waters (Conley, 1997; Ragueneau et al., 2002, 2005), as indicated by the high sensitivities to the deposition (F_{s2s4}) and subsequent benthic dissolution of bSiO₂ (F_{s4s3}).

Changes in Si cycling at the land-ocean transition may also be caused by changes in the water cycle. Nevertheless, reliable scenarios for the future evolution of the water cycle are difficult to constrain. In addition to bSiO₂ retention, river damming causes a decrease of net river flow to the oceans. In the proximal coastal zone, a reduction by 20% of the river discharge (W_{1a2}) to the oceans results,

after 150 years, in a relatively small decrease (4 %) in the concentration of DSi, but no change in that of bSiO₂. For the distal coastal zone, the corresponding changes are 3 and 4 % reductions in the concentrations of DSi and bSiO₂. The latter concentrations are further reduced (by 5 and 4 %, respectively) when the decrease in river discharge by 20% is accompanied by a 20% reduction in the coastal upwelling water flux (W_{43}). On longer time scales, changes in the water cycle (e.g., upwelling) may have significantly larger effects on global Si cycling (e.g., Yool and Tyrell, 2005).

3.3. Applications

Temperature rise

The three temperature scenarios yield the same general trends, but with different magnitudes (Figure 5). Except for open surface ocean DSi, increasing temperatures result in higher water column DSi and bSiO₂ concentrations. bSiO₂ concentrations in sediments of the continents and deep-sea are hardly affected, while they show opposite trends in the proximal (increase) and distal coastal ocean (decrease).

Rising concentrations of DSi and bSiO₂ in the continental aquatic environment (Box 1a, Figure 2) reflect enhanced DSi fluxes from weathering and bSiO₂ dissolution in soils. In combination with the relatively small volume of the aquatic environment, this causes significant, and parallel, increases in the DSi and bSiO₂ concentrations. Because of more rapid bSiO₂ dissolution kinetics, the additional reactive Si mobilized does not accumulate in sediments and soils, but is exported to the ocean.

Increased continental supply of reactive Si enhances siliceous productivity in proximal and distal coastal ecosystems. The largest relative change is observed in the bSiO₂ concentration of nearshore waters. That is, increased temperatures further decrease the water column DSi/bSiO₂ ratio of the proximal zone. The higher deposition flux of bSiO₂ offsets the faster bSiO₂ dissolution kinetics, resulting in a net increase in the bSiO₂ concentration of proximal coastal sediments. Sediment bSiO₂ concentrations in the distal coastal zone show an opposite response, reflecting the very different recycling efficiencies of reactive Si in the two coastal systems

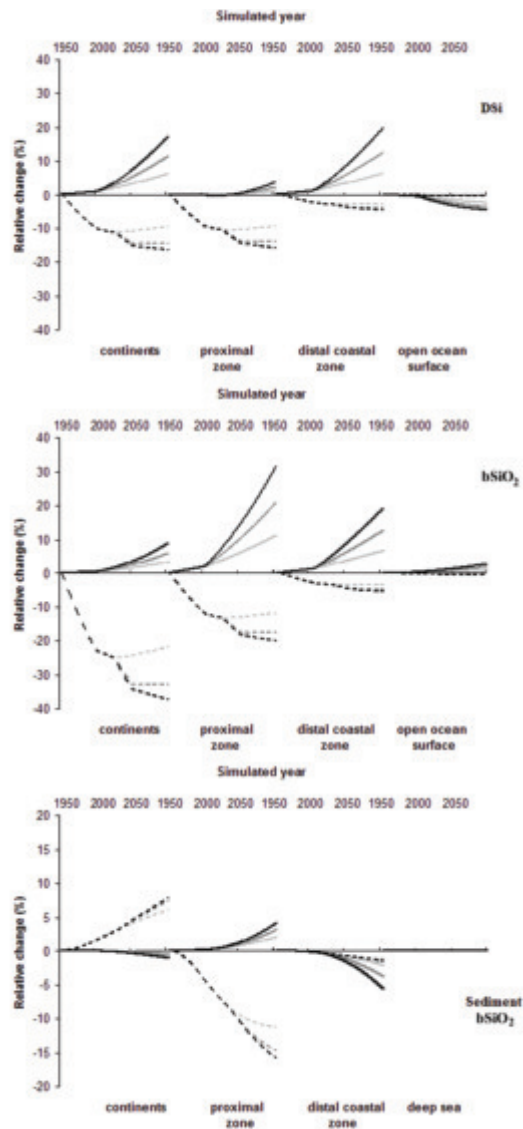


Figure 5: Relative changes in DSi (top), water column bSiO₂ (middle) and sediment bSiO₂ (bottom) reservoir sizes versus time for the three different temperature (continuous lines), and damming (dashed lines) scenarios. In black, the high temperature or damming scenario, in gray the medium temperature or damming scenario, and in light gray the low temperature or damming scenario.

(Figure 2). The latter is also reflected in the relative increases in water column DSi and bSiO₂ concentrations. In the proximal zone, rising temperatures cause a larger relative increase in bSiO₂, compared to DSi, while the reverse is observed for the distal zone. Possible indicators of a global warming effect on the Si cycle thus include opposite changes of water column DSi/bSiO₂ ratios and sediment bSiO₂ accumulation rates in proximal versus distal coastal environments.

Because of its much larger volume and of the buffering effect of the coastal zone, the open ocean exhibits much smaller modifications in Si cycling. The most pronounced changes are in the surface ocean, as it directly experiences changes in air temperature. Both DSi uptake and bSiO₂ dissolution rates are enhanced by rising temperature, resulting in faster Si turnover in the upper ocean. For the model structure and parameter values used here, the net effect is a slight increase in the bSiO₂ standing stock, at the expense of the DSi pool.

River damming

River damming leads to opposite trends of DSi and bSiO₂ concentrations compared to those of temperature rise, with the exception of bSiO₂ in distal coastal sediments (Figure 5, broken lines). Predicted concentration changes also imply that damming should increase water column DSi/bSiO₂ ratios in continental aquatic systems and the proximal coastal zone. A number of studies have indeed reported measurable increases in DSi/bSiO₂ ratios of riverine and nearshore waters (Conley 1997, 2002b; Friedl and Wuest, 2002).

As expected, the sedimentary bSiO₂ pool on the continents increases as biosiliceous debris accumulates behind the growing number of dams. The decreased continental supply of reactive Si causes a relative drop in sediment bSiO₂ in nearshore marine sediments and an increase on the continents. It should be borne in mind, however, that the reservoir size of proximal coastal zone sediment bSiO₂ (110 Tmol Si) is much smaller than that of continental sediments (1417 Tmol Si). At the scale investigated in our simulations, damming causes more bSiO₂ to be trapped in continental sediments than lost from proximal sediments.

A general feature of the response of Si cycling to changes in damming is the “dilution” of the relative effects from rivers to the open ocean (Figure 5).

Typically, the largest changes in reactive Si concentrations are observed in aquatic systems on land and in the proximal coastal zone, while the open ocean system experiences little changes. For example, the open ocean surface DSi concentration is predicted to change by less than 1% after 150 years, even for the highest damming scenario.

According to the damming scenarios, the largest increase in the number of dams should have taken place between the 1950s and the present. After 2000, the different damming scenarios hypothesize the same decreasing damming pressure until 2025, after which the three scenarios diverge (Figure 4). The time-dependent features imposed to the damming scenarios are recorded nearly instantaneously by the water column DSi and bSiO₂ concentrations in the continental aquatic system and the proximal coastal zone, because of the correspondingly very short residence times of reactive Si (2.1 and 0.7 years, Table 4). This is not the case for the sediment bSiO₂ concentrations in the same reservoirs. Because of much longer residence, and hence response times, the initial trends (i.e., for the period 1950-2000) are projected into the future with still little differentiation in sediment bSiO₂ concentrations among the scenarios by the year 2050.

Combined river damming and temperature rise

A set of nine permutations of the three temperature and three damming scenarios were run. The results are illustrated in Figure 6 for the intermediate temperature rise plus maximum damming scenario. This particular scenario was selected because it exhibits the main features observed in all the various simulations. The comparison between Figures 5 and 6 suggests that river damming is driving the changes in Si cycling in the combined scenario, particularly during the initial period (1950-2000). On the continents, the results of the combined simulation closely follow those of the damming-only simulation, except for the slight rise in water column DSi concentration simulated beyond 2050. The slowing down of dam construction after 2000 and continued rise in temperature cause much more pronounced reversals in the water column DSi concentrations of the coastal ocean. By the end of the simulation, the DSi concentration in the proximal zone has returned to within 2% of its starting value, while in the distal zone the DSi

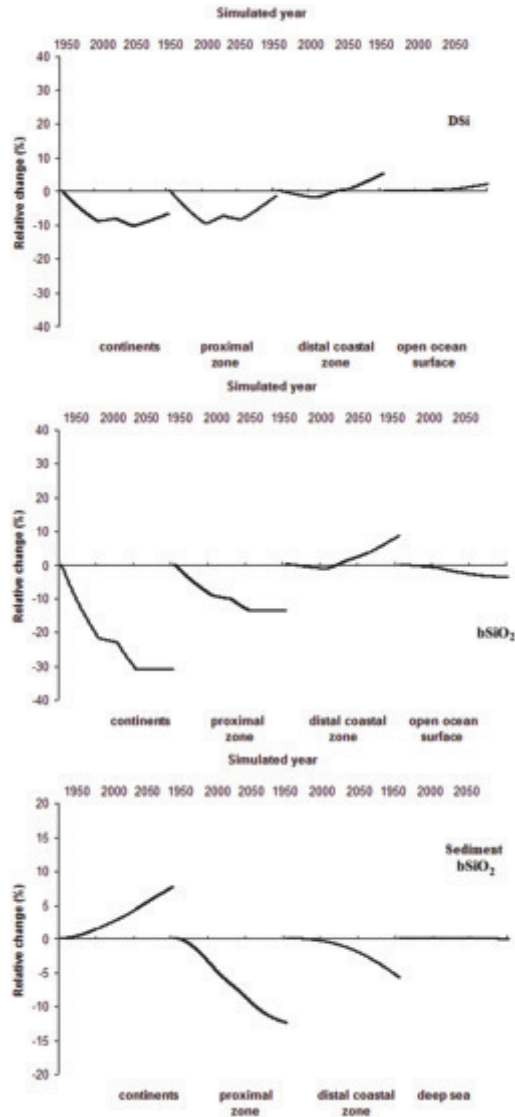


Figure 6: Relative changes in DSi (top), water column bSiO₂ (middle) and sediment bSiO₂ (bottom) reservoir sizes versus time for the combined scenario with high damming and medium temperature forcing.

concentration increases above the initial value.

The water column bSiO₂ concentration in the proximal coastal zone mainly records the changing damming pressure. This is no longer the case for the distal

coastal zone, since reactive Si cycling in this reservoir is largely driven by internal recycling, via temperature-dependent DSi uptake and bSiO₂ dissolution. Thus, as far as the water column DSi and bSiO₂ concentrations are concerned, when moving from the continents to the open ocean, the relative influence of changes in river damming decreases, while that of global warming increases.

Changes in sediment bSiO₂ concentrations in the combined scenario are essentially the same as in the damming-only scenario, for all reservoirs. The lack of temperature-induced changes reflects the much longer residence times of reactive Si in the sediment reservoirs, relative to the water column. That is, over the 150 years of simulation time, the sediments only record the initial rapid growth in the number of dams after the 1950s. The observed loss of sediment bSiO₂ in coastal environments over the simulation period is therefore mainly due to reactive Si retention by dams.

The results presented in Figures 5 and 6 illustrate the complex response of Si cycling to human influences. In particular, the temporal trends in DSi and bSiO₂ concentrations in the combined damming plus temperature rise scenario are not simply the sum of the individual responses to the two perturbations. Nonetheless, the results also indicate that by combining temporal trends in DSi and bSiO₂ concentrations in multiple reservoirs it may become possible to extricate the relative effects of the different anthropogenic forcings acting on the biogeochemical Si cycle.

4. Conclusions

Silicon is a key nutrient whose biogeochemical cycling is closely coupled to those of carbon, nitrogen, phosphorus, iron and trace compounds. Large amounts of dissolved Si (DSi) are biologically fixed annually as biogenic silica (bSiO₂), both on land (89 Tmol y⁻¹) and in the oceans (240 Tmol y⁻¹). The estimated residence time of reactive Si on the continents (775 years), however, is about 20 times smaller than for the oceans (17037 years), reflecting the much larger marine reservoir of reactive Si.

While reactive Si is mainly exported from the continents as riverine DSi (6.2 Tmol y⁻¹), a non-negligible fraction is delivered to the oceans as bSiO₂ in

river suspended matter and in eolian dust deposits (1.6 Tmol y⁻¹), and as DSi in submarine groundwater discharge (0.4 Tmol y⁻¹). Because of the net transformation of DSi into bSiO₂ in nearshore waters, nearly half (43%) of land-derived reactive Si reaching the distal coastal zone is in the form of bSiO₂. Nevertheless, the major input of reactive Si to the continental shelves is via coastal upwelling.

The coastal ocean represents a dynamic interface between the continents and the open ocean. Although coastal and shelf environments account for only 18% of all biological Si fixation in the oceans, an estimated 40% of all marine bSiO₂ burial takes place in nearshore and shelf sediments (3.2 Tmol y⁻¹). Nearshore ecosystems also attenuate the downstream propagation of land-based perturbations of the Si cycle that results from damming of rivers or land-use changes.

The biogeochemical Si cycle is currently undergoing significant modifications due to human activities. The proposed model can help delineate the expected changes, through sensitivity analyses and scenario simulations. A major difficulty is that multiple anthropogenic perturbations are simultaneously acting on the Si cycle. The results presented here, and observed changes in rivers and nearshore waters, indicate that riverine export of reactive Si, and the riverine bSiO₂/DSi ratio, are likely to continue to drop in the near future, as a result of reactive Si retention by dams. However, enhanced bSiO₂ dissolution due to global warming may ultimately allow coastal siliceous productivity to recover from the downward trend caused by river damming.

Our work represents a first step towards modeling the global biogeochemical Si cycle along the entire land to ocean continuum. Further progress will rely especially on the increased understanding and characterization of the spatial heterogeneity of continental Si cycling, caused by differences in lithology, vegetation, land-use and hydrology. This information is needed to account for the regional variability in reactive Si delivery to the coastal zone by rivers and submarine groundwater discharge.

Acknowledgements

This project was initiated during the 2004 Summer School of the EU-funded Research Training Network SiWEBS (contract number HPRN-CT-2002-000218).

Further work on the project was made possible by financial support from the EU (SiWEBS), Utrecht University (High Potential project G-NUX to C.P. Slomp) and the Netherlands Organisation for Scientific Research (NWO Pioneer grant to P. Van Cappellen). We thank the editor and the anonymous reviewers for their useful and constructive comments.

References

- Alexandre, A., J.-D. Meunier, F. Colin and J. M. Koud (1997) Plant impact on the biogeochemical cycle of silicon and related weathering processes. *Geochim. Cosmochim. Acta*, 61, 677-682.
- Alvarez-Salgado, X.A., C.G. Castro, F.F. Pérez and F. Fraga (1997) Nutrient mineralization patterns in shelf waters of the Western Iberian upwelling, *Continental Shelf Research* 17, 1247–1270.
- Anikouchine, W.A and R.W. Sternberg (1981) *The World Ocean: An Introduction to Oceanography*, Prentice-Hall, NJ, USA.
- Appelo, C. A. J. and D. Postma (1993) *Geochemistry, Groundwater and Pollution*, Balkema, Amsterdam.
- Arhondistis, G. E. and M. T. Brett (2005) Eutrophication model for Lake Washington (USA) Part II—model calibration and system dynamics analysis. *Ecological Modelling*, 187, 179-200.
- Batjes, N.H. (1997) A world data set of derived soil properties by FAO UNESCO soil unit for global modeling, *Soil Use Manage.* 13, 9–16.
- Bartoli, F. (1983) The biogeochemical cycle of silicon in two temperate forest ecosystems. *Ecological Bulletin* 35, 469–476.
- Berelson, W. M., D. E. Hammond and K. S. Johnson (1987) Benthic fluxes and the cycling of biogenic silica and carbon in the two southern California Borderland Basins. *Geochim. Cosmochim. Acta*, 51, 1345–1363.
- Berner, E. A. and R. A. Berner (1996) *Global Environment: Water, Air and Geochemical Cycles* Prentice-Hall.
- Biscaye, P. E., C. N. Flagg and P. G. Falkowski (1994) The shelf edge exchange processes experiment, SEEP-II: an introduction to hypotheses, results and conclusions. *Deep-Sea Res. II*, 41, 231-252.
- Blum, A.E. and L.L. Stillings (1995) Feldspar dissolution kinetics, in *Chemical Weathering Rates of Silicate Minerals* edited by A.E. White and S.L. Brantley, pp. 291-351. Mineralogical Society of America.
- Bonn, W.J. (1995) Biogenic opal and barium: Indicators for late Quarternary changes in productivity at the Antarctic continental margin, Atlantic Sector. *Reports on Polar Research*, 180, 186pp., Alfred Wegener Institute

for Polar and Marine Research, Bremerhaven.

- Brink, K. H., F. F. G. Abrantes, P. A. Bernal, R. C. Dugdale, M. Estrada, L. Hutchings, R. A. Jahnke, P. J. Muller and R. L. Smith (1995) Group report: How do coastal upwelling systems operate as integrated physical, chemical, and biological systems and influence the geological record?, in *Upwelling in the Ocean: Modern Processes and Ancient Records* edited by C. P. Summerhayes, K.-C. Emeis, M. V. Angel, R. L. Smith and B. Zeitzeschel, pp. 103–124.
- Broecker, W.S. and T.-H. Peng (1982) *Tracers in the Sea*. A publication of the L-D geological Observatory. Columbia University, Palisades, New York. Eldigio Press.
- Brzezinski, M.A., D. R. Phillips, F. P. Chavez, G. E. Friederich and R. C. Dugdale (1997) Silica production in the Monterey, California, upwelling system. *Limnol. Oceanogr.*, 42, 1694-1705.
- Chauvaud, L., F. Jean, O. Ragueneau and G. Thouzeau (2000) Long-term variation of the Bay of Brest ecosystem: benthic–pelagic coupling revisited. *Mar. Ecol. Prog. Series*, 200, 35–48.
- Chameides, W. L. and E. M. Perdue (1997) *Biogeochemical Cycles. A Computer-Interactive Study of Earth System Science & Global Change*. Oxford University Press, New York / Oxford, 1997
- Clarke, J. (2003) The occurrence and significance of biogenic opal in the regolith, *Earth Sci Rev.*, 60, 175-194.
- Cole, J. M., Goldstein, S. L., deMenocal, P. B., Hemming, S. R. and F. E. Grousset (2009) Contrasting compositions of Saharan dust in the eastern Atlantic Ocean during the last deglaciation and African Humid Period. *Earth and Planetary Science Letters*, 278, 257–266.
- Conkright, M., S. Levitus and T. P. Boyer (1994) NOAA Atlas NESDIS 1. World Ocean Atlas 1994, Nutrients, vol. 1, U.S. Government Printing Office, Washington, D.C., USA.
- Conley, D. J. (1988) Biogenic silica as an estimate of siliceous microfossil abundance in Great-Lakes sediments. *Biogeochemistry*, 6(3), 161-179.
- Conley, D. J. (1997) Riverine contribution of biogenic silica to the oceanic silica

- budget. *Limnol. Oceanogr.*, 42, 774-777.
- Conley, D. J. (2002a) The biogeochemical silica cycle: Elemental to global scales. *Océanis*, 28, 353-368.
- Conley, D. J. (2002b) Terrestrial ecosystems and the global biogeochemical silica cycle. *Global Biogeochem. Cycle*, 16, 1121, doi: 10.1029/2002GB001894.
- Conley D.J., Kilham, S.S. and E. Theriot (1989) Differences in silica content between marine and freshwater diatoms. *Limnol. Oceanogr.* 34, 205-213.
- Conley, D. J., C.L. Schelske, and E.F. Stoermer (1993) Modification of the biogeochemical cycle of silica with eutrophication. *Mar. Ecol. Prog. Series*, 101, 179-192.
- Conley, D. J., P. Stålnacke, H. Pitkänen, and A. Wilander (2000) The transport and retention of dissolved silicate from rivers in Sweden and Finland. *Limnol. Oceanogr.*, 45, 1850-1853.
- Conley, D. J. and T. C. Malone (1992) Annual cycle of dissolved silicate in Chesapeake Bay-implications for the production and fate of phytoplankton biomass. *Mar. Ecol. Prog. Series*, 81, 121-128.
- Conley D. J. and C. L. Schelske (2001) Biogenic silica. in: *Tracking Environmental Changes Using Lake Sediments: Biological Methods and Indicators*, edited by J. P. Smol, H. J. B. Birks and W. M. Last, pp. 281-293. Kluwer Academic Press, Dordrecht.
- Conley D. J., G. E. Likens, D. Buso, L. Saccone, S. W. Bailey, and C. Johnson (2008) Deforestation causes increased dissolved silicate losses in the Hubbard Brook Experimental Forest. *Global Change Biol.* 14, 2548-2554.
- Cossins, A.R. and K. Bowler (1987) *Temperature biology of animals*. Chapman and Hall, New York, New York.
- Datnoff, L. E., G. H. Snyder and G. H. Korndörfer (2001) *Silicon in agriculture*, edited by L. E. Datnoff, G. H. Snyder and G. H. Korndörfer, Elsevier Sci., Amsterdam.
- Del Amo, Y. and M.A. Brzezinski (1999) The chemical form of dissolved Si taken up by marine diatoms. *Journal of Phycology*, 35 (6), 1162-1170.

- De La Rocha, C. L. and M. J. Bickle (2005) Sensitivity of silicon isotopes to whole-ocean changes in the silica cycle, *Mar. Geol.*, 217, 267–282.
- DeMaster, D.J., (2002) The accumulation and cycling of biogenic silica in the Southern Ocean: revisiting the marine silica budget. *Deep-Sea Res. II*, 49, 3155-3167.
- Dittmar, T. and M. Birkicht (2001) Regeneration of nutrients in the northern Benguela upwelling and the Angola-Benguela Front areas, *South African Journal of Science*, 97(5-6), 239-246.
- Dixit, S. and P. Van Cappellen, (2003) Predicting benthic fluxes of silicic acid from deep-sea sediments. *J. Geophys. Res.*, 108(C10), 3334, doi:10.1029/2002JC001309.
- Dürr H.H., Meybeck M., Hartmann J., Laruelle G.G., Roubeix V. (submitted). Global spatial distribution of natural riverine silica inputs to the coastal zone. under review in *Biogeosciences Discussions*
- Egge, J.K. and D.L. Aksnes (1992) Silicate as a regulating nutrient in phytoplankton competition. *Mar. Ecol. Prog. Series*, 83, 281-189.
- Eppley, R. W. (1972) Temperature and phytoplankton growth in the sea. *Fishery Bull.*, 70, 1063-1085.
- Epstein, E. (1999) Silicon. *Ann. Rev. Plant Physiol. Plant Molec. Biol.*, 50, 641-664.
- Fekete, B.M., Vörösmarty, C.J. and W. Grabs (2002). High-resolution fields of global runoff combining observed river discharge and simulated water balances. *Global Biogeochemical Cycles*, 16(3), 1042, doi:10.1029/1999GB001254.
- Food and Agriculture Organization/U.N. Educational, Scientific and Cultural Organization (FAO/UNESCO), (1986). Gridded FAO/UNESCO soil units: UNEP/GRID, FAO soil map of the world in digital form, digital raster data on 2-minute geographic (lat x lon) 5400 x 10800 grid, Carouge, Switzerland.
- Friedl, G. and A. Wüest, (2002) Disrupting biogeochemical cycles – Consequences of damming. *Aquatic Science*, 64, 55-65.
- Friedl, G., C. Teodoru and B. Wehrli (2004) Is the Iron Gate I reservoir on the

- Danube River a sink for dissolved silica? *Biogeochemistry*, 68, 21-32.
- Garnier, J., A. D'Aygués, J. Billen, D. J. Conley and A. Sferratore (2002) Silica dynamics in the hydrographic network of the Seine River. *Océanis*, 28, 487-508.
- Garrels, R. M. and F. T. Mackenzie (1971) *Evolution of Sedimentary Rocks*, edited by W.W. Norton, 397pp., New York.
- Gerard, F. and J. Ranger (2002) Silicate weathering mechanisms in a forest soil. *Océanis*, 28, 384-415.
- Gibson, C.E., B.M. Stewart and R.J. Gowen (1997) A synoptic study of nutrients in the north-west Irish Sea, *Estuarine, Coastal and Shelf Science* 45, 27-38.
- Gleick, P.H. (2003) Global freshwater resources: Soft-path solutions for the 21st Century. *Science*, 302, 1524-1528.
- Heinze, C., E. Maier-Reimer, A. M. E. Winguth and D. Archer (1999) A global oceanic sediment model for long-term climate studies, *J. Geophys. Res.*, 13(1), pp. 221, doi:98GB02812.
- Heiskanen, A.S. and A. Keck (1996) Distribution and sinking rates of phytoplankton, detritus, and particulate biogenic silica in the Laptev Sea and Lena River (Arctic Siberia), *Mar. Chem.* 53, 229-245.
- Hill, J.K. and P. A. Wheeler (2002) Organic carbon and nitrogen in the northern California current system: comparison of offshore, river plume and coastally upwelled water. *Progress in Oceanography*, 53, 369-387.
- Humborg, C., D. J. Conley, L. Rahm, F. Wulff, A. Cociasu and V. Ittekkot (2000) Silicon retention in river basins: far-reaching effects on biogeochemistry and aquatic food webs in coastal marine environments. *Ambio*, 29(1), 45-51.
- Humborg, C., M. Pastuszak, J. Aigars, H. Siegmund, C. M. Morth, V. Ittekkot (2006) Decreased silica land-sea fluxes through damming in the Baltic Sea catchment - Significance of particle trapping and hydrological alterations. *Biogeochemistry* 77(2), 265-281.
- Jahnke, R. A., S. R. Emerson and J. W. Murray (1982) A model of oxygen reduction, denitrification, and organic matter mineralization in marine sediments.

- Limnol. Oceanogr., 27, 610-630.
- Johnson, H. P., S. L. Hautala, T. A. Bjorklund, and M. R. Zarnetske (2006) Quantifying the North Pacific silica plume. *Geochem., Geophys., Geosys.* 7: doi:10.1029/2005GC001065.
- Kendrick, K. J. and R. C. Graham. (2004) Pedogenic silica accumulation in chronosequence soils, Southern California. *Soil Sci. Soc. Amer. J.* 68, 1295-1303.
- Koning, E., G.-J. Brummer, W. Van Raaphorst, J. Van Bennekom, W. Helder and J. Van Ipperen (1997) Settling, dissolution and burial of biogenic silica in the sediments off Somalia (northwestern Indian Ocean). *Deep-Sea Res. II*, 44, 1341–1360.
- Lacroix, G., Ruddick, K., Park, Y., Gypens, N. and C. Lancelot (2007). Validation of the 3D biogeochemical model MIRO&CO with field nutrient and phytoplankton data and MERIS-derived surface chlorophyll a images. *Journal of Marine Systems* 64 (1–4), 66–88.
- Lasaga, A. C. (1981) Rate laws of chemical reactions, in *Kinetics of Geochemical Processes*, Vol. 8, edited by Lasaga, A. C. and R. J. Kirkpatrick, pp. 1–169. Mineralogical Society of America.
- Lasaga, A.C. (1998) *Kinetic Theory in the Earth Sciences*. Princeton, New Jersey: Princeton University Press.
- Ledford-Hoffman, P. A., D. J. DeMaster and C. A. Nittrouer (1986) Biogenic silica accumulation in the Ross Sea and the importance of Antarctic continental-shelf deposits in the marine silica budget. *Geochim. Cosmochim. Acta*, 50, 2099-2110.
- Levitus, S.J.L., T.P. Antonov, Boyer, and C. Stephens, (2000) Warming of the world ocean. *Science*, 287., 2225 – 2229.
- Leynaert, A., P. Tréguer, and C. Lancelot (2001) Silicic acid limitation of Equatorial Pacific diatom populations : evidence from ³²Si kinetic experiments. *Deep-Sea Res.*, 48, 639-660.
- Macdonald, A. M. (1998) The global ocean circulation: a hydrographic estimate and regional analysis. *Progress in Oceanography*, 41, 281–382.
- Mackenzie, F. T. and R.A. Garrels (1966) Chemical mass balance between rivers

- and oceans. *Amer. J. Sci.*, 264, 507-525.
- Mackenzie, F. T., A. Lerman, and L. M. Ver (1998) Role of the continental margin in the global carbon balance during the past three centuries. *Geology*, 26, 423–426.
- Mackenzie, F. T., L. M. Ver and A. Lerman (2000) Coastal-zone biogeochemical dynamics under global warming. *Int. Geol. Rev.*, 42, 193–206.
- Mackenzie, F. T., L. M. Ver, C. Sabine, M. Lane and A. Lerman (1993) C, N, P, S global biogeochemical cycles and modeling of global change. in *Interactions of C, N, P and S Biogeochemical Cycles and Global Change*, edited by Wollast, R., F. T. Mackenzie and L. Chou, pp.1–62. Springer-Verlag.
- Maher, K., DePaolo D. J. and Lin J. C.-F. (2004) Rates of silicate dissolution in deep-sea sediment: in situ measurement using $^{234}\text{U}/^{238}\text{U}$ of pore fluids. *Geochim. Cosmochim. Acta*, 68(22), 4629-4648.
- Meunier, J.D., F. Colin, C. Alarcon (1999) Biogenic silica storage in soils. *Geology*, 27 (9), 835-838.
- Meybeck M, L. Laroche, H. H. Dürr and J. P. M. Syvitski (2003) Global variability of daily total suspended solids and their fluxes in rivers. *Global and Planetary Change*, 39 (1-2), 65-93
- Meybeck, M. and A. Ragu (1995), *River discharges to oceans: An assessment of suspended solids, major ions and nutrients*, report, U.N. Environ. Programme, Nairobi.
- Michalopoulos, P. and R. C. Aller (1995) Rapid clay mineral formation in Amazon delta sediments: reverse weathering and oceanic elemental fluxes. *Science*, 270, 614–617.
- Michalopoulos, P and R.C. Aller (2004) Early diagenesis of biogenic silica in the Amazon delta: alteration, authigenic clay formation, and storage, *Geochim. Cosmochim. Acta*, 68, 1061–1085.
- Michalopoulos P., Aller R. C., and Reeder R. J. (2000) Conversion of diatoms to clays during early diagenesis in tropical, continental shelf muds. *Geology*, 28, 1095–1098.
- Nelson, D.M., P. Tréguer, M. A. Brzezinski, A. Leynaert and B. Queguiner (1995)

Production and dissolution of biogenic silica in the ocean: revised global estimates, comparison with regional data and relationship to biogenic sedimentation. *Global Biogeochem. Cycles*, 9, 359–372.

- Paasche, E. (1980) Silicon. in *The Physiological Ecology of Phytoplankton*, edited by Morris, I., pp. 259-284. Blackwell Scientific Publications, Oxford.
- Pasquer, B., G. Laurelle, S. Bequevort, V. Schoemann, H. Goosse and C. Lancelot (2005) Linking ocean biochemical cycles and ecosystem structure and function: results of the complex SWAMCO model, *J. Sea Res.*, 53, 93–108.
- Piperno D. R. (1988) Phytolith analysis – an archeological and geological perspective. pp. 280, Academic Press, London.
- Pouba, Z. (1968). *Geologische Kartierung (czech.)*. NAKLAD. Ceskoslowenske, Akademie Ved, Prague.
- Presti, M., and P. Michalopoulos. (2008) Estimating the contribution of the authigenic mineral component to the long-term reactive silica accumulation on the western shelf of the Mississippi River Delta. *Continental Shelf Research*, 28, 823-838.
- Rabouille, C., F.T. Mackenzie, and L.M. Ver (2001) Influence of the human perturbation on carbon, nitrogen, and oxygen biogeochemical cycles in the global coastal ocean. *Geochim. Cosmochim. Acta*, 65(21), 3615-3641.
- Rabouille, C., P. Crassous, A. Kripounoff, J.-F. Gaillard, R. Jahnke, C. Pierre and J.-C. Relexans. (1993) A model of early diagenesis in the tropical North Atlantic: Processes and mass balances in the sediments of the EUMELI program, *Chemical Geology*, 107, 463-466.
- Ragueneau, O., Dittert, N., Corrin, L., Tréguer, P. and P. Pondaven (2002). Si:C decoupling in the world ocean: is the Southern Ocean different ? *Deep-Sea Research II*, 49 (16), 3127-3154.
- Ragueneau, O., Chauvaud, L., Moriceau, B., Leynaert, A., Thouzeau, G., Donval, A., Le Loc'h, F. and F. Jean (2005) Biodeposition by an invasive suspension feeder impacts the biogeochemical cycle of Si in a coastal

- ecosystem (Bay of Brest, France). *Biogeochemistry*, DOI 10.1007/s10533-004-5677-3.
- Ragueneau, O., S. Schultes, K. Bidle, P. Claquin, and B. Moriceau (2006a) Si and C Interactions in the world ocean: Importance of ecological processes and implications for the role of diatoms in the biological pump, *Global Biogeochemical Cycles*, 20, GB4S02, doi:10.1029/2006GB002688.
- Ragueneau, O., D. J. Conley, S. Ni Longphuir, C. P. Slomp, A. Leynaert (2006b) A review of the Si biogeochemical cycle in coastal waters, I. Diatoms in coastal food webs and the coastal Si cycle. in: *Land-ocean nutrient fluxes: silica cycle*, edited by Ittekkot, V., C. Humborg and J. Garnier. SCOPE, in press.
- Ragueneau, O., D.J. Conley, S. Ni Longphuir, C.P. Slomp, A. Leynaert. (2006c) A review of the Si biogeochemical cycle in coastal waters, II. Anthropogenic perturbation of the Si cycle and responses of coastal ecosystems. in: *Land-ocean nutrient fluxes: silica cycle*, edited by Ittekkot, V., C. Humborg and J. Garnier. SCOPE, in press.
- Rao, A. M. F. and R. A. Jahnke (2004) Quantifying porewater exchange across the sediment-water interface in the deep sea with in situ tracer studies, *Limnol. Oceanogr.: Methods*, 2, 75–90.
- Rickert, D. (2000) Dissolution kinetics of biogenic silica in marine environments. in : *Reports on Polar Research*, vol. 351, pp. 211., Alfred Wegener Institute for Polar and Marine Research.
- Rosenberg, D.M., P. McCully, and C. M. Pringle. (2000) Global-scale environmental effects of hydrological alterations: introduction. *BioScience*, 50, 746-751.
- Saccone, L., D. J. Conley, G. E. Likens, S. W. Bailey, D. C. Buso, and C.E. Johnson (2008) Distribution of amorphous silica in soils of the Hubbard Brook Experimental Forest. *Soil Sci. Soc. J. Amer.* 72, 1637-1644.
- Seitzinger, S.P. and A.E. Giblin. (1996) Estimating denitrification in North Atlantic continental shelf sediments. *Biogeochemistry*, 35, 235-259.
- Serebrennikova, Y.M. and K.A. Fanning (2004) Nutirents in the Southern Ocean GLOBEC region: variations, water circulation, and cycling, *Deep-Sea*

- Research, Part II 51, 1981–2002.
- Schroeder, D. (1978). *Bodenkunde in Stichworten*. Verlag Ferdinand Hirt, 154 pp
- Simpson, T.L. and B. E. Volcani (1981) *Silicon and siliceous structures in biological systems*. Springer-Verlag, New York.
- Sferratore, A., J. Garnier, G. Billen, D. Conley, and S. Pinault (2006). Silica diffuse and point sources in the Seine watershed. *Environmental Science & Technology*, 40: 6630-6635.
- Slomp, C. P. and P. Van Cappellen (2004) Nutrient inputs to the coastal ocean through submarine groundwater discharge: Controls and potential impact, *J. Hydrol.*, 295, 64-86.
- Sverdrup, H. V., M. W. Johnson and R. H. Fleming (1942) *The Oceans*. Englewood Cliffs, N. J., Prentice-Hall.
- Tréguer, P., D. M. Nelson, A. J. Van Bennekom, D. J. DeMaster, A. Leynaert, and B. Queguiner (1995) The silica balance in the world ocean: A reestimate, *Science New Series*, 268(5209), 375-379.
- Van Cappellen, P., S. Dixit and J. Van Beusekom (2002) Biogenic silica dissolution in the oceans: reconciling experimental and field-based dissolution rates. *Global Biogeochem. Cycles*, 16(4),1075, doi:10.1029/2001GB001431.
- Van Cappellen, P. (2003) Biomineralization and global biogeochemical cycles. in: *Biomineralization* edited by Dove, P., J. DeYoreo and S. Weiner, pp. 357-381, *Reviews in Mineralogy and Geochemistry*, 54, Mineral. Soc. Amer., Washington, D. C.
- Ver, L. M. (1998) *Global kinetic models of the coupled C, N, P, and S biogeochemical cycles: Implications for global environmental change*. Ph.D. dissertation, University of Hawaii.
- Winkler, J. P., R. S. Cherry and W. H. Schlesinger (1996) The Q10 relationship of microbial respiration in a temperate forest soil. *Soil Biol. Biochem.*, 28, 1067–1072.
- Wollast, R. (1974) The silica problem. in: *The Sea* edited by Goldberg E. D. pp. 359-392, Wiley.
- Wollast, R. (1991) The coastal organic carbon cycle: Fluxes, sources, and sinks. in: *Ocean Margin Processes in Global Change*, edited by Mantoura, R.

- F. C., J. M. Martin, and R. Wollast, pp. 365–381. Wiley-Interscience.
- Wollast, R. (1993) Interactions of carbon and nitrogen cycles in the coastal zone. in : Interactions of C, N, P and S Biogeochemical Cycles and Global Change, edited by. Wollast, R., F. T. Mackenzie, and L. Chou, pp. 195–210, Springer-Verlag.
- Woodwell, G. M., Rich P. H., and Hall C. A. S. (1973) Carbon in estuaries. in Carbon and the Biosphere. edited by Woodwell G. M. and E. V. Pecan, pp. 221–240. U.S. Atomic Energy Commission, CONF-720510.
- Yool, A. and T. Tyrrell (2003) The role of diatoms in regulating the ocean's silicon cycle. *Glob. Biogeochem. Cycles*, 17, 1103, doi:10.1029/2002GB002018.
- Yool, A. and T. Tyrrell (2005) Implications for the history of Cenozoic opal deposition from a quantitative model. *Palaeogeography, Palaeoclimatology, Palaeoecology*, 218, 239–255.
- Zhang, J. (2002) Biogeochemistry of Chinese estuarine and coastal waters: nutrients, trace metals and biomarkers. *Reg. Environ. Change*, 3, 65-76.

CHAPTER 3

Impact of changes in river nutrient fluxes on the global marine silicon cycle: a model comparison

C. Y. Bernard, G. G. Laruelle, C. P. Slomp, C. Heinze

Biogeosciences Discussion, 6:4463-4492

March 2009

Abstract

The availability of dissolved silica in the ocean provides a major control on the growth of siliceous phytoplankton. Diatoms in particular account for a large proportion of oceanic primary production. The original source of the silica is rock weathering, followed by transport of dissolved and biogenic silica to the coastal zone. This model study aims at assessing the sensitivity of the global marine silicon cycle to variations in the river input of silica and other nutrients on timescales ranging from several centuries to millennia. We compare the performance of a box model for the marine Si cycle to that of a global biogeochemical ocean general circulation model (HAMOCC2 and 5). Results indicate that the average global ocean response to changes in river input of Si is surprisingly similar in the models on time scales up to 150 kyrs. While the trends in export production and opal burial are the same, the box model shows delayed response to the imposed perturbations compared the general circulation model. Results of both models confirm the important role of the continental margins as a sink for silica at the global scale. While general circulation models are indispensable when assessing the spatial variation in opal export production and biogenic Si burial in the ocean, this study demonstrates that box models provide a good alternative when studying the average global ocean response to perturbations of the oceanic silica cycle (especially on longer time scales).

1. Introduction

The marine biogeochemical cycle of silica depends on the weathering of rocks on the continents. This temperature-dependant process releases dissolved silica (dSi) into ground waters and rivers which ultimately may discharge into the ocean. All along the transport route over the continents, the dissolved silica may be used by fresh water diatoms and plants to build up biogenic forms of silica (bSiO₂) (Conley and Schelske, 2001). Part of the bSiO₂ is deposited in riverine sediments, but a significant fraction reaches the coastal waters thus contributing to the total riverine input of silica (Conley, 1997). In coastal waters, silica input creates favourable conditions for diatom production, which can account for up to 75 % of total primary production (Nelson et al., 1995). The high level of opal production combined with the shallow settings, commonly allow a rapid settling and efficient burial of biogenic silica in coastal sediments (DeMaster, 2002). In the open ocean, an estimated 50% of the opal produced is exported from the euphotic layer (Van Cappellen et al., 2002) and only about 3% is permanently incorporated in seabed sediments (Treguer et al., 1995). The burial of biogenic silica in coastal and open ocean environments varies spatially. Despite their small surface area (8%), continental margins are suggested to account for a significant percentage of total accumulation in sediments (DeMaster, 2002; Laruelle et al., 2009)

River inputs of silica to the oceans vary on geological time scales, given the important role that climate and land surface hydrology play in controlling silicate weathering and the transport of silica to the ocean (White and Blum, 1995). For example, geological events such as the uplift of the Himalayan plateau may have accelerated silicate weathering during the late Cenozoic by increasing the exposure of crustal rock and by increasing the monsoon regime (Raymo, 1991). Changes in river inputs of silica likely also affected marine Si cycling over glacial-interglacial cycles. Thus, Tréguer and Pondaven (2000) and Ridgwell (2002) suggest that increased river input of silica during the last glacial maximum, possibly combined with increased dust input (Harrison, 2000) may have contributed to the glacial/interglacial changes in the oceanic carbon pump and atmospheric CO₂ concentrations.

More recently, human activities (damming, land use practices, deforestation,

and the introduction of invasive species) are affecting the natural terrestrial cycle of silica and its delivery to the ocean (Conley et al., 1993;Ragueneau et al., 2005;Humborg et al., 2000). The effects are particularly evident in changes in nutrient ratios involving Silica (Si), Nitrogen (N) and Phosphorus (P) in surface waters of many coastal areas over the past decades (Rabalais et al., 1996;Conley et al., 1993). The observed decrease of Si:N and Si:P ratios are the combined effect of increased human inputs of N and P to rivers and decreased river loads of Si due to retention of biogenic Si in reservoirs behind dams. Note that deforestation increases the continental input of silica to the ocean by increasing the exposure of rocks to weathering (Conley et al., 2008). However, this effect is not large enough to balance the general worldwide decline in riverine silica input (Conley et al., 2008). The major consequence of changes in nutrient ratios is a shift in planktonic species composition in the near coastal zone, with flagellates, cyanobacteria and other non-siliceous phytoplankton replacing diatoms (Egge and Aksnes, 1992;Humborg et al., 2000). In some cases, toxic blooms of harmful algal species may develop and strongly impact coastal ecosystems and fisheries (Roelke, 2000).

Several modelling tools have been developed to investigate the dynamics of the marine silica cycle at the global scale and its sensitivity to natural and anthropogenic perturbation. These tools consist of mass balance or box models (Yool and Tyrrell, 2003;Laruelle et al., 2009) and Global Biogeochemical Ocean General Circulation Models (Heinze et al., 2003;Bernard et al., 2009). While box models mostly rely on first order kinetic rate laws (Mackenzie et al., 1993), general circulation models include a more robust and mechanistic description of biogeochemical and physical processes in the ocean (Heinze et al., 2003). Both approaches have been used to gain insight in marine silicon cycling and its response to river inputs of silicon. Results of global scale box modelling of the coming century, for example, indicate that enhanced biogenic silica dissolution due to global warming may ultimately allow coastal siliceous productivity to recover from the downward trend caused by river damming (Laruelle et al., 2009). Inclusion of present-day river inputs of Si in a high resolution general circulation model indicate that the effects of river inputs on coastal marine Si cycling are most pronounced in hot spots, such as the Amazon plume, the Arctic and Southern Asia

(Bernard et al., 2009). Given that box models are more easily accessible and less computationally demanding than general circulation models, and to increase their use as a prognostic and predictive tool, it is of interest to compare the response of both types of models to similar perturbations, both on human and geological time scales.

In this study, we make such a comparison using the box model for the global Si cycle of Laruelle et al. (2009) as well as the Hamburg Ocean Carbon Cycle Model in its annually averaged coarse resolution version for long time integrations (HAMOCC2) and the high resolution version that includes the continental margins and a more detailed silica cycle (HAMOCC5). We first compare the marine Si budget inherent to each model and the model assumptions. Then long term (0-15 kyrs) and short term (0-150 yrs) simulations are performed to test the response of the models to changes in river inputs of nutrients. We demonstrate that the trends at the global scale obtained with the general circulation model (GCM) and the box model are surprisingly similar both for short and long term simulations. The critical role of the continental margins in the global cycling of silica as well as their higher reactivity to riverine perturbations is highlighted using results of the box model and HAMOCC5.

2. Model description and comparison:

2.1. The box model

The box model used in this study, for both short-term and long-term simulations, is described in Laruelle et al (2009). The model is based on an updated budget of the global biogeochemical cycle of reactive silicon, including both the terrestrial and oceanic realms. The earth surface is divided into 4 compartments along the land ocean continuum: continents (box 1), proximal coastal zone (box 2), distal coastal zone (box 3) and open ocean (box 4). Coastal regions receive particular attention given their role as a filter between the continents and the ocean. The proximal coastal zone consists of large bays, the open water parts of estuaries, inner deltas, inland seas and coastal marshes (Woodwell et al., 1973; Smith and Hollibaugh, 1993). The distal zone comprises the rest of the continental margins up to the shelf break.

In each compartment, an estimate of the amount of dissolved (dSi) and biogenic silica (bSiO₂) was established for the water column and the upper layer of the sediment. Yearly averaged fluxes between these silica reservoirs were based on previous budgets (Alexandre et al., 1997; Conley, ; DeMaster, 2002; Treguer et al., 1995) or were estimated independently. The Si cycle was linked to a steady state hydrological cycle and the advection fluxes for dSi and bSiO₂ were calculated as follows;

$$\frac{F_{ij}}{S_i} = \frac{Q_{ij}}{V_i}, \quad (1)$$

where F_{ij} and Q_{ij} are the fluxes of reactive Si and water from reservoir i to reservoir j , respectively, S_i is the mass of dSi or bSi in reservoir i , and V_i is the volume of the reservoir. The remaining transport fluxes correspond to sedimentation and deposition of bSiO₂ in the sediment and the efflux of dSi from sediments to the water column.

Simple first order kinetic relationships were obtained for all fluxes that were not linked to the water cycle by deriving a rate constant k_{ij} from the steady state Si budget using the values of the flux F_{ij} and the size of the reservoir from which the flux originates;

$$k_j = \frac{F_j}{S_i}. \quad (2)$$

The reaction network was completed by including the input fluxes through terrestrial rock and seafloor weathering and hydrothermal activities (Treguer et al., 1995) and the ultimate sinks are burial of bSiO₂ within freshwater and marine sediments (DeMaster, 2002; Conley, 2002b; Treguer et al., 1995) as well as reverse weathering reactions in shelf sediments (Mackenzie and Garrels, 1966).

2.2. HAMOCC2

In order to test the long-term effect of changes in Si supply to the ocean, we employ the HAMOCC global biogeochemical ocean model (Maier-Reimer,

1993;Maier-Reimer et al., 2005a) in its computationally efficient annual average version “HAMOCC2s” (Heinze et al., 2006;Heinze et al., 2003;Heinze et al., 1999). Annual average velocity and thermohaline fields are taken from the Large Scale Geostrophic dynamical ocean general circulation model with climatological atmospheric data (details are given in Winguth et al. (1999), for their “interglacial first guess” circulation). The effect of deep convective mixing at high latitudes is represented in the annual average velocity field, which is used for transporting the dissolved tracer substances within the model water column. The horizontal resolution is $3.5^{\circ} \times 3.5^{\circ}$. The water column is structured into 11 layers (centered at 25, 75, 150, 250, 450, 700, 1000, 2000, 3000, 4000, and 5000 m). The bioturbated top sediment zone is structured into 10 layers, with interfaces at 0, 0.3, 0.6, 1.1, 1.6, 2.1, 3.1, 4.1, 5.1, 7.55, and 10 cm down from the water sediment interface.

The biogeochemical model includes the following processes: air-sea gas exchange, biogenic particle export production out of the ocean surface layer, particle flux through the water column and particle degradation by dissolution as well as remineralisation, transport of dissolved substances with ocean currents, deposition of particulate constituents on the ocean floor, pore water chemistry and diffusion, advection of solid sediment weight fractions, bioturbation, and sediment accumulation (export out of the sediment mixed layer). The model predicts the following tracer concentrations in the ocean water column, the sediment pore waters, and the solid sediment: water column - DIC (dissolved inorganic carbon), POC (particulate organic carbon), DOC (dissolved organic carbon), CaCO_3 (calcium carbonate or particulate inorganic carbon) of ^{12}C and ^{13}C , dissolved oxygen O_2 , dissolved PO_4^{3-} as biolimiting nutrient, silicic acid $\text{Si}(\text{OH})_4$ and opal (biogenic particulate silica BSi); sediment pore waters - the same dissolved substances as in the water column; and solid sediment – clay, CaCO_3 , opal, and organic carbon. For inorganic carbon chemistry, the dissociation constants of carbonic and boric acid according to Mehrbach et al. (1973), the solubility product for CaCO_3 after Ingle (1975), and the pressure dependencies of Edmond and Gieskes (1970) were applied.

The ocean surface and water column processes and the pore water chemistry are parameterized as described in previous applications of the model (Heinze et

al., 2006;Heinze et al., 1999;Heinze et al., 2003). Opal export production and respective depletion of silicic acid in the ocean surface layer are simulated by Michaelis Menten nutrient uptake kinetics. The higher maximum nutrient uptake velocity is higher for Si than for P, leading to a concentration of opal export in upwelling regions. Through this approach, silicic acid is depleted in surface waters before phosphate is completely used up through primary production. The resulting variable Si:C ratios correspond well with trends as given by Brzezinski (Brzezinski, 1985). The overall coupling of the P and Si cycles in the model is thus governed by vertical (upwelling) velocity and sedimentation rates. For the opal flux through the water column, an implicit numerical algorithm is used involving an independent choice of the particle sinking velocity and the opal dissolution rate. Pore water chemistry follows Archer et al. (1993) “*burial = rain minus re-dissolution*”, but allows for time dependent exchange with ocean bottom water in the free water column (Heinze et al., 2003) and includes efficient numerics for the vertical sediment advection following Maier-Reimer et al. (2005a). The re-dissolution constant of opal within the bioturbated sediment zone was adjusted to be lower than the one for the water column. This is in line with the presumed alteration of biogenic silica particles during their aging process in the water column and surface sediment (Van Cappellen et al., 2002). Bioturbation is implemented through diffusion of solid materials, where non-local mixing and particle size dependent mixing have been neglected. The early diagenetic model is based on the concept of conservation of volume (or geometry) where all sediment layers do not change their geometric shape according to a fixed porosity profile (after Ullmann and Aller, 1982) with time. Thus, gaps in the solid sediment are instantaneously closed, either by shifting of material from the respective sediment layer above (in the case where rain exceeds re-dissolution) or from erosion of material from the layer below.

The model is initialized with clay sediment only and run to quasi-equilibrium after 120,000 years of integration before any sensitivity experiments are started. At model equilibrium, the global burial rate of Si corresponds to the given input rate from riverine material. However, the local opal production, deposition, re-dissolution and burial (sediment accumulation) rates are prognostic.

2.3. HAMOCC5

HAMOCC5 was used for short timescale simulations (150 yr). Given the high resolution of its grid and detailed description of the Si cycle, the model is not suitable for long term simulations.

HAMOCC5-MPIOM results from the interactive coupling of the Max Plank Institute Ocean Model (MPI-OM), a full primitive equation dynamical ocean model which computes thermohaline circulation and assures the advection and diffusion of biogeochemical tracers of the HAMburg Oceanic Carbon Cycle Circulation Model. The two fully coupled models receive the same radiative forcing. HAMOCC5 includes a more comprehensive description of biogeochemical processes. The model grid used in this simulation is an orthogonal curvilinear C-grid with an average resolution of 3° . To optimize calculations, the North Pole is artificially located over Greenland and the South Pole over Antarctica. The resulting resolution is 29 km in the Arctic to about 390 km in the Tropics. The water column is divided into 40 vertical levels whose thickness gradually increases with depth, from 12 meters at the surface to a maximum of 600 m in the deep ocean. This resolution resolves the continental margins, although in a coarse manner. In this study, the continental shelf is represented by grid cells shallower than 1500 m, of which the integrated surface covers 8% of the world ocean ($27 \cdot 10^6 \text{ km}^2$). The average depth is 530 m, 50 % of this surface is shallower than 300 m. The time step is 0.1 day.

Only the features relevant to the silica cycle will be described here. For a full description of HAMOCC5 and MPI-OM, we refer to the technical reports that are available online (Maier-Reimer et al., 2005b; Wetzler et al.). Riverine inputs of nutrients were implemented according to Bernard et al. (2009) using the COSCAT segmentation of the coast line (Dürr et al., 2009).

In HAMOCC5, opal production is computed as a fraction of the dead material produced by zooplankton and phytoplankton (including the pseudo faeces); the model calculates opal and calcium carbonate production as the two fractions of the non living part of the detritus, the shells. A main difference with HAMOCC2 is that the opal export production is dependent on primary production. The competition between opal production and calcium carbonate production is

regulated by the silica availability (Leynaert et al., 2001; Paasche, 1980). It is assumed that phytoplankton consists of diatoms, coccolithophorids, and flagellates. As diatoms are known to be the fastest competitors (Egge and Aksnes, 1992), opal production by diatoms will be preferred to CaCO_3 production if sufficient dSi is available in the ocean surface layer.

The flux of particles through the water column redistributes phosphorous, silica and associated tracers during sinking, thus enriching the deep waters in nutrients. In the default version of the code, particles have constant sinking speeds, w_{DET} , w_{CaCO_3} , w_{Opal} and w_{Dust} for organic detritus, CaCO_3 , opal and clay, respectively. The export production is computed as the POC (particulate organic carbon), opal and CaCO_3 leaving the euphotic layer, i.e. the material sinking below 90 m depth in the surface ocean. Remineralisation of opal and CaCO_3 occurs during sinking of particles after they have left the euphotic layer. As the model only computes the last step of the living part of the silica cycle, hardly any of the opal produced in the euphotic layer is remineralized in the surface ocean. This simplification implies that primary production of opal is not computed in HAMOCC5, and we therefore only refer to exported opal production.

Fluxes from the bottom ocean layer in each ocean grid cell provide the boundary condition for the sediment module that includes 4 sediment weight fractions and 12 layers following Heinze et al. (1999). The sediment module computes the accumulation of deposited material on the sea floor as well as remineralisation in the sediments and the release of redissolved tracers to the lowest level of the water column.

2.4. Model comparison

The box model and the two GCMs compared in this study present many conceptual and structural differences. The major differences between the box model and GCMs are the inclusion of other elements than silica and the spatially-explicit description of biogeochemical processes (Table 1). Note also that the GCMs differ in their description of biogeochemical cycling of silica and in the representation of the continental margins. While coastal zone processes are resolved in the box model and roughly in HAMOCC5, they are not included in HAMOCC2. Thus,

Table 1. Key characteristics of the three models used in this study

	Box model	HAMOCC2	HAMOCC5
Nutrients	Single nutrient (Si)	Multi-nutrient (Si, P)	Multi-nutrient (Si, N, P, Fe)
Geographical extent	Land, Continental margin, Open ocean	Open ocean	Continental margin, Open ocean
Time scale of simulations	Short + long term simulations	Long term simulations (millennia)	Short term simulations (centuries)
Temporal resolution, time step	Annually averaged, high resolution: 0.01 year	Annually averaged, low resolution: 1 year	Seasonal cycle, high resolution: 0.1 day
Horizontal resolution	Global average	3.5°×3.5°	Average 3°×1.8° (29 to 390 km)
Vertical resolution	Vertical resolution in the ocean: 3 layers	11 layers	40 layers
Processes formulation	First-order rate laws for fluxes	Mechanistic and empirical rate laws	Mechanistic and empirical rate laws
Hydrodynamics	Steady state water cycle	Fixed flow field (modern-day circulation)*	On-line coupling of biogeochemical ocean model to MPI-OM**
Si Residence time	17000 yrs	22900 yrs	No steady state reached
Si phases	dSi / bSiO ₂	dSi, bSiO ₂	dSi, bSiO ₂

* Large Scale Geostrophic dynamical ocean general circulation model (Winguth et al., 1999), ** MPI-OM: Max Planck Institute Ocean Model (Marsland et al., 2003), *** dSi: dissolved Si; bSiO₂: biogenic silica.

given the computational demands of HAMOCC5, only the box model allows the assessment of the effects of coastal zone processes on the long-term silica cycle.

The steady state budgets for Si in all three models show general similarities (Fig. 1), in particular with respect to rates of sediment burial in the coastal zone and benthic recycling. There are also significant differences, for example, in the biogeochemistry of the euphotic zone (0- 100 m) and intermediate waters (100-1000 m). Conceptually, it must be remembered that the steady state Si cycle of the box model is the hypothesis on which the model itself is built. The budgets calculated by the GCMs, in contrast, result from calibration and optimization processes (Heinze et al., 2003). The 3 models are fed with similar inputs of dSi (Dürr et al., 2009) to allow a better inter-comparison. The box model, also includes other sources of Si: bSiO₂ (Conley, 1997), ground water inputs (Slomp and Van Cappellen, 2004) and aeolian dust deposition on the open ocean (Treguer et al., 1995).

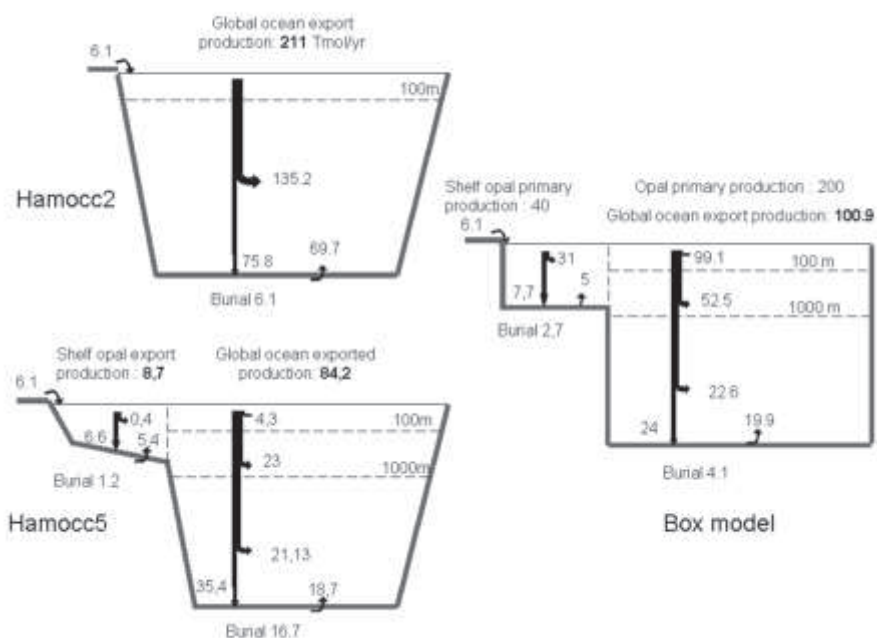


Figure 1. Schematic representation of the silica budget of each model. Global Si fluxes in HAMOCC2, HAMOCC5 and in the box model represented in a similar fashion (separating out the coastal sections, surface, intermediate and deep ocean, where possible).

The spatial resolution of HAMOCC2 does not allow the coastal zone to be resolved and its global budget is, therefore, the most simple. 211 Tmol yr⁻¹ of Si are exported as opal from the euphotic layer of the ocean. About two thirds of this amount redissolves in the water column before reaching the sediment. To ensure a steady state, a massive recycling takes place, leading to an efflux of 69.7 Tmol yr⁻¹ from the sediments. The net burial, perfectly balances the riverine inputs (6.1 Tmol yr⁻¹). HAMOCC5, on the other hand, can not be run to full steady state including the slowest reservoirs because of overwhelming computation costs associated with its higher spatial resolution, a more complex biogeochemical module and a much higher temporal discretisation. In this model, 10% of the export production takes place on the continental margins where 1.2 Tmol yr⁻¹ of Si is buried. Out of the 84.2 Tmol yr⁻¹ of opal exported from the euphotic layer in the open ocean,

35.4 Tmol yr⁻¹ reaches the sediment. This compartment is not at steady state and the burial is 16.7 Tmol yr⁻¹, which is likely too high. However, given the long residence time of Si in the ocean, this approximation is not expected to affect the trends in simulations on the time scale of a few centuries.

The box model not only calculates export production but also the total dSi uptake. This number is not calculated in the GCMs but is based on the study of Tréguer et al. (1995). In the model, it is assumed that 20% of the 240 Tmol yr⁻¹ of dSi uptake takes place on the continental shelf. Due to rapid pelagic recycling, only 7.7 Tmol yr⁻¹ enters the sediment, which is close to the estimate of 6.6 Tmol yr⁻¹ obtained with HAMOCC5. However, the coastal burial flux is more than twice as large in the box model as in HAMOCC5 (2.7 Tmol yr⁻¹ versus 1.2 Tmol yr⁻¹). Note that this former number includes the coastal reverse weathering of 1 Tmol Si yr⁻¹ while the additional shelf burial in the box model is 1.7 Tmol yr⁻¹. In both models burial fluxes are significantly higher than Tréguer's estimate of 0.6 Tmol/yr (1995), thus supporting the suggestion of DeMaster (2002) that silica burial in shelf sediments has been underestimated so far.

In the box model, only 50% of the opal primary production is recycled in the euphotic layer of the open ocean (based on Treguer et al., 1995; Van Cappellen et al., 2002). The resulting export production of opal is similar in both models (103 Tmol yr⁻¹ and 84.7 Tmol yr⁻¹, respectively). The dissolution in the remainder of the water column is 75%, which compares well with values for the other models (64% in HAMOCC2 and 58% in HAMOCC5). Only 4.1 Tmol yr⁻¹ of a total deposition of 24 Tmol Si yr⁻¹ remains permanently in the sediment. This implies a Si recycling in the sediment of 83% which lies between those of the GCMs (92% and 53% for HAMOCC2 and HAMOCC5, respectively).

3. Model scenarios and results

3.1. Long-term effects of changes in river inputs (HAMOCC2 vs box model).

The long term response of the box model and HAMOCC2 to changes in river inputs of silica was investigated through a set of simulations run over 150 kyrs. The perturbations selected were taken from Heinze et al. (2006) using updated river fluxes as described in Bernard et al. (Bernard et al.) :

Simulation 1: reduction to 75% of Si inputs.

Simulation 2: increase to 400% of Si inputs.

Simulation 3: reduction to 0 of Si inputs.

Simulation 4: step function simulating a 10-fold increase Si inputs during 20 kyrs after 10 kyrs of unmodified inputs and followed by 20 kyrs with no inputs. After 50 kyrs, the Si delivery returns to its original level. For each of the 3 first scenarios, an initial spin-up period of 10 kyrs with unmodified inputs was applied before the perturbation.

Export production of opal and burial of Si in the sediment were used as indicators of pelagic and benthic Si processing in the box model and HAMOCC2 as done by Heinze (2006). Export production provides insight into the biological activity of diatoms. Sediment burial is the ultimate sink for the marine biogeochemical cycle of Si and is a key process in determining the long term mass balance of silica in the ocean. In the box model, all sediment sink terms are included, and the silica lost to reverse weathering on the continental shelf is considered as part of the 'burial term'. Both models are fed with comparable Si deliveries (6.2 and 7.4 Tmol Si yr⁻¹ for HAMOCC2 and the box model, respectively), and the inputs are balanced by Si burial at the beginning of the simulations.

Results show that a 25% reduction in Si inputs induces comparable decreases in both models for export production and sediment burial (Fig. 2a, 2b). While the response in export production represents -10% for HAMOCC2, it reaches -25% in the box model. The quasi-instantaneous drop following the perturbation in the box model is the result of the dynamics of Si in the coastal zone; the characteristic residence time for Si on the continental margins is significantly shorter (2.3 kyrs) than that of Si in the open ocean (17 kyrs). As a consequence, this box responds to each perturbation much faster. The same general decrease is observed in opal burial. Overall, while HAMOCC2 appears to reach a new steady state after only 20-30 kyrs, despite a residence time for Si of 23 kyrs. While it takes about 100 kyrs for the box model, with the shorter residence time of 17 kyrs, to reach a new equilibrium. This suggests that the higher spatial resolution and shorter residence time of the individual grid cells in HAMOCC2 compared to the box model, allows a faster collective response of the whole ocean system to

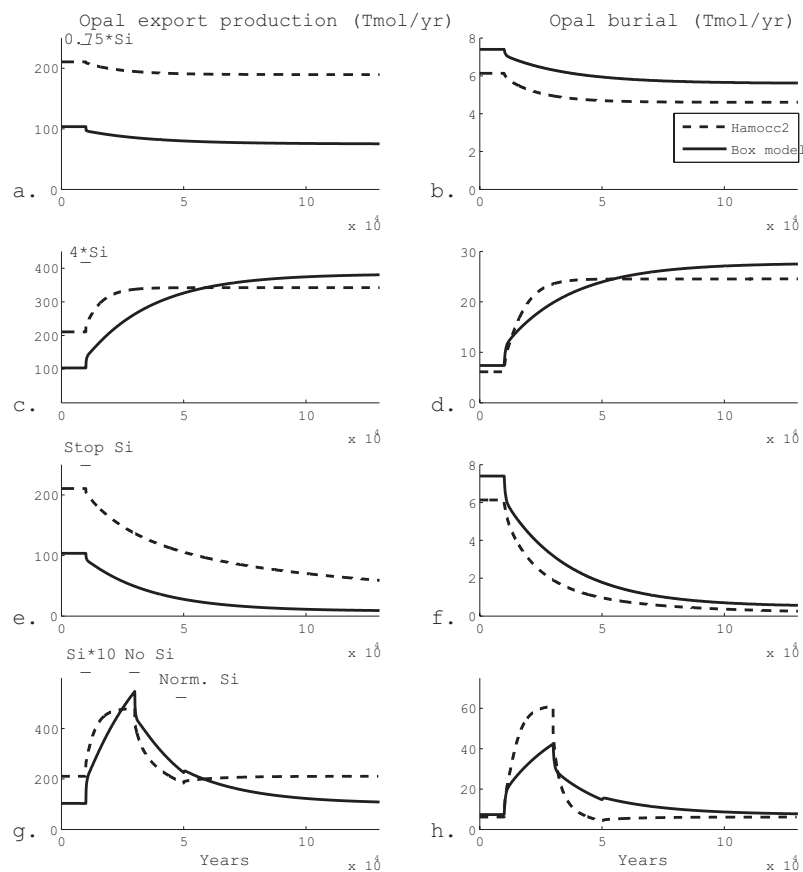


Figure 2. Long term scenarios Box Model versus HAMOCC2: Run 1. The riverine Si input is decreased by 25%. Model experiment Run 2: The riverine Si input is increased by a factor 4. Model experiment Run 3: The riverine Si input is completely stopped. Model experiment Run 4: The riverine Si input is suddenly increased (*10), suddenly stopped (0) and returned to the normal value.

a perturbation. A similar lowering of the response time as the result of collective behaviour, has been demonstrated for box models of the global carbon cycle (Lasaga, 1980).

The scenario assuming a 4-fold increase of river Si inputs (Fig. 2c, 2d) yields an opposite response, with increases in export production and sediment

burial for the box model as well as HAMOCC2. Again, HAMOCC2 reaches a steady state much faster than the box model (after ~30 kyrs as opposed to ~120 kyrs), and the magnitude of the increase is less than that of the box model. Export production reaches a maximum at 150% of its original value in HAMOCC2, while it reaches a maximum at 300% in the box model. This is partially explained by the structure of the model itself which only allows dSi availability to limit opal production. Hence, dSi uptake (not shown) and export production in the box model follow the inputs of Si delivery to the ocean almost linearly, whereas in HAMOCC2, phosphorus may also limit diatom growth (see Table 1). Despite the difference in export production, opal burial increases by a factor of 4 in both models. This can be explained by a lower redissolution of the sinking bSiO₂ in HAMOCC2 compared to the box model.

A simulation without any Si inputs (Fig. 2e, 2f) drives export production and opal burial in both models towards zero as the ocean becomes depleted of Si. Export production decreases faster in the box model than in HAMOCC2, reaching only 25% of its initial value after less than 50 kyrs. The opposite trend is observed with Si burial, which drops significantly faster in HAMOCC2 than in the box model at the beginning of the simulation. However, more than 150 kyrs are required for either model to remove all oceanic Si through burial.

The step function, imposing a very strong increase of riverine Si input (10-fold) followed by a shutdown results, in a strong increase in export production and opal burial followed by a significant drop 50 kyrs after the beginning of the simulation in both models. In agreement with the previous results, export production reaches much higher values; the increases in sediment burial in both models remain comparable in magnitude in the box model. However, the temporal response of the models, strongly differs because of the smoother behaviour of HAMOCC2. In the box model, the short residence time on the continental shelf leads to very steep increases in production and sediment burial during the first centuries following the perturbation and slower rates later on. Between 30 and 50 kyrs, without Si inputs, HAMOCC2 reaches slightly lower values for both fluxes than the initial conditions. Despite sharp initial decreases, the box model still exhibits higher export production (500 Tmol Si yr⁻¹) and sediment burial (18 Tmol

Si yr⁻¹) after 50kyr than at the beginning of the simulation. This difference between the models leads to opposite trends during the remainder of the simulations while they slowly return to their original steady states, reached at 80 kyrs and 150 kyrs for HAMOCC2 and the box model, respectively.

Overall, both models present similar qualitative responses to major long term variations in silica inputs from the rivers. Quantitatively however, discrepancies are observed: HAMOCC2 shows a faster return to steady state than the box model while the latter always exhibits larger changes in export production. In fact, the box model shows a quasi-linear response to the imposed perturbations. Hence, its export production varies within a significantly larger range of values than that of HAMOCC2. Nonetheless, the long term responses of both models are comparable and similar with respect to opal burial. The differences in transient behaviour mainly concern export production and essentially affect the first 20-30 kyr of the simulations. The two major differences between both models are due to the higher sensitivity of the export production in the box model to Si inputs and the higher resolution in the GCM which allows a faster return to steady state despite the similarity in the overall residence time of Si (Table 1).

3.2. Short-term effects of changes in river inputs (HAMOCC5 vs box model)

The effects of short term changes in the riverine input of silica were tested in the box model through a perturbation of the terrestrial silica cycle induced by river damming (Laruelle et al., 2009). This scenario relies on projected changes in the number of dams until 2025 (Gleick, 2003), combined with a relation between global water use and the number of new dams (Rosenberg et al., 2000), and an estimate of global population changes throughout the 21st century. The HAMOCC5 equivalent scenario was implemented by imposing a reduction of the riverine silica flux. The coefficient was computed as the silica flux reduction ratio at the proximal/distal interface in the box model. In addition, a scenario was run without any silica input for the box model and HAMOCC5, and without any input of other nutrients (nitrogen and phosphorus) for HAMOCC5 alone. HAMOCC5 requires a spin up time of 100 yrs.

The damming scenario assumes a maximum decrease of 17% in riverine

silica input to the ocean in the year 2100. At the scale of the global ocean, this does not cause a significant decrease of the opal export production and burial (Fig. 3a and 3b.). Thus, the box model shows a 1% decrease in export production, while the decrease is insignificant compared to the inter-annual variability for HAMOCC5. The response to a total shutdown of riverine Si input has a much stronger effect, with a decrease in export production of 7% for the box model and 6% for HAMOCC5. Switching off all riverine nutrients in HAMOCC5, leads to a slightly stronger response, reflecting the additional dependency of opal production on the availability of other nutrients.

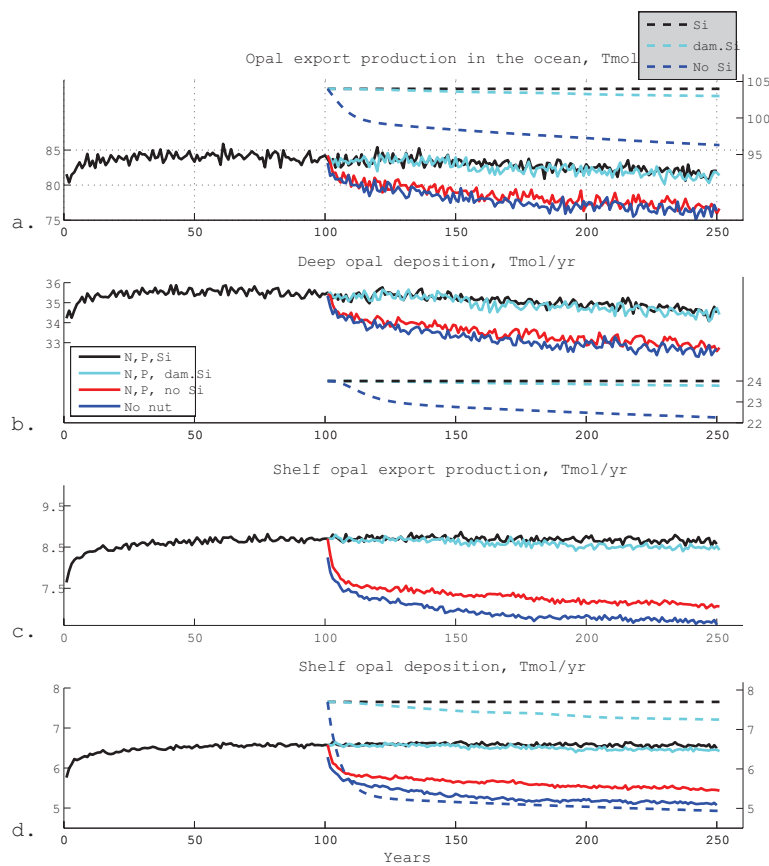


Figure 3. Short term scenarios for variations in Si inputs and resulting export production, and burial of biogenic Si in the coastal zone and Open Ocean in HAMOCC5 (left axis) and the box model (right axis). Plain and dashed lines represent the HAMOCC5 and the box model runs, respectively.

The Si cycle on the continental margins is significantly affected by changes in river inputs of nutrients (Fig. 3c and d). Since the box model does not explicitly compute shelf opal export production, only results for HAMOCC5 are shown in Fig. 3c. The decrease in export production is difficult to quantify because of the inter-annual variability but the relative change is larger than for the open ocean. The strongest response to the damming scenario is observed for opal deposition in the box model (Fig. 3d). At the end of the simulation, the box model shows a 0.5 Tmol reduction of the opal deposition (-5.8%), compared to a 0.1 Tmol decrease for HAMOCC5 (-1.5%).

The production and export of bSiO_2 in the box model is only limited by dSi availability. This makes the box model much more sensitive to variations in the riverine input of silica than HAMOCC5. The multi nutrient limitation (N, P, Fe and Si) of HAMOCC5 makes it more stable and reduces the effects of changes in riverine silica alone. The modest response of the GCM shows that opal production on the shelf does not suffer only by silica limitation. The opal production is limited by other nutrients such as N, P or Fe. As a consequence, switching off the riverine input of N and P (Fig. 3d) causes a stronger decrease of the opal export production (-22%) than switching off the riverine silica input alone (-16.6%).

A major difference between the two models is the description of riverine input of silica. The box model explicitly receives both riverine bSiO_2 and dSi , while HAMOCC5 is only fed with dSi . In rivers, lakes and artificial reservoirs, the water residence time increases leading to more efficient retention of bSiO_2 than that of dSi . This feature, observed in the field (Humborg et al., 2000), and implemented in the box model, modifies the particulate/dissolved ratio for silica. As a consequence, the lower relative input of bSiO_2 further enhances the drop in bSiO_2 sedimentation in the distal zone of the box model while HAMOCC5 can not capture this process. However, the buffer effect of the proximal zone in the box model, limits the variations of the particulate/dissolved ratio to marginal changes (a few percent at most). Overall, the major factor explaining the differences in the response of the models is the inclusion of multiple nutrient limitations in the GCM.

Shelf opal deposition drops by 16.6% when cutting off the riverine input of silica in HAMOCC5 (Fig. 3d). The drop is 35.7% for the box model, which is

higher than when cutting off of all riverine nutrients in HAMOCC5 (21.9%). In comparison, the box model's linear response to changes in silica supply highlights the buffer effect of the multi nutrient limitation of the primary production in HAMOCC5. In the box model, only silica drives bSiO₂ production, and a change in the riverine input has a direct effect on the opal production. In HAMOCC5, changes in the dSi availability will have little effect on the opal production, unless dSi itself is the limiting factor driving the opal production.

The explicit spatial component of HAMOCC5 allows the visualization of the complex interaction of lateral advection of riverine silica with regional nutrient limitation. A global map of opal deposition obtained from HAMOCC5 for a 150 yr simulation (Fig. 4.a) illustrates the large spatial heterogeneity of opal deposition including the major role of the Austral Ocean, the Equatorial Pacific upwelling as well as coastal upwellings off Mauritania, Peru, Chile, western South Africa (Benguela) and eastern New Zealand. The change in opal deposition relative to the reference run for a model scenario without a riverine Si contribution (Fig. 3b) demonstrates the contribution of terrestrial Si input to the marine silica cycle. Although most of the opal sedimentation supported by the riverine input occurs near to the coast, the response in the Pacific differs from that in the Atlantic Ocean. While opal deposition decreases in the Sargasso Sea and the Eastern North Atlantic, a minor increase is observed in the central Pacific. Results of the model run without riverine nutrients (N, P and Si; Fig. 3c) display a decrease of opal deposition of at least 20 mmol m⁻² yr⁻¹ for the whole North Atlantic Ocean. This illustrates the role of regional limitation: in the Atlantic Ocean, primary production is nitrogen limited and thus will be affected by a drop in riverine inputs of N. In contrast, the Pacific is largely limited by iron (except for the equatorial region), thus a change in the Si, N or P will have a smaller impact.

As discussed in Bernard et al (2009), the effect of silica largely depends on the location of its release to the ocean. Thus, a small reduction of the riverine input of silica, as prescribed for the river damming scenario (-17%), will have a minor effect in the Pacific Ocean. The main effect is seen in the Gulf of Bengal where a local drop of more than 50 mmol m⁻² yr⁻¹ is observed, and in the Amazon plume and the Gulf of Mexico. The reduced input of the Congo River and other

minor rivers of Central Africa lowers opal deposition in the central South Atlantic Ocean by $25 \text{ mmol m}^{-2} \text{ yr}^{-1}$.

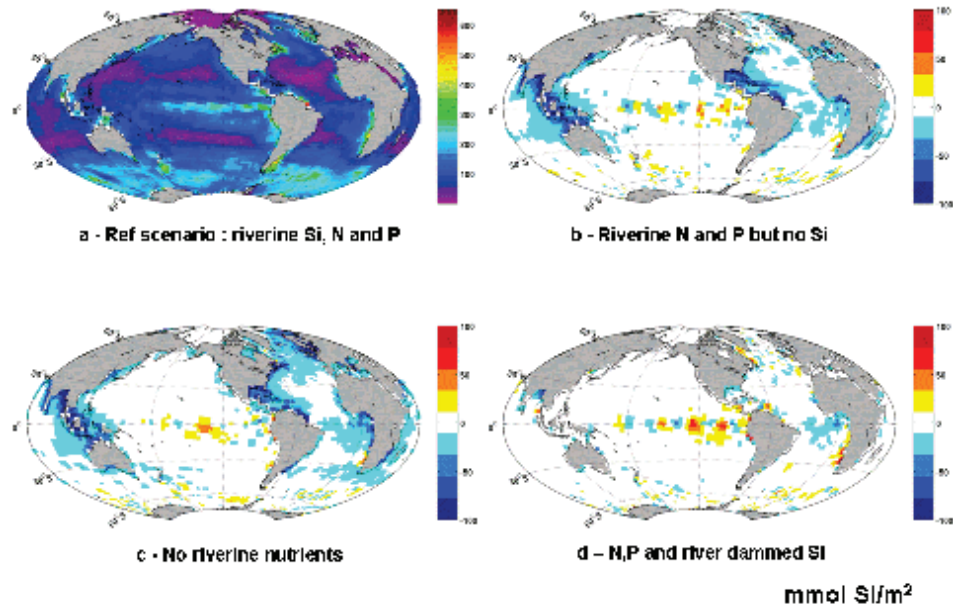


Figure 4: HAMOCC5 opal sediment deposition $\text{mmol m}^{-2} \text{ yr}^{-2}$ (a), and the effect of perturbation of the riverine Si input after a simulation time of 150 yrs (computed difference between the scenario runs and the reference run (N, P and Si)); without the riverine Si input (b), without any riverine input (c), with reduction of riverine Si corresponding to a river damming scenario.

As an advantage compared to the box model, the GCM describes the circulation in the North Atlantic Ocean and provides insight in the fate of the Amazon River plume. The strong current moving northwest along the coast of Brazil distributes opal deposition into the Caribbean Sea and mixes with the silica rich waters in the Gulf of Mexico. The Amazon River alone contributes to a large fraction of the offshore North Atlantic pool of silica (Shipe et al., 2006; Froelich et al., 1978); with a flux of Si that is estimated to be on the order of $1\text{-}1.5 \text{ Tmol Si.yr}^{-1}$ (Johnson et al., 2005). Such a massive input likely supports most of the North Atlantic siliceous uptake (DeMaster et al., 1996).

While the effect of damming on Si dynamics on the global scale is limited (Fig. 3), the distribution of opal burial for this scenario (Fig. 4d) suggest that locally, effects may be significant, even in the open ocean. The regional details of the riverine silica contribution make the general damming scenario assumed here somewhat unrealistic, however. Indeed, a homogeneous increase in river damming all over the world is unlikely. A realistic approach would take into account regional characteristic (e.g. population, land use, water demand) for a spatially explicit global damming scenario. Unfortunately, such a scenario is unavailable at the present time.

4. Conclusions

Despite their different structures, the box model and general circulation model for the marine silica cycle used in this study show surprisingly comparable responses to changes in river input on long and short time scales. Thus, HAMOCC2 and the box model predict a similar export production and opal burial on a time scale of 150 kyrs although the temporal dynamics differ slightly. For simulations of 150 years, the box model and HAMOCC5 forecast comparable decreases in export production and sediment burial on the continental margins and in the open ocean in response to increased Si retention in rivers. Only the amplitude of change in the results of the box model is slightly higher than in the results of the GCM due to the absence of other nutrients in the former model. Results of both models also demonstrate the role of the continental shelf as a major sink of silica at the global scale. Furthermore, coastal waters appear to be more sensitive to perturbations of riverine inputs than the open ocean.

Ultimately, the choice of one model over another should be based on the availability of data and technical limitations as much as on model performance. For structural reasons, the box model can not be applied to problems requiring explicit spatial representations. Nevertheless, box models remain suitable tools to evaluate the global scale response of both continental margins and the open ocean to global scale perturbations, especially on longer time scales. Given its low data demand and computational requirements, the box model is the most user friendly of the modeling tools compared here. The performance of our box

model could be further improved by coupling it to models for other nutrients, such as N and P (e.g. Wallmann, 2003; Slomp and Van Cappellen, 2007). Such an implementation would potentially show the sensitivity of the marine silica cycle to anthropogenic perturbations of Si:N and Si:P. HAMOCC2 is a well-tested GCM that has been used in many long term studies of biogeochemical cycles of various nutrients (Heinze et al., 2003; Heinze and Maier-Reimer, 1999; Heinze et al., 1999). The strength of the HAMOCC2 model is that it can be integrated over thousands of years in an acceptable amount time while retaining a relatively high horizontal resolution. Its spatial resolution does however not allow for a full representation of the continental margins, however, and the regional effects of riverine inputs cannot be assessed well. HAMOCC5 is, by far, the most demanding model in terms of computer power and requires high performance parallel clusters to run efficiently. Its spatial resolution is sufficient to spatially resolve current riverine inputs (Dürr et al., 2009; Seitzinger et al., 2005) and paves the way for a detailed assessment of global and regional riverine contributions to marine nutrient cycling. Future work with HAMOCC5 could include spatially explicit scenarios for human-induced alterations in river biogeochemistry. Given the spin-up time required for equilibration with the sediment, its use in global oceanic budgeting is limited.

Acknowledgments:

This work was co-funded through the EU FP6 Integrated Project CARBOOCEAN (contract. 511176 GOCE), the Bjerknes Centre for Climate Research – University of Bergen, the EU (Si-WEBS, contract number HPRN-CT-2002-000218), Utrecht University (High Potential project G-NUX) and the Netherlands Organisation for Scientific Research (NWO-VIDI grant 864.05.004). Sybil Seitzinger and Emilio Mayorga (Institute of Marine & Coastal Sciences, Rutgers University, USA) are acknowledged for the communication of the merged Global-NEWS data sets as well as Hans Dürr from Utrecht University for the communication of the riverine silica data set. Computations were carried out under project nn2980k at the Norwegian Metacenter for Computational Science NOTUR. This is publication no. XXXX from the Bjerknes Centre for Climate Research.

References

- Alexandre, A., Meunier, J. D., Colin, F., and Koud, J. M.: Plant impact on the biogeochemical cycle of silicon and related weathering processes, *Geochimica Et Cosmochimica Acta*, 61, 677-682, 1997.
- Archer, D., Lyle, M., Rodgers, K., and Froelich, P.: What controls opal preservation in tropical deep-sea sediments?, *Paleoceanography*, 8, 7-21, 1993.
- Bernard, C. Y., Durr, H. H., Heinze, C., Segsneider, J., and Maier-Reimer, E.: Contribution of riverine nutrients to the silicon biogeochemistry of the global ocean - a model study, *Biogeosciences Discuss.*, 6, 1091-1119, 2009.
- Brzezinski, M. A.: The Si:C:N ratio of marine diatoms: interspecific variability and the effect of some environmental variables, *J. Phycol.*, 21, 347-357, 1985.
- Conley, D. J., Schelske, C. L., and Stoermer, E. F.: Modification of the Biogeochemical Cycle of Silica with Eutrophication, *Marine Ecology Progress Series*, 101, 179-192, 1993.
- Conley, D. J.: Riverine contribution of biogenic silica to the oceanic silica budget, *Limnology and Oceanography*, 42, 774-777, 1997.
- Conley, D. J., and Schelske, C. L.: Biogenic silica. In *Tracking Environmental Change Using Lake Sediments: Biological Methods and Indicators*, Smol, J. P., H. J. B. Birks & W. M. Last, (Editors), Kluwer Academic Press, pp. 281-293., 2001.
- Conley, D. J.: Terrestrial ecosystems and the global biogeochemical silica cycle, *Global Biogeochemical Cycles*, 16, 8, 1121, 10.1029/2002gb001894, 2002a.
- Conley, D. J.: The biogeochemical silica cycle: Elemental to global scales., *Océanis*, 28, 353-368, 2002b.
- Conley, D. J., Likens, G. E., Buso, D. C., Saccone, L., Bailey, S. W., and Johnson, C. E.: Deforestation causes increased dissolved silicate losses in the Hubbard Brook Experimental Forest, *Global Change Biology*, 14, 2548-2554, 10.1111/j.1365-2486.2008.01667.x, 2008.
- DeMaster, D. J., Smith, W. O., Nelson, D. M., and Aller, J. Y.: Biogeochemical

- processes in Amazon shelf waters: Chemical distributions and uptake rates of silicon, carbon and nitrogen, *Continental Shelf Research*, 16, 617-643, 1996.
- DeMaster, D. J.: The accumulation and cycling of biogenic silica in the Southern Ocean: revisiting the marine silica budget, 2002, ISI:000176691300004, 3155-3167,
- Dürr, H. H., Meybeck, M., Hartmann, J., Laruelle, G. G., and Roubéix, V.: Global spatial distribution of natural river silica inputs to the coastal zone., *Biogeosciences Discuss.*, 6, 1345–1401, 2009.
- Edmond, J. M., and Gieskes, J. M. T. M.: What controls opal preservation in tropical deep-sea sediments ?, *Geochim. Cosmochim. Acta*, 34, 1261-1291, 1970.
- Egge, J. K., and Aksnes, D. L.: Silicate as Regulating Nutrient in Phytoplankton Competition, *Marine Ecology-Progress Series*, 83, 281-289, 1992.
- Froelich, P. N., Atwood, D. K., and Giese, G. S.: Influence of Amazon River discharge on surface salinity and dissolved silicate concentration in the Caribbean Sea, *Deep Sea Research*, 25, 735-744, 1978.
- Gleick, P. H.: Global freshwater resources: Soft-path solutions for the 21st century, *Science*, 302, 1524-1528, 2003.
- Harrison, K. G.: Role of increased marine silica input on paleo-pCO₂ levels, *Paleoceanography*, 15, 292-298, 2000.
- Heinze, C., Maier-Reimer, E., Winguth, A. M. E., and Archer, D.: A global oceanic sediment model for long-term climate studies, *Global Biogeochemical Cycles*, 13, 221-250, 1999.
- Heinze, C., and MaierReimer, E.: The Hamburg Oceanic Carbon Cycle Circulation Model version "HAMOCC2s" for long time integrations. Technical Report 20.
- Deutsches Klimarechenzentrum, Modellberatungsgruppe, Hamburg., 1999.
- Heinze, C., Hupe, A., Maier-Reimer, E., Dittert, N., and Ragueneau, O.: Sensitivity of the marine biospheric Si cycle for biogeochemical parameter variations, *Global Biogeochemical Cycles*, 17, 2003.
- Heinze, C.: The long-term oceanic Si cycle and the role of opal sediment. In: *The silicon cycle - human perturbations and impacts on aquatic systems*,

- SCOPE 66. Chicago, IL 60628, USA: Island Press, p. 229-243, 2006.
- Heinze, C., Gehlen, M., and Land, C.: On the potential of Th-230, Pa-231, and Be-10 for marine rain ratio determinations: A modeling study, *Glob. Biogeochem. Cycle*, 20, 12, Gb2018 10.1029/2005gb002595, 2006.
- Humborg, C., Conley, D. J., Rahm, L., Wulff, F., Cociasu, A., and Ittekkot, V.: Silicon retention in river basins: Far-reaching effects on biogeochemistry and aquatic food webs in coastal marine environments, *Ambio*, 29, 45-50, 2000.
- Ingle, S. E.: Solubility of calcite in the ocean, *Marine Chemistry*, 3, 301-319, 1975.
- Laruelle, G. G., Roubex, V., Sferratore, A., Brodherr, B., Ciuffa, D., Conley, D. J., Dürr, H. H., Garnier, J., Lancelot, C., Le Thi Phuong, Q., Meunier, J.-D., Meybeck, M., Michalopoulos, P., Moriceau, B., Ní Longphuirt, S., Loucaides, S., Papush, L., Presti, M., Ragueneau, O., Regnier, P. A. G., Saccone, L., Slomp, C. P., Spiteri, C., and P. Van Cappellen. Anthropogenic perturbations of the silicon cycle at the global scale: the key role of the land-ocean transition., *Global Biogeochemical Cycles*. Accepted, 2009.
- Leynaert, A., Treguer, P., Lancelot, C., and Rodier, M.: Silicon limitation of biogenic silica production in the Equatorial Pacific, *Deep-Sea Research Part I-Oceanographic Research Papers*, 48, 639-660, 2001.
- Mackenzie, F. T., and Garrels, R. M.: Chemical mass balance between rivers and oceans, *American Journal of Science*, 264, 507-&, 1966.
- Mackenzie, F. T., Ver, L. M., Sabine, C., Lane, M., and Lerman, A.: C, N, P, S global biogeochemical cycles and modeling of global change. in *Interactions of C, N, P and S Biogeochemical Cycles and Global Change*, edited by Wollast, R., F. T. Mackenzie and L. Chou, pp.1-62. Springer-Verlag., 1993.
- Maier-Reimer, E.: Geochemical cycles in an ocean general circulation model. Preindustrial tracer distributions., *Glob. Biogeochem. Cycle*, 7, 645-677, 1993.
- Maier-Reimer, E., Kriest, I., Segschneider, J., and Wetzel, P.: The HAMburg Ocean Carbon Cycle Model HAMOCC 5.1 - Technical Description Release 1.1, 2005a.

- Maier-Reimer, E., Kriest, I., Segschneider, J., and Wetzel, P.: Technical description of the HAMburg Ocean Carbon Cycle model, version 5.1 (HAMOCC5.1), and of its interface to MPI-OM, available at: <http://www.mpimet.mpg.de/wissenschaft/modelle/mpiom/mpiom-description.html>, 2005b.
- Mehrbach, C., Culberso, Ch, Hawley, J. E., and Pytkowic, Rm: Measurement of the apparent dissociation constants of carbonic acid in seawater at atmospheric pressure, *Limnology and Oceanography*, 18, 897-907, 1973.
- Nelson, D. M., Treguer, P., Brzezinski, M. A., Leynaert, A., and Queguiner, B.: Production and Dissolution of Biogenic Silica in the Ocean - Revised Global Estimates, Comparison with Regional Data and Relationship to Biogenic Sedimentation, *Global Biogeochemical Cycles*, 9, 359-372, 1995.
- Paasche, E.: Silicon content of five marine plankton diatom species measured with a rapid filter method, *Limnology and Oceanography*, 25, 474-480, 1980.
- Rabalais, N. N., Wiseman, W. J., Turner, R. E., SenGupta, B. K., and Dortch, Q.: Nutrient changes in the Mississippi River and system responses on the adjacent continental shelf, *Estuaries*, 19, 386-407, 1996.
- Ragueneau, O., Chauvaud, L., Moriceau, B., Leynaert, A., Thouzeau, G., Donval, A., Le Loc'h, F., and Jean, F.: Biodeposition by an invasive suspension feeder impacts the biogeochemical cycle of Si in a coastal ecosystem (Bay of Brest, France), *Biogeochemistry*, 75, 19-41, 10.1007/s10533-004-5677-3, 2005.
- Raymo, M. E.: Geochemical evidence supporting T. C. Chamberlin's theory of glaciation, *Geology*, 19, 344-347, 1991.
- Ridgwell, A. J., Watson, A. J., and Archer, D. E.: Modeling the response of the oceanic Si inventory to perturbation, and consequences for atmospheric CO₂, *Global Biogeochemical Cycles*, 16, 26, 1071, 10.1029/2002gb001877, 2002.
- Roelke, D. L.: Copepod food-quality threshold as a mechanism influencing phytoplankton succession and accumulation of biomass, and secondary productivity: a modeling study with management implications, *Ecol. Model.*, 134, 245-274, 2000.

- Rosenberg, D. M., McCully, P., and Pringle, C. M.: Global-scale environmental effects of hydrological alterations: Introduction, *Bioscience*, 50, 746-751, 2000.
- Seitzinger, S. P., Harrison, J. A., Dumont, E., Beusen, A. H. W., and Bouwman, A. F.: Sources and delivery of carbon, nitrogen, and phosphorus to the coastal zone: An overview of Global Nutrient Export from Watersheds (NEWS) models and their application, *Global Biogeochemical Cycles*, 19, GB4S01, doi:10.1029/2005GB002606. , 2005.
- Shipe, R. F., Curtaz, J., Subramaniam, A., Carpenter, E. J., and Capone, D. G.: Diatom biomass and productivity in oceanic and plume-influenced waters of the western tropical Atlantic Ocean, *Deep-Sea Research Part I-Oceanographic Research Papers*, 53, 1320-1334, 10.1016/j.dsr.2006.05.013, 2006.
- Slomp, C. P., and Van Cappellen, P.: Nutrient inputs to the coastal ocean through submarine groundwater discharge: controls and potential impact, *Journal of Hydrology*, 295, 64-86, 2004.
- Slomp, C. P., and Van Cappellen, P.: The global marine phosphorus cycle: sensitivity to oceanic circulation, *Biogeosciences*, 4, 155-171, 2007.
- Smith, S. V., and Hollibaugh, J. T.: Coastal Metabolism and the Oceanic Organic-Carbon Balance, *Rev. Geophys.*, 31, 75-89, 1993.
- Treguer, P., Nelson, D. M., Vanbennekom, A. J., Demaster, D. J., Leynaert, A., and Queguiner, B.: The Silica Balance in the World Ocean: A Reestimate, *Science*, 268, 375-379, 1995.
- Treguer, P., and Pondaven, P.: Global change - Silica control of carbon dioxide, *Nature*, 406, 358-359, 2000.
- Ullmann, W. J., and Aller, R. C.: Diffusion coefficients in nearshore marine environments, *Limnology and Oceanography*, 27, 552-556, 1982.
- Van Cappellen, P., Dixit, S., and van Beusekom, J.: Biogenic silica dissolution in the oceans: Reconciling experimental and field-based dissolution rates, *Glob. Biogeochem. Cycle*, 16, 10, 1075, 10.1029/2001gb001431, 2002.
- Wallmann, K.: Feedbacks between oceanic redox states and marine productivity: A model perspective focused on benthic phosphorus cycling, *Global Biogeochemical Cycles*, 17, 18, 1084, 10.1029/2002gb001968, 2003.

- Wetzel, P., Haak, H., Jungclauss, J., and Maier-Reimer, E.: The Max-Planck-Institute Global Ocean/Sea-Ice Model MPI-OM; technical documentation, 90p,
- White, A. F., and Blum, A. E.: Effects of climate on chemical weathering in watersheds, *Geochimica Et Cosmochimica Acta*, 59, 1729-1747, 1995.
- Winguth, A. M. E., Archer, D., Duplessy, J. C., Maier-Reimer, E., and Mikolajewicz, U.: Sensitivity of paleonutrient tracer distributions and deep-sea circulation to glacial boundary conditions, *Paleoceanography*, 14, 304-323, 1999.
- Woodwell, G. M., Rich, P. H., and Hall, C. A. S.: Carbon in estuaries, *Brookhaven Symposia in Biology*, 221-240, 1973.
- Yool, A., and Tyrrell, T.: Role of diatoms in regulating the ocean's silicon cycle, *Global Biogeochemical Cycles*, 17, 21, 1103, 10.1029/2002gb002018, 2003.

CHAPTER 4

World-wide typology of near-shore coastal systems: defining the estuarine filter of river inputs to the oceans

Hans H. Dürr*, Goulven G. Laruelle*, Cheryl M. van Kempen, Caroline P. Slomp, Michel Meybeck and Hans Middelkoop

*H.H. Dürr and G.G. Laruelle have contributed equally to this manuscript.

Submitted to *Estuaries and Coasts*

June 2009

Abstract

We present a spatially-explicit global overview of near-shore coastal types, based on hydrological, lithological and morphological criteria. A total of 4 main operational types act as active filters of both dissolved and suspended material entering the ocean from land: small deltas (type I), tidal systems (II), lagoons (III) and fjords (IV). Large rivers (V) bypass the nearshore zone, while karstic (VI) and arctic coasts (VII) act as inactive filters. This typology provides new insight in the spatial distribution and inherent heterogeneity of the estuarine filter worldwide. The relative importance of each type at the global scale is calculated and types I, II, III and IV account for 32, 22, 8 and 26% of the global coastline, respectively, while 12% does not possess a coastal filter. As an application of this typology, a re-estimate of the global estuarine surface area is provided.

1. Introduction

The coastal zone is the highly dynamic transition area where the land meets the ocean. It constitutes one of the most active interfaces of the biosphere (Gattuso et al. 1998) and provides important human ecosystem services (Crossland et al. 2005, Kempe 1988). Despite its limited surface area compared to the open ocean, the coastal zone plays an important role in the global cycling of many biogeochemically important elements given. For example, it receives major inputs of terrestrial material through river and groundwater discharge and exchanges large amounts of energy and matter with the open ocean (Alongi 1998; Rabouille et al. 2001; Slomp and Van Cappellen 2004).

A large and increasing proportion of the global population lives in this domain and this makes it one of the most vulnerable and perturbed areas. While many models exist to describe the biogeochemistry of estuaries and other coastal systems on a local and regional scale (Allen et al. 2001; Lohrenz et al. 2002; Moll and Radach 2003), the incorporation of the near-shore coastal zone into global oceanic models remains limited by resolution constraints. As yet, the spatially complex pattern of incoming riverine fluxes is commonly either simplified or ignored when defining boundary conditions of Ocean General Circulation Models (Aumont et al. 2001; Da Cunha et al. 2007; Bernard et al. 2009).

But how is the coastal zone defined exactly? This depends on the point of interest. Oceanographers tend to use the term for the continental shelves as a whole (Smith and Hollibaugh 1993; Crossland et al. 2005) where the shelves are seen as a filter between the realm of rivers and other continental influences and the open ocean. The shelves are often approached as a system of several layers, with the first level being the transition zone between riverine (fresh) and marine waters, generally termed as ‘estuaries’ (Woodwell et al. 1973).

A large body of literature exists on definitions of the different types of near-shore coastal systems. These definitions are commonly based on their origin, geomorphology, dynamics, sediment balance, biogeochemistry, or ecology (Elliott and McLusky 2002; Meybeck et al. 2004; Schwartz 2005; Meybeck and Dürr 2009). The most well-known global scale “coastal typology” established to date is the one of LOICZ (Talaue-McManus et al. 2003; Crossland et al. 2005;

Buddemeier et al. 2008), which describes nutrient levels in individual coastal cells at 0.5° resolution. The types are derived from a statistical treatment of a large number of physical and morphological criteria combining terrestrial and marine realms and including human impacts (Gordon et al. 1996). The LOICZ typology is of great value for coastal zone biogeochemical flux assessments, and is the only comprehensive, spatially-explicit global scale effort we are aware of. However, the results are not easily used outside the context of analysis of groups of cells with similar characteristics, since cells belonging to the same estuarine entity can be attributed to different clusters.

Other typologies have been developed, but their geographical extent is mostly limited to only part of the world (e.g. Australia in Digby et al. 1998; USA in Engle et al. 2007) and they sometimes also originate from cluster analysis and thus do not provide easy-to-use criteria (e.g., Engle et al. 2007). Often, typologies are developed for a particular purpose and only describe single physical or geographical parameters, such as the hydrodynamics of a system (Carter and Woodroff 1994), the degree of openness of an estuary (Bartley et al. 2001), or one particular type of coast such as deltas (Davis and Fitzgerald 2004). Coastal segmentation approaches (Meybeck et al. 2006) provide geographical limits for budgeting of incoming riverine material fluxes at the global scale, but do not delineate the various types of coastal areas specifically. Finally, available maps of the global geographic distribution of coastal types typically leave some regions unclassified or include overlapping sections (Dolan et al. 1975). There is thus still a need for a global, comprehensive morphological coastal typology useable to distinguish types of coast that can be identified in terms of the filtering effect of incoming riverine material.

Here, we present an object-based, spatially-explicit global typology at a 0.5 degree resolution that is based on hydrological, lithological and morphological criteria. The typology was developed in a GIS framework, making it easy to use and distribute. Nearly 300 individual objects are described using higher resolution data sets. Our operational typology provides a direct link to well-established databases for continental river basins at the same scale (Vörösmarty et al. 2000 a, b). The typological approach allows the development of tools for inventory

and comparison of systems. Hence, this typology can find applications that range from global mapping, regional and global budgeting of material fluxes, to nutrient modelling. Furthermore, we provide an inter-type comparison of basic hydrodynamical properties, and propose a revised number for Woodwell et al.'s (1973) estimate of the global estuarine surface area.

2. Methods

2.1. General approach

Here, we define a set of four main estuarine filter types, plus three additional types for other types of coast. They are mapped according to the limits of the STN-30 river basins (Vörösmarty et al. 2000 a, b), and each final terrestrial cell is labelled with a typology code for the type of receiving coastal water body: type I – small deltas, type II – tidal systems, type III – lagoons, type IV – fjords and fjärds, plus large rivers (type V) as well as karst-dominated stretches of coast (type VI) and arheic areas (type VII).

The systems included in our analysis include all near-shore filter types, i.e. 'estuaries' in the widest sense (Schwartz 2005), representing the body of water bordered by rivers on the upstream boundary and the open waters of the continental shelf on the downstream boundary. This is consistent with boundaries found in the literature for individual systems. We are aware that different types of near-shore coastal water bodies can be divided into dozens of additional second-order or third-order types (e.g. Meybeck et al. 2004; Vafeidis et al. 2008). However, when mapping types at a global scale, there is a need for simplification and the introduction of groups of types where specialists would suggest important differences.

2.2. Conceptual definition of types

Our typology only concerns exorheic river basins and aims at describing the interface between continents and the open ocean. Hence, large inner parts of continents are not included in this study for the sole reason that they flow towards enclosed internal seas such as the Caspian Sea. The physical characteristics of all 7 types are shown in Figure 1.

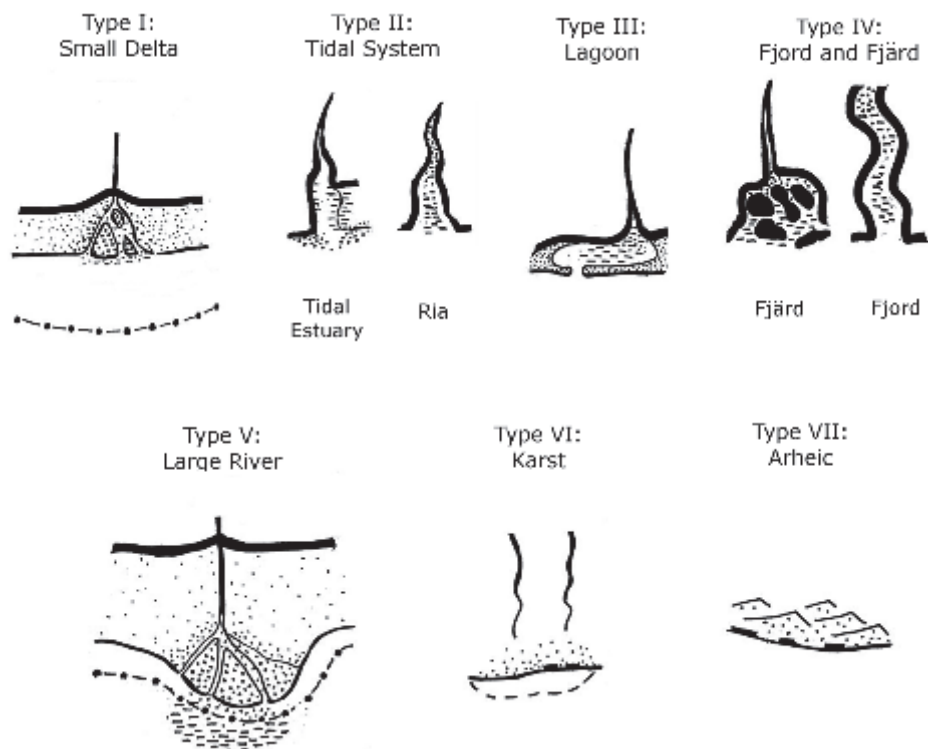


Figure 1: Estuarine filter types with their physical boundaries. For further details: see text.

Type I: Small deltas

A delta is a coastal landform created by sediment deposition at the mouth of a river, forming an alluvial landscape, and where the sediment supplied to the coastline is not removed by tides or waves. (Schwartz 2005). Several forms of deltas are distinguished, e.g. river-dominated, wave-dominated or tide-dominated deltas, not all leading to the classical deltaic form, coined after the Nile River delta by Herodotus (Schwartz 2005). However, many deltas world-wide have such high discharge and incoming material rates, that limited filtering occurs in the internal delta channels (Meybeck et al. 2004). As such, most of the deltas mapped in this class are comparatively small, while many of the rivers possessing larger, well-known deltas, have been indicated as ‘large rivers’ (type V).

Type II: Tidal systems

As opposed to river deltas that protrude onto the receiving shelves, tidal systems are here defined as a river stretch of water that is tidally influenced. This definition includes rias and tidal embayments and classical funnel-shaped estuaries which are usually characterised by comparable residence times.

Type III: Lagoons

Coastal lagoons are comparatively shallow water bodies that are separated from the open ocean by a barrier, such as sandbanks, coral reefs, or barrier islands (Schwartz 2005). Lagoons are generally less than 5 meters deep, very elongated but narrow, and are commonly orientated parallel to the coast. The definition extends to any enclosed shallow body of water situated between the river and the coast where tidal influence in general is minimal.

Type IV: Fjords and fjärds

Fjords are classical U-shaped valleys created by glaciers that were drowned and are thus characterized by long, often narrow inlets with very steep topographies (Syvitski et al. 1987). Major fjords can be very deep, such as the Sognefjord in Norway that reaches depths under 1000 m (Sørnes and Aksnes 2006). Fjords generally are separated from the open sea by a sill or rise at their mouth, due to the presence of the former glacier's terminal moraine. Fjärds are wider and shallower, and have more gentle, lateral slopes. They share the glacial origin, and are characterized by many islands. A typical representative of this type of coast is the Swedish coast around Stockholm.

Non-filter types:

Type V: Large rivers

In this type, the major biogeochemical processing of incoming river fluxes takes place in a plume on the continental margin (type V – large rivers, or 'RiOMars', i.e. River dominated Ocean Margins, McKee 2003; Dagg et al. 2004; McKee et al. 2004). Some of these large systems may be influenced by tides, and we therefore include a subtype (type V_b) for tidal large rivers.

Type VI : Karst-dominated coast

Karsts are landforms that are dominated by dissolution of carbonate rock (Ford and Williams 1989). This leads to distinct landscapes, such as observed along the coasts of the Eastern Adriatic, Borneo, and Ha-Long Bay in Vietnam (Herak and Springfield 1972). Submarine groundwater discharge is important in these areas (Slomp and Van Cappellen 2004; Fleury et al. 2007). While multiple submarine ‘point’ sources of continental waters thus occur, surface fluxes are generally negligible.

Type VII : Arheic coast

In arid regions, such as deserts, runoff is so low that significant stretches of coast are characterized by a near-total absence of water inputs (arheism) from the continent to the ocean.

2.3. Determination of types of estuarine coastal filters

The development of the typology consisted of several successive steps, following a decision tree (Figure 2) using an iterative process that included multiple verifications, and decisions on the identification and clustering of various coastal types.

Step 1: Exorheic vs. endorheic parts of the continents

Endorheic river basins flow towards internal seas and lakes. Hence, the material carried never reaches the ocean. The digitized global potential river network (Vörösmarty et al. 2000 a, b) was used to distinguish between systems draining to the external parts of the continents (exorheism) vs. internal basins (endorheism).

Step 2: Absence of filter: Rheism – arheism, karst

The second step involved establishing whether a river basin is intercepted by an estuarine filter before reaching the coastal ocean. Such a filter can be absent due to arheism, or submarine groundwater discharge. Rheic systems were differentiated from arheic systems based on average runoff over the whole

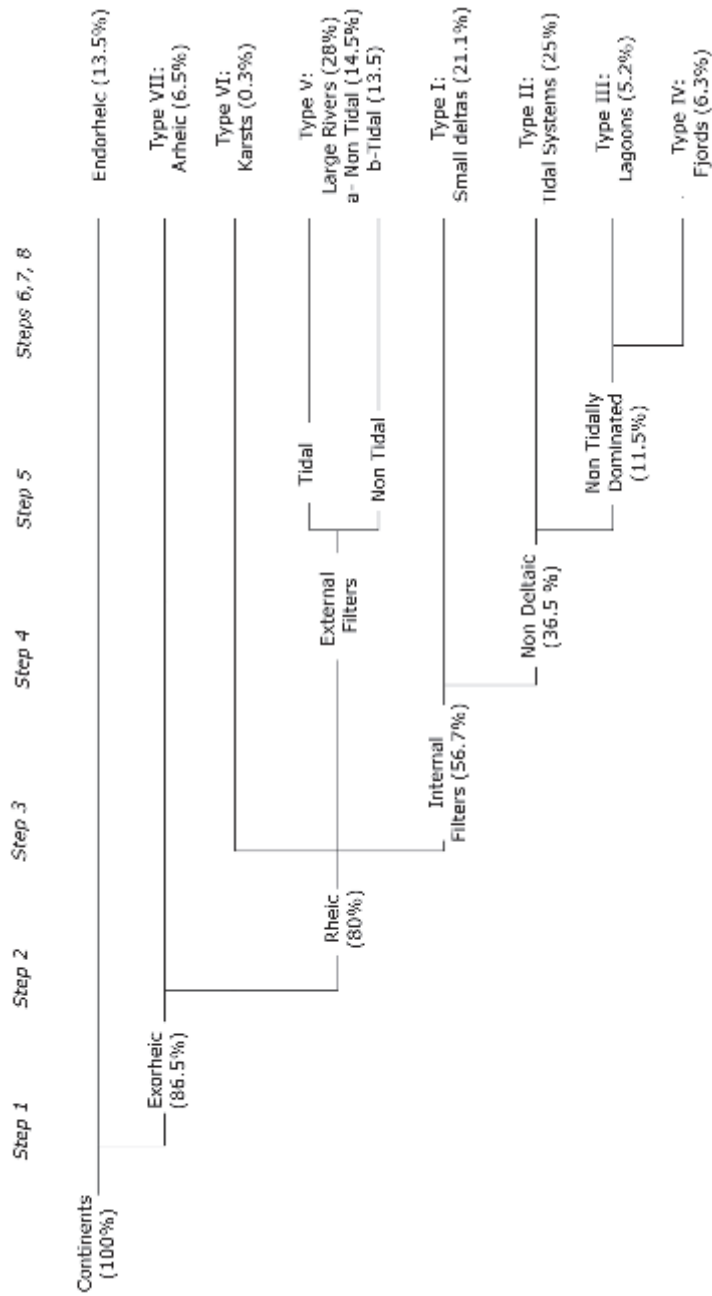


Figure 2: Schematic of the hierarchical steps for type determination plus surface distribution of river basins catchments connected to the different types.

watershed (arheic when runoff $< 3 \text{ mm y}^{-1}$) (Vörösmarty et al. 2000 a, b; Fekete et al. 2002). Carbonate rock dominance on the last terrestrial cell of the upstream river basin (Dürr et al. 2005) was used to indicate karst occurrence (type VI). Larger systems mostly develop other dominant types of coast, and dominant coastal karst occurrence is thus mostly limited to catchments with very few upstream cells.

Step 3: Estuarine filters – external filters

Large rivers produce estuarine plumes that extend far beyond the defined limits of our estuarine filters and they are thus considered external filters (Meybeck and Dürr 2009). Based on McKee (2003), McKee et al. (2004) and Dagg et al. (2004), we assume that the Rhône River (with a discharge of $52 \text{ km}^3 \text{ y}^{-1}$) is the smallest large river. The geographic distribution of large river deltas was assessed using available literature (Davis and Fitzgerald 2004; Ericson et al. 2006). Protruding deltas were identified one by one using the form of the coastal morphology and the shape around the 200 m bathymetry line from the Smith and Sandwell (1997) dataset. Case by case verification revealed that most of the major deltas were associated to large rivers (type V). In some cases, large river systems were connected to large estuarine systems and were assigned to another type. Prominent examples are the Ob, St. Lawrence, and the Parana and Uruguay (Rio de la Plata) rivers.

Step 4: Remaining smaller deltas

Small deltas (type I) were identified as remaining smaller deltas, mostly with surface areas (total delta area) $< 1.000 \text{ km}^2$. Additionally, small basins without distinct features, as well as rocky coasts, and other miscellaneous types that could not be attributed to one of the other major coastal types, were clustered here.

Step 5: Tidal Systems

Tidally dominated systems were identified by combining coastline maps showing coastal embayments with global tide amplitude maps (Hayes 1979; Stewart 2000). All such systems with tidal amplitude $> 2 \text{ m}$ were included. Furthermore, some selected systems with tidal amplitude $> 1 \text{ m}$ were also chosen, based on shape

and when tidal energy > river energy. Additionally, rias were identified using the ‘submerging’ type on the map of Kelletat (1995). Systems such as the Delaware, Chesapeake Bay and San Francisco Bay are included here.

In some of the ‘large river’ systems (type V), tides can be important, when they propagate into the estuary. We have identified these systems (type Vb), using the information on tidal amplitude, combined with more detailed information for individual systems, such as the Amazon and Tocantins (Gallo and Vinzon 2005), and several Indian rivers (Harrison et al. 1997; Selvam 2003).

Step 6. Lagoons

River basins passing through coastal lagoons on their way to the sea were identified, based on coastal morphology (Kelletat 1995). We used a combination of the coastline shape with information derived from atlases (New York Times, 1992) or imagery sources such as Google Earth (Google, 2009). Lagoons unconnected to rivers were not included.

Step 7: Fjords and fjärds

In our typology, fjords and fjärds were identified by systems characterised by combined (i) hard rock lithology and (ii) maximum Quaternary glacier coverage extent, both derived from Dürr et al. (2005), and (iii) coastline shape (New York Times, 1992) and bathymetry (Smith & Sandwell, 1997).

Step 8: Overlapping types

In some cases, for single cells containing different types a choice of a dominant type had to be made or several cells were grouped to a main type. The final type assignment was based on the net filter function of different types of coastal zones. Mostly, the order of priority for the attribution of the different types was established as follows (from highest to lowest): Large Rivers, Lagoon, Arheic, Karst, Fjord, Tidal systems (Estuary and Ria), Identifiable deltas, Fjärd, Miscellaneous, mostly remaining stretches of coast (mainly assigned as small deltas).

The four types of estuarine filters that are distinguished here are ranked

in an increasing order of fresh water residence time, also called flushing time (Sheldon and Alber 2006). Table 1 summarizes how the morphological subtypes were derived from various sources.

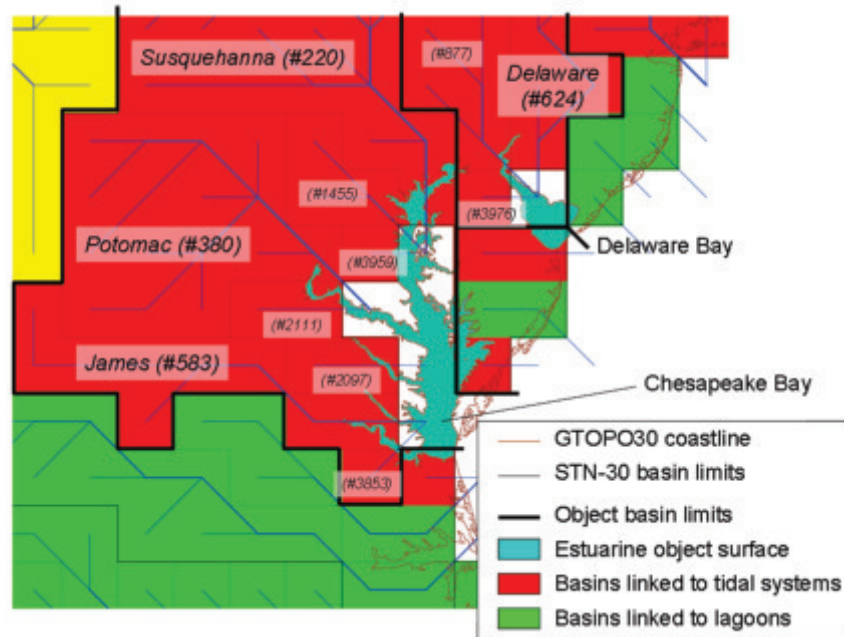


Figure 3: Examples of estuarine objects along the Eastern coast of the USA. Physical boundaries of objects are detailed, connected river basins at STN-30 resolution (0.5 deg.) are shown, together with the colour of the corresponding coastal type. Names of major river basins are highlighted and STN-30 v.6 basin numbers of all river systems connected to a single coastal entity / object are given. Estuarine surface area is also shown.

2.4. Individual object description

A set of 302 of the most important individual estuarine systems distributed world wide were manually delimited on the GIS using the ‘GTOPO30’ coast limit (USGS-EDC, 1996), at a 0.5 minute resolution (about 1 km²). Figure 3 presents an example stretch of coast showing several of these systems along the North East Atlantic coast of the United States. The systems widely vary in size and morphological structure. The area of each system was established by delimiting

Table 1: Main sources used for the step by step determination of coastal types and their certainty (from –very uncertain to ++ highly certain).

Step	Coastal type	Description	Map				Tides				Remarks	References	Degree of certainty
			Map	Satellite imagery	Lithology	River discharge	Ice extent	Bathymetry	Morphology	Tides			
1	0	Endorheic										Vorosmarty et al. 2000 a, b	++
	VII	Arctic				X						Fekete et al. 2002	++
2	VI	Karst	X		X							Durr et al. 2005	+
3	V	Large rivers	X									Herak and Springfield 1972, Sweeting 1972	
4	I	Small deltas	X									McKee 2003	+
												Davis and Fitzgerald 2004	+/-
												Various sources	+/-
5	II	Tidal systems	X									LOICZ database (Stewart 2000), Hayes 1979	+
												Kellert 1995	+/-
												Meybeck et al. 2004	+
												Google Earth	
	V _b	Tidal large rivers		X								Various sources	+
												(see main text)	
6	III	Lagoons	X									Davis and Fitzgerald 2004,	+/-
												Google Earth, Sea-WIFS (NASA 2006)	+
												Durr et al. 2005	+
7	IV	Fjords and fjords	X		X							Gregory 1913,	--
			X									Meybeck et al. 2004	+
												Smith and Sandwell 1997	
												GTOPO30 coastline	+/-
8	I	Miscellaneous systems		X								Google Earth (Google 2009)	
				X								Sea-WIFS (NASA 2006)	
												Various	
	II	Non-tidal estuarine-shaped systems	X									Gregory 1913,	--
												Google Earth (Google 2009),	+
												various other sources	+/-

the GTOPO30 coastline by a virtual prolongation of the external coastline. Note that the surface area defined here represents the water surface and does not include internal islands, salt-marshes and other emerging features. This distinction is particularly important for deltas, since the delta surfaces available in the literature (Ericson et al. 2006) usually refer to the whole deltaic domain including the terrestrial part. Each system was then assigned to a river basin via its STN-30 v.6 basin number (Vörösmarty et al. 2000 a, b), at the 30 minute scale.). For each coastal object, we then calculated the water discharge (based on Fekete et al., 2002), sediment fluxes (based on Beusen et al. 2005) and associated river basin population (Vörösmarty et al., 2000c). In several cases, such as the Chesapeake Bay, the Ob / Pur-Taz basins, or major lagoons (Patos, Laguna Madre), several STN-30 basins connect to the same coastal object (e.g., bay or lagoon), and the ensemble of the connected systems was considered when calculating the incoming fluxes and basin pressures.

The volume of each individual estuarine filter was established by a GIS standard algorithm transforming geographical shapes into grids. Then, a depth was assigned to each grid cell at a resolution of 1 minute, corresponding to the highest resolution of globally available consistent bathymetry data sets, in order to calculate the volumes. The global bathymetric dataset used for this purpose was Smith and Sandwell (1997). Several other global bathymetry datasets were tested (ETOPO2 dataset (U.S. D.C. – NOAA 2006) and the GEBCO database (GEBCO 2007)), but the Smith and Sandwell (1997) data gave the best overall picture when compared to high-resolution data available for individual systems in the literature.

For validation purposes, surface areas and volumes of 18 systems were collected from the literature (Table 2). Despite the emphasis on tidal temperate estuaries and, lagoons in many coastal studies, our collection was as representative as possible, and also included fjords and several small deltas. A good correlation was observed for the surface areas between the GIS calculation and the literature values (Figure 4a). The robustness of the method decreases for estuaries smaller than 300 km² (about the size of the Scheldt estuary or Apalachee Bay). In some cases, the complex boundary of a system makes a proper definition of the deltaic shape difficult. For example, this is the case for the Pearl River, which is described

as having a surface area of 1970 km² by Wong and Cheung (2000), while we estimate an area of 2753 km².

The calculated volumes for the validation set correlate well with the

Table 2: Calculated and observed (when available) estuarine surface areas (Ae) and estuarine volumes for selected near shore coastal systems that were manually delimited. N.a.: not available.

System Name	Type	Ae (km ²)		Volume (10 ⁶ m ³)		Ref.
		Calculated	Observed	Calculated	Observed	
Bug	II	61	50	n.a.	n.a.	(1)
Chesapeake Bay	II	10073	11542	82656	69252	(2)
Delaware Bay	II	1980	1989	15403	19293	(2)
Dnieper	II	741	750	8321	3000	(1)
Gironde	II	604	635	n.a.	n.a.	(3)
Ob	II	34790	408000	813452	612000	(4)
Pearl River	II	2753	1970	19613	11578	(5)
Scheldt	II	383	277	4124	3102	(2)
Apalachicola Bay	III	813	260	n.a.	n.a.	(6)
Curonian Lagoon	III	1602	1584	7794	6200	(7)
Don (Azov Sea)	III	37077	40000	347158	320000	(8)
Maracaibo Lake	III	12695	13210	263058	28000	(9)
Oder Lagoon	III	844	1000	9197	3500	(10)
Patos Lagoon	III	9851	10000	n.a.	n.a.	(11)
Venice Lagoon	III	388	500	4594	1000	(12)
Vistula Lagoon	III	740	838	4250	2300	(13)
Aysen Fjord	IV	263	350	n.a.	n.a.	(14)
Sognefjord	IV	898	950	310816	530000	(15)

(1) Dziganshin and Yurkova 2001, (2) Nixon et al, 1996, (3) Audry et al, 2007 (4) Invanov 1991 (5) Wong and Cheung, 2000, (6) Mortazavi et al., 2000, (7) Stankevicius, 1995, (8) Tolmazin 1985 (9) Laval et al, 2005 (10) Grelowski 2000, (11) Castelao and Moller 2006, (12) Solidoro et al, 2005 (13) Chubarenko and Margoński 2008 (14) Marin et al. 2008 (15) Sørnes and Asknes 2006

observed values (Figure 4b). In contrast to the trend observed for the surface area, the largest systems do not necessarily show the best fit. This is partly due to the deep fjords which are poorly described in bathymetric datasets (Smith and Sandwell 1997). Overall, systems larger than 4000 M m³ do not differ by more than 50%, which is the order of magnitude of the tidal prism in many macrotidal systems (Monbet 1992).

3. Results and Discussion

3.1. Spatial distribution and heterogeneity of types

The world-wide distribution of the various types of estuarine filters reveals a large heterogeneity between continents and between oceanic basins, but

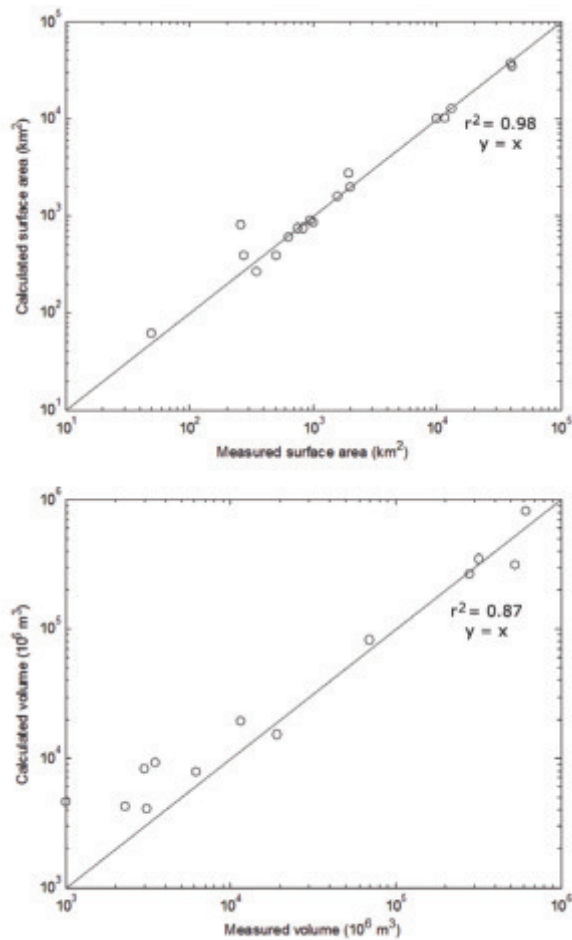


Figure 4: Comparison of measured and calculated surface areas and volumes for 18 systems (see Table 3) for validation. The regression equations ($y = x$) are forced.

also very clear geographical patterns (Figure 5). Major world river basins and their coastal type are described in table 3. The observed distribution stems from a complex interplay of different factors influencing the coastal morphology, from genetic origins such as geological or glacial history, to differences between the energy provided by rivers or tides, to differences between types due to a varying influx of water and sediments associated with climate, vegetation, relief, soils and other characteristics of the upstream basin.

Table 3: List of the world's 100 largest river basins and the type of filter per continent.

	<i>Endorhetic</i>	<i>Type I</i>	<i>Type II</i>	<i>Type III</i>	<i>Type IV</i>	<i>Type V</i>
North America		Nelson	Saint Lawrence San Francisco Bay Baker		Frasier Churchill Colombia	Mississippi Colorado RioGrande Mackenzie Yukon
South America		Salado	Parana Chubut Uruguay Paratiba			Amazon Orinoco Tocantins Magdalena Colorado
Europe	Volga		Dvina	Dnepr Don		Negro Arg. Danube Neva Pechora Zaire Nile Niger Zambezi
Africa	Lake Chad, Tamanrasset, Bode le Depr, Okavango Lake Rudolf	Volta Orange Jubba	Ogooue Senegal	Kouliou		
North Asia		Limpopo Yana Olenek	Yenisei Ob Amur Khatanga Kolyma	Anadyr		Lena Indigirka
South East Asia	Amu-Darya, Tarim, Kerulen, Syr-Darya, Farah, Garagum, Ruo Dong, Shur, Dzungarian, Jaji, Ural, Lake Balkhas, Kure, Ili, Qarqan, Za'gya Bogea Great Artesia Mac Key Lake Frome	Krishna, Hai Ho	Chang Jiang Zhujiang Shatt el Arab Liao Huai			Ganges Mekong Irrawaddy Salween Godavari Huang He Indus
Australia/Oceania		Taymyr		Murray		

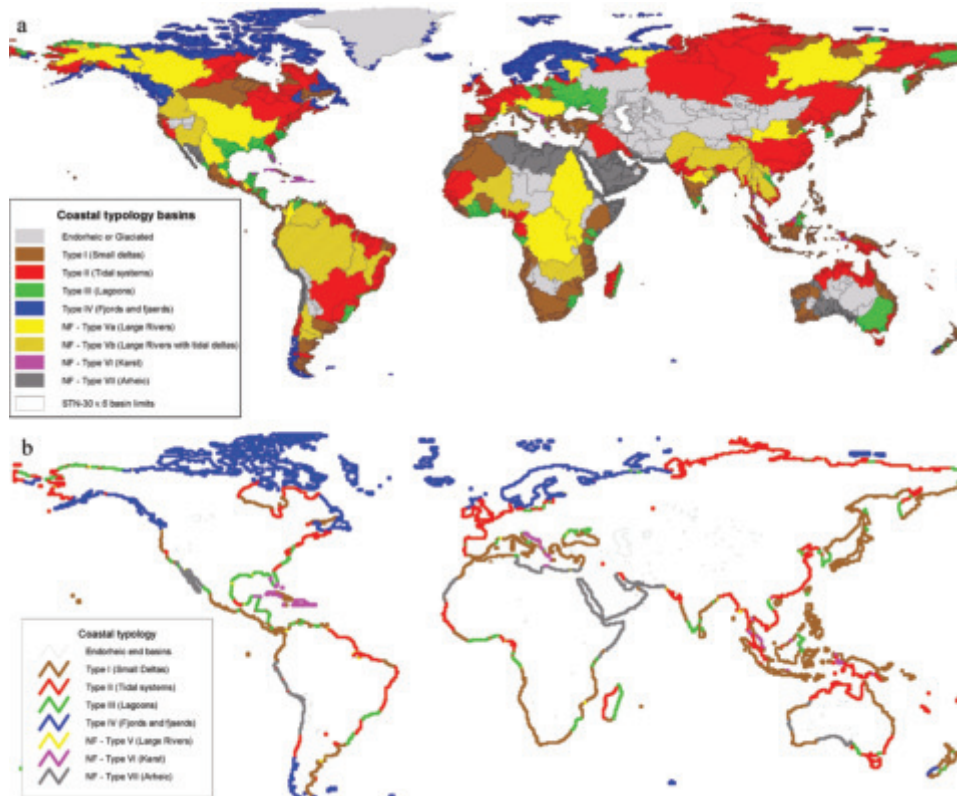


Figure 5: Spatial distribution of the internal filters according to their type. On the top panel (a), the whole watersheds are coloured while only the coastline is designated on the bottom panel (b).

The majority of endorheic river basins are located in Eastern Europe and Central Asia (62% of the endorheic continental area). The surfaces of the remaining continental surface landmass are widely dominated by exorheic river basins. In South and North America as well as Africa, the fraction of the watershed surface occupied by large rivers is the largest. These systems contribute to 41.6% of the continental water discharge, 25.7% of sediment load (mostly from tidal large rivers) and 33.6% of the exorheic land area, but they provide runoff to less than 1% of the global coastline (table 4). This also leads to a biased distribution of the population. While 26.4% of the total population live in these areas, only 1.9% live in coastal areas connected to large rivers.

Table 4: Global riverine connection to estuarine filter for river basin area (Ab), coastal length, total population, coastal population (at mouth), water discharge (Q) and sediment load per type.

Type	River basin area (Ab) (10 ⁶ km ²)	Coastline length (km)	%	Total Population (10 ⁶ p)	%	Coastal Population (at mouth) (10 ⁶ p)	%	Water Discharge (km ³)	%	Sediment Load (10 ⁶ t)	%
I-Small deltas	21.1	131167	30.1	1273	20.7	405	43.1	6458	16.5	7305	42.5
II-Tidal Systems	34.8	91326	21.0	2163	35.2	281	29.9	10718	27.4	2732	15.9
III-Lagoons	7.2	33286	7.6	399	6.5	102	10.9	1824	4.7	801	4.7
IV-Fjords	8.7	105657	24.3	44	0.7	20	2.1	2732	7.0	815	4.7
Va- Large Rivers	20.1	2945	0.7	649	10.6	6.8	0.7	4400	11.3	672	3.9
Vb-Tidal Large Rivers	18.7	13.5	0.4	972	15.8	10.9	1.2	11858	30.3	3746	21.8
VI- Karst	0.5	10543	2.4	58	0.9	34.4	3.7	310	0.8	284	1.7
VII- Atheic	9.1	35979	8.3	172	2.8	69.7	7.4	32	0.1	75	0.4
Total Exorheic	120.1	387103	94.4	5730	93.3	929.3	99.0	38333	98.1	16431	95.6
Endorheic	18.8	24469	5.6	409	6.7	9.4	1.0	757	1.9	748	4.4
Grand Total	138.9	411572	100	6139	100	938.7	100	39090	100	17179	100

Other coasts without estuarine filters (types VI and VII) are mainly located in tropical and subtropical regions where they represent 22% of the coastline between 30°N and 30°S, and 11% of the global coastline. Coastal karst is primarily found in tropical and equatorial, well-known, areas including Florida. They only represent 2.4% of the world's coastline and account for only 0.8% of its river discharge. The remainder of the non-filter coast consists of arid regions such as the Arabian Peninsula, northern Africa and along subtropical borders of the West Pacific. Australia alone accounts for 7% of the arctic coastline.

Nearly 57% of the world's exorheic river water discharge and 71% of the sediment discharge to the oceans passes through estuarine filters (Table 4). In terms of coastline distribution, estuarine filters account for approximately 88% of the world-wide exorheic coastline. Types I and III are heterogeneously distributed around the globe. Long stretches of the Siberian coast consist of large rias (type II). Lagoons are particularly well represented between the equator and 40°N. This is largely due to the, sometimes nested, lagoons of the Gulf of Mexico, Florida and the South East coast of the US. In Europe, the northern part of the Black Sea including the Azov Sea is treated as a mega lagoon. The remainder of the lagoons is distributed more or less equally along all continents and latitudes. Tidal systems and small deltas (types II and I) occur across all climate zones. Their distribution varies significantly from one continent to the other. Western Europe, northern Asia and South East China can be qualified as dominated by tidal-type coasts, while sub-equatorial Africa, India, Indonesia, North-East China and Japan are dominated by small deltas. North America as well as eastern South America exhibit significant stretches of coastline from each type and Central America appears dominated by lagoons (type III) on its Atlantic side and by small deltas (type I) on its Pacific side. Fjords (type IV), however, are essentially concentrated in Scandinavia, Canada, Alaska and southern Chile, plus a few coasts of New Zealand, due to their origin in formerly glaciated areas. Fjords account for 75% of the coastline north of 70°N.

Differences also show up when mapping river basins connected to a particular type of coast and coastal cells alone (Figures 5a and b, respectively). This is indeed somewhat a consequence of our type definition, and is particularly evident in regions such as East Asia where most of the major watersheds are

connected to tidal systems (type II) while most of the coastline actually consists of small deltas. This discrepancy between watershed area and coastline length is also observed for lagoons that typically have comparatively small river basins, as for the Brazilian coast. Although fjords are completely absent in Africa and almost non-existent in Asia and Oceania, the other types are represented on all continents. Consequently, there is a real difference between the spatial distribution of estuarine filters along the coastline (Figure 5b) and the watershed area connected to the filters (Figure 5a). While the first provides a realistic representation of estuarine filters, the latter provides an indicator of relative river contribution. As an example, 61% of the water flowing into the Atlantic does not encounter an estuarine filter, due to the large contributions of the Amazon ($6548 \text{ km}^3 \text{ y}^{-1}$), Mississippi ($639 \text{ km}^3 \text{ y}^{-1}$) and Congo/Zaire ($1330 \text{ km}^3 \text{ y}^{-1}$). The contribution of the Orinoco ($1106 \text{ km}^3 \text{ y}^{-1}$), in contrast, is filtered by an estuary.

3.2. Clusters of types and their origins

To highlight some of the key characteristics of each coastal type with respect to runoff and sediment transport characteristics, a cluster analysis was carried out for a subset of the ~300 individual objects. We used the estuarine surface area (A_e), estuarine volume (V_e), watershed surface area (A_b), annual river water discharge (Q) and sediment load (S) (Figures 6 and 7). The latter three data sets were obtained from global statistical model outputs within the GlobalNEWS-framework (Vörösmarty et al. 2000 a, b; Seitzinger et al. 2005). In order to comply to guidelines regarding the accuracy of these values (Seitzinger et al. 2005), the smallest watersheds (<8 continental cells) were excluded from the analysis. Due to the very limited number of objects that can actually be spatially delimited for small deltas (<5 items), we included 7 large deltas world-wide where the GTOPO30 detailed coastline allowed an identification of the estuarine water surface area. While these systems are different from small deltas in terms of filtering (e.g., external plumes vs. internal filtering), most of the ‘large rivers’ are actually deltas and can be studied together from a geomorphological point of view for the cluster analysis. Included are the Amazon, Nile, Mississippi, Lena, Mackenzie, Indus and Yukon deltas, attributed as ‘large rivers’ (type V). This procedure allowed us to

obtain a somewhat larger set of data for deltas.

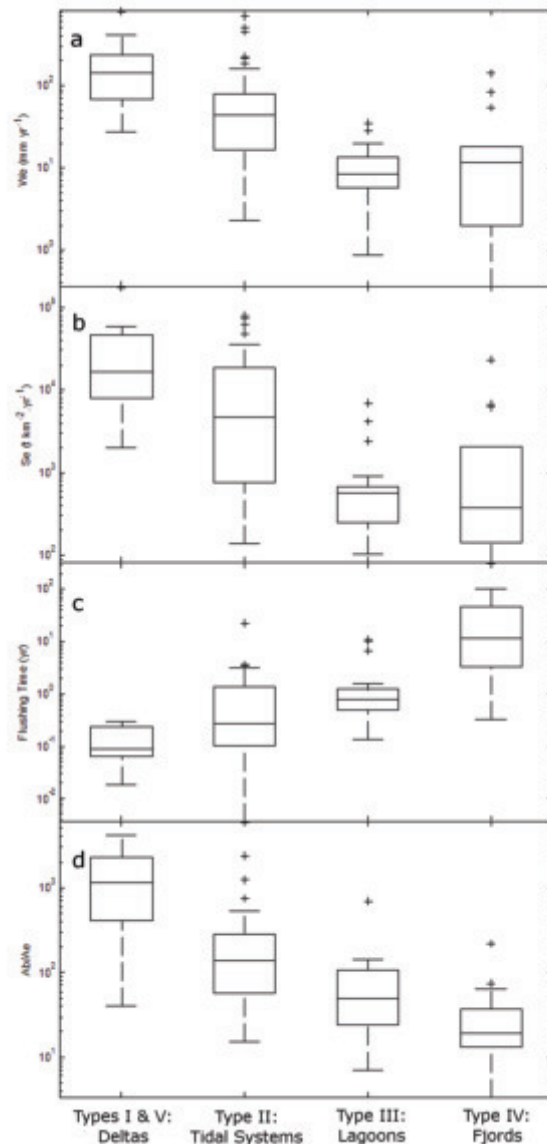


Figure 6: Boxplot of the distribution of the We , which is defined as the annual rivers discharge divided by the estuarine surface area (Q/A_e), (a), Se , which is the ratio of the annual sediment load and estuarine surface area (S/A_e) (b), Flushing time (c) and ratio of the estuarine surface area and river basin area (A_e/A_b) (d) per filter type.

We calculated various parameters (Figures 6 a-d) for each type: (a) the We index which is defined as the annual river water discharge divided by the estuarine surface area (Q/A_e), thus representing the average amount of water received per unit area collected by the estuarine object. (b) the Se index, which is calculated in the same way using the annual sediment wash load (S/A_e), (c) the flushing time, or river water residence time, for each system (V_e/Q) and (d) the ratio of basin area to estuarine surface area (A_b/A_e). Despite a wide heterogeneity, the We index tends to be high for tidal systems and low for lagoons. Both types comprise small and large watersheds, unlike fjords which are mainly fed by river basins of modest size ($<10^5 \text{ km}^2$), and consequently rather limited incoming discharge. For the Se index, the heterogeneity within types is larger than for the We index but, in general, tidal systems exhibit a higher sediment charge per estuarine area while few lagoons and fjords reach $10^3 \text{ t sediment km}^{-2} \text{ yr}^{-1}$. Overall, it appears that, in spite of their usually large surfaces, fjords collect relatively modest discharge and sediment per surface area. Lagoons and tidal systems can have a wide range of river basin sizes but the latter is characterized by higher We and Se . The relation between incoming riverine water fluxes and estuarine area and volume is indicated by the varying flushing times per coastal type.

The relation between incoming riverine water fluxes and estuarine area and volume is reflected in varying flushing times per coastal type. Overall, tidal systems have shorter residence times than lagoons while fjords possess the longest residence times. Deltas have comparatively low flushing times (Figure 6c), due to the interplay of high incoming water fluxes from large river basin areas (Figure 6d; Figure 7a) with often comparatively low estuarine volumes. A comparison between flushing times and river basin area (Figure 7b) exhibits a trend for shorter water residence time with increasing watershed area. Fjords (type IV) stand out clearly with high flushing times and modest basin areas, whereas lagoons have slightly elevated flushing times with restricted variability, despite large variation in basin areas (Figure 6c; Figure 7b). The median flushing times are 0.08, 0.27, 0.78 and 10.2 yrs for types I, II, III and IV, respectively.

The direct comparison of sediment loads against water discharge displays a linear relationship, well known from the literature on river sediment load (Walling

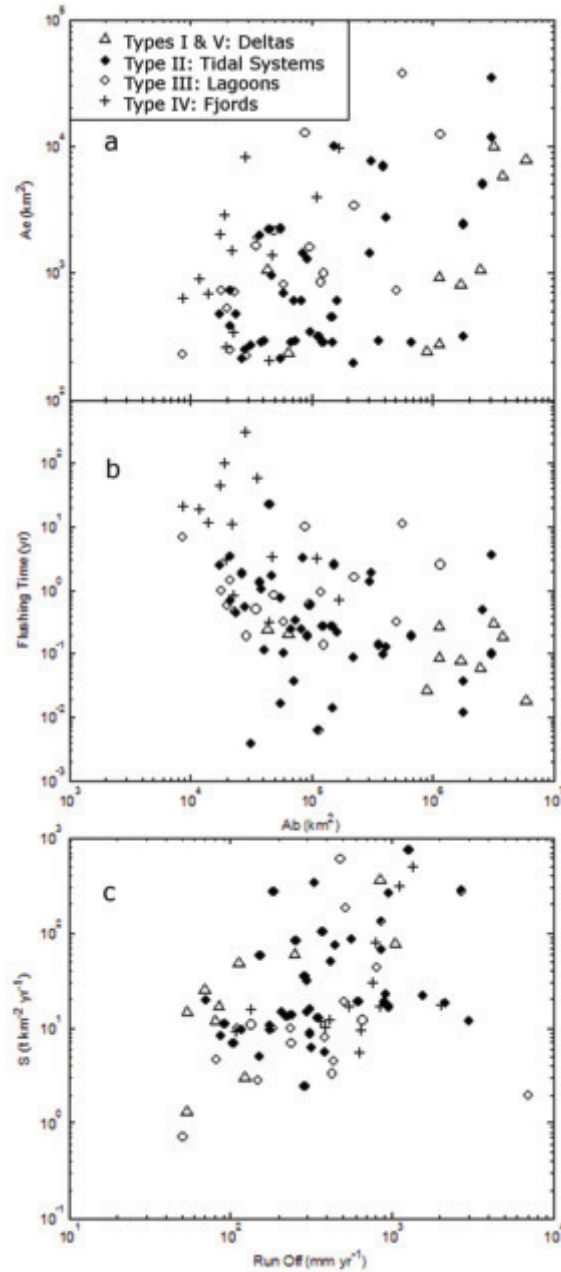


Figure 7: Cluster analysis. Triangles represent deltas (type I), black filled circles represent tidal systems (type II), white filled circles represent lagoons (type III) and '+' signs represent fjords (type IV).

and Fang, 2003), and here we chose to rather report these values against river basin area, i.e., sediment yield vs. river runoff (Figure 7c). The data, however, are very scattered. As to be expected, lagoons have rather low sediment yields and river runoff, with few exceptions, and deltas tend to have higher incoming yields. Fjords tend to range towards higher runoffs, whereas the overall variability for tidal systems is largest.

As our typology was established independently from the factors used in the cluster analysis, these observations serve as a validation of our approach and highlight the differences between the various factors responsible for the morphology of today's coastlines and their effects on the estuarine filtering of riverine inputs. The estuarine zone is clearly a variable filter. While the effects of human activities have not been included explicitly here, they certainly will have altered the filter efficiency for the different coastal types. Thus, for example, the filtering capacity of deltas likely has increased due to lower runoff linked to water extraction for irrigation, while the filter function of navigated estuaries likely has decreased.

3.3. Limitations of our approach

The geographic distribution of the coastal types is assessed based on different sources of information (Table 1), and most of the sources used serve to determine a single morphology or filtering type. The accuracy of the typology presented here depends on several factors, such as resolution and precision of source material, transfer of information from the source material (which often was not available in digital form) to the GIS and the decision to give one morphology priority over another in cases of overlap. In general, highest uncertainty prevails when very coarse-scale maps are scanned or digitized from books, and then geo-referenced in the GIS.

For some types, the uncertainty depends on the region, mainly due to the variety of sources available. Limitations of the typology are highest in cold climates, as the main source clearly delimiting the different types consists of a single map at coarse resolution (Gregory 1913), although other sources such as atlases or Google Earth were used as well. Furthermore, some areas in Siberia are

morphologically defined as rias, but might behave as a more passive filter system as they are frozen a large part of the year. Yet, the overall error induced by these uncertainties for the northern high latitudes is probably limited as coastal zones of the Arctic Ocean only receive 6% of the global sediment load and 7% of water discharge. The tidal systems of Europe are probably better defined than the same type in Asia. However, the Mediterranean coast of Europe is very heterogeneous, and at our resolution (0.5°), the exact boundary of morphological variations is sometimes difficult to establish, and different small-scale features might show frequent overlap, especially for type I. Whereas the small deltas (type I) represent 73% of the sediment load discharged to the Mediterranean and Black Sea, they only represent a few percent of the global water (1%) and sediment (7%) fluxes. In Asia, the coasts of Japan, China and Indonesia have larger stretches of coast without distinct embayments or prominent features, that were thus assigned to the ‘type I’ (small deltas) coasts. Here, the importance of type I is much larger: small deltas receive 49% of the total sediment load and 29% of the water load of the coasts of Asia, and still represent 29% and 8% of the global total sediment and water loads, respectively. As a consequence, we estimate that the general uncertainty is <2% for systems with > 10 or 15 river basin cells, and around 15% for the smaller basins. This is not higher than other global scale attempts at a similar scale, such as the Global-NEWS approach for land-based nutrient inputs (Seitzinger et al. 2005).

4. Application: estuarine surface area

A first application of the typology consists of a re-estimate of the water surface area of the world’s estuarine filters. In the early 1970’s, a first attempt was made by Woodwell et al. (1973) to quantify the surface area of the world’s estuaries. The area from their pioneering work continues to be used (e.g. Frankignoulle et al. 1998, Borges et al. 2005) and has not been updated since. Here we propose a revised figure, based on more extensive data on estuarine area for several regions of the world. Woodwell et al. (1973) define the term ‘estuary’ as systems being within the realm of tidal influence and upstream of the virtual prolongation of the external coastline. This definition essentially covers our definition of near-shore coastal zone filters, but Woodwell et al. (1973) also included large enclosed

bodies of water such as the Baltic Sea. Woodwell et al. (1973) calculated a ratio of estuarine surface area per km of coastline (A_e/C_e) for a continent's known area and length of internal coastline, i.e., inside the prolongation of the external coastline. At the time, the only region with sufficient data coverage was the USA and the global extrapolation thus solely relied on a unique ratio established for the US coast, which was then extrapolated, using these ratios, by multiplying them with the known coastline length of the remaining continents.

Here, we use our typology to establish these “w-ratios” (for ‘*Woodwell-ratio*’) for each of the four types of coast representing our estuarine filters (types I-IV) and extrapolate the results to the total world coastline (Antarctica and glaciated parts of Greenland were excluded). The data available for our study are from the conterminous USA without Alaska (Engle et al. 2007), the UK with the exclusion of Northern Ireland and Scotland (DEFRA 2008), Sweden (SMHI 2009) and Australia (Digby et al. 1998; AED 1999). Each of our coastal types is represented in at least two of these regions and the total coastline used is 32,700 km (8% of the world). The coastline lengths were calculated at 0.5° resolution. The use of the same method for the calculation of these lengths throughout our whole analysis ensures consistency between the values obtained.

The w-ratio obtained for each type may vary significantly for each region, and generally increases with the number of the type of coast (I to IV) (Table 5). The only exception to this rule is the very large w-ratio for US tidal systems, but this number includes large internal macrotidal bays such as the Chesapeake Bay (10.072km²), accounting alone for 44% of the estuarine surface area of the country.

The weighted averages of the w-ratio for each type vary within one order of magnitude from small deltas (type I: 0.64 km²/km) to lagoons (type III: 7.57 km²/km). The global extrapolation leads to a fairly modest surface area for type I despite the longest coastline. Tidal systems (type II) and lagoons (type III) contribute equally with 0.28 and 0.25 10⁶ km², respectively. Fjords (type IV), having the second largest coastline and second-highest w-ratio, reach 0.46 10⁶ km², accounting for 43% of the total surface area of estuarine filters (1.07 10⁶ km²). This number, however, should not be compared directly to Woodwell et al.'s. Indeed, in their work, out of 1.75 Mkm², 0.38 10⁶ km² are salt marshes and another

Table 5: Calculation of w-ratios (ratio of estuarine surface area per km of coastline for a continent's known area and length of internal coastline from Woodwell et al. (1973)) for each type and estimation of the global surface area of estuarine filters.

Type	Country	Coastline	Surface	w-Ratio	Global Coastline	Surface Extrapolation
		<i>km</i>	<i>km²</i>	<i>km²/km</i>	<i>km</i>	<i>km²</i>
Type I	US	1458	1298	0.89		
	Australia	7091	4179	0.59		
	Total	8549	5477	0.64	131167	84033
Type II	US	2889	23141	8.01		
	Australia	9948	18331	1.84		
	UK	3350	7362	2.20		
	Total	16187	48834	3.02	91326	275518
Type III	US	4521	39604	8.17		
	Australia	1044	2546	2.44		
	Total	5565	42150	7.57	33286	252112
Type VI	US	500	2638	5.276		
	Sweden	2576	10624	4.12		
	Total	3076	13262	4.31	105657	455535
Grand Total					1067198	

0.42 10^6 km² represent large bays, deltas and regional seas such as the Baltic Sea. Hence, the estuarine surface area in its most conservative sense amounts to less than 10^6 km². In addition, Woodwell et al. exclude surface areas North of 60°N latitude (except the Baltic Sea coastline), the west-coast of Norway from 60° to 70°N and the United Kingdom. This leaves out 30% of the world coastline. This implies, with our typology, a reduction of the fjords by 69% and the comparable estuarine surface area being only 0.64 10^6 km² (33% less than Woodwell et al.'s).

The main reason for this lower value is an inconsistency in the coastline length used by Woodwell et al. Coasts are known to possess a fractal property and their length varies with the scale of measurement (Mandelbrot, 1967). In their study, Woodwell et al. used a coastline length estimated by the National Estuarine Pollution Study (USDOI 1970) for the USA. The w-ratios were then extrapolated to the coastline of entire continents of which the length was deduced from a single map (Man's Domain/ A Thematic Atlas of the World). The smaller

scale of measurement of the local studies of the USA led to an overestimation of the relative contribution to the world's coastline (5% in Woodwell et al.'s study without Alaska and 2.5% in our study, in agreement with official measurements of the CIA (CIA, 2009), using a consistent 0.5° scale for the world-wide coastline). In conclusion, our calculation provides the first – to our knowledge – exhaustive estimate for the global estuarine surface area.

5. Conclusions / Perspectives

In this work, we present the first spatially-explicit, global typology for near shore coastal systems which is GIS-based and directly applicable for a wide range of purposes. Besides the update of the estimate for the global estuarine surface area presented here, multiple additional applications have been shown, linking coastal types to incoming river fluxes or related population pressure. Others can be envisioned for riverine nutrient discharge (Seitzinger et al. 2005; Laruelle et al. in prep). Despite all the possible applications of this typology, it is only a first step in the development of tools to describe the interface between continental and oceanic sciences at the global scale. Depending on the subject of interest, our current types could be further refined, for example, through the definition of subtypes or the addition of new types such as mangroves. Also, our typology for the near coastal zone could be expanded to include the continental shelves (or distal zone) including the area of influence of the world's largest rivers (McKee 2003).

Some future evolution of the typology itself might be expected based on changes in human and climate-induced changes in water regimes and sea level rise. For example, an increase of the sea level by 42-58 cm around 2080 (Horton et al., 2008), will particularly affect small deltas and some lagoons. Yet, most morphological types such as drowned river valleys or fjords will not change.

Our surface areas are of direct use for biogeochemical budget calculations for the coastal zone (e.g. Borges et al., 2005) and modeling of nutrient cycling as done in the companion paper by Laruelle et al. (in prep) where a set of generic biogeochemical box models has been developed for each type and applied to estimate the estuarine retention of N and P from rivers. This typology-based modeling tool can provide an interface between spatially-explicit global models for

river discharge of nutrients (Seitzinger et al., 2005) and Ocean Global Circulation Models (Bernard et al. 2009, Heinze et al. 1999, 2003).

Finally, several studies and generic models exist that apply to a particular type of estuarine setting (Valiela et al., 2004, Arndt, 2008). These settings may be related to one of the present types of our typology and, hence, an explicit global distribution of the applicability domain would be available opening the door to potential global or regional extrapolations.

Acknowledgements

This work was funded by Utrecht University (High Potential Project G-NUX) and the Netherlands Organisation for Scientific Research (NWO Vidi grant 864.05.004). We are greatly indebted to Sybil Seitzinger and Emilio Mayorga (Institute of Marine & Coastal Sciences, Rutgers University, USA) for the communication of the merged Global-NEWS data sets.

References:

- Australian Estuarine Database 1999 A Physical Classification of Australian Estuaries http://www.precisioninfo.com/rivers_org/au/library/nrhp/estuary_clasifn/ Accessed 1 May 2009
- Allen, J.I., J. Blackford, J. Holt, R. Proctor, M. Ashworth, and J. Siddorn. 2001. A highly spatially resolved ecosystem model for the North West European Continental Shelf. *SARSIA*. 86 (6): 423-440.
- Alongi, D.M. 1998. Coastal Ecosystem Processes. Marine Science Series, eds. M.J. Kennish and P.L. Lutz. CRC Press LLC.
- Arndt, S. 2008 Biogeochemical transformations and fluxes in redox-stratified environments: from the shallow coastal ocean to the deep subsurface. Ph-D thesis, Utrecht, Utrecht University.
- Audry, S., G. Blanc, J. Schäfer, F. Guérin, M. Masson, and S. Robert. 2007 Budgets of Mn, Cd and Cu in the macrotidal Gironde estuary (SW France) *Mar. Chem.* 107(4): 433-448, doi:10.1016/j.marchem.2007.09.008
- Aumont, O., J.C. Orr, P. Monfray, W. Ludwig, P. Amiotte-Suchet, P., and J.-L. Probst. 2001 Riverine-driven interhemispheric transport of carbon. *Global Biogeochemical Cycles*. 15: 393-405.
- Bartley, J.D., R.W. Buddemeier and D.A. Bennett. 2001. Coastline complexity: a parameter for functional classification of coastal environments. *J. Sea Res.* 46: 87–97.
- Bernard, C.Y., H.H. Dürr, C. Heinze, J. Segschneider, and E. Maier-Reimer. 2009. Contribution of riverine nutrients to the silicon biogeochemistry of the global ocean - a model study: *Biogeosciences Discuss.* 6:1091-1119.
- Beusen, A.H.W., A.L.M. Dekkers, A.F. Bouwman, W. Ludwig, and J. Harrison. 2005. Estimation of global river transport of sediments and associated particulate C, N, and P, *Global Biogeochem. Cycles*, 19, GB4S05, doi:10.1029/2005GB002453.
- Borges, A.V., B. Delille, and M. Frankignoulle. 2005. Budgeting sinks and sources of CO₂ in the coastal ocean: Diversity of ecosystems counts. *Geophysical Research Letters*. 32: L14601, doi:10.1029/2005GL023053

- Buddemeier, R.W., S.V. Smith, D.P. Swaney, C.J. Crossland and B.A. Maxwell. 2008. Coastal typology: An integrative “neutral” technique for coastal zone characterization and analysis. *Estuarine, Coastal and Shelf Science*. 77 (2):197-205. doi:10.1016/j.ecss.2007.09.021
- CIA. 2009. The World Factbook: <https://www.cia.gov/library/publications/the-world-factbook/fields/2060.html> Accessed 1 May 2009.
- Carter, R.W.G., and C.D. Woodroffe. 1994. Coastal evolution. Edited by Carter, R.W.G., and C.D. Woodroffe, Cambridge: Cambridge University Press.
- Castelao, R.M., and O.O. Moller Jr. 2006. A modeling study of Patos Lagoon (Brazil) flow response to idealized wind and river discharge: Dynamical analysis. *Brazilian Journal of Oceanography* 54(1):1-17.
- Chubarenko, B., and P. Margoński. 2008. The Vistula Lagoon. In *Ecology of Baltic Coastal waters; Ecological Studies*, Vol. 197, eds. Schiewer, 167-195, Berlin: Springer-Verlag.
- Crossland C.J., H.H. Kremer, H.J. Lindeboom, J.I. Marshall Crossland, and M.D.A. LeTissier. 2005. *Coastal Fluxes in the Anthropocene*. Global Change - The IGBP Series: Berlin, Heidelberg, Springer.
- Da Cunha, L.C., E.T. Buitenhuis, C. Le Quéré, X. Giraud, and W. Ludwig. 2007. Potential impact of changes in river nutrient supply on global ocean biogeochemistry: *Global Biogeochemical Cycles*, 21, GB4007, doi:10.1029/2006GB002718.
- Dagg, M., R. Benner, S. Lohrenz, and D. Lawrence. 2004. Transformation of dissolved and particulate materials on continental shelves influenced by large rivers: plume processes: *Cont. Shelf Res.*, 24:833-858.
- Davis, R.A.J., and D.M. Fitzgerald. 2004. *Beaches and Coasts*. Oxford: Blackwell Publishing.
- Department for Environment, Food and Rural Affairs. 2008. The estuary guide <http://www.estuary-guide.net/search/estuaries/> Accessed 18 Feb 2009.
- Digby, M.J., P. Saenger, M.B. Whelan, D. McConchie, B. Eyre, N. Holmes, and D. Bucher. 1998. A Physical Classification of Australian Estuaries. Report prepared for the Urban Water Research Association of Australia by the Centre for Coastal Management, Southern Cross University, Lismore, NSW.

- Dolan, R., B. Hayden, and M. Vincent. 1975. Classification of coastal landform of the Americas. *Zeitschrift für Geomorphologie, Supp. Bull.*, 22:72-88.
- Dürr, H., M. Meybeck, and S.H. Dürr. 2005. Lithologic composition of the Earth's continental surfaces derived from a new digital map emphasizing riverine material transfer. *Global Biogeochemical cycles*, 19, GB4S10:1-22.
- Dziganshin, G.F., and I.Y. Yurkova. 2001. Interannual variability of the river discharge into the North-western part of the Black Sea. In *Systems of Environmental Control: Collected papers*, eds. V.N. Eremeev, 267-272. Sevastopol: MHI NAS (in Russian).
- Elliott, M., and D.S. McLusky. 2002. The need for definitions in understanding estuaries, *Estuarine, Coastal and Shelf Science* 55:815-827.
- Engle, V.D., J.C. Kurtz, L.M. Smith, C. Chancy, and P. Bourgeois. 2007. Environmental monitoring and assessment 129(1-3):397-412.
- Ericson, J.P., C.J. Vorosmarty, S.L. Dingman, L.G. Ward, and M. Meybeck. 2006. Effective sea-level rise and deltas: Causes of change and human dimension implications. *Global and Planetary Change*, 50 (1-2): 63-82.
- Fekete, B.M., C.J. Vörösmarty, and W. Grabs. 2002. High-resolution fields of global runoff combining observed river discharge and simulated water balances: *Global Biogeochemical Cycles*, 16, 1042, doi: 10.1029/1999GB001254.
- Fleury, P., M. Bakalowicz, and G.D. Marsily. 2007. Submarine springs and coastal karst aquifers: A review: *Journal of Hydrology*, 339:79-92.
- Ford, D.C., and P.W. Williams. 1989. *Karst Geomorphology and Hydrology*. Unwin Hyman, London, Boston, Sydney, Wellington.
- Frankignoulle, M., G. Abril, A. Borges, I. Bourge, C. Canon, B. Delille, E. Libert, and J.-M. Théate. 1998. Carbon dioxide emission from European estuaries, *Science*, 282:434-436
- Gallo, M.N., and S.B. Vinzon. 2005. Generation of overtides and compound tides in Amazon estuary: *Ocean Dynamics*, 55:441-448.
- Gattuso, J.-P., M. Frankignoulle, and R. Wollast. 1998. Carbon and Carbonate Metabolism in Coastal Aquatic Ecosystems. *Annual Review of Ecology and Systematics* 29: 405-434.
- GEBCO 2007. General Bathymetric Chart of the Oceans. <http://www.ngdc.noaa>.

- [gov/mgg/gebco/](http://www.gov/mgg/gebco/) Accessed 28 Dec 2006.
- Google. 2009. Google Earth. <http://earth.google.com/> Accessed 1 May 2009.
- Gordon, J.D.C., P.R. Boudreau, K.H. Mann, J.E. Ong, W.L. Silvert, S.V. Smith, G. Wattayakorn, F. Wulff, and T. Yanagi. 1996. LOICZ Biogeochemical Modelling Guidelines. LOICZ Reports & Studies, 5, Texel, The Netherlands: LOICZ.
- Gregory, J.W. 1913. The nature and origin of fiords. (ed.), London: John Murray.
- Grelowski, A., M. Pastuszek, S. Sitek, and Z. Witek. 2000. Budget calculations of nitrogen, phosphorus and BOD5 passing through the Oder estuary. *Journal of Marine Systems* 25 (3-4): 221-237.
- Harrison, P.J., N. Khan, K. Yin, M. Saleem, N. Bano, M. Nisa, S.I. Ahmed, N. Rizvi, and F. Azam. 1997. Nutrient and phytoplankton dynamics in two mangrove tidal creeks of the Indus River delta, Pakistan, *Marine Ecology Progress Series* 157:13-19.
- Hayes, M.O. 1979. Barrier island morphology as a function of wave and tide regime In *Barrier islands from the Gulf of St. Lawrence to the Gulf of Mexico*, eds. S.P. Leatherman, 1-29, New York: Academic Press.
- Heinze, C., and E. Maier-Reimer. 1999. The Hamburg Oceanic Carbon Cycle Circulation Model version "HAMOCC2s" for long time integrations. Technical Report 20. Hamburg: Deutsches Klimarechenzentrum, Modellberatungsgruppe.
- Heinze, C., A. Hupe, E. Maier-Reimer, N. Dittert, and O. Ragueneau. 2003. Sensitivity of the marine biospheric Si cycle for biogeochemical parameter variations, *Global Biogeochemical Cycles*, 17, 3, doi:10.1029/2002GB001943.
- Herak, M., and V.T. Stringfield. 1972. *Karst - Important Karst Regions of the Northern Hemisphere*. Amsterdam, Elsevier.
- Horton, R., C. Herweijer, C. Rosenzweig, J. Liu, V. Gornitz, and A.C. Ruane. 2008. Sea level rise projections for current generation CGCMs based on the semi-empirical method. *Geophysical Research Letters* 35, L02715, doi:10.1029/2007GL032486.
- Ivanov, V.V. 1991. The estimation of water reserves in the Arctic estuaries with closed estuarine systems. *Problems of Arctic and Antarctic* 66:224-238. (In Russian)

- Kelletat, D.H. 1995. Atlas of coastal geomorphology and zonation. *Journal of Coastal Research*, special issue 13.
- Kempe, S. 1988. Estuaries – Their Natural and Anthropogenic Changes. In: *Scales and Global Change*. SCOPE, eds. T. Rosswall, R.G. Woodmansee, and P.G. Risser, 251-285, Wiley & Sons.
- Laruelle, G.G., H.H. Dürr, C.P. Slomp, C. van Kempen, M. Meybeck. Nitrogen and phosphorus retention in nearshore coastal environments: a global-scale modeling approach. In preparation.
- Laval, B.E., J. Imberger, and A.N. Findikakis. 2005. Dynamics of a large tropical lake: Lake Maracaibo. *Aquatic Sciences - Research Across Boundaries* 67(3): 337-349, 10.1007/s00027-005-0778-1
- Lohrenz, S.E., D.G. Redalje, P.G. Verity, C. Flagg, and K.V. Matulewski. 2002. Primary production on the continental shelf off Cape Hatteras, North Carolina. *Deep-Sea Research II* 49 (20):4479-4509.
- Mandelbrot, B. 1967. How Long Is the Coast of Britain? Statistical Self-Similarity and Fractional Dimension. *Science, New Series*, 156(3775):636-638. doi: 10.1126/science.156.3775.636
- Marín, V.H., L.E. Delgado, and P. Bachmann. 2008. Conceptual PHES-system models of the Aysén watershed and fjord. (Southern Chile): Testing a brainstorming strategy. *Journal of Environmental Management* 88:1109-1118.
- McKee, B. A. 2003. RiOMar: The Transport, transformation and fate of carbon in river-dominated ocean margins. In the riomar workshop: Tulane university, new Orleans, LA.
- McKee, B.A., R.C. Aller, M.A. Allison, T.S. Bianchi, and G.C. Kineke. 2004. Transport and transformation of dissolved and particulate materials on continental margins influenced by major rivers: benthic boundary layer and seabed processes. *Cont. Shelf Res.*, 24:899-926.
- Meybeck, M., and H.H. Dürr. 2009. Cascading Filters of River Material from Headwaters to Regional Seas: The European Example. In: *Watersheds, Bays, and Bounded Seas - The Science and Management of Semi-Enclosed Marine Systems*, SCOPE Series 70, eds. E.R. Urban Jr., B. Sundby, P. Malanotte-Rizzoli, and J.M. Melillo, 115-139, Washington, Island Press.

- Meybeck, M., H. Dürr, J. Vogler. 2004. River/coast relations in European regional seas. Eurocat WP 5.3. Report
- Meybeck, M., H. Dürr, and C.J. Vörosmary. 2006. Global coastal segmentation and its river catchment contributors: A new look at land-ocean linkage. *Global Biogeochemical Cycles*, 20, GB1S90:1-15, doi: 10.1029/2005GB002540.
- Moll, A., and G. Radach. 2003. Review of three-dimensional ecological modelling related to the North Sea shelf system Part 1: models and their results, *Progress in Oceanography* 57:175–217.
- Monbet, Y. 1992. Control of phytoplankton biomass in estuaries a comparative analysis of microtidal and macrotidal estuaries, *Estuaries* 15:563–571.
- Mortazavi, B., R.L. Iverson, W. Huang, F.G. Lewis, and J.M. Caffrey. 2000. Nitrogen budget of Apalachicola Bay, a bar-built estuary in the northeastern Gulf of Mexico. *Marine Ecology Progress Series* 195:1-14.
- NASA 2006 SeaWiFS. <http://oceancolor.gsfc.nasa.gov/SeaWiFS/BACKGROUND/> Accessed 12 Apr 2007.
- USDOI 1970 The national estuarine pollution study. Report of the Secretary of Interior to the U.S. Congress pursuant to Public Law 89-753, the Clean Water Restoration Act of 1966. Document No. 91-58. Washington, DC.
- New York Times. 1992. *Times Atlas of the World: Comprehensive Edition*, 9th ed. New York: New York Times.
- Nixon S.W, J.W. Ammerman, L.P. Atkinson, V.M. Berounsky, G. Billen, W.C. Boicourt, W.R. Boynton, T.M. Church, D.M. Ditoro, R. Elmgren, J.H. Garber, A.E. Giblin, R.A. Jahnke, N.J.P. Owens, M.E.Q. Pilson and S.P. Seitzinger. 1995. The fate of nitrogen and phosphorus at the land–sea margin of the North Atlantic Ocean. *Biogeochemistry* 3:141-180.
- Rabouille, C., F.T. Mackenzie, and L.M. Ver. 2001. Influence of the human perturbation on carbon, nitrogen, and oxygen biogeochemical cycles in the global coastal ocean. *Geochim. Cosmochim. Acta*, 65(21): 3615-3641.
- Schwartz, M.L. 2005. *Encyclopedia of Coastal Science*. Dordrecht: Springer.
- Seitzinger, S.P., J.A. Harrison, E. Dumont, A.H.W. Beusen, and F.B.A. Bouwman. 2005. Sources and delivery of carbon, nitrogen, and phosphorus to the coastal zone: An overview of Global Nutrient Export from Watersheds (NEWS)

- models and their application. *Global Biogeochemical Cycles*, 19, GB4S01:1-11, doi: 10.2029/2005GB002606.
- Selvam, V. 2003. Environmental classification of mangrove wetlands of India: *Current Science*, 84 (6):757-765.
- Sheldon, J.E., and M. Alber. 2006. The calculation of estuarine turnover times using freshwater fraction and tidal prism models: a critical evaluation, *Estuaries Coasts* 29:133-146.
- SMHI 2009 Swedish Oceanographic Data Center, <http://www.smhi.se/cmp/jsp/polopoly.jsp?d=5431&l=sv> Accessed 1 May 2009
- Smith, W.H.F., and D.T. Sandwell. 1997. Global Seafloor Topography from Satellite Altimetry and Ship Depth Soundings, version 9.1b, http://topex.ucsd.edu/marine_topo/ Accessed 20 Dec 2007
- Smith, S.V., and J.T. Hollibaugh. 1993. Coastal metabolism and the oceanic carbon balance. *Reviews of Geophysics* 31:75–89.
- Slomp, C.P., and P. Van Cappellen. 2004. Nutrient inputs to the coastal ocean through submarine groundwater discharge: controls and potential impact. *Journal of Hydrology* 295 (1-4): 64-86.
- Solidoro, C., R. Pastres, and G. Cossarini, 2005. Nitrogen and plankton dynamics in the lagoon of Venice. *Ecological Modelling*, 184 (1):103-124.
- Sørnes, T.A., and D.L. Aksnes. 2006. Concurrent temporal patterns in light absorbance and fish abundance. *Marine Ecology Progress Series* 325:181-186.
- Stewart, J.S. 2000. Tidal Energetics: studies with a barotropic model. PhD thesis, Boulder: University of Colorado.
- Sweeting, M.M. 1972. *Karst Landforms*. The Macmillan Press LTD.
- Syvitski, J.P.M., D.C. Burrell, and J.M. Skei. 1987. *Fjords: processes and products*. New York: Springer Verlag.
- Talaue-McManus, L.T., S.V. Smith, and R.W. Buddemeier. 2003. Biophysical and socio-economic assessments of the coastal zone: the LOICZ approach. *Ocean and Coastal Management* 46:323-333.
- Tolmazin, D. 1985. Economic impact on the riverine-estuarine environment of the USSR: the Black Sea Basin. *GeoJournal*, 11(2):137-152, 10.1007/BF00212915.

- U.S. Department of Commerce, National Oceanic and Atmospheric Administration, National Geophysical Data Center. 2006. 2-minute Gridded Global Relief Data (ETOPO2v2) <http://www.ngdc.noaa.gov/mgg/fliers/06magg01.html> Accessed 26 Dec 2008.
- Vafeidis, A.T., R.J. Nicholls, L. McFadden, R.S.J. Tol, J. Hinkel, T. Spencer, P.S. Grashoff, G. Boot, and R.J.T. Klein. 2008. A new global coastal database for impact and vulnerability analysis to sea-level rise. *Journal of Coastal Research* 24(4):917-924.
- Valiela, I., S. Mazzilli, J. L. Bowen, K. D. Kroeger, M. L. Cole, G. Tomasky, and T. Isaji. 2004. ELM, an estuarine nitrogen loading model: Formulation and verification of predicted concentrations of dissolved inorganic nitrogen. *Water Air and Soil Pollution* 157:365-391.
- Walling, D.E., and D. Fang. 2003. Recent trends in the suspended sediment loads of the world's rivers. *Global and Planetary Change* 39:111-126.
- Wong, M.H., and K.C. Cheung. 2000. Pearl River Estuary and Mirs Bay, South China. In *Estuarine Systems of the South China Sea Region: Carbon, Nitrogen and Phosphorus Fluxes*. LOICZ Reports and Studies 14, eds. V. Dupra, S.V. Smith, J.I. Marshall Crossland, and C.J. Crossland, 7-16, Texel: LOICZ.
- Woodwell, G.M., P.H. Rich, and C.A.S. Hall. 1973. Carbon in estuaries, In *Carbon and the biosphere*, eds. G.M. Woodwell and E.V. Pecan, 221-240, Springfield, Virginia.
- Vörösmarty, C.J., B.M. Fekete, M. Meybeck, and R.B. Lammers. 2000a. The global system of rivers: its role in organizing continental land mass and defining land-to-ocean linkages: *Global Biogeochemical Cycles* 14:599-621.
- Vörösmarty, C.J., B.M. Fekete, M. Meybeck, and R.B. Lammers. 2000b. Geomorphometric attributes of the global system of rivers at 30-minute spatial resolution. *Journal of Hydrology*, 237 (1-2):17-39.
- Vörösmarty C.J.; P. Green, J. Salisbury, R.B. Lammers. 2000c. Global water resources: vulnerability from climate change and population growth. *Science* 289(5477):284-288.

CHAPTER 5

Nitrogen and phosphorus retention in nearshore coastal environments: a global-scale modeling approach

Goulven G. Laruelle, Hans H. Dürr, Caroline P. Slomp, Cheryl van Kempen, Michel Meybeck.

Manuscript in preparation

July 2009

Abstract

A global scale, spatially-explicit model of the coupled nitrogen (N) and phosphorus (P) cycles in the estuarine zone is presented. The model consists of a “ribbon” of cells distributed along the entire global coast-line at a half degree resolution. The model calculates the nutrient retention in each coastal cell using generic box models. Different parameterizations for the models are established using a global estuarine typology that identifies small delta’s, tidal systems, lagoons and fjords. The modeled retention of N and P for individual boxes compares well to data for local studies. Our model results indicate that, on average, only 22% of the riverine N and 24% of the riverine P that enters an estuarine environment is retained there. We demonstrate which types of coastal systems and which regions most efficiently filter continental nutrient inputs to the oceans and where nutrients bypass estuaries and are discharged directly onto the continental shelves.

1 Introduction

Human activities are leading to major increases in terrestrial nitrogen (N) and phosphorus (P) inputs to the coastal ocean (Crossland, 2003; Mackenzie et al., 1993; Seitzinger et al., 2005). Estuarine environments such as delta's, tidal ecosystems, lagoons and fjords may provide a natural filter for this N and P during its transfer from land to shelf seas and the open ocean. For example, estuarine processes at the land-sea margin of the North Atlantic Ocean have been estimated to retain and remove 30-65% of the total N and 10-55% of the total P that would otherwise pass into shelf seas (Nixon et al., 1996). On a global scale, average N and P retention in the nearshore coastal zone has been estimated at 60% (Rabouille et al., 2001) and 40% of total inputs (Slomp and Van Cappellen, 2004), respectively.

The efficiency of this nearshore N and P retention strongly depends on the water residence time (Nixon et al., 1996), although other characteristics of coastal systems such as the floral and faunal activity (Heip et al, 1995), temperature (Eppley, 1972), tidal energy (Monbet et al, 1992), and geomorphology also play a role (Meybeck et al., 2006). For denitrification, the availability of nitrate is an additional important requirement (Nedwell et al., 1999; Tappin et al., 2002), while P removal through sediment burial is strongly affected by ambient redox conditions (Ruttenberg, 2004).

Various approaches have been used to estimate nutrient budgets for estuarine systems. These range from detailed local and regional studies using mechanistic, reactive transport models in which biogeochemical processes and hydrodynamics are closely coupled (Soetaert and Herman, 1995; Arndt et al, 2007, Laruelle et al, 2009a, Plus et al, 2006) to regional biogeochemical budgets based on mass balances for salt, water and nutrients (LOICZ project; Gordon et al, 1996; Smith et al., 2005) and global scale studies with box models (Rabouille et al, 2001; Slomp and Van Cappellen, 2004). The reactive transport models commonly lead to excellent descriptions of nutrient dynamics (Tappin et al, 2002), but they have a high data demand and thus can be applied to a limited number of well-monitored systems only. Information from regional biogeochemical budgets is not easily upscaled, since techniques aiming at extrapolating fluxes to unmeasured systems are not yet fully developed (Smith et al., 2005; Buddemeier et al., 2008).

In addition, such budgets do not allow quantitative predictions and do not capture the transient nature of estuarine processes. In current global box models, the nearshore environment (or “estuarine filter”) is either combined with the distal shelf zone (Ver et al., 1999) or treated as a single, homogeneous reservoir with a single river input (Rabouille et al, 2001; Laruelle et al, 2009b). Thus, the spatial heterogeneity in input fluxes (Smith et al., 2003; Seitzinger et al., 2005) and coastal ecosystem characteristics (Nedwell et al., 1999; Meybeck et al., 2006) is ignored. Moreover, the exact definition of the proximal coastal zone is often unclear (Elliott and McLusky, 2002), as illustrated by the inclusion of large enclosed systems such as the Baltic Sea in the domain in several studies (Woodwell et al, 1973; Nixon et al, 1996).

To adequately capture the heterogeneity at the global land-ocean interface and predict the modulation of terrestrial nutrient fluxes in nearshore coastal environments on a global scale, spatially-explicit process-based models that account for the differences in nutrient cycling between the various coastal systems across landscapes and climatic zones are needed. An important additional application of such models is their use as an interface between spatially-explicit models for nutrient export from watersheds (e.g. Global NEWS; Seitzinger et al, 2005) and biogeochemical ocean general circulation models that currently do not adequately resolve coastal zone processes (Da Cunha et al, 2007; Sarmiento and Gruber, 2006; Heinze et al, 2003; Bernard et al., 2009).

In this study, we present a spatially-explicit global model of the N and P cycles in the estuarine zone that can act as such an interface. The model consists of a set of box models that are distributed along the global coast-line and explicitly differentiates between 4 coastal types (small delta’s, tidal systems, lagoons and fjords) using the coastal typology of Dürr et al. (2009). We validate the box model on local studies and compare its performance to that of an empirical model for nutrient retention (Nixon et al., 1996). Modelled retention of riverine N and P and export to the shelves is presented per coastal type for the global coast line, per cell (0.5 x 0.5 degree) and per ocean basin. Finally, the sensitivity of the coastal filter for N and P to changes in river inputs of water is assessed. Our work shows that nutrient retention in estuaries at the global scale is less efficient than reported in earlier studies.

2. Methods

2.1. Model structure

Our model consists of a “ribbon” of 6200 model units that are run in parallel. The units are distributed along the entire global coastline at 0.5 degree resolution in order to match the river mouths of the global continental watershed basins defined by Vörösmarty et al (2000 a, b). Retention of N and P in each unit is calculated using a box model as detailed below. The model specifically focuses on nutrient cycling in estuaries, which are here assumed to include river sections from the first onset of tidal influence to the river mouth and enclosed features such as lagoons and tidal embayments (Dürr et al, 2009). Retention of N and P is calculated for a steady state situation corresponding to the year 1995. Note that many large estuaries are fed by several river basins (e.g., Chesapeake Bay, Patos Lagon, Gulf of Ob). For each of these coastal entities, only one modeling unit is defined, and inputs are determined as the sum of the inputs from all connecting watersheds.

2.2. Coastal typology

In the model, we use a world wide typology for estuarine filters (Figure 1a) developed by Dürr et al (2009). This typology identifies the presence or absence of an estuarine filter for each of the watersheds of Vörösmarty (2000 a, b). Estuarine filters consist of small delta’s (Type I), tidal systems (Type II), lagoons (type III) and fjords (Types IV).

Small delta’s are estuarine systems that develop in settings with high sediment discharge and low hydrodynamics. They typically protrude onto the continental shelves and possess low water residence times. Many deltas world-wide have such high discharge and incoming material rates, that only limited filtering occurs in the internal delta channels (Meybeck et al, 2004).

Tidal systems include rias, tidal embayments and classical funnel-shaped estuaries where tidal energy is the dominant driver of the local hydrodynamics.

Coastal lagoons are generally shallow water bodies, separated from the open ocean by a barrier, such as sandbanks, coral reefs, or barrier islands (Schwartz, 2005). They are characterised by relatively calm waters and long residence times (several months to several years).

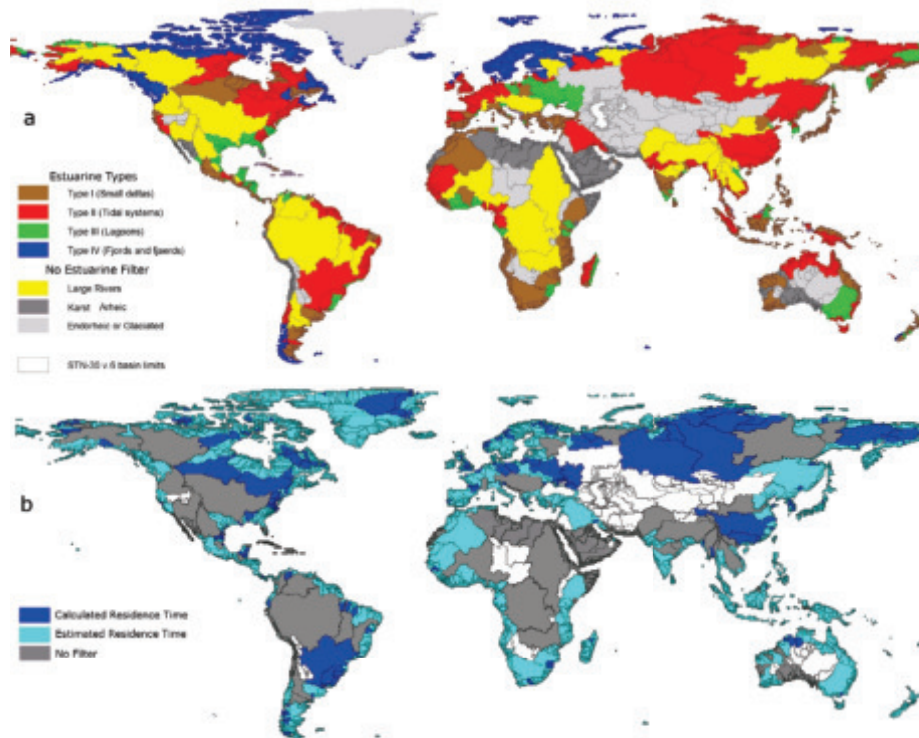


Figure 1: Typology of near-shore coastal environments (modified from Dürr et al, 2009) (a) and global overview of river basins with an estuarine filter for which a residence time was either calculated based on the volume of the system and yearly river discharge or estimated based on the coastal type (b).

For further details, see text.

Fjords and fjærds include classical U-shaped valleys created by glaciers that were drowned and are thus characterized by long, often narrow inlets with very steep topographies (Syvitski et al, 1987). They also include complex archipelagos such as the Swedish coast around Stockholm. These waters are generally cold, deep and stratified and characterised by very long residence times on the order of years or decades.

Non filtering types are arheic coasts (Type VII), karsts (Type VI) and large rivers (Type V). Large rivers include most of the 40 largest rivers of the world (Ericson et al, 2006) which usually develop a plume extending far beyond the limits of an estuary. Most of the nutrient cycling and removal occurs within

the continental shelf waters (McKee, 2003) making the system an external filter (Meybeck et al, 2006). As such, they are not part of the estuarine filter.

A total of 110 of the world's largest estuaries were identified and geographically delimited, constrained by the GTOPO world coastline (U.S. Geological Survey EROS Data Center, 1996) and a manual definition of the upper and lower boundaries. For each system, the surface area (S) and volume (V) were calculated using a Geographical Information System and the global bathymetric data set from Smith and Sandwell (1997). The accuracy of the method was validated for volumes greater than 4 km³. These volumes, divided by the Global NEWS yearly average water discharge for each river basin (Q; Seitzinger et al, 2005, Fekete et al, 2002) provided fresh water residence times for each estuary (τ). These residence times were then used to calculate median residence times for each coastal type (with values of 0.08, 0.27, 0.78 and 10.2 yrs for types I, II, III and IV, respectively, Dürr et al, 2009). The geographical distribution of river basins for which an individual residence time for the estuarine filter was calculated, and river basins for which only the median residence time for the corresponding coastal type was available is shown in Figure 1b. Approximately 19% and 13% of the global riverine N and P input enters estuaries with a calculated, i.e. well-constrained residence time.

2.3. Model formulation

Box model

Our model for the biogeochemical cycling of N and P (Figure 2) is modified from two earlier box models for global coastal nutrient cycling (Rabouille et al., 2001; Slomp and Van Cappellen, 2004). For both nutrients, we distinguish between total dissolved N and P (DN and DP), riverine particulate N and P (PN_r and PP_r) and estuarine particulate N and P (PN_m and PP_m). The latter material is assumed to be produced within the estuary through biological uptake.

Input of N and P from rivers is assumed to occur both in dissolved (DN, DP) and particulate form (PN_r and PP_r). We assume that 20% of the particulate P in rivers is reactive and is released directly in dissolved form, while 80% is assumed to consist of unreactive P phases (Froelich et al, 1988; Compton et al., 2000).

Uptake of dissolved N and P by phytoplankton results in the production of marine particulate matter (PN_m and PP_m, respectively), while remineralization leads to removal of these forms and the release of dissolved P and N. Denitrification and burial of both marine and riverine particulate material are responsible for retention of N. Retention of P includes burial of riverine and marine organic matter, and formation and burial of inorganic P minerals such as Fe-bound and Ca-bound P (e.g. Slomp et al, 1998; Ruttenberg, 2004). Atmospheric inputs of N and P to estuaries are assumed to be negligible (Rabouille et al., 2001; Slomp and Van Cappellen, 2004). Net export of marine and riverine particulate and dissolved N and P to the continental shelves is linked to the water cycle. Although the carbon cycle is not explicitly included in the model, the primary productivity in each coastal unit is calculated and used to estimate the uptake of dissolved N and P by phytoplankton.

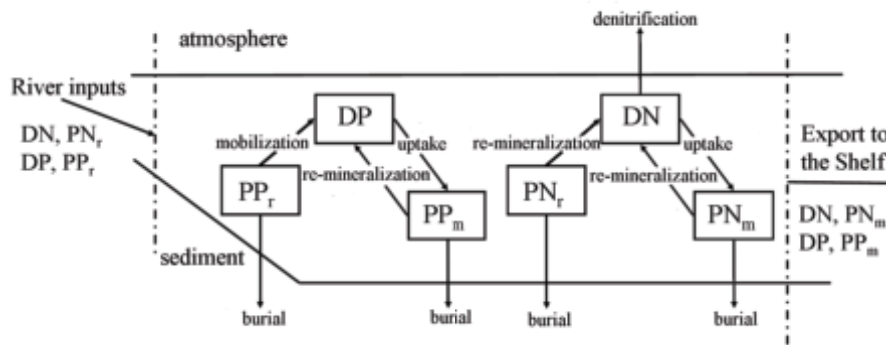


Figure 2: Conceptual scheme of the generic box model for N and P cycling in the coastal zone.

The biogeochemical processes in the model are described with simple rate laws that are parameterized using data sets on coastal nutrient cycling compiled in this study (Appendix). Primary productivity (P_{Prod} in mol C yr^{-1}) is assumed to be limited by either N or P, depending on whether the ratio of DN and DP in the water column is above or below Redfield ($N/P = 16$). P_{Prod} is also assumed to be dependent on the mean depth of the water column (H in m) and the yearly averaged temperature (T in $^{\circ}\text{C}$), following Eppley's empirical law (Eppley, 1972):

$$P_{Prod} = k_{P_{Prod}} \times \min(DN, DP \times 16) \times e^{(0.07 T)/H} \quad (1)$$

The value of the rate constant for primary production (k_{pprod} ; $0.0906 \text{ mol C yr}^{-1} \text{ m}^{-1}$) is obtained by fitting equation (1) to data for 15 coastal sites (Figure 3a). Surface water temperatures for each cell of the model are obtained from Reynolds et al. (2002; Table 1) and water depth is either calculated from the volume and surface area of an individual system or a type dependant median value (Dürr et al, 2009). Uptake of DN and DP is calculated from rates of PProd assuming the Redfield C:N:P ratio of 106:16:1 (Redfield, 1934; Redfield et al, 1963).

Table 1: Inputs and forcings used in the model with their symbol, definition and the source or data base used.

<i>Symbol</i>	<i>Name</i>	<i>Reference</i>
Q	Water discharge	Seitzinger et al, 2005
DN	Riverine Dissolved Nitrogen Loads	Dumont et al, 2005
DP	Riverine Dissolved Phosphorus Loads	Harrison et al, 2005a,b
PNr	Riverine Particulate Nitrogen Loads	Beusen et al, 2005
PPr	Riverine Particulate Phosphorus Loads	Beusen et al, 2005
V, H	Volume, Depth	Dürr et al, 2009
T	Temperature	Reynolds et al, 2002

Denitrification of DN is assumed dependent on the amount of DN in a coastal unit and a denitrification rate constant (k_{denit} , 0.05 yr^{-1}) following a first-order rate law. The value of the rate constant was obtained by fitting the rate law to data for 11 estuaries (Figure 3a). Remineralization of particulate N and P is described as a first order process, with rate constants (k_{minN} , k_{minP} in yr^{-1}) that are adjusted for surface water temperature following:

$$k_{min} = k_{minT0} \times e^{(0.07 T)} \quad (2)$$

Values for k_{minP} and k_{minN} for a temperature of 0 C° (yr^{-1}) and for the constant b ($k_{minN0} = 0.0812 \text{ yr}^{-1}$ and $k_{minP0} = 0.0812 \text{ yr}^{-1}$) are obtained by fitting equation (2) to calculated k values for 8 coastal systems (Figure 3c, d).

Burial of particulate N and P is assumed to be dependent on the mass of PN and PP, respectively, and a rate constant adjusted for the depth of the water column following Nixon et al (1996):

$$NBurial = kNb \times PN/H \quad (3)$$

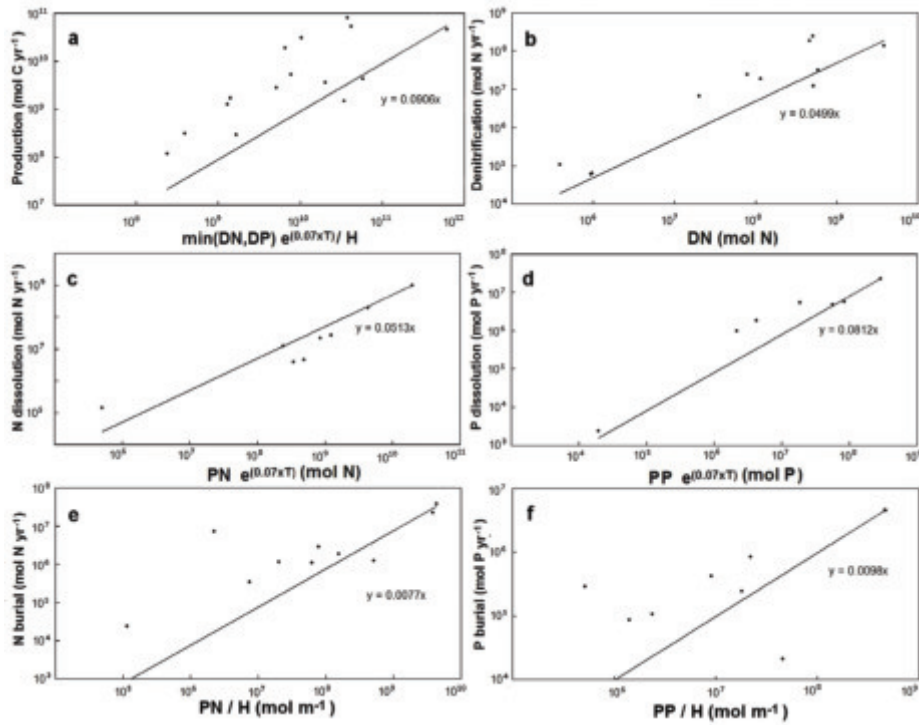


Figure 3: Calibration of the empirical relations used in the model for primary production (a), denitrification (b), N remineralization (c), P remineralization (d), N burial (e) and P burial (f). For equations: see text. The regressions are forced through zero.

The values of kN_b ($0.0077 \text{ yr}^{-1} \text{ m}^{-1}$) and kP_b ($0.0098 \text{ yr}^{-1} \text{ m}^{-1}$) are obtained by fitting equation (3) to data for 10 local studies (Figure 3e, f). Export of dissolved and particulate N and P is calculated as the product of the average concentration of each nutrient form in the coastal unit (mass divided by V) and the yearly river discharge (where, for example, $DN \text{ export} = \text{mass of DN} \times Q/V$). This leads to an inverse relationship between the water residence time ($\tau = V/Q$) and DN export:

$$DN \text{ export} = \text{mass of DN in coastal zone} / \tau \quad (4)$$

Empirical model

Retention of N and P in all 6200 model units was also calculated using empirical relationships between the export of N and P and the mean water residence time (τ in months) in estuaries (Nixon et al., 1996). Assuming that all N and P that is not exported, is retained in the estuary through burial and denitrification, the “retention efficiency”, (which we define here as the percentage of the N and P entering estuaries that is retained) is calculated as follows:

$$Ret(N) = 35.2 + 27 \log(\tau) \quad (5)$$

$$Ret(P) = 19.2 + 31.83 \log(\tau) \quad (6)$$

Hence, the amount of N retained equals the product of Ret(N) and the sum of the dissolved and particulate N inputs to the estuary (Nload). A similar calculation can be made for P. For our global scale calculations, we use the calculated or estimated residence times for each coastal unit (Figure 1b) and N and P loads for the associated river basins using output from the Global NEWS models (Table 1; Seitzinger et al, 2005).

2.4. Model solution

The set of ordinary differential equations for all 6200 model units is solved with MATLAB-software (version 6.5) using Euler’s method with an integration time step of 0.001 yr. Initial conditions are provided by a spin up simulation of 10 years to ensure the steady state of all cells.

2.5. Model Validation

The performance of the box model was validated by comparing modeled and observed N and P retention (Figure 4) for individual coastal systems. We also include data for calibration systems in the figure for comparison (see Appendix). Overall, the box model explains 66% and 96% of the variability in N and P retention, respectively.

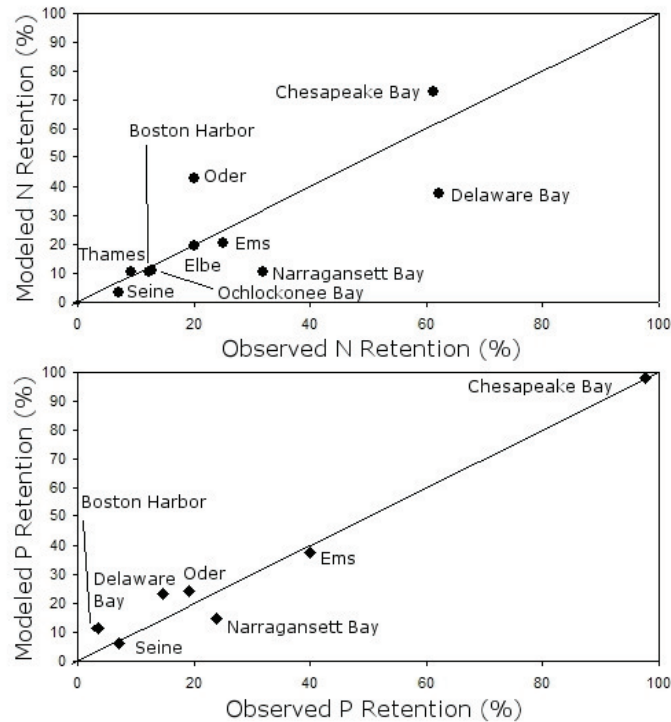


Figure 4: Validation of the box model for N (a) and P (b). The modeled retentions are plotted against observations for coastal systems.

3. Results

3.1. N and P retention per coastal type

The median values of the retention efficiency of N and P for all box models along the global coast-line show a clear relationship with coastal type and residence time (Figure 5). The highest nutrient retention is observed for fjords, while delta's show very little retention. Tidal systems and lagoons display intermediate behaviour. The variation in nutrient retention per type is significantly larger for P than for N (as indicated by the size of the box and length of the whiskers). The outliers in the box plot (light grey points in Figure 5) represent a limited number of the total of systems with a retention that is significantly different from the median value. Note that the heterogeneity is maximal for tidal systems (type II) and that only very few lagoons (type III) have a retention below the lower boundary of the whisker.

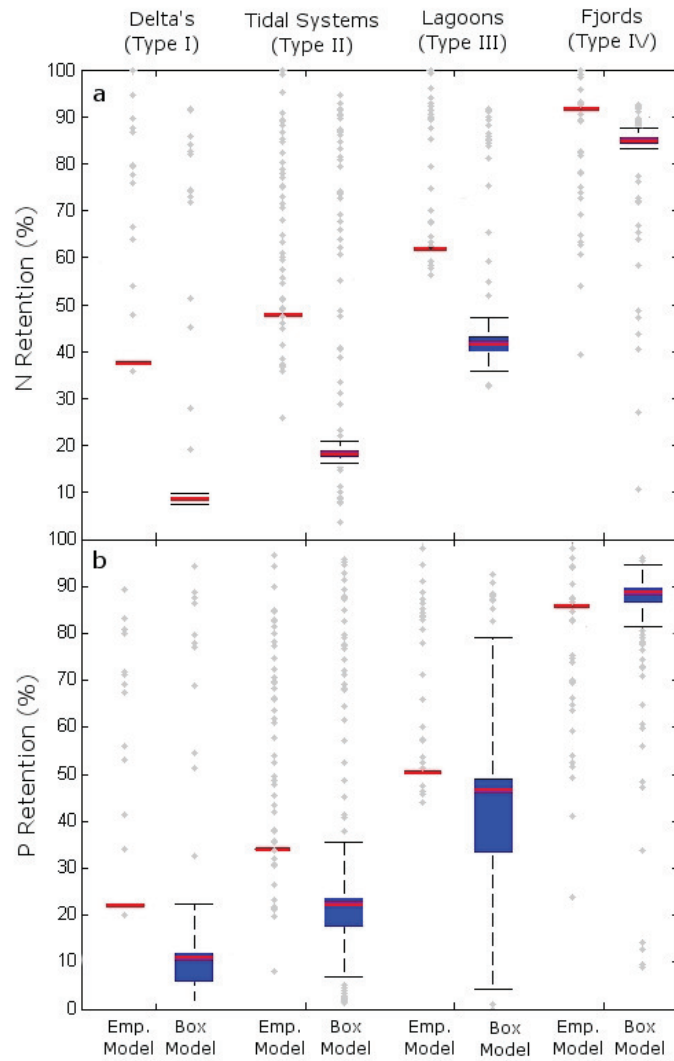


Figure 5: Box plot of the retention efficiency (in %) per estuarine type for N (a) and P (b) for the empirical model and the box model. The red line indicates the median value, the blue box is bounded by the first and third quartile and the whisker includes data values within twice the interquartile range of the sample set, representing over 95% of the distribution. Outliers are indicated as light grey dots.

For comparison, we also plot the median values calculated with the empirical model of Nixon et al. (1996) in Figure 5. Overall, the empirical model predicts a stronger nutrient retention than the box model, especially for N. The difference is most pronounced for systems with relatively short residence times, i.e. small delta's and tidal systems (Types I and II). For small deltas, for example, N and P retention amount to 8% and 12%, respectively, in the box model, compared to 37% and 22% for the empirical model. Given that, in the empirical model, the nutrient retention is only dependent on the residence time, there is no variability around the median value for most systems and only a limited number of systems with a residence time that is very different from the median value are visible as outliers.

3.2. Global distribution of N and P retention

Global patterns of N and P retention in the coastal zone as calculated with the box model and plotted per river basin (Figure 6) are relatively similar, despite a strong overall geographic heterogeneity. High latitude regions, especially in the northern hemisphere, are characterized by high retention of N and P with notable hotspots in Scandinavia and Canada. Similarly, in the southern hemisphere, the fjord coastline of Chile is a region of intense nutrient retention. Temperate regions show a very wide range of results with high retention areas such as the coastal systems along the Gulf of Mexico or moderate retention areas such as along the coastline of the Pacific. Several well-studied coastal systems, such as the Chesapeake Bay (Boynton et al, 1995), emerge as hotspots for P and N retention. The same holds for several coastal systems in Western Europe and Central America, where rivers flow to single cells that act as a highly efficient local filter within a stretch of coastal cells characterized by low retention.

In the tropics, retention is limited in high run-off areas such as Indonesia, and low runoff (ahreic) areas such as the Red Sea coastline, the Northern coast of Africa and part of the Arabic peninsula. A high retention is observed in several parts of central and South America, including Patos Lagoon and the Rio de la Plata which collects waters from the Parana and Uruguay rivers. Only minor differences in the modeled retention for N and P at the global scale are visible.

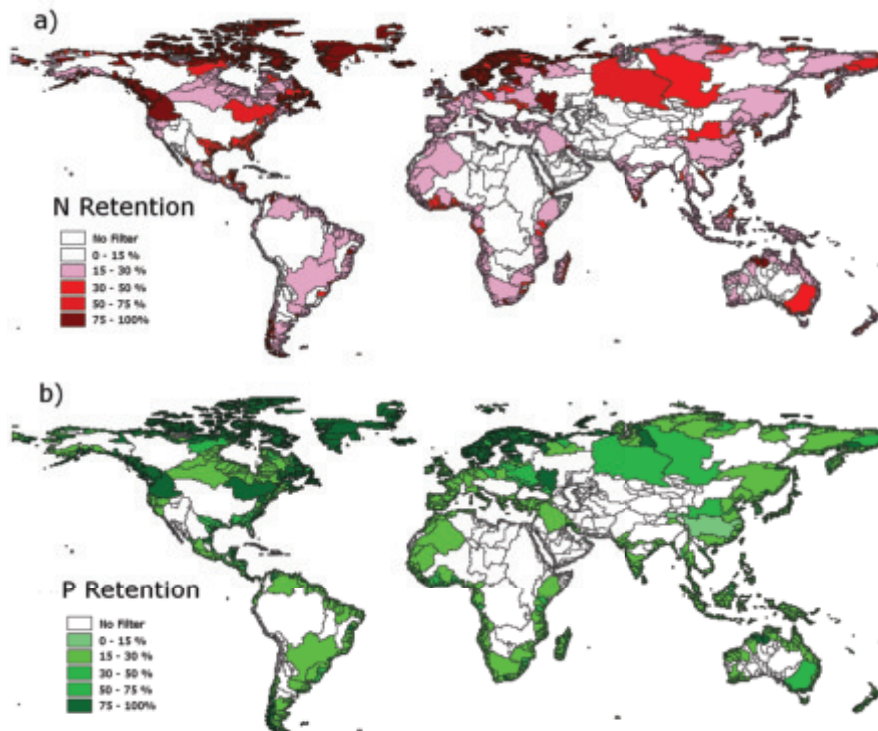


Figure 6: Global map of retention of N (a) and P (b) simulated by the model.

Figure 7 illustrates the latitudinal distribution of water and nutrient loads. More than 60% of the world's river discharge takes place in latitudes between 20°S and 30°N. The major contribution of large rivers is very clear – especially that of the Amazon and Zaire around the equator and of the Mississippi and Yangtze around the Tropic of Cancer. About half of the water discharge in the tropics bypasses the estuarine filter and is carried onto the continental margins by the four above mentioned rivers. The same holds for N and P deliveries (Figure 7b, c). Moreover, the efficiency of the estuarine filter is often minimal in these regions and the overall nutrient retention is lower than 15% for both nutrients. In the Northern hemisphere, the retention efficiency increases with latitude as the contribution of large rivers decreases. North of 45°N, 40% of the N and 45% of the P is retained in estuaries. In absolute terms, the amount of N and P trapped in

these high latitude estuaries represents about half of the total retention of N and P in nearshore environments.

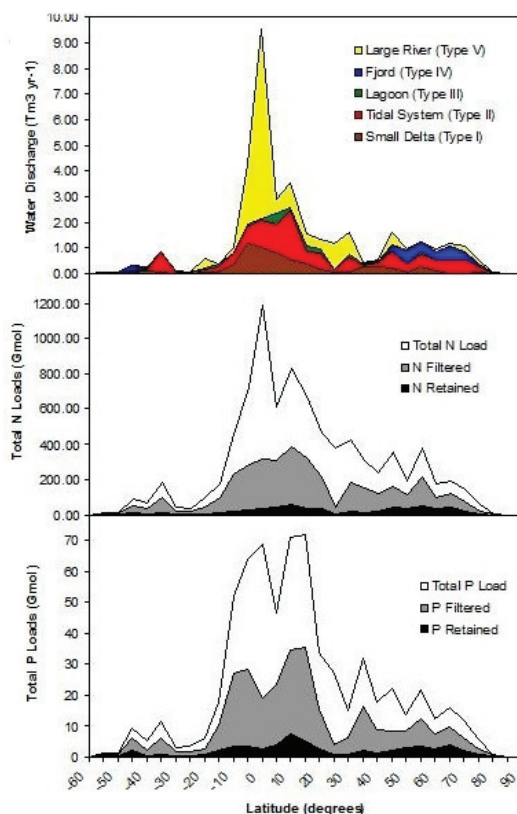


Figure 7: Latitudinal distribution of the water discharge (in $\text{Tm}^3 \text{yr}^{-1}$) per type of estuarine filter (a), N loads and retention (in 10^9mol y^{-1}) (b) and P loads and retention (in 10^9mol y^{-1}) (c) Values are integrated over 5 degrees.

In Table 2, we compare the N and P inputs and retention for each type of system per oceanic basin. Significant differences in N and P retention are observed for the 5 oceanic basins. The table also indicates the differences between the efficiency of the estuarine filter (types I-IV) and the retention calculated based on the total nutrient loads (i.e. including deliveries from large rivers without estuarine filter). The Atlantic and Pacific coastal areas are both characterized by retentions close to 15%. However, the Atlantic Ocean receives input from several of the largest rivers of the world (Amazon, Mississippi, Zaire), which lowers the

effective retention. When correcting for this, the Atlantic proximal filter is in fact more active than the Pacific one (29% versus 16% for N and 32% versus 20% for P, respectively). The Mediterranean coastal zone is slightly less efficient as a filter: it is not fed by many large rivers (mainly the Rhone and the Nile which do not represent very large inputs of water or nutrients compared to the other large river systems) and instead has long stretches of karstic (East Adriatic Sea) and arheic (Africa) coastline. The coastline of the Indian Ocean is the least efficient as a filter with an overall retention of 9% and 12% for N and P, respectively. Note, for example, that a large fraction of the Indonesian coastline is dominated by small delta's and short residence time systems. The Arctic Ocean is by far the most efficient proximal filter with overall retention efficiencies reaching 45% for N and 50% for P. These proximal filters are mainly fjords or large gulfs (e.g. associated with the Ob and Taz rivers).

4. Discussion

4.1. Modeling Global Coastal Nutrient Retention

Quantifying the role of nearshore environments as a filter for nutrients at the regional and global scales has been a challenge for oceanographers for more than a decade. While various empirical (Nixon et al., 1996) and box models (e.g. Rabouille et al., 2001) for nutrient cycling are available, none of the current modelling tools adequately accounts for the heterogeneity of coastal systems and their variable response to environment change. The spatially-explicit model for nutrient retention that we present here is unique in that it captures both differences in nutrient cycling in the various coastal types, and the spatial heterogeneity of nutrient inputs at the global scale (Seitzinger et al., 2005).

Our model results generally capture observed trends in nutrient retention in local studies (Figure 4). The emergence of various small coastal areas in Western Europe and Central America as hotspots for nutrient retention in coastal stretches that otherwise retain little nutrients is in accordance with field studies for these systems (e.g. Boynton et al., 1995; Nixon et al., 1996). While a more extensive validation is currently limited by the lack of complete data sets for coastal systems, these results suggest that the model adequately reproduces the

Table 2: Riverine inputs and calculated N and P retention per oceanic basin and per type in 10⁶ mol. Values in parentheses are calculated retention efficiencies.

Oceanic Basin	Element	No Filter	Small delta's (Type I)	Tidal Systems (Type II)	Lagoons (Type III)	Fjords (Type IV)	Whole Estuarine Filter	Total
Atlantic	N inputs	992	125	600	161	66	953	1954
	<i>N retention</i>	-	11 (9%)	132 (22%)	77 (48%)	55 (82%)	274 (29%)	274 (14%)
	P inputs	57	10	31	12	4	56	113
	<i>P retention</i>	-	1 (11%)	7 (23%)	7 (55%)	3 (84%)	18 (32%)	18 (16%)
Pacific	N inputs	110	884	381	60	90	1415	1525
	<i>N retention</i>	-	74 (8%)	55 (15%)	25 (42%)	76 (84%)	231 (16%)	231 (15%)
	P inputs	8	92	20	5	8	126	134
	<i>P retention</i>	-	11 (12%)	4 (19%)	2 (47%)	7 (89%)	25 (20%)	25 (18%)
Indian	N inputs	401	243	201	33	0	477	878
	<i>N retention</i>	-	20 (9%)	44 (22%)	14 (43%)	-	77 (16%)	77 (9%)
	P inputs	28	26	15	2	0	44	71
	<i>P retention</i>	-	3 (12%)	4 (28%)	1 (48%)	-	8 (20%)	8 (12%)
Arctic	N inputs	31	4	77	3	50	134	166
	<i>N retention</i>	-	0 (9%)	31 (40%)	1 (44%)	42 (83%)	74 (55%)	74 (45%)
	P inputs	3	1<	6	1<	5	11	14
	<i>P retention</i>	-	0 (12%)	3 (44%)	0 (52%)	4 (87%)	7 (61%)	7 (50%)
Med.Sea	N inputs	44	78	2	9	0	89	132
	<i>N retention</i>	-	8 (10%)	0 (22%)	6 (70%)	-	14 (16%)	14 (11%)
	P inputs	3	6	1<	1	0	7	11
	<i>P retention</i>	-	1 (11%)	0 (15%)	0 (57%)	-	1 (16%)	1 (11%)

small scale heterogeneity in nutrient retention along the global coast line.

The box model used to calculate nutrient retention for each coastal unit is deliberately kept very simple because of limitations in data availability at the global scale. Moreover, the current available inputs for small rivers are subject to large uncertainties (Seitzinger et al, 2005). Because the N and P cycles are coupled to the water cycle, the residence time of water plays an important role in determining the concentration of nutrients in a given model unit (see equation 4) and thus the potential for nutrient removal. Nutrient retention thus increases with residence time from delta's, tidal systems and lagoons to fjords. Other factors, such as differences in temperature, water depth and types of nutrient inputs also play a role, however, and are mostly responsible for the spread in P and N retention (i.e. the length of the whiskers) calculated for each coastal type with the box model (Figure 5).

On average, our model predicts much lower N and P retention for the various coastal types than values obtained with the empirical model of Nixon et al. (1996). The latter model calculates nutrient retention based only on water residence time with equations that were calibrated for sites that were mostly located in temperate regions at latitudes above 40°N (equations 5 and 6). Our work shows that nutrient retention in temperate regions is much higher than in nearshore environments in the tropics and sub-tropics (Figure 7).

In various global scale studies, the values of Nixon et al. (1996) for temperate regions have been assumed to be representative at the global scale (e.g. Rabouille et al., 2001; Slomp and Van Cappellen, 2004). This clearly leads to an overestimation of the role of estuaries as a filter for N and P. Our work suggests that, instead of a retention of 60 and 40% of total inputs of N and P, respectively, as suggested in these earlier studies, the estuarine filter efficiency is 22% for N and 24% for P. Moreover, only 64% of the riverine inputs of N and 69% of the inputs of P actually will journey through estuaries before reaching shelf waters. Ultimately, only on average 14% of riverine N and 17% of riverine P is retained in estuarine environments. Further work, especially in tropical and subtropical systems is needed to improve these estimates of nutrient retention in the global coastal zone.

A relevant issue in this context is the exact definition and the geographical boundary of the nearshore environment in the various models. In our model, we follow the coastal typology of Dürr et al. (2009) and specifically focus on the estuarine filter, which is not assumed to extend onto the continental shelf and excludes large enclosed seas such as the Baltic Sea. In the model of Rabouille et al. (2001), in contrast, the dimensions of the coastal zone are based on earlier work of Woodwell et al (1973) and enclosed seas and the open water part of estuaries and delta's are explicitly included. As a consequence, the residence time for water assumed by Rabouille et al. (2001) for the global coastal zone is estimated at 1 yr¹. This value is at the high end of the range of residence times observed in nearshore systems, and while reasonable for lagoons and fjords, does not capture the dynamics of delta's and tidal systems (Durr et al., 2009). Such differences in model domains and assumptions will affect both the total retention of nutrients calculated for the global coastal zone and the response of the coastal system to perturbation.

4.2. Sensitivity of the box model to perturbations

A sensitivity analysis was performed to assess the potential response of modeled estuarine nutrient retention at the global scale to long-term changes in river water discharge. We specifically focused on active coastal filters (types I-IV), thus excluding large rivers (type V) and varied the water inputs by dividing or multiplying them by a factor of 2 and allowed the system to return to steady state. In all cases, a decrease in water discharge induces an increase in nutrient retention (Table 3). An increase in water discharge generates the opposite response. While fjords are only mildly sensitive to changes in water discharge, the filtering capacity of the three other types changes by ca. 50 to 100%.

The sensitivity analyses demonstrate that changes in water inputs significantly affect nutrient processing and retention in nearshore environments, particularly in estuaries and lagoons. These systems are also the most impacted by human activities (Walsh et al., 1988; Dürr et al., 2009) and are expected to be subject to major changes over the coming century. Further work will focus on assessing spatially-explicit changes in coastal nutrient cycling as a result of human

Table 3: Nutrient retention per type for N and P under 3 different scenarios for river discharge of water: present day, steady state situation (Reference), a decrease of river discharge by a factor 2 (Q/2) and an increase of river discharge by a factor 2 (Qx2).

Scenario	Element	Small delta's (Type I)	Tidal Systems (Type II)	Lagoons (Type III)	Fjords (Type IV)	Whole Estuarine Filter	Total
Reference	N Retention	8%	21%	47%	83%	22%	14%
	P Retention	12%	24%	53%	87%	24%	17%
Q / 2	N Retention	15%	32%	62%	88%	31%	20%
	P Retention	21%	37%	67%	91%	34%	24%
Q x 2	N Retention	5%	13%	32%	76%	15%	10%
	P Retention	6%	15%	38%	81%	17%	12%

activities, preferably using results of scenario studies with global watershed models when they become available.

5. Summary

Here, we present the first global scale spatially-explicit model for N and P cycling in nearshore environments. The model, which consists of a ribbon of 6200 box models arranged along the global coast-line, is used to quantify nutrient retention in 4 types of coastal environments: small delta's (type I), tidal systems (type II), lagoons (type III) and fjords (type IV) at the global scale. The model is validated on data sets for selected coastal systems and has a low data demand. The retention of N and P is shown to vary greatly with coastal type and latitude. Fjords are particularly effective in retaining nutrients while small delta's have a low filtering capacity. Estuaries in temperate regions in the Northern hemisphere are particularly important as a sink for nutrients. In tropical and sub-tropical regions, retention is much less efficient and a large proportion of the nutrient inputs to the ocean bypass the coastal filter by discharging directly onto the shelves in large rivers.

With the model, we demonstrate that nearshore environments account for a retention of 14% and 17% of river inputs of N and P, respectively, on the global scale. Of the nutrient inputs that enter the coastal filter, an estimated 22% of the riverine N and 24% of the riverine P is retained. These estimates are significantly lower than earlier global scale estimates for nutrient retention in estuaries. This is because these earlier estimates did not account for nutrient processing in tropical areas and because there is a bias in the available data towards large systems with a relatively long residence time. Because of the spatially-explicit nature of our model, it can be used as an interface between spatially-explicit global models for river inputs of nutrients to the ocean (Seitzinger et al, 2005) and biogeochemical ocean models. Potential future applications include dynamic simulations to assess the response of the estuarine filter to changes in nutrient inputs from rivers on time scales of decades to a century.

Acknowledgements

This research was made possible by financial support from Utrecht University (HiPo project G-NUX to C.P. Slomp) and the Netherlands Organisation for Scientific Research (NWO Vidi grant 864.05.004). We are greatly indebted to Sybil Seitzinger and Emilio Mayorga (Institute of Marine & Coastal Sciences, Rutgers University, USA) for the communication of the merged Global-NEWS data sets.

References

- Arndt, S., J.-P. Vanderborgh, and P. Regnier. 2007. Diatom growth response to physical forcing in a macrotidal estuary: coupling hydrodynamics, sediment transport and biogeochemistry. *Journal of Geophysical Research* 12. doi:10.1029/2006JC003581
- Bernard C.Y., G.G. Laruelle, C.P. Slomp, and C. Heinze. 2009. Impact of changes in river nutrient fluxes on the global marine silicon cycle: a model comparison. *Biogeosciences Discussions* 6: 4463-4492.
- Berner, E.A., and R.A. Berner. 1996. *Global Environment: Water, Air and Geochemical 31 Cycles* Prentice-Hall.
- Beusen, A.H.W., A.L.M. Dekkers, A.F. Bouwman, W. Ludwig, and J. Harrison. 2005. Estimation of global river transport of sediments and associated particulate C, N, and P, *Global Biogeochem. Cycles*, 19, GB4S05, doi:10.1029/2005GB002453.
- Boynton, W.R., J.H. Garber, R. Summers, and W.M. Kemp. 1995. Inputs, transformations and transport of nitrogen and phosphorus in Chesapeake Bay and selected tributaries. *Estuaries* 18(1B):285-314.
- Brion, N., W. Baeyens, S. De Galan, M. Elskens, R.W.P.M. Laane. 2004. The North Sea: source or sink for nitrogen and phosphorus to the Atlantic Ocean? *Biogeochemistry* 68: 277–296.
- Buddemeier, R.W., S.V. Smith, D.P. Swaney, C.J. Crossland and B.A. Maxwell. 2008. Coastal typology: An integrative “neutral” technique for coastal zone characterization and analysis. *Estuarine, Coastal and Shelf Science*. 77 (2):197-205. doi:10.1016/j.ecss.2007.09.021
- Chapelle, A., A. Ménesguen, J.-M. Deslous-Paoli, P. Souchu, N. Mazouni, A. Vaquer, and B. Millet. 2000. Modelling nitrogen, primary production and oxygen in a Mediterranean lagoon. Impact of oysters farming and inputs. *Ecological Modelling* 127: 161–181.
- Compton, J., D. Mallinson, C.R. Glenn, G. Filippelli, K Föllmi, G. Shields, and Y. Zanin. 2000. Variations in the Global Phosphorus Cycle. *Marine Authigenesis: From Global to Microbial*, SEPM Special Publication, 66: 21-33.
- Contreras, F. 1993. *Ecosistemas Costeros Mexicanos*. Comision Nacional Para el

Conocimiento y Uso de la Biodiversidad. Universidad Autónoma Metropolitana
Unidad Iztapalapa.

- Crossland C.J., H.H. Kremer, H.J. Lindeboom, J.I. Marshall Crossland, and M.D.A. LeTissier. 2003. *Coastal Fluxes in the Anthropocene*. Global Change - The IGBP Series: Berlin, Heidelberg, Springer.
- Da Cunha, L.C., E.T. Buitenhuis, C. Le Quéré, X. Giraud, and W. Ludwig. 2007. Potential impact of changes in river nutrient supply on global ocean biogeochemistry: *Global Biogeochemical Cycles*, v. 21, GB4007, doi:10.1029/2006GB002718.
- Day Jr., J.W., C. Coronado-Molina, F.R. Vera-Herrera, R. Twilley, V.H. Rivera-Monroy, H. Alvarez-Guillen, R. Day, and W. Conner. 1996. A 7 year record of above-ground net primary production in a southeastern Mexican mangrove forest. *Aquatic Botany* 55: 39-60.
- Dumont, E., J.A. Harrison, C. Kroeze, E.J. Bakker, and S.P. Seitzinger. 2005. Global distribution and sources of dissolved inorganic nitrogen export to the coastal zone: Results from a spatially explicit, global model, *Global Biogeochem. Cycles*, 19, GB4S02, doi:10.1029/2005GB002488.
- Dürr, H.H., G.G. Laruelle, C.M. van Kempen, C.P. Slomp, M. Meybeck, and H. Middelkoop. 2009. World-wide typology of near-shore coastal systems: defining the estuarine filter of riverine inputs to the oceans. Submitted to *Estuaries and Coasts*.
- Elliott, M., and D.S. McLusky. 2002. The need for definitions in understanding estuaries, *Estuarine, Coastal and Shelf Science* 55:815-827.
- Eppley, R.W. 1972. Temperature and phytoplankton growth in the sea. *Fishery Bull.*, 70:1063-1085.
- Ericson, J.P., C.J. Vorosmarty, S.L. Dingman, L.G. Ward, and M. Meybeck. 2006. Effective sea-level rise and deltas: Causes of change and human dimension implications. *Global and Planetary Change*, 50 (1-2): 63-82.
- Eyre, B.D, and L.J. McKee. 2002, Carbon, nitrogen and phosphorus budgets for a shallow sub-tropical coastal embayment (Moreton Bay, Australia) *Limnology and Oceanography*, 47(4):1043-1055.
- Fekete, B.M., C.J. Vorosmarty, and W. Grabs. 2002. High-resolution fields of global

- runoff combining observed river discharge and simulated water balances: *Global Biogeochemical Cycles*, 16, 1042, doi: 10.1029/1999GB001254.
- Froelich, P.N., M.A. Arthur, W.C. Burnett, M. Deakin, V. Hensley, R. Jahnke, L. Kaul, K.H. Kim, K. Roe, A. Soutar, and C. Vathakanon. 1988. Early diagenesis of organic-matter in Peru continental-margin sediments - phosphorite precipitation, *Mar. Geol.* 80:309-343.
- Gordon, J.D.C., P.R. Boudreau, K.H. Mann, J.E. Ong, W.L. Silvert, S.V. Smith, G. Wattayakorn, F. Wulff, and T. Yanagi. 1996. LOICZ Biogeochemical Modelling Guidelines. LOICZ Reports & Studies, 5, Texel, The Netherlands: LOICZ.
- Grelowski, A., M. Pastuszek, S. Sitek, and Z. Witek. 2000. Budget calculations of nitrogen, phosphorus and BOD₅ passing through the Oder estuary. *Journal of Marine Systems* 25:221–237
- Gilmartin, M., and N. Revelante. 1978. The phytoplankton characteristics of the barrier island lagoons of the Gulf of California. *Estuarine And Coastal Marine Science*, 7: 29-47.
- Harrison, J. A., S. P. Seitzinger, A. F. Bouwman, N. F. Caraco, A. H. W. Beusen, and C. J. Vörösmarty. 2005a. Dissolved inorganic phosphorus export to the coastal zone: Results from a spatially explicit, global model, *Global Biogeochem. Cycles*, 19, GB4S03, doi:10.1029/2004GB002357.
- Harrison, J. A., N. Caraco, and S. P. Seitzinger. 2005b. Global patterns and sources of dissolved organic matter export to the coastal zone: Results from a spatially explicit, global model, *Global Biogeochem. Cycles*, 19, GB4S04, doi:10.1029/2005GB002480.
- Heinze, C., A. Hupe, E. Maier-Reimer, N. Dittert, and O. Ragueneau. 2003. Sensitivity of the marine biospheric Si cycle for biogeochemical parameter variations, *Global Biogeochemical Cycles*, 17.
- Heip, C.H.R., N.K. Goosen, P.M.J. Herman, J. Kromkamp, J.J. Middelburg and K. Soetaert. 1995. Production and consumption of biological particles in temperate tidal estuaries. *Oceanogr Mar Biol Annu Rev*, 33:1-150.
- Huret, M., I. Dadou, F. Dumas, P. Lazure, and V. Garçon. 2005. Coupling physical and biogeochemical processes in the Río de la Plata plume. *Continental Shelf*

Research 25: 629–653.

- Kelly, J.R. 1998. Quantification and potential role of ocean nutrient loading to Boston Harbor, Massachusetts, USA. *Marine Ecology Progress Series*. 173:53-65.
- Laruelle, G.G., P. Regnier, O. Ragueneau, M. Kempa, B. Moriceau, S. Ni Longphuir, A. Leynaert, G. Thouzeau, and L. Chauvaud. 2009a. Benthic-pelagic coupling and the seasonal silica cycle in the bay of Brest (France): New insights from a coupled physical-biological model. *Marine Ecology Progress Series*. 385:15-32, doi: 10.3354/meps07884.
- Laruelle G.G., V. Roubex, A. Sferratore, B. Brodherr, D. Ciuffa, D.J. Conley, H.H. Dürr, J. Garnier, C. Lancelot, Q. Le Thi Phuong, J.-D. Meunier, M. Meybeck, P. Michalopoulos, B. Moriceau, S. Ni Longphuir, S. Loucaides, L. Papush, M. Presti, O. Ragueneau, P.A.G. Regnier, L. Saccone, C.P. Slomp, C. Spiteri, P. Van Cappellen. 2009b. Anthropogenic perturbations of the silicon cycle at the global scale: the key role of the land-ocean transition. *Global Biogeochemical Cycles*. in press.
- Mackenzie, F. T., L. M. Ver, C. Sabine, M. Lane and A. Lerman. 1993. C, N, P, S global biogeochemical cycles and modeling of global change. In *Interactions of C, N, P and S Biogeochemical Cycles and Global Change*, eds Wollast, R., F. T. Mackenzie and L. Chou, 1-62, Springer-Verlag.
- Machado, E.C., and B. Knoppers. 1988. Sediment oxygen consumption in an organic rich subtropical lagoon, Brazil. *Science of the Total Environment* 75: 341-349.
- Meybeck, M., H. Dürr, and J. Vogler. 2004. River/coast relations in European regional seas. Eurocat WP 5.3. Report.
- Meybeck, M., H. Dürr, and C.J. Vörosmary. 2006. Global coastal segmentation and its river catchment contributors: A new look at land-ocean linkage. 20:1-15 *GBIS90*, doi:10.1029/2005GB002540.
- McKee, B.A. 2003. RiOMar: The Transport, transformation and fate of carbon in river-dominated ocean margins. In the riomar workshop: Tulane university, New Orleans, LA.
- Monbet, Y. 1992. Control of phytoplankton biomass in estuaries a comparative

- analysis of microtidal and macrotidal estuaries, *Estuaries* 15:563-571.
- Nedwell, D.B. 1999. Effect of low temperature on microbial growth: lowered affinity for substrates limits growth at low temperature, *FEMS Microbiol. Ecol.* 30:101-111.
- Nielsen, K., L.P. Nielsen, and P. Rasmussen. 1995. Estuarine nitrogen retention independently estimated by the denitrification rate and mass balance methods: a study of Norsminde Fjord, Denmark. *Marine Ecology Progress Series*. 119:275-283.
- Nixon S.W, J.W. Ammerman, L.P. Atkinson, V.M. Berounsky, G. Billen, W.C. Boicourt, W.R. Boynton, T.M. Church, D.M. Ditoro, R. Elmgren, J.H. Garber, A.E. Giblin, R.A. Jahnke, N.J.P. Owens, M.E.Q. Pilson and S.P. Seitzinger. 1996. The fate of nitrogen and phosphorus at the land-sea margin of the North Atlantic Ocean. *Biogeochemistry* 3:141-180.
- Nixon, S.W., S.L. Granger, and B.L. Nowicki. 1995. An assessment of the annual mass balance of carbon, nitrogen, and phosphorus in Narragansett Bay. *Biogeochemistry* 31: 15-61
- Plus, M., I.L. Jeunesse, F. Bouraoui, J.-M. Zaldivar, A. Chapelle, and P. Lazure. 2006. Modelling water discharges and nitrogen inputs into a Mediterranean lagoon: Impact on the primary production. *Ecological Modelling*, 193 (1-2): 1-69.
- Prego, R. 2002. Nitrogen fluxes and budget seasonality in the Ria Vigo (NW Iberian Peninsula) *Hydrobiologia* 475/476: 161-171.
- Rabouille, C., F.T. Mackenzie, and L.M. Ver. 2001. Influence of the human perturbation on carbon, nitrogen, and oxygen biogeochemical cycles in the global coastal ocean. *Geochim. Cosmochim. Acta*, 65(21): 3615-3641.
- Redfield, A.C. 1934. On the proportions of organic derivations in sea water and their relation to the composition of plankton. In James Johnstone Memorial. ed R.J. Daniel, 177-192, University Press of Liverpool.
- Redfield, A.C., B.H Ketchum, and F.A. Richards. 1963. The influence of organisms on the composition of sea water. In *the Sea*, ed Hill, M.N. 26-77, Interscience.
- Reynolds, R.W., N.A. Rayner, T.M. Smith, D.C. Stokes, and W. Wang. 2002: An Improved In Situ and Satellite SST Analysis for Climate. *J. Climate*, 15:1609-

1625.

- Ruttenberg, K.C. 2004. The Global Phosphorus Cycle, In *Treatise on Geochemistry*, eds Holland, H.D. and Turekian, K. K, 585-643, Elsevier, Amsterdam.
- Salazar, J. 1996. Hidrografía y sedimentología de la laguna de La Restinga, Isla de Margarita, Venezuela. Trabajo de ascenso, Univ. Oriente.
- Sanders, R., C. Klein, and T. Jickells. 1997. Biogeochemical Nutrient Cycling in the Upper Great Ouse Estuary, Norfolk, U.K. *Estuarine, Coastal and Shelf Science*. 44:543-555.
- Sarmiento, J.L., and N. Gruber. 2006. *Ocean Biogeochemical Dynamics*. Princeton University Press, Princeton.
- Schwartz, M.L. 2005. *Encyclopedia of Coastal Science*. Dordrecht: Springer.
- Seitzinger, S.P., J.A. Harrison, E. Dumont, A.H.W. Beusen, and F.B.A. Bouwman. 2005. Sources and delivery of carbon, nitrogen, and phosphorus to the coastal zone: An overview of Global Nutrient Export from Watersheds (NEWS) models and their application. *Global Biogeochemical Cycles*, 19, GB4S01:1-11, doi: 10.2029/2005GB002606.
- Seitzinger, S.P. and A.E. Giblin. 1996. Estimating denitrification in North Atlantic continental shelf sediments. *Biogeochemistry*, 35:235-259.
- Slomp, C.P., J.F Malschaert, and W. Van Raaphorst. 1998. The role of absorption in sediment-water exchange of phosphate in North Sea continental margin sediments. *Limnology and Oceanography*, 43(5):832-846.
- Slomp, C. P., and P. Van Cappellen. 2004. Nutrient inputs to the coastal ocean through submarine groundwater discharge: controls and potential impact. *Journal of Hydrology*, 295 (1-4):64-86.
- Smith, S.V., D.P. Swaney, L. Talaue-McManus, J.D. Bartley, P.T. Sandhei, C. McLaughlin, V.C. Dupra, C.J. Crossland, R.W. Buddemeier, B.A. Maxwell, and F. Wulff. 2003. Humans, hydrology, and the distribution of inorganic nutrient loading to the ocean. *BioScience* 53:235-245.
- Smith, S.V., D.P. Swaney, R.W. Buddemeier, M.R. Scarsbrook, M.A. Weatherhead, C. Humborg, H. Eriksson, and F. Hannerz. 2005. River nutrient loads and catchment size. *Biogeochemistry* 75:83-107.
- Smith, W.H.F., and D.T. Sandwell. 1997. *Global Seafloor Topography from*

- Satellite Altimetry and Ship Depth Soundings, version 9.1b, http://topex.ucsd.edu/marine_topo/ Accessed 20 Dec 2007
- Smith, S.V., and T. Yanagi. 1997. NP budgets for three Japanese Bays. <http://data.ecology.su.se/MNODE/> Accessed 21 Jun 2008.
- Soetaert, K. and P.M.J. 1995. Herman, Nitrogen dynamics in the Westerschelde estuary (SW Netherlands) estimated by means of the ecosystem model MOSES, *Hydrobiologia* 311:225-246.
- Solidoro, C., R. Pastres, and G. Cossarini. 2005. Nitrogen and plankton dynamics in the lagoon of Venice. *Ecological Modelling* 184:103-124.
- Syvitski, J.P.M., D.C. Burrell, and J.M. Skei. 1987. *Fjords: processes and products*. New York: Springer Verlag.
- Tanaka, K., and F.T. Mackenzie. 2005. Ecosystem behavior of southern Kaneohe Bay, Hawaii: A statistical and modelling approach. *Ecological Modelling* 188:296-326.
- Tappin, A. D. 2002. An Examination of the Fluxes of Nitrogen and Phosphorus in Temperate and Tropical Estuaries: Current Estimates and Uncertainties. *Estuarine, Coastal and Shelf Science*, 55:885-901, doi:10.1006/ecss.2002.1034.
- Torres-Valdés, S., and D.A. Purdie. 2006. Nitrogen removal by phytoplankton uptake through a temperate non-turbid estuary. *Estuarine, Coastal and Shelf Science*. 70: 473-486.
- Trimmer, M., D.B. Nedwell, D.B. Sivyer, and S.J. Malcom. 2000. Seasonal benthic organic matter mineralization measured by oxygen uptake and denitrification along a transect of the inner and outer River Thames estuary, UK. *Marine Ecology Progress Series* 197:103-119.
- U.S. Department of Commerce, National Oceanic and Atmospheric Administration, National Geophysical Data Center. 2006. 2-minute Gridded Global Relief Data (ETOPO2v2) <http://www.ngdc.noaa.gov/mgg/fliers/06mgg01.html> Accessed 26 Dec 2008.
- Van Beusekom, J.E.E., and V.N. De Jonge. 1998. Retention of Phosphorus and Nitrogen in the Ems Estuary. *Estuaries* 21(4A):527-539.
- Vant, W.N., and B.L. Williams 1992. Residence times of Manukau Harbour, New Zealand. *New Zealand Journal of Marine and Freshwater Research* 26: 393-

404.

- Ver, L.M., F.T. Mackenzie, and A. Lerman. 1999. Biogeochemical responses of the carbon cycle to natural and human perturbations: Past, present, and future. *Am. J. Sci.* 299:762–801.
- Walsh, J.J. 1988. *On the nature of continental shelves*. Academic Press, San Diego, California.
- Witek, Z., C. Humborg, O. Savchuk, A. Grelowski, and E. Łysiak-Pastuszek. 2003. Nitrogen and phosphorus budgets of the Gulf of Gdańsk (Baltic Sea). *Estuarine, Coastal and Shelf Science* 57: 239-248.
- Woodwell, G.M., P.H. Rich, and C.A.S. Hall. 1973. Carbon in estuaries, In *Carbon and the biosphere*, eds. G.M. Woodwell and E.V. Pecan, 221-240, Springfield, Virginia.
- Vörösmarty, C.J., B.M. Fekete, M. Meybeck, and R.B. Lammers. 2000a. The global system of rivers: its role in organizing continental land mass and defining land-to-ocean linkages: *Global Biogeochemical Cycles* 14:599-621.
- Vörösmarty, C.J., B.M. Fekete, M. Meybeck, and R.B. Lammers. 2000b. Geomorphometric attributes of the global system of rivers at 30-minute spatial resolution. *Journal of Hydrology*, 237 (1-2):17-39.

Appendix: Systems used for calibration and validation of the box model for Primary production, denitrification and N and P burial. For further details: see text.

Calibration/Validation	Site	Process(es)	References
Calibration	Boston Harbor	N&P burial	Nixon et al, 1996, Kelly 1998
	Carretas-Pereyra	Production	Contreras, 1993
	Chantuto_Panzacola	Production	Contreras, 1993
	Chesapeake Bay	Production, Denitrification, N&P burial	Nixon et al, 1996, Boyton et al, 1995
	Delaware Bay	N&P burial	Nixon et al, 1996
	Ems estuary	denitrification, N&P remineralization, N&P burial	van Beusekom and De Jonge, 1998
	Ensenada de la Paz	Production	Gilmartin and Revelante. 1978
	Estero La Cruz	Production	Gilmartin and Revelante. 1978
	Great Ouse	N&P remineralization, denitrification	Sanders et al, 1997
	Kaneohe	Denitrification	Tanaka and Mackenzie 2005
	Laguna de Terminos	Production	Day Jr et al, 1996
	Laguna Restinga	Production	Salazar, 1996
	Manukau Harbor	Production	Vant and Williams, 1992
	Marica-Guarapina	Production	Machado and Knoppers, 1988
	Moreton Bay	Denitrification, N&P burial	Eyre and McKee, 2002
	Narragansett Bay	Production, N&P burial	Nixon et al, 1996, Nixon et al, 1995
	Norsminde fjord	Denitrification	Nielsen et al, 1995
	Ochlocknee Bay	Production, N burial	Nixon et al, 1996

Osaka Bay	Production	Smith and Yanagi 1997
Ria of Vigo	Production	Prego, 2002
Rio de la Plata	N remineralization	Huret et al, 2005
Solent Estuary	Production	Torres-Valdés and Purdie, 2006
Szczecin lagoon	Production, denitrification, N&P remineralization, N&P burial	Grełowski et al, 2000, Witek et al, 2003
Thau Lagoon	Production, N&P remineralization, N&P burial	Plus et al, 2006, Chapelle et al, 2000
Venice lagoon	Production, denitrification, N&P remineralization, N&P burial	Solidoro et al, 2005
Boston Harbor	N & P Retention	Nixon et al, 1996
Chesapeake Bay	N & P Retention	Nixon et al, 1996
Delaware Bay	N & P Retention	Nixon et al, 1996
Elbe	N Retention	Brion et al, 2004
Ems	N & P Retention	van Beusekom and De Jonge, 1998
Narragansett Bay	N & P Retention	Nixon et al, 1996
Ochlockonee Bay	N Retention	Nixon et al, 1996
Seine	N & P Retention	Brion et al, 2004
Szczecin lagoon	N & P Retention	Grełowski et al, 2000
Thames	N Retention	Trimmer et al, 2000

CHAPTER 6

Re-evaluation of air-water exchange of CO₂ in the global coastal ocean using a spatially-explicit typology

Goulven G. Laruelle, Hans H. Dürr, Caroline P. Slomp, Alberto V. Borges

Submitted to *Geophysical Research Letters*

July 2009

Abstract

We re-evaluate the exchange of CO₂ between the atmosphere and the global coastal ocean (the sum of continental shelf seas and near-shore ecosystems) based on a compilation of air-water CO₂ fluxes that are scaled using a spatially-explicit global typology of estuaries and continental shelves. The re-evaluated emission of CO₂ to the atmosphere from estuaries to the atmosphere is ~50% lower than previous flux estimates (0.23 Pg C yr⁻¹ versus 0.45 Pg C yr⁻¹), due to a lower total estuarine surface area estimate, and because the data are scaled based on 4 different types of near-shore ecosystems with different CO₂ emission rates. The sink of atmospheric CO₂ of continental shelf seas is ~33% lower than previous flux estimates (-0.11 Pg C yr⁻¹ versus -0.37 Pg C yr⁻¹). The present work presents an improved typology to scale CO₂ fluxes in continental shelf seas and near-shore ecosystems, hence, the largest uncertainty in evaluating the sinks or sources of CO₂ in the global coastal ocean remains in the adequacy of CO₂ data to describe the spatial variability and extent, and to capture relevant temporal scales of variability.

1 Introduction

The quantification of CO₂ fluxes between the ocean and the atmosphere has been a major topic of research for more than four decades since the pioneering study of Takahashi (1961), leading to the most recent climatology of the partial pressure of CO₂ (pCO₂) in the oceans combining ~3 10⁶ measurements (Takahashi et al. 2009). The world ocean is a net sink for anthropogenic CO₂, accounting for ~48% of the total fossil-fuel and cement-manufacturing CO₂ emissions since the onset of the industrial revolution (Sabine et al. 2004). While the atmospheric CO₂ sink is reasonably well-constrained for the open ocean, with estimates ranging between -1.4 Pg C yr⁻¹ and -2.2 PgC yr⁻¹ (e.g., Gruber et al. 2009; Takahashi et al. 2009), CO₂ flux estimates for the coastal ocean are subject to large uncertainties (Borges 2005; Crossland et al. 2005). The global CO₂ uptake by continental shelf seas has been evaluated by several authors based on the global extrapolation of a flux value from a single shelf sea (Tsunogai et al. 1999; Thomas et al. 2004) or from the compilation of literature data in several shelf seas (Borges 2005; Borges et al. 2005; Cai et al. 2006; Chen and Borges 2009), and values range between -0.2 Pg C yr⁻¹ and -1.0 PgC yr⁻¹.

Estuaries and other near-shore ecosystems are net sources of CO₂ to the atmosphere (e.g., Frankignoulle et al. 1998; Borges et al. 2003) and may account for a global emission of CO₂ of a similar order of magnitude as the CO₂ sink from continental shelf seas, ranging between 0.4 and 0.6 PgC yr⁻¹ (Abril and Borges 2004; Borges 2005; Borges et al. 2005; Chen and Borges 2009). This wide range of flux values reflects the heterogeneity and complexity of these highly active biogeochemical environments at the interface between the land and the ocean, but also demonstrates the insufficient data coverage both in time and space, and the lack of appropriate spatially-explicit numerical models for carbon cycling in the global coastal ocean.

As an alternative, scaling approaches can be used where a reasonable flux value for a coastal system is multiplied by the respective surface area (Abril and Borges 2004; Borges 2005; Borges et al. 2005; Cai et al. 2006; Chen and Borges 2009). The success of such scaling approaches not only depends on the quality and quantity of the measurements and how representative they are for a given coastal

environment, but also on the accurate determination of the surface area. In this study, we re-evaluate the air-water CO₂ fluxes in the global coastal ocean using a scaling approach, based on a spatially-explicit coastal typology and surface areas of both estuaries and continental shelf seas.

2 Budget calculations

We calculate air-water CO₂ fluxes for estuaries using the data compilation of Borges et al. (2005), expanded with more recent studies (cf. Auxiliary material), and revised estimates of the surface areas of various types of near-shore environments. The surface areas for near-shore coastal systems are based on a spatially explicit typology of coastal entities consisting of four different types of estuaries based on morphological differences: I – small deltas and miscellaneous small estuaries, II – tidal systems and embayments, III – lagoons, IV – fjords and fjärds. Large rivers often produce an estuarine plume that protrudes past the conventional geographical limits of estuaries and even continental shelves (McKee 2003). These systems are not considered estuaries in the present study but rather continental shelves (Dürr et al. 2009). Average air-water CO₂ fluxes are then calculated for each estuarine type and extrapolated to the global near-shore coastal zone, based on the type-specific surface areas reported by Dürr et al. (2009) (Table 1).

Table 1: Air water CO₂ fluxes and global extrapolation for the 4 different types of near-shore coastal types. Positive values represent a source of CO₂ to the atmosphere.

<i>Type</i>	<i>Surface (10⁶ km²)</i>	<i>Avg. CO₂ flux (mol C m⁻² yr⁻¹)</i>	<i>Total CO₂ flux (Pg C yr⁻¹)</i>
Small deltas	0.084	25.0	0.025
Tidal Systems	0.276	37.3	0.124
Lagoons	0.252	17.3	0.052
Fjords	0.456	4.4	0.024
Total	1.067		0.225

The CO₂ flux estimates for the continental margins rely on a similar typological approach based on 138 shelf units with surface areas calculated using a geographical information system (GIS). The limit of the continental shelf is set to 200 m depth based on the common convention (Walsh 1988; Gattuso et al. 1998; Wollast 1998) and the related isobath was extracted from the 1' resolution global bathymetry of Smith and Sandwell (1997). Each shelf unit was defined by

perpendicularly extrapolating the limits of coastal segments from the shoreline (Meybeck et al. 2006). These segments were designed to identify homogeneous stretches of coast according to a set of parameters such as morphology, lithology, oceanic currents and climate, not biased by national or political boundaries. This segmentation has been used previously to gather spatially explicit riverine inputs as boundary conditions for an oceanic general circulation model (Bernard et al. 2009). A type was attributed to each continental shelf sea unit: Type 1 corresponds to enclosed shelves as proposed by Meybeck et al. (2009) and comprises the Hudson Bay, the Baltic Sea, the Adriatic Sea, the Persian Gulf and the shelf of the Black Sea. Type 2 includes all Western and Eastern boundary currents characterized by coastal upwelling. The California Current, Humbolt Current, Canary Current, Leeuwin Current include the coasts of California, Peru, Chile, Iberia, Morocco, Mauritania, Benguela shelf and North East Australia (Xie and Hsich 1975). The last type consists of all other open shelf areas which are ranked by climatic zones (Type 3a: 0-30°, Type 3b: 30-60°, Type 3c: 60-90°). Based on the data compilation by Borges et al. (2005), we used average CO₂ fluxes of 1.09 mol C m⁻² yr⁻¹ for upwelling regions, 1.74 mol C m⁻² yr⁻¹ for Type 3a, -1.74 mol C m⁻² yr⁻¹ for Type 3b and -1.88 mol C m⁻² yr⁻¹ for Type 3c (Table 2). An average flux value of -1.50 mol C m⁻² yr⁻¹ was used for type 1, based on data for the Baltic Sea (Thomas and Schneider 1999).

Table 2: Air-water CO₂ fluxes and global extrapolation for the different types of continental shelves along different climatic zone. Positive values represent a source of CO₂ to the atmosphere.

<i>Area</i>	<i>Surface (10⁶ km²)</i>	<i>Avg. CO₂ flux (mol C m⁻² yr⁻¹)</i>	<i>Total CO₂ flux (Pg C yr⁻¹)</i>
<i>Polar</i>			
Enclosed	0.189	-1.5	-0.003
Open Shelf	5.477	-1.88	-0.124
Upwelling	0.086	1.09	0.001
	5.752		-0.126
<i>Temperate</i>			
Enclosed	1.410	-1.5	-0.025
Open Shelf	7.170	-1.74	-0.150
Upwelling	0.629	1.09	0.008
	9.209		-0.167
<i>Tropical</i>			
Enclosed	0.231	-1.5	-0.004
Open Shelf	7.909	1.74	0.165
Upwelling	1.540	1.09	0.020
	9.680		0.181
Total	24.641		-0.112

3. Results

A detailed description of the typology of near-shore environments is given by Dürr et al. (2009). In brief, fjords and fjärds (Type IV) are the most extensive near-shore types (~43% of the total surface area and 26% of the world-wide exorheic coast line). They are dominant at latitudes north of 45°N (Scandinavia, Canada and Alaska) and south of 45°S (southern Chile) (Fig. 1a). Tidal systems (Type II) and lagoons (Type III) are the second and third most abundant near-shore types (~26% and 24% of the total surface area, respectively). While no clear spatial pattern is apparent for tidal systems (Type II), lagoons (Type III) are dominant in the tropics and subtropics of the Northern Hemisphere (0°-45°N). Small deltas (Type I) represent ~8% of the total surface area, and do not show a clear latitudinal pattern. The total surface area of estuaries is $1.1 \cdot 10^6 \text{ km}^2$ and ~81% is located in the Northern Hemisphere, with ~58% North of 45°N.

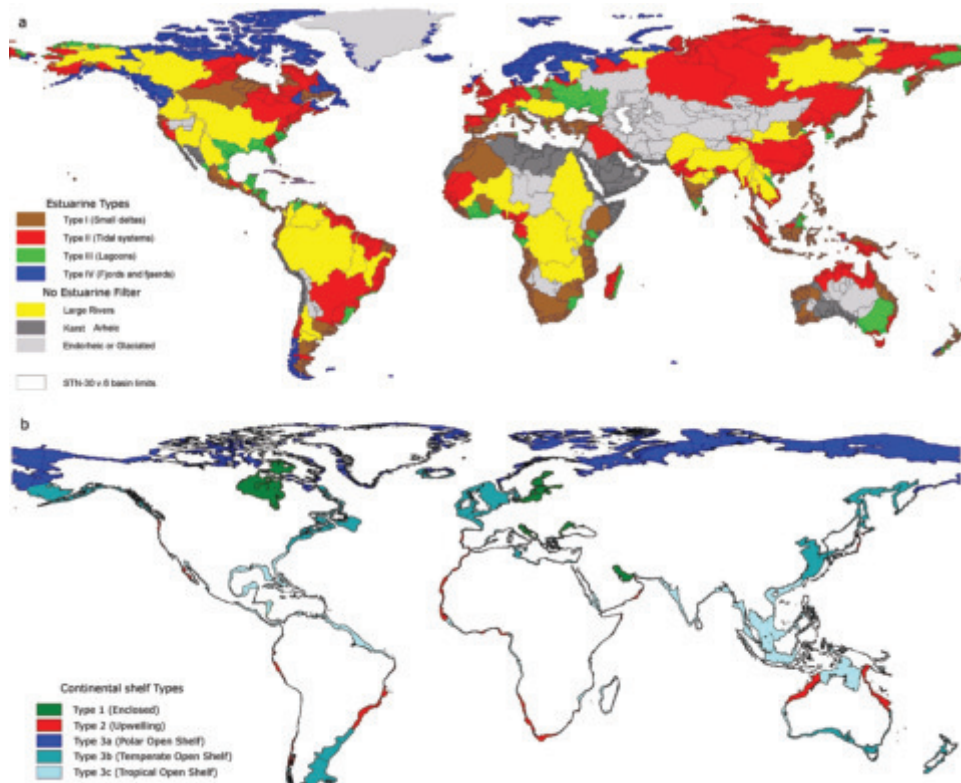


Figure 1: Typology of near-shore coastal environments (modified from Dürr et al., 2009) (a) and continental shelf seas (b)

The typology of continental shelf seas is shown in Figure 1b. Enclosed shelves (Type 1) represent 6%, coastal upwelling systems (Type 2) represent 9% and the remaining continental shelves (Type 3a,b,c) represent 82% of the total surface (24.6 10^6 km²). About 75% of the surface area of continental shelf seas is located in the Northern Hemisphere, and ~45% is located north of 45°N.

The emission of CO₂ to the atmosphere from near-shore environments shows two maxima, one at the equator and another at ~65°N (Fig. 2a). These two maxima correspond to a small peak in surface area (associated to Types I, II and III with high air-water CO₂ fluxes) and a large peak in surface area (associated to Type IV with lower air-water CO₂ flux), respectively (Fig. 2d). The overall emission of CO₂ to the atmosphere from near-shore environments is estimated at 0.23 PgC yr⁻¹. Tidal systems (Type II) contribute 61%, lagoons (Type III) contribute 22%, fjords and fjärds (Type IV) contribute 9% and small deltas (Type I) contribute 8% of the total CO₂ emission to the atmosphere from near-shore ecosystems. About 74% of the total CO₂ emission to the atmosphere from near-shore ecosystems occurs in the Northern Hemisphere.

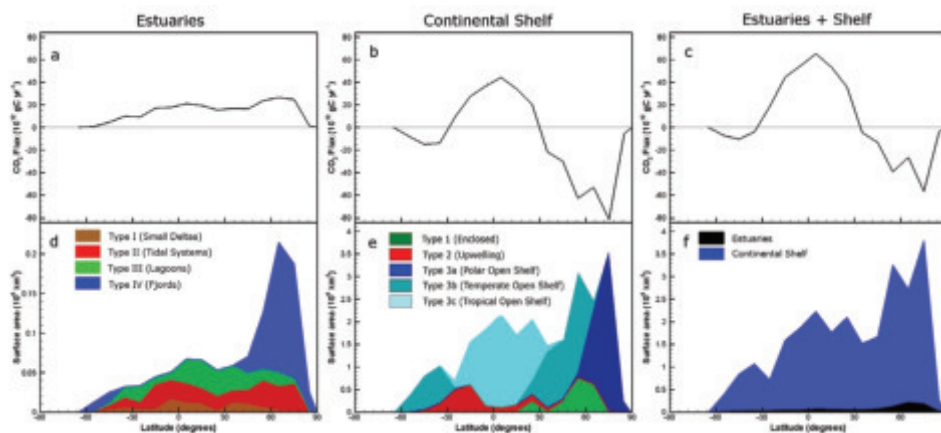


Figure 2: Latitudinal distribution of the air-water CO₂ fluxes (in 10^{12} g C yr⁻¹, top panels) and cumulated surface areas (in 10^6 km², bottom panels) in estuaries (left) and continental shelf seas (center) and the whole coastal ocean (right).

The exchange of CO₂ between continental shelf seas and the atmosphere as a function of latitude shows a clear asymmetry with regions between 30°S and 30°N (Fig. 2e) acting as a source of CO₂ to atmosphere and temperate and high

latitude areas (south of 30°S, north of 30°N) acting as a sink for atmospheric CO₂ (Fig. 2b). The continental shelf seas of the Northern Hemisphere are a net sink of CO₂ of -0.15 PgC yr⁻¹ and the continental shelf seas of the Southern Hemisphere are a source of CO₂ of 0.44 PgC yr⁻¹. Globally, continental shelf seas are a net sink of atmospheric CO₂ of -0.11 PgC yr⁻¹.

The integrated air-water CO₂ flux in the global coastal ocean (near-shore ecosystems and continental shelves) gives an overall source of CO₂ of 0.15 PgC yr⁻¹. The latitudinal pattern of a CO₂ source in low latitudes and sink of CO₂ at temperate and high latitudes is still observed. The global coastal ocean (near-shore ecosystems and continental shelves) in the Northern Hemisphere is a smaller CO₂ source (0.04 PgC yr⁻¹) than in the Southern Hemisphere (0.11 PgC yr⁻¹).

4. Discussion

The general patterns of the integrated of air-water CO₂ fluxes from the present study are similar to those reported by Borges et al. (2005). Continental shelf seas in the tropics and subtropics are a source of CO₂ to the atmosphere, while temperate and high latitude continental shelf seas are sinks for atmospheric CO₂. The overall emission of CO₂ from near-shore environments is of the same order of magnitude as the sink of CO₂ of continental shelf seas. Integrated CO₂ fluxes from both continental shelf seas and near-shore environments are more intense in the Northern than Southern Hemisphere.

However, there are marked differences in values of globally integrated air-water CO₂ fluxes, despite the use of a similar air-water CO₂ flux data set. The integrated fluxes are lower for continental shelf seas (-0.11 Pg C yr⁻¹ compared to -0.37 Pg C yr⁻¹; Borges et al., 2005). The total surface area of continental shelf seas used in the present study (24.6 10⁶ km²) is similar to the one used by Borges et al. (2005) (26.0 10⁶ km²) based on Walsh (1988). However, in the Borges et al. (2005) study the total surface area of continental shelf seas located between 30°N and 30°S (3 10⁶ km²) was under-estimated compared to that of the present typology (10 10⁶ km²). Since, these areas are assumed to act as a source of CO₂ to the atmosphere, the overall sink of CO₂ in continental shelf seas thus decreases.

The emission of CO₂ from near-shore estuaries in the present study is also

markedly lower than the one reported by Borges et al. (2005), and is estimated at 0.23 PgC yr^{-1} compared to $0.45 \text{ Pg C yr}^{-1}$. For more than 3 decades, the only global available estimate for the estuarine surface area was based on the study of Woodwell et al. (1973). The present typology provides a significantly lower estimate of the total estuarine area of $\sim 40\%$. Moreover, a large fraction of the surface area corresponds to fjords and fjärds that are characterized by the lowest air-water CO_2 flux rates of the 4 types of near-shore ecosystems.

We describe a detailed typology that can be used to scale air-water CO_2 fluxes in the coastal ocean. The typology of continental shelf seas could be further improved by distinguishing between coastal upwelling systems with and without an oxygen minimum zone (OMZ). This would allow the separation of coastal upwelling systems that can act both as sources (Goyet et al. 1998; Friederich et al. 2009) and sinks of atmospheric CO_2 (Borges and Frankignoulle 2002). The typology of near-shore ecosystems could be improved by distinguishing between micro-tidal and macro-tidal systems, since the former are usually highly stratified and are lower sources of CO_2 to the atmosphere than the latter that are usually permanently well-mixed (e.g. Borges 2005; Koné et al. 2009). However, the degree of detail in a typology depends on the availability of appropriate data for each type. At present, the lack of sufficient data is the major limitation in the quantification of the spatial and temporal variability of CO_2 fluxes in coastal environments. In near-shore environments there is a fair amount of data to characterize tidal systems (Type II) and small deltas (Type I). However, for fjords and fjärds (Type IV), that represent 43% of the total estuarine surface area, there are data from only one location. For lagoons (Type III), most of the available data were obtained from 5 contiguous systems located in Ivory Coast ($\sim 5^\circ\text{N}$) although these near-shore ecosystems are ubiquitous at all latitudes (Fig. 1). Finally, for near-shore environments, one source of uncertainty to be resolved lies in the computation of the gas transfer velocity (k) to calculate the CO_2 flux from pCO_2 data. Most available CO_2 flux data in near-shore estuaries have been computed from k parameterizations as a function of wind speed. However, in estuaries, tidal currents (Zappa et al. 2004; 2007; Borges et al. 2004a), fetch (Borges et al. 2004b) or turbidity (Abril et al. 2009) strongly modulate the gas transfer velocity, hence k parameterizations as a function of wind

speed are strongly site specific.

The data availability in continental shelf seas is strongly biased towards the temperate regions of the Northern Hemisphere, while coastlines of the Russian Arctic, western South America, eastern Africa, large sections of western Africa, and most of Antarctica (between 90°W and 180°W) are dramatically under-sampled. Finally, pCO₂ temporal variability ranges from daily (Dai et al. 2009) to inter-annual (Friederich et al. 2002; Borges et al. 2008a;b) scales. The (in)adequate representation of the full range of temporal variability can impact the evaluation of the overall net annual air-sea CO₂ fluxes. Overall, adequate data-sets to describe the relevant temporal and spatial scales of air-water CO₂ fluxes in continental shelf seas are lacking at present. For a more robust evaluation of CO₂ fluxes in continental shelf seas, an intensive, integrated, international and interdisciplinary program of observational efforts is required.

Acknowledgements

This work was funded by Utrecht University (High Potential Project G-NUX) and the Netherlands Organisation for Scientific Research (NWO Vidi grant 864.05.004). It is a contribution to EU IP CARBOOCEAN (511176), to EU CSA COCOS (212196) and to COST Action 735. AVB is a research associate at the FRS-FNRS.

References

- Abril G. and A. V. Borges (2004) Carbon dioxide and methane emissions from estuaries. in Greenhouse gases emissions from natural environments and hydroelectric reservoirs: fluxes and processes, edited by A. Tremblay, L. Varfalvy, C. Roehm and M. Garneau. Chapter 7: 187-207, Environmental Science Series, Springer, Berlin, Heidelberg, New York.
- Abril G., M. V. Commarieu, A. Sottolichio, P. Bretel and F. Guérin (2009) Turbidity limits gas exchange in a large macrotidal estuary. *Estuarine Coastal and Shelf Science*, 83(3) 342-348
- Bernard, C. Y., H. H. Dürr, C. Heinze, J. Segschneider and E. Maier-Reimer (2009) Contribution of riverine nutrients to the silicon biogeochemistry of the global ocean - a model study, *Biogeosciences Discuss.*, 6:1091-1119.
- Borges A.V. (2005) Do We Have Enough Pieces of the Jigsaw to Integrate CO₂ Fluxes in the Coastal Ocean? *Estuaries*. 28(1):3–27.
- Borges, A. V., S. Djenidi, G. Lacroix, J. Théate, B. Delille and M. Frankignoulle (2003), Atmospheric CO₂ flux from mangrove surrounding waters, *Geophys. Res. Lett.*, 30(11), 1558, doi:10.1029/2003GL017143
- Borges A.V., J.-P. Vanderborght, L.-S. Schiettecatte, F. Gazeau, S. Ferrón-Smith, B. Delille and M. Frankignoulle (2004a) Variability of the gas transfer velocity of CO₂ in a macrotidal estuary (The Scheldt), *Estuaries*, 27(4): 595-605
- Borges A.V., B. Delille, L.-S. Schiettecatte, F. Gazeau, G. Abril and M. Frankignoulle (2004b) Gas transfer velocities of CO₂ in three European estuaries (Randers Fjord, Scheldt and Thames), *Limnology and Oceanography*, 49(5): 1630-1641
- Borges A.V., B. Delille And M. Frankignoulle (2005) Budgeting sinks and sources of CO₂ in the coastal ocean: Diversity of ecosystems counts. *Geophysical Research Letters* 32, L14601, doi:10.1029/2005GL023053.
- Borges A.V., K. Ruddick, L.-S. Schiettecatte and B. Delille (2008a) Net ecosystem production and carbon dioxide fluxes in the Scheldt estuarine plume, *BMC Ecology*, 8:15, doi:10.1186/1472-6785-8-15
- Borges A.V., B. Tilbrook, N. Metzl, A. Lenton and B. Delille (2008b) Inter-annual variability of the carbon dioxide oceanic sink south of Tasmania, *Biogeosciences*, 5:141–155

- Cai W.-J., M. H. Dai and Y. C. Wang (2006) Air-sea exchange of carbon dioxide in ocean margins: A province-based synthesis. *Geophysical Research Letters*, 33, L12603, doi:10.1029/2006GL026219.
- Chen C. T. A. and A. V. Borges (2009) Reconciling opposing views on carbon cycling in the coastal ocean: continental shelves as sinks and near-shore ecosystems as sources of atmospheric CO₂, *Deep-Sea Research II*, 56 (8-10):578-590.
- Crossland, C. J., H. H. Kremer, H. J. Lindeboom, J. I. M. Crossland and M. D. A. Le Tissier (2005) *Coastal Fluxes in the Anthropocene*. Springer, Berlin, 231 pp.
- Dai, M., Z. Lu, W. Zhai, B. Chen, Z. Cao, K. Zhou, W.-J. Cai, and C.-T.A. Chen (2009) Diurnal variations of surface seawater pCO₂ in contrasting coastal environments, *Limnology & Oceanography*, 54(3):735-745
- Dürr, H. H., G. G. Laruelle, C. M. van Kempen, C. P. Slomp, M. Meybeck and H. Middelkoop, World-wide typology of near-shore coastal systems: defining the estuarine filter of riverine inputs to the oceans, *Submitted to Estuaries and Coasts*
- Frankignoulle, M., G. Abril, A. Borges, I. Bourge, C. Canon, B. Delille, E. Libert and J.-M. Théate (1998) Carbon dioxide emission from European estuaries, *Science*, 282:434–436
- Friederich, G. E., P. M. Walz, M. G. Burczynski and F. P. Chavez (2002) Inorganic carbon in the central California upwelling system during the 1997-1999 El Niño-La Niña event. *Progress In Oceanography* 54(1-4):185-203.
- Friederich, G.E., J. Ledesma, O. Ulloa and F.P. Chavez (2008) Air–sea carbon dioxide fluxes in the coastal southeastern tropical Pacific, *Progress in Oceanography*, 79(2-4):156-166.
- Gao, X. L., J. M. Song, X. Q. Li, H. M. Yuan and N. Li (2005) Spatial and temporal variations in pH and total alkalinity at the beginning of the rainy season in the Changjiang Estuary, China. *Acta Oceanologica Sinica* 24 (5):68-77.
- Gattuso, J.-P., M. Frankignoulle and R. Wollast. (1998) Carbon and carbonate metabolism in coastal aquatic ecosystems. *Annual Review Ecology Systematics* 29:405–433.

- Goyet, C., F. J. Millero, D. W. O'Sullivan, G. Eiseheid, S. J. McCue and R. G. J. Bellerby. (1998) Temporal variations of pCO₂ in surface seawater of the Arabian sea in 1995. *Deep-Sea Research Part I* 45(4-5):609-623.
- Gruber N., M. Gloor, S. E. Mikaloff Fletcher, S. C. Doney, S. Dutkiewicz, M. J. Follows, M. Gerber, A. R. Jacobson, F. Joos, K. Lindsay, D. Menemenlis, A. Mouchet, S. A. Müller, J. L. Sarmiento and T. Takahashi (2009) Oceanic sources, sinks, and transport of atmospheric CO₂, *Global Biogeochem. Cycles*, 23, GB1005, doi:10.1029/2008GB003349.
- Koné, Y. J. M., G. Abril, K. N. Kouadio, B. Delille and A. V. Borges (2009) Seasonal Variability of Carbon Dioxide in the Rivers and Lagoons of Ivory Coast (West Africa) *Estuaries and Coasts* 32:246–260
- Meybeck, M., H. H. Dürr and C. J. Vörosmary. (2006) Global coastal segmentation and its river catchment contributors: A new look at land-ocean linkage. *Global Biogeochemical Cycles*, 20, GB1S90:1-15, doi: 10.1029/2005GB002540.
- Meybeck, M., and H. H. Dürr (2009) Cascading Filters of River Material from Headwaters to Regional Seas: The European Example. In: *Watersheds, Bays, and Bounded Seas - The Science and Management of Semi-Enclosed Marine Systems*, SCOPE Series 70, edited by E.R. Urban Jr., B. Sundby, P. Malanotte-Rizzoli, and J.M. Melillo, 115-139, Washington, Island Press.
- McKee, B. A. (2003) RiOMar: The Transport, transformation and fate of carbon in river-dominated ocean margins, in the riomar workshop: Tulane university, new Orleans, LA, 54 p.
- Sabine, C. L., R. A. Feely, N. Gruber, R. M. Key, K. Lee, J. L. Bullister, R. Wanninkhof, C. S. Wong, D. W. R. Wallace, B. Tilbrook, F. J. Millero, T.-H. Peng, A. Kozyr, T. Ono, and A. F. Rios (2004) The oceanic sink for anthropogenic CO₂. *Science* 305:367–371.
- Smith, W. H. F. and D. T. Sandwell (1997) Global Seafloor Topography from Satellite Altimetry and Ship Depth Soundings, version 9.1b, http://topex.ucsd.edu/marine_topo/ Accessed 20 Dec 2007
- Takahashi, T., S. C. Sutherland, R. Wanninkhof, C. Sweeney, R. A. Feely, D. W. Chipman, B. Hales, G. Friederich, F. Chavez, C. Sabine, A. Watson, D. C. E. Bakker, U. Schuster, N. Metzl, Hi. Yoshikawa-Inoue, M. Ishii, T. Midorikawa,

- Y. Nojiri, A. Körtzinger, T. Steinhoff, M. Hoppema, J. Olafsson, T. S. Arnarson, B. Tilbrook, T. Johannessen, A. Olsen, R. Bellerby, C. S. Wong, B. Delille, N. R. Bates, H. J. W. de Baar (2009) Climatological Mean and Decadal Change in Surface Ocean pCO₂, and Net Sea-air CO₂ Flux over the Global Oceans, *Deep-Sea Research II*, 56(8-10):554-577
- Takahashi, T. (1961) Carbon dioxide in the atmosphere and in the Atlantic Ocean water. *J. Geophys. Res.* 66:477–494.
- Thomas, H. and B. Schneider (1999) The seasonal cycle of carbon dioxide in Baltic Sea surface waters, *J. Mar. Sys.*, 22(1):53-67.
- Thomas, H., Y. Bozec, K. Elkalay and H. J. W. de Baar (2004) Enhanced open ocean storage of CO₂ from shelf sea pumping. *Science* 304(5673):1005-1008.
- Tsunogai, S., S. Watanabe, and T. Sato (1999) Is there a “continental shelf pump” for the absorption of atmospheric CO₂? *Tellus* 51B:701–712.
- Walsh, J. J. (1988) *On the nature of continental shelves*. Academic Press, San Diego, New York, Berkeley, Boston, London, Sydney, Tokyo, Toronto.
- Wollast, R. (1998) Evaluation and comparison of the global carbon cycle in the coastal zone and in the open ocean, p. 213-252. *In* K. H. Brink and A. R. Robinson (eds.), *The Global Coastal Ocean*. John Wiley & Sons.
- Woodwell, G. M., P. H. Rich and C. A. S. Hall (1973) Carbon in estuaries. *in*: *Carbon and the biosphere*, edited by G. M. Woodwell and E. V. Pecan, 221-240, Springfield, Virginia.
- Xie, L. and W.W. Hsieh (1975) Global wind-induced upwelling, *Fisheries Oceanography* 4: 52–67.
- Zappa, C. J., P. A. Raymond, E. A. Terray and W. R. McGillis (2003) Variation in surface turbulence and the gas transfer velocity over a tidal cycle in a macrotidal estuary. *Estuaries* 26: 1401–1415.
- Zappa, C. J., W. R. McGillis, P. A. Raymond, J. B. Edson, E. J. Hints, H. J. Zemmelen, J. W. H. Dacey and D. T. Ho (2007) Environmental turbulent mixing controls on air-water gas exchange in marine and aquatic systems, *Geophys. Res. Lett.*, 34, L10601, doi:10.1029/2006GL028790.

Auxiliary Material:

Table 1: Air-water CO₂ fluxes for each estuarine type based on field studies. Positive values represent a source of CO₂ to the atmosphere. * indicates a study site used in Borges et al. (2005).

<i>Site</i>	<i>Longitude</i>	<i>Latitude</i>	<i>CO₂ flux</i>	<i>Reference</i>
Small deltas (I)				
Mandovi-Zuari	73.5	15.3	14.2	Sarma et al. (2001)*
Gaderu Creek	82.3	16.8	20.4	Borges et al. (2003)*
Nagada Creek	145.8	-5.2	15.9	Borges et al. (2003)*
Mooringanga Creek	89	22	8.5	Borges et al. (2003)*
Saptamukhi Creek	89	22	20.7	Borges et al. (2003)*
Itacuruca Creek	-44	-23	41.4	Borges et al. (2003)*
Rio San Pedro	-5.7	36.6	39.4	Ferrón et al. (2007)
Kidogoweni creek	39.5	-4.4	23.7	Bouillon et al. (2007a)
Kiên Vãng creeks	105.1	8.7	34.2	Koné and Borges (2008)
Matolo/Ndogwe/ Kalota/Mto Tana creeks	40.1	-2.1	25.8	Bouillon et al. (2007b)
Ras Dege creek	39.5	-6.9	12.4	Bouillon et al. (2007c)
Shark River	-81.1	25.2	18.4	Koné and Borges (2008)
Tam Giang creeks	105.2	8.8	49.3	Koné and Borges (2008)
<i>Average</i>			25.0	
Tidal systems (II)				
Elbe	8.8	53.9	53	Frankignoulle et al. (1998)*
Ems	6.9	53.4	67.3	Frankignoulle et al. (1998)*
Rhine	4.1	52	39.7	Frankignoulle et al. (1998)*
Thames	0.9	51.5	73.6	Frankignoulle et al. (1998)*
Scheldt	3.5	51.4	63	Frankignoulle et al. (1998)*
Tamar	-4.2	50.4	74.8	Frankignoulle et al. (1998)*
Loire	-2.2	47.2	64.4	Abril et al. (2003, 2004)*
Gironde	-1.1	45.6	30.8	Frankignoulle et al. (1998)*
Douro	-8.7	41.1	76	Frankignoulle et al. (1998)*
Sado	-8.9	38.5	31.3	Frankignoulle et al. (1998)*
York River	-76.4	37.2	6.2	Raymond et al. (2000)*
Hooghly	88	22	5.1	Mukhopadhyay et al. (2002)*
Satilla River	-81.5	31	42.5	Cai and Wang (1998)*
Duplin River	-81.3	31.5	23.5	Wang and Cai (2004)*
Tana	40.1	-2.1	47.9	Bouillon et al. (2007b)
Altamaha Sound	-81.3	31.3	32.4	Jiang <i>et al.</i> (2008)
Betsiboka	46.3	-15.7	3.3	Ralison <i>et al.</i> (2008)
Changjiang (Yantze)	120.5	31.5	24.9	Gao et al. (2005), Zhai et al. (2007)
Chilka	85.5	19.1	25.0	Gupta et al. (2008)
Doboy Sound	-81.3	31.4	13.9	Jiang et al. (2008)
Godavari	82.3	16.7	5.5	Bouillon et al. (2003)
Guadalquivir	-6.0	37.4	31.1	de la Paz et al. (2007)
Mekong	106.5	10.0	30.8	Chen and Borges (2009)
Sapelo Sound	-81.3	31.6	13.5	Jiang et al. (2008)
Saja-Besaya	-2.7	43.4	52.2	Ortega et al. (2005)
<i>Average</i>			37.3	
Lagoons (III)				
Aby Lagoon	-3.3	4.4	-3.9	Koné et al. (2009)
Potou Lagoon	-3.8	4.6	40.9	Koné et al. (2009)
Tagba Lagoon	-5.0	4.4	18.4	Koné et al. (2009)
Tendo Lagoon	-3.2	4.3	5.1	Koné et al. (2009)
Ebrié Lagoon	-4.3	4.5	31.1	Koné et al. (2009)
Aveiro lagoon	-8.7	40.7	12.4	Chen and Borges (2009)
<i>Average</i>			17.3	
Fjords (IV)				
Randers Fjord	10.3	56.6	4.4	Gazeau et al. (2004)*

Associated references :

- Abril, G., H. Hetcher, B. Delille, M. Frankignoulle and A.V. Borges (2003) Carbonate dissolution in the turbid and eutrophic Loire estuary. *Marine Ecology-Progress Series* 259:129–138.
- Bouillon, S., M. Frankignoulle, F. Dehairs, B. Velimirov, A. Eiler, G. Abril, H. Etcheber and A. V. Borges (2003) Inorganic and organic carbon biogeochemistry in the Gautami Godavari estuary (Andhra Pradesh, India) during pre-monsoon: The local impact of extensive mangrove forest. *Global Biogeochemistry Cycles* 17 (4), 1114, doi:10.1029/2002GB002026.
- Bouillon, S., F. Dehairs, B. Velimirov, G. Abril and A. V. Borges (2007a) Dynamics of organic and inorganic carbon across contiguous mangrove and seagrass systems (Gazi bay, Kenya). *Journal of Geophysical Research – Biogeosciences* 112, G02018, doi:10.1029/2006JG000325.
- Bouillon, S., F. Dehairs, L.-S. Schiettecatte and A.V. Borges (2007b) Biogeochemistry of the Tana estuary and delta (northern Kenya). *Limnology and Oceanography* 52 (1): 45-59.
- Bouillon, S., J. J. Middelburg, F. Dehairs, A. V. Borges, G. Abril, M. R. Flindt, S. Ulomi and S. Kristensen (2007c) Importance of intertidal sediment processes and porewater exchange on the water column biogeochemistry in a pristine mangrove creek (Ras Dege, Tanzania). *Biogeosciences* 4 :311-322.
- Cai, W.-J., and Y. Wang (1998) The chemistry, fluxes, and sources of carbon dioxide in the estuarine waters of the Satilla and Altamaha Rivers, Georgia, *Limnol. Oceanogr.*, 43(4):657-668.
- de la Paz, M., A. Gómez-Parra and J. Forja (2007) Inorganic carbon dynamic and air - water CO₂ exchange in the Guadalquivir Estuary. *Journal of Marine Systems*, 68:265-277.
- Ferrón, S., T. Ortega, A. Gómez-Parra and J. M. Forja (2007) Seasonal study of dissolved CH₄, CO₂ and N₂O in a shallow tidal system of the bay of Cadiz (SW Spain). *Journal of Marine Systems* 66 (1-4):244-257.
- Gazeau, F., A. V. Borges, C. Barrón, C. M. Duarte, N. Iversen, J. J. Middelburg, B. Delille, M.-D. Pizay, M. Frankignoulle and J.-P. Gattuso (2005), Net ecosystem metabolism in a micro-tidal estuary (Randers Fjord, Denmark): evaluation of

- methods and interannual variability. *Mar. Ecol. Prog. Ser.*, 301:23-41.
- Jiang, L.-Q., W.-J. Cai and Y. Wang (2008) Carbon dioxide degassing in river- and marine-dominated estuaries: Importance of freshwater runoff. *Limnology and Oceanography*, 53 (6): 2603–2615.
- Koné, Y. J. M. and A. V. Borges (2008) Dissolved inorganic carbon dynamics in the waters surrounding forested mangroves of the Ca Mau Province (Vietnam) *Estuarine Coastal and Shelf Science*, 77(2): 409-421.
- Mukhopadhyay, S. K., H. Biswas, T. K. De, S. Sen and T. K. Jana (2002) Seasonal effects on the air-water carbon dioxide exchange in the Hooghly estuary, NE coast of Gulf of Bengal, India, *J. Environ. Monit.*, 4(4):549-552.
- Ortega, T., R. Ponce, J. Forja and A. Gómez-Parra (2005) Fluxes of dissolved inorganic carbon in three estuarine systems of the Cantabrian Sea (north of Spain). *Journal of Marine Systems* 53 (1-4):125-142.
- Ralison, O. H., A. V. Borges, F. Dehairs, J. J. Middelburg and S. Bouillon (2008) Carbon biogeochemistry of the Betsiboka Estuary (north-western Madagascar). *Organic Geochemistry*, 39:1649–1658
- Raymond, P. A. and J. J. Cole (2001) Gas exchange in rivers and estuaries: Choosing a gas transfer velocity, *Estuaries*, 24(2):312-317.
- Sarma, V. V. S. S., M. D. Kumar and M. Manerikar (2001) Emission of carbon dioxide from a tropical estuarine system, Goa, India, *Geophys. Res. Lett.*, 28(7): 1239-1242, doi:10.1029/2000GL006114.
- Wang, Z. A. and W. -J. Cai (2004) Carbon dioxide degassing and inorganic carbon export from a marsh-dominated estuary (the Duplin River): A marsh CO₂ pump, *Limnol. Oceanogr.*, 49(2): 341-354.
- Zhai W., Dai, M., Guo, X., 2007. Carbonate system and CO₂ degassing fluxes in the inner estuary of Changjiang (Yangtze) River, China. *Marine Chemistry* 107 (3), 342-356.

SUMMARY

Coastal waters extend from the mouths of rivers to the edge of the continental shelves, thus forming the zone of transition between land and the ocean. This highly dynamic narrow ribbon of coastal ecosystems is of major ecological and economical interest. It also plays a key role in global ocean biogeochemistry through its removal and transformation of terrestrial and marine nutrient inputs. Over the past century, human activities have led to drastic increases in nitrogen (N) and phosphorus (P) concentrations in rivers, while in some areas silica (Si) concentrations have declined due to damming. As a consequence of these changes in nutrient loads and ratios, many coastal ecosystems are suffering from problems related to eutrophication, such as increased primary production, the occurrence of harmful algal blooms and hypoxia.

The research presented in this thesis focuses on the biogeochemical cycles of carbon and nutrients in the global coastal ocean and their response to perturbation, mostly on time scales of decades to a century. In chapter 1, a local model is developed and used to assess the biological response of a small tidal bay (Bay of Brest, France) to increased nutrient loads from agriculture and colonization by an invasive filter feeder. Results of the fully transient, two dimensional hydrodynamic model coupled with a biogeochemical model for N and Si cycling show that the benthic nutrient dynamics in the bay are highly variable and depend on the spatial distribution of benthic filter feeders. Monthly Si budgets calculated with the model demonstrate the importance of benthic recycling for the supply of dissolved silica (dSi) for primary production in the bay. The results suggest that removal of the benthic filter feeders might enhance the development of harmful dinoflagellate blooms. Thus, the invasion of benthic filter feeders may actually have increased the resistance of the ecosystem to water quality problems associated with eutrophication.

To assess the role of perturbations of the Si cycle at the global scale, a budget and box model for the global Si cycle was developed (Chapter 2). The model focuses on the land-ocean continuum and comprises of 4 compartments:

continents, proximal coastal zone, distal coastal zone and open ocean. All relevant reservoir sizes and fluxes were newly estimated based on an extensive and systematic review of existing data. A sensitivity analysis of the global Si cycle to temperature rise and to river damming demonstrates the high sensitivity of the biogeochemical cycle of Si in the near coastal zone to anthropogenic pressures on the time scale of a century. This work represents a first step towards modeling of the global biogeochemical cycle of Si along the entire land to ocean continuum.

The performance of the box model for the global Si cycle described in Chapter 2 is compared to that of a Ocean General Circulation Model (HAMOCC2 and HAMOCC5) in Chapter 3. Similar scenarios are run on short (150 yrs) and long (150,000 yrs) time scales with a particular focus on the temporal evolution of Si burial rates in oceanic sediments with changing river inputs. While the trends in opal burial are generally the same, the box model shows a delayed response to the imposed perturbations compared to the general circulation model. Results of both models confirm the role of the continental margins as a sink for silica on the global scale. While general circulation models are indispensable when assessing the spatial variation in opal burial in the ocean, this study demonstrates that box models provide a good alternative when studying the average global ocean response to perturbations of the silica cycle.

In order to better account for the spatial heterogeneity of carbon and nutrient dynamics in near shore environments, a spatially explicit global typology for estuarine ecosystems was developed (Chapter 4). This typology defines 7 coastal types and distinguishes between ecosystems with an active estuarine filter (small deltas, tidal estuaries, lagoons and fjords) and those without (large rivers with an external plume, karstic systems and arctic coasts). Each river basin, at 0.5 degree resolution, is associated with a coastal type. Overall, 42% of the world's water discharge bypasses the estuarine filter and is directly exported to continental shelf waters. Using ratios of the estuarine surface area over coastal length per type for well studied regions, the global estuarine surface area is re-estimated at 1 million km².

The efficiency of the estuarine filter for nutrients is assessed with a spatially explicit global model for N and P cycling in near-coastal waters (chapter

5). The model consists of a ribbon of 6200 generic box models distributed along the world coastline. Box models for each coastal type (as defined in chapter 4) were calibrated separately and the model was run with riverine fluxes obtained as output from GIS-based global watershed models for N and P (GlobalNEWS). Steady state simulations suggest that 20% and 18% of the incoming riverine P and N, respectively, is retained in the near coastal zone. These global estimates for N and P retention are lower than values reported for the global estuarine filter in previous studies. This is likely due to a bias in those earlier studies towards high latitude areas in the Northern hemisphere where retention is most efficient.

In Chapter 6, global estimates for CO₂ exchange at the air-water interface in the coastal zone are re-evaluated using a typology for estuaries (Chapter 4) and the continental shelves. When compared to earlier work, the improved estimates for surface areas, and spatially-explicit typological approach used here allow for a more accurate upscaling of average CO₂ exchange fluxes from local studies to the global scale. The new estimate for CO₂ exchange suggests that the overall coastal ocean is only a limited source of CO₂ (0.12 PgC yr⁻¹) due to the contrasting behaviour of estuaries (0.23 PgC yr⁻¹) and continental margins (-0.11 PgC yr⁻¹) in the air-water exchange of CO₂.

SAMENVATTING

Kustwateren strekken zich uit van riviermondingen tot de rand van het continentale plat en vormen zo de overgangszone tussen het land en de open oceaan. Deze zeer dynamische en smalle kuststrook is van groot ecologisch en economisch belang. Kustwateren spelen ook een centrale rol in de mondiale kringlopen van elementen in de oceaan vanwege hun rol in de retentie en transformatie van voedingstoffen die zowel van het land als vanuit zee aangevoerd kunnen worden. Gedurende de afgelopen eeuw zijn de concentraties stikstof (N) en fosfor (P) in rivieren door toedoen van de mens sterk toegenomen. Silica (Si) concentraties, daarentegen, zijn in sommige gebieden afgenomen, vooral als gevolg van het plaatsen van dammen in rivieren. De veranderingen in nutriëntconcentraties en -ratios leiden tot veel waterkwaliteitsproblemen in kustgebieden, zoals eutrofiëring, toegenomen primaire productie, de aanwezigheid van schadelijke algen en zuurstofloosheid.

Het onderzoek dat wordt gepresenteerd in dit proefschrift richt zich op de biogeochemische cycli van koolstof en nutriënten in kustwateren op mondiale schaal en het effect van verstoring van deze cycli op tijdschalen van decennia tot een eeuw. In Hoofdstuk 1 wordt een lokaal biogeochemisch model gepresenteerd voor de Baai van Brest in Frankrijk. Het model is gebruikt om te onderzoeken wat de effecten zijn van veranderingen in nutriëntentoevoer en de recente kolonisatie van de baai door een zeeslakkensoort (*Crepidula fornicata*) die zich voedt door het water te filtreren. De resultaten van het dynamische, 2-dimensionale hydrodynamisch en biogeochemisch model voor de cycli van N en Si laten zien dat de benthische nutriëntendynamiek in de baai zeer variabel is en afhangt van de ruimtelijke verspreiding van de zeeslak. Maandelijkse Si budgetten die berekend zijn met het model tonen het belang aan van regeneratie van opgelost silica (dSi) uit het sediment compartiment voor primaire productie in de baai. De resultaten suggereren dat het verwijderen van de benthische organismen die het water filtreren de ontwikkeling van schadelijke algenbloeien (met name die van dinoflagellaten) zou kunnen bevorderen. De kolonisatie van de baai door *Crepidula fornicata* lijkt de weerstand van het ecosysteem tegen waterkwaliteitsproblemen gerelateerd aan

eutrofiëring te hebben verhoogd.

Om de rol van verstoringen van de Si kringloop op wereldschaal te onderzoeken is een *box model* voor de mondiale Si kringloop ontwikkeld (Hoofdstuk 2). Het model richt zich vooral op de beschrijving van de overgang van het land naar de oceaan en bestaat uit 4 compartimenten: continenten, de kustnabije zone, het resterende deel van het continentale plat en de open oceaan. Alle relevante reservoirs en fluxen werden opnieuw geschat op basis van een uitgebreid en systematisch literatuuronderzoek. Een gevoeligheidsanalyse waarbij specifiek gekeken is naar de rol van temperatuursveranderingen en het plaatsen van dammen in rivieren toont aan dat menselijke activiteiten grote effecten kunnen hebben op de biogeochemische kringloop van Si in estuaria op een tijdschaal van een eeuw. Dit werk is de eerste stap op weg naar een gedetailleerd model van de mondiale geochemische kringloop van Si.

De prestaties van het *box model* voor de mondiale Si kringloop dat is beschreven in Hoofdstuk 2 worden in Hoofdstuk 3 vergeleken met die van een Mondiaal Oceaan Circulatie Model (*Ocean General Circulation Model*; HAMOCC2 en HAMOCC5). Vergelijkbare scenarios zijn uitgevoerd op korte (150 jaar) en lange (150 000 jaar) tijdschalen met speciale aandacht voor de respons van de begraving van Si in mariene sedimenten bij veranderingen in de rivierinvoer van Si. Terwijl de kwalitatieve trends in resultaten voor beide modellen hetzelfde zijn, laat het *box model* een vertraagde respons op de verstoringen zien in vergelijking met het *general circulation model*. De resultaten van beide modellen bevestigen de rol van het continentale plat als begravingsplaats voor Si op mondiale schaal. Hoewel *general circulation models* onmisbaar zijn voor het onderzoeken van de ruimtelijke variatie in begraving van Si in de oceaan, laat deze studie zien dat *box models* een goed alternatief vormen en inzicht bieden in de gemiddelde respons van de mondiale oceaan op een verstoring.

Om de ruimtelijke heterogeniteit van de koolstof- en nutriëntendynamiek in kustnabije milieus beter te kunnen kwantificeren, is een classificatie voor kustnabije ecosystemen (estuaria) ontwikkeld en met behulp van een geografisch informatie systeem (GIS) toegepast op de hele mondiale kustzone (Hoofdstuk 4). Deze *typology* die daarmee ruimtelijk expliciet is, onderscheidt 7 kust-types

waarbij ecosystemen met een actief estuarien filter (kleine deltas, getijdenestuaria, lagunes en fjorden) en die zonder filter (grote rivieren met een extern estuarium, karstsystemen en kusten zonder afwatering of drainage) apart beschouwd worden. Elk rivierbekken sluit aan op een kust-type. In totaal passeert 42 % van het water dat uit rivieren naar de oceaan stroomt het kustnabije filter en wordt direct naar het continentale plat geëxporteerd. Gebruikmakend van de ratios tussen het oppervlak van de verschillende kustnabijesystemen en de kustlengte per type voor goedbestudeerde gebieden, wordt het mondiale oppervlak aan estuaria geschat op 1 miljoen km².

De efficiëntie van het estuariene filter in het vasthouden van nutriënten is onderzocht met een ruimtelijk expliciet en mondiaal model voor de N and P kringlopen in kustnabije wateren (Hoofdstuk 5). Het model bestaat uit een strook van 6200 generieke *box modellen* die zich langs de kustlijn van de wereld uitstrekken. *Box modellen* voor elk kust-type (zoals gedefinieerd in Hoofdstuk 4) zijn apart gecalibreerd. Het model maakt gebruik van rivierfluxen die berekend zijn met behulp van mondiale, GIS-modellen voor rivierinvoer van N en P (GlobalNEWS). *Steady state* simulaties suggereren dat 20% van het P en 18% van het N dat door rivieren wordt aangevoerd in de kustnabije zone wordt vastgehouden. Deze globale schattingen voor N en P retentie zijn lager dan de waarden voor het mondiale estuariene filter die in eerdere studies worden gegeven. Dit komt waarschijnlijk doordat die eerdere studies hun schatting vooral gebaseerd hebben op resultaten voor gebieden op een hoge breedtegraad op het noordelijk halfrond, waar de retentie het meest effectief is.

In Hoofdstuk 6 worden nieuwe schattingen gepresenteerd voor de mondiale uitwisseling van CO₂ op het grensvlak tussen zeewater en de atmosfeer. Deze schattingen maken gebruik van de classificatie (*typology*) voor estuaria uit Hoofdstuk 4. De verbeterde schattingen voor het oppervlak van estuaria en de mondiale *typology* maken een nauwkeuriger opschaling van CO₂ fluxen uit lokale studies mogelijk dan in eerder werk. De nieuwe schatting voor CO₂ uitwisseling suggereert dat kustwateren op mondiale schaal slechts een geringe bron van CO₂ zijn (0.12 PgC yr⁻¹). Dit komt mede door het contrasterende gedrag van estuaria (0.23 PgC yr⁻¹) en de rest van het continentale plat (-0.11 PgC yr⁻¹) wat betreft de

lucht-water uitwisseling van CO₂.

ACKNOWLEDGMENTS

I know this may not be the most critical piece of text I have to write for my thesis but it is likely to become the most read. First, by my friends and colleagues, seeking a funny quote of checking if their name is written somewhere. Then, by most of the people attending the defence to keep them busy after the second question. Later, by various people looking at this book on a desk or on a shelf out of boredom or curiosity and wishing to start with the easiest. Last, in a few years, by a nervous soon-to-be doctor in the exact same position I am right now: browsing through old PhD thesis looking for inspiration to write his or her acknowledgments. And so goes life. Patterns and cycles, all over again...

Nonetheless, these acknowledgments truly matter to me because the past 4 years of work were a very important period of my life and, like most journeys, the people I met and travelled with were just as important to me as the travel itself.

My first thoughts are for the members of G-NUX, which proved to be an ambitious but very exciting and enjoyable project. I first want to greatly thank Caroline Slomp for offering me the chance to be part of this experience. More importantly, I thank her for the attention she gave to me and my work all through my PhD. As time passed, our collaboration only improved and she helped me develop the confidence I often lacked before. I also thank my promotor Philippe van Cappellen for his kindness, his sharp mind and his ability to make any discussion interesting and even sometimes challenging. Then, I have to thank Hans Dürr for his friendship and support but also because this thesis definitely is also a bit his as well. For the same reason, I thank Cheryl van Kempen who shared with Hans and I some of the most exciting moments of our project when ideas started to shape up. Iana, Sibren and Hans M., it was a pleasure to be part of the G-NUX adventure with you and, looking back, these 4 years bring back many good memories.

I am also grateful to many of the Si-Webs folks. Without this project, I would never have moved to Utrecht in the first place and it is hard for me

to imagine what my life would look like then. I met so many great people through this program that it's impossible to name everyone. Hard work turned into friendship with many members, either junior (Briva, Chris, Vincent, Massimo...) or senior scientists (Michel, Josette, Daniel...). But above all, I would like to say "Trugarez Olivier" for all he did for me since we first met. Then, I also want to thank Christiane and Pierre for their confidence and support when I worked for them.

I also met fantastic people in the department of Geochemistry of Utrecht during these last years among which David, who was the first one to welcome me and help me feel comfortable, Sandra and Vincent, my beloved Breitnerlaan-mates, Peter and Claudette, my current and former office mates... From my first seminar in a shaky English to countless parties, discussions and concerts, I have so many great memories with Sir Andrew Dale, Jeff, Doug, Rinske and Darren, Haydon, Dan, Socratis, Tom... So many souvenirs, so many people, so little space to name everyone...

Of course, I want to thank all the friends I have outside of the academic realm. It's for a large part thanks to them that I decided to stay in Utrecht. From the first persons I met (Roxane, Tijn, Youval, Bram, Thierry...) to all of the Noorderwind fellows (Reinier and Veya, Shanna, Jogchem, Araceli, Gregal...), I thank you for making me feel at home here. I also want to thank my family for their support and all my long-time friends (Claude, Dom, Ded, Tanguy, Yann, Cedric...) as well as my less-long-time-but-still-quite-long-time-friends (Bénédicte, Edo, Saki, Cyril, Maëva, Diane, Christelle, Shutan...). Distance and work often kept us apart but it really helps to know that people think about you somewhere. There are so many people I can think of like Julien, the first person who brought me to the Netherlands or Pien, the one I probably fought the most with... Thanks to you all.

Extra thanks are awarded to Béatrice Inthavong for the beautiful illustration of the Global Water Cycle she kindly drew for me (Chapt. 1, Fig. 1).

CURRICULUM VITAE

Goulven Gildas Laruelle was born on May 1st 1978 in Morlaix, France. After his graduation, he first studied General Biology and then, Marine Biology at the University of Western Brittany (Brest, France) where he received a Bachelor's degree in 2000. He moved to Belgium, to the University of Liège, where he obtained a DEA (Master's degree equivalent) in Marine Environment Modeling in 2002. Later that year, he was hired as research assistant at the Free University of Bruxelles under the supervision of Prof. Dr. C. Lancelot. In November 2003, he joined the Geochemistry Department at the Faculty of Earth Sciences of Utrecht University as a research assistant under the supervision of Dr. P.A.G. Regnier within the Si-Webs Research and Training Network coordinated by Dr. O. Ragueneau. He began working on this thesis in March 2005 under the supervision of Prof. Dr. P. van Cappellen and Dr. C. P. Slomp. Since June 2009, Goulven Laruelle is working at Utrecht University as a Postdoc in the framework of the SOWACOR programme.

